

**PALACKY UNIVERSITY OLOMOUČ**

Faculty of Science  
Department of Organic Chemistry



**Development of new fluorescent conjugates for  
intracellular imaging, drug delivery and diagnostics**

**DISSERTATION THESIS**

**Author:** Mgr. Martin Porubský

**Supervisor:** prof. RNDr. Jan Hlaváč, Ph.D.

**Academic Year:** 2021/2022

---

Prohlašuji, že jsem dizertační práci vypracoval/a samostatně s vyznačením všech použitých pramenů a spoluautorství. Souhlasím se zveřejněním dizertační práce podle zákona č. 111/1998 Sb., o vysokých školách, ve znění pozdějších předpisů. Byl jsem seznámen s tím, že se na moji práci vztahují práva a povinnosti vyplývající ze zákona č. 121/2000 Sb., autorský zákon, ve znění pozdějších předpisů.

V Olomouci dne .....

---

## Bibliografická identifikace

<b>Autor:</b>	Mgr. Martin Porubský
<b>Název práce:</b>	Vývoj fluorescenčních konjugátů pro intracelulární zobrazování, dopravení léčiva a diagnostiku
<b>Studijní program:</b>	Chemie
<b>Studijní obor:</b>	Organická chemie
<b>Pracoviště:</b>	Katedra organické chemie Přírodovědecká fakulta, Univerzita Palackého
<b>Vedoucí práce:</b>	Prof. RNDr. Jan Hlaváč, Ph.D.
<b>Akademický rok:</b>	2021/2022
<b>Počet stran:</b>	130
<b>Počet příloh:</b>	31
<b>Jazyk:</b>	Anglický
<b>Klíčová slova:</b>	BODIPY, konjugáty, zobrazování, cílení na rakovinové buňky, 3-hydroxy-2-fenylchinolony, fluorescence, kaspázy, syntéza na pevné fázi, FRET, matematický model

---

## Bibliographical identification

<b>Author:</b>	Mgr. Martin Porubský
<b>Title of Thesis:</b>	Development of new fluorescent conjugates for intracellular imaging, drug delivery and diagnostics
<b>Degree program:</b>	Chemistry
<b>Field of Study:</b>	Organic Chemistry
<b>Department:</b>	Department of Organic Chemistry Faculty of Science, Palacky University
<b>Supervisor:</b>	Prof. RNDr. Jan Hlaváč, Ph.D.
<b>Academic Year:</b>	2021/2022
<b>Number of pages:</b>	130
<b>Number of appendices:</b>	31
<b>Language:</b>	English
<b>Keywords:</b>	BODIPY, conjugates, intracellular imaging, cancer cell targeting, 3-hydroxy-2-phenylquinolones, fluorescence, caspases, solid phase synthesis, FRET, mathematical model

---

## Abstract

Ratiometric fluorescent intracellular imaging and drug delivery represent interesting strategy in current medicinal chemistry and study of various therapeutics for its personalized approach and deeper study of drug penetration and localization in cells taking advantage mainly of being non-destructive technique. Controlled and targeted delivery and real-time monitoring of drug release is of great importance due to reducing or lessening of adverse side effects in process of medication.

In the first part of this thesis, the design, synthesis and spectral properties of fluorescent conjugates of BODIPY and 3-hydroxyquinolinones (3HQs) are discussed. First generation involves BODIPY-3HQ conjugates connected with disulfide linker allowing a cleavage by increased level of glutathione. Second generation of conjugates were equipped either with two fluorescent dyes to allowing the FRET ratiometric detection or with one fluorescent tag and targeting unit to provide selective localization in the cancer cells. Both generations of conjugates were studied with respect to biological activity and fluorescent properties.

The second part is dedicated to description of design, synthesis and optimization of novel fluorescent three-fluorophore dual-FRET peptide probe for detection and quantification of proteolytic enzymes – caspase 8 and caspase 9. The probe was designed as a ratiometric single-excitation triple-emission system which function is driven by a change of fluorescence intensities during the enzymatic cleavage of specific linkers. Several probes were prepared by solid-phase chemistry approach and mathematical model for unambiguous caspases detection and determination of their relative activities was developed. The functionality of proposed system was tested in biological media, specifically on cell lysates with selectively activated caspase-8 and caspase-9.

---

## Abstrakt

Poměrové fluorescenční zobrazování uvnitř buněk a systémy pro doručování léků představují v současné medicíně zajímavou strategii zejména pro její osobní přístup a detailnější studium penetrace a lokalizace léků v buňkách s využitím nedestruktivních technik. Řízené a cílené doručování léků a monitorování jejich uvolňování v reálném čase má velký význam kvůli snížení nebo zmírnění nežádoucích vedlejších účinků v procesu léčby.

V první části této disertační práce je diskutován design, syntéza a spektrální vlastnosti fluorescenčních konjugátů BODIPY a 3-hydroxychinolonů. První generace těchto látek zahrnuje konjugáty BODIPY-3HQ spojené disulfidovým linkerem, aby se umožnilo štěpení díky zvýšené koncentraci glutathionu. Druhá generace konjugátů byla vybavena buď dvěma fluorescenčními barvivy umožňujícími FRET poměrovou detekci nebo jednou fluorescenční značkou a cílicí jednotkou tak, aby byla umožněna selektivní lokalizace v rakovinných buňkách. Aktivita obou generací konjugátů byla studována na buněčných liniích za použití fluorescenční mikroskopie.

Druhá část disertační práce je věnována popisu designu, syntézy a optimalizace nové tří-fluoroforové duální-FRET sondy pro detekci a kvantifikaci proteolytických enzymů – kaspázy-8 a kaspázy-9. Sonda byla navržena jako poměrová s jednou excitací a trojitou emisí, které se mění během enzymatického štěpení specifických linkerů. Testované sondy byly připraveny syntézou na pevné fázi a byl vyvinut matematický model pro jednoznačnou detekci obou kaspáz samostatně nebo ve směsi a pro stanovení jejich relativní aktivity. Funkčnost navrhovaného systému byla testována v biologickém médiu, konkrétně na buněčných lyzátech se selektivně aktivovanými kaspázami -8 a -9.

---

“The best teacher is experience and not through someone's distorted point of view”

— Jack Kerouac

“Whatever you are, be a good one.”

— Abraham Lincoln

“Everything you can imagine is real.”

— Pablo Picasso

---

## Acknowledgement

It was a long journey accompanied by many heroes without whom it would not be possible to get to the last stop. During this journey full of ascents and usually steep descents, enriched by several summits, some of these heroes showed me the good path whereas some helped me to recognize the wrong, misleading and dangerous ones. Nevertheless, I am grateful for both.

On the first place I would like to express my gratitude to my boss Honza Hlaváč for the opportunity to work under his supervision, for his optimism and patience which shed the light during the darkest passages of my PhD journey, for giving me a free hand to come up with new projects and for giving me a second chance always I did not respect some basic rules. I would like to thank to all former and current members of our group and other colleagues at IMTM and faculty who were helpful, enriched my scientific knowledge and also provided pleasant atmosphere during long hours of lab work – mainly Tanas, Kristýna, Soňa, Zuza, David, Soňa and Kateřina.

Furthermore, I am grateful to analytical support team – Terka Volná, Sandra Benická, Adam Příbylka and Soňa Krajčovičová who provided everything that I wished for – HRMS measurements, assistance with HPLC analyses and purification and all kinds of NMR experiments.

Next, I thank to co-authors of our publications - Soňa Gurská, Jarka Stanková, Petr Džubák from IMTM and Eva Řezníčková and Vladimír Kryštof from Department of Experimental Biology for doing the hard work in biological lab and testing of our compounds for cytotoxicity and all other biological experiments.

I am also thankful to Josef Vagner who was my temporary boss during the internship in Tucson, USA for his help and long inspiring talks by the window with the best view on the mountains in Arizona.

I am really grateful to Foundation “Nadání Josefa, Marie a Zdeňky Hlávkových” for a financial contribution for the internship at The University of Arizona, AZ, USA.

V neposlednom rade ďakujem rodičom a bratovi Tomášovi za podporu počas celého života nevyvímajúc obdobie PhD, vďaka ktorej môžem robiť to čo ma baví. Za to, že mi píľili uši rôznymi, pre doktoranda neoblíbenými otázkami.no stáli pri mne vždy, keď som to najviac potreboval. Ďakujem !

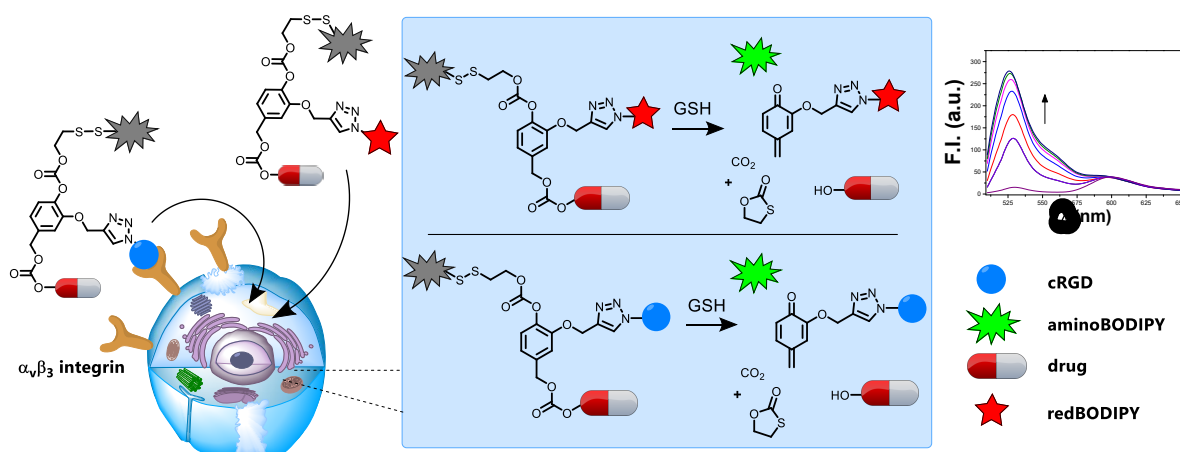
---



## Thesis objectives

This work is divided into three separate parts which discuss design, synthesis, optimization and biological activity of conjugates that may be generally assigned as theranostics or diagnostic tools. The common denominator of all projects is the use of fluorescent labels for intracellular imaging or diagnostic purposes. The chemistry of fluorescent labels was not thoroughly established previously in the group of Jan Hlaváč and this work may provide new insight in development of intracellular ratiometric imaging agents and theranostics. Currently, a lot of effort in medicinal chemistry is put into development of more selective and personalized chemotherapeutic agents together with reduction of undesired effects. Moreover, ratiometric or “OFF-ON” fluorescent probes are attractive for their ability to selectively visualize tumor sites what may be utilized in imaging-guided surgery.

The first project was devoted to various ways of conjugation of model drug 3-hydroxyquinolinone with fluorescent tag and to monitor the fate of these conjugates in biological medium. 3HQs were synthesized and derivatized previously in our group as novel anticancer agents. Some derivatives were therefore used as model drugs for conjugates development. The aim was to prepare various conjugates bearing fluorescent dye - BODIPY that would easily penetrate and would be cleaved readily in the presence of microenvironment stimuli inside the cancer cells releasing the free drug. Our goal was also to study the optical properties and compare biological activity of cleavable and non-cleavable conjugates. Further, our intention was also to incorporate targeting unit specific for cancer cells such as biotin or cRGD peptide to the previously prepared conjugates and monitor their cleavability as well as biological activity.



The second project deals with design and synthesis of dual-FRET probes for detection of caspases -8 and -9, proteolytic enzymes that take a part in programmed cell death – apoptosis. Chosen caspases represent two main initiator caspases which are activated in the cells by different pathways and facile distinguishing between them would provide valuable information about mechanism of action of drugs. Synthesis of dual-FRET probes by solid phase chemistry approach would lead to optimization of structure for optimal caspase cleavage selectivity and FRET efficiency. Further, the functionality of probes was aimed to be tested with active recombinant enzymes and cell lysates with selectively activated caspases. The big challenge remained to develop mathematical model that would be able to provide detection and relative quantification of enzymes as well.

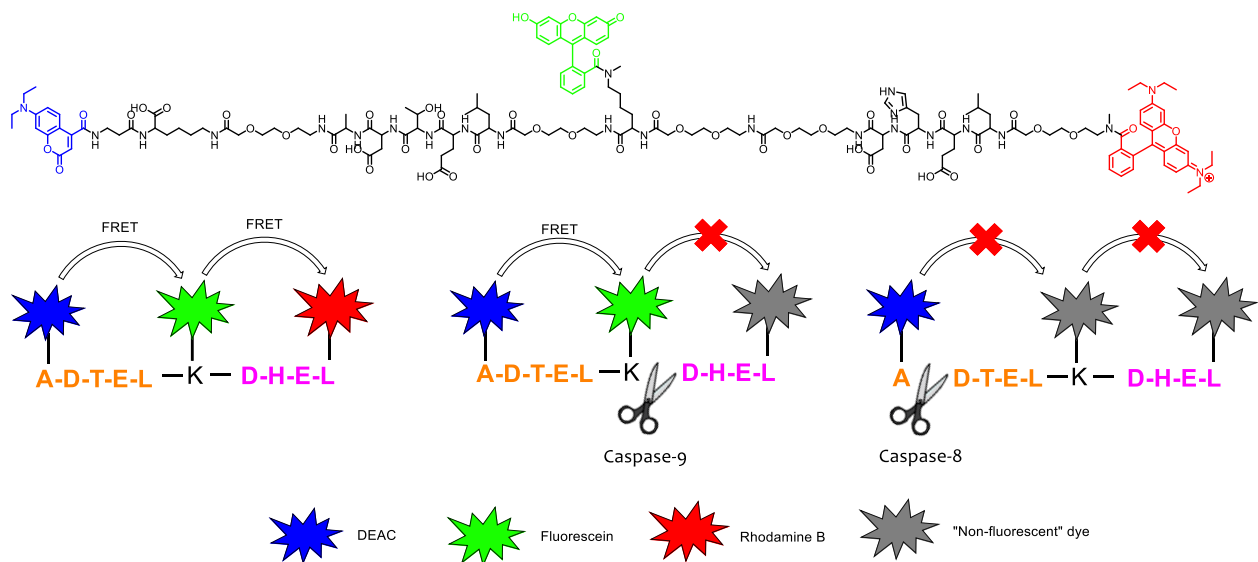


## Table of Contents

Part I: Fluorescent conjugates for delivery of 2-phenyl-3-hydroxy-4(1H)-quinolinones to the cancer cells and their release monitoring .....	16
1 Introduction .....	17
1.1 Short overview of 3-hydroxy-2-phenyl-4(1 <i>H</i> )-quinolinones .....	17
1.1.1 Quinolones .....	18
1.1.2 Overview of 3-hydroxyquinolones.....	19
1.2 Fluorescent dyes .....	24
1.2.1 Synthesis of BODIPY dyes and their application in chemical biology .....	25
1.2.2 BODIPY fluorescent probes.....	28
1.3 Targeting cancer cells.....	34
1.3.1 Passive targeting.....	35
1.3.2 Active targeting .....	36
1.4 Cell-penetrating peptides.....	42
1.5 Linkers for stimulus responsive targeting .....	44
2 Results and discussion.....	48
2.1 1 <sup>st</sup> generation of 3HQ conjugates .....	50
2.1.1 Synthesis of BODIPY dyes .....	51
2.1.2 Synthesis and modification of 3HQs.....	51
2.1.3 Synthesis of linkers .....	53
2.1.4 Synthesis of conjugates .....	55
2.1.5 Fluorescent properties of BODIPY dyes and its conjugates .....	58
2.1.6 GSH-mediated cleavage .....	59
2.1.7 Biology .....	67
2.2 Second generation conjugates .....	72
2.2.1 Synthesis.....	73
2.2.2 cRGD synthesis .....	82
2.2.3 Fluorescent properties and GSH-cleavage .....	83
2.2.4 Biology .....	91
2.3 Conclusion.....	94
Part II: Development of dual FRET probes for detection and quantification of caspases -8 and -9.....	97
3 Introduction .....	98

---

3.1	Multi-analyte detection probes .....	98
3.2	Caspases .....	102
4	Results and discussion.....	106
4.1	Synthesis of dual-FRET probes.....	107
4.2	Caspase cleavage studies.....	110
4.3	Mathematical “sun watch” model .....	114
4.4	Biology .....	117
4.5	Conclusion.....	122
5	Literature .....	124
6	Appendices .....	131

---

## List Of Abbreviations

<b>3HQ</b>	3-hydroxy-2-phenyl-4(1 <i>H</i> )-quinolinone	<b>DIPEA</b>	Diisopropylethylamine
<b>AA</b>	Amino acid	<b>DIC</b>	N,N'-Diisopropylcarbodiimide
<b>AcOH</b>	Acetic acid	<b>DM1</b>	Maytansinoid
<b>ADC</b>	Antibody drug conjugate	<b>DMAP</b>	4-(Dimethylamino)pyridine
<b>ALP</b>	Alkaline Phosphatase	<b>DMF</b>	Dimethylformamide
<b>a-QM</b>	Aza-quinone methide	<b>DMSO</b>	Dimethylsulfoxide
<b>ATP</b>	adenosine triphosphate	<b>DNA</b>	Deoxyribonucleic acid
<b>bFGF</b>	Basic fibroblast growth factor	<b>DNBS</b>	Dinitrobenzenesulfonyl
<b>BODIPY or BDP</b>	4,4-difluoro-4-bora-3a,4a-diaza-s-indacene	<b>DOXO</b>	Doxorubicine
<b>Btz</b>	Benzotriazole	<b>DPPA</b>	Diphenylphosphoryl azide
<b>CHX</b>	Cycloheximide	<b>DTT</b>	Dithiothreitol
<b>CPP</b>	Cell penetrating peptide	<b>DTX</b>	Docetaxel
<b>CPT</b>	Camptothecin	<b>EDTA</b>	Ethylenediamine tetraacetic acid
<b>cRGD</b>	Cyclic RGD peptide	<b>eEF1A1</b>	Eukaryotic Translation Elongation Factor 1-alpha 1
<b>CTP</b>	Cell targeting peptide	<b>EPR</b>	Enhanced permeability and retention
<b>DABCYL</b>	4-(dimethylaminoazo)benzene-4-carboxylic acid	<b>ESIPT</b>	Excited-state intramolecular proton-transfer
<b>DBU</b>	1,8-Diazabicyclo(5.4.0)undec-7-ene	<b>Fl</b>	Fluorescein
<b>DCM</b>	Dichloromethane or 4-(Dicyanomethylene)-2-methyl-6-(4-(dimethylamino)styryl)-4H-pyran	<b>FRET</b>	Forster resonance energy transfer
<b>Dde</b>	1-(4,4-Dimethyl-2,6-dioxocyclohex-1-ylidene)ethyl	<b>HCy</b>	Homocysteine
<b>DDQ</b>	2,3-Dichloro-5,6-dicyano-p-benzoquinone	<b>HEPES</b>	4-(2-hydroxyethyl)-1-piperazineethanesulfonic acid
<b>DDS</b>	Drug delivery system	<b>HOBt</b>	1-Hydroxybenzotriazole
<b>DEAC</b>	7-(diethylamino)- coumarin	<b>HPLC</b>	High performance liquid chromatography

---

<b>HPMA</b>	N-(2-Hydroxypropyl) methacrylamide	<b>TCEP</b>	tris(2-carboxyethyl)phosphine
<b>HRMS</b>	High resolution mass spectrometry	<b>TEA</b>	Triethylamine
<b>KFL</b>	KeioFluors BODIPY dyes	<b>TES</b>	Triethylsilane
<b>LC/MS</b>	Liquid chromatography with mass detection	<b>TFA</b>	Trifluoroacetic acid
<b>mAb</b>	Monoclonal antibody	<b>THF</b>	tetrahydrofuran
<b>MDR</b>	Multidrug resistance	<b>TfR</b>	Transferrin
<b>MeCN</b>	Acetonitrile	<b>QM</b>	Quinone methide
<b>MeOH</b>	Methanol	<b>RES</b>	Reticulo-endothelial system
<b>Mesyl</b>	Methanesulfonyl	<b>RhB</b>	Rhodamine B
<b>MMP</b>	Matrix metalloproteinase	<b>ROS/RNS</b>	Reactive oxygen/nitrogen species
<b>MPS</b>	Mononuclear phagocyte system	<b>SAR</b>	Structure-activity relationship
<b>NEM</b>	N-ethylmaleimide	<b>SD</b>	Standard deviation
<b>NIR</b>	Near-infrared	<b>SEAr</b>	Aromatic electrophilic substitution
<b>NLS</b>	Nuclear localization sequence	<b>SS</b>	disulfide
<b>NMP</b>	N-methylpyrrolidone	<b>TAX</b>	Taxol
<b>Nosyl</b>	4-Nitro-toluenesulfonyl	<b>TMSCl</b>	Trimethylsilyl chloride
<b>NPs</b>	Nanoparticles	<b>TNF</b>	Tumor necrosis factor
<b>NQO</b>	NAD(P)H:quinone oxidoreductase	<b>Tosyl</b>	Toluenesulfonyl
<b>NTR</b>	Nitroreductase	<b>Trt</b>	Trityl
<b>PARP-1</b>	Poly [ADP-ribose] polymerase 1	<b>Val-Cit</b>	Valine-citrulline
<b>PBS</b>	Phosphate buffered saline	<b>VEGF</b>	Vascular endothelial growth factor
<b>PEG</b>	Polyethyleneglycol	<b>WT</b>	Wild type
<b>PeT</b>	Photoinduced electron transfer		
<b>PLA</b>	Polylactic acid		

---

## Foreword

This PhD thesis consists of two main projects, which results have been published during my PhD thesis or are submitted and waiting for publication. Both projects contain concise literature review in the *Introduction* chapters that serves as a guidance for a reader.

*Results and discussion* parts summarize all relevant approaches towards the synthesis and optimization of synthetic routes. Further it deals with evaluation of fluorescence properties and biological activity.

The discussed manuscripts are attached as *Appendices* at the end of the thesis.

The *Supporting information* contain all relevant experimental data and is attached as an electronic file on CD or following QR code. They can also be found on the web pages of the corresponding publisher.



<https://docs.google.com/document/d/1u2-MdbBBiq5S1VKGUDCpxV4Bm-CwW1ft/edit?usp=sharing&oid=114037866727996604255&rtpof=true&sd=true>

---

## Part I:

Fluorescent conjugates for delivery of 2-phenyl-3-hydroxy-4(1H)-quinolinones to the cancer cells and their release monitoring

---



# 1 Introduction

## 1.1 Short overview of 3-hydroxy-2-phenyl-4(1*H*)-quinolinones

Despite the fact that only few new derivatives 3-hydroxy-2-phenyl-4(1*H*)-quinolinones (3HQs) were synthesized during my Ph.D. and without particular intention for optimization of their inherent biological activity, I believe that short introduction into the chemistry of these compounds should be brought since they were used as model drugs through this work. As the complexity of the compounds related to 3HQs is beyond the scope of this short introduction and therefore I will focus on narrower range of quinolones and 3HQs.

3-HQs represent isosteric aza-analogues to flavonols – derivatives of flavones. In general, flavone derivatives represent large group of mainly phenolic or polyphenolic structures belonging to a class of natural products and plant secondary metabolites with occurrence in mostly fruits and vegetables.<sup>1</sup> Flavones possess interesting biochemical and antioxidant properties linked with diseases such as cancer or Alzheimer's disease.<sup>2</sup> Flavonols, the closest structurally related flavones to 3HQs, are associated with wide range of beneficial effects such as protection against oxidative stress<sup>3</sup>, reduce risk of vascular diseases<sup>4</sup>, anti-inflammatory activity<sup>5</sup> and antibiotic activity<sup>6</sup>. Bioisosteric replacement of chromone core of flavones with nitrogen containing ring affords quinolone derivatives (Figure 1).

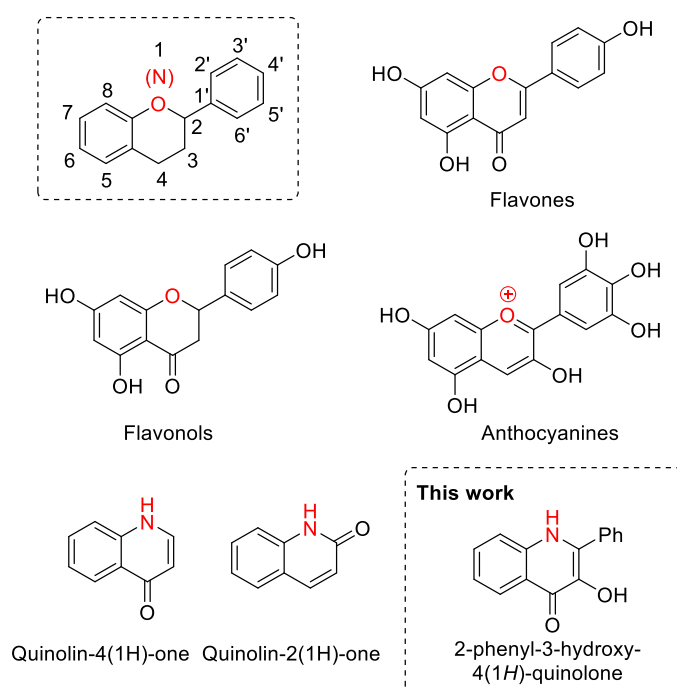


**Figure 1** Structures of biologically important groups derived from flavonols.

### 1.1.1 Quinolones

Since the discovery of the first quinolone nalidixic acid in 1962 used for treatment of urinary tract infections<sup>7</sup>, various structural modifications of the quinolone core resulted in one of the major classes (>10 000 analogs) in heterocyclic chemistry led by significant expansion of fluoroquinolones and next generations of quinolone-based antibiotics.<sup>8</sup> Thanks to its diverse spectrum of biological activity the quinolone structural unit is seen in wide spectrum of antibiotics<sup>9</sup>, chemotherapeutic agents<sup>10,11</sup>, anti-viral<sup>12</sup>, anti-inflammatory<sup>13</sup>, neuroprotective, anti-tubercular drugs<sup>14</sup>. Currently 4-quinolones are the third most prescribed class of antibiotics after macrolides and beta-lactams.<sup>15</sup>

Although the dominant role of quinolones lies in antibacterial treatment a lot of effort was oriented in the synthesis and evaluation of quinolones for their anti-cancer activity in last decades. Broad spectrum of compounds was discovered to have promising properties and some of them reached different stages of clinical trials.<sup>16–18</sup>

Since inhibition of prokaryotic DNA topoisomerases causes antimicrobial activity, targeting its eukaryotic equivalent may be used for effective anticancer medication.<sup>19</sup> Mammalian topoisomerase (mainly type II) as well as bacterial is essential for living cells, maintaining the proper DNA topology.<sup>20,21</sup> They act as regulators of DNA during replication, transcription, and repair processes by providing single (type I) or double strand breaks (type II) and taking a part during re-ligation.<sup>22</sup> The correct way of these operations is indispensable and vital for cell survival. Since the expression of topoisomerase II $\alpha$  is connected with division of cells, it represents an attractive drug target especially for rapidly dividing cancer cells.<sup>23</sup>

To reorientate antimicrobial agents to anticancer drugs certain modifications such as lowering the zwitterionic character at carboxylic acid at C-3, adjusting the basic site at C-7, incorporating aromatic substitution at C-7, derivatization at N-1 and maintaining planarity by substitution at C-5 were necessary<sup>24</sup>. Among the most prominent examples of quinolone anticancer agents belong **Camptothecin**, **Ciprofloxacin**, **Moxifloxacin** or **Voreloxin**, also used as antibiotic agents (Figure 2).<sup>25</sup> Fluoroquinolone **Quarfloxin** was promising, first in class of G-quadruplex inhibitors that reached Phase II clinical trials. However, due to low bioavailability it failed to proceed to the Phase III.<sup>26</sup> Furthermore, newly synthesized compound **91i** (Figure 2) showed superior activity to A549 (IC<sub>50</sub> 0.009  $\mu$ M), HL-60 (IC<sub>50</sub> 0.008  $\mu$ M) and HeLa (IC<sub>50</sub> 0.010  $\mu$ M) cell lines along with excellent topoisomerase inhibitory activity thanks to difluorophenyl substitution at N-1 and CF<sub>3</sub> group at the phenyl ring of sulfonamide.<sup>27</sup>

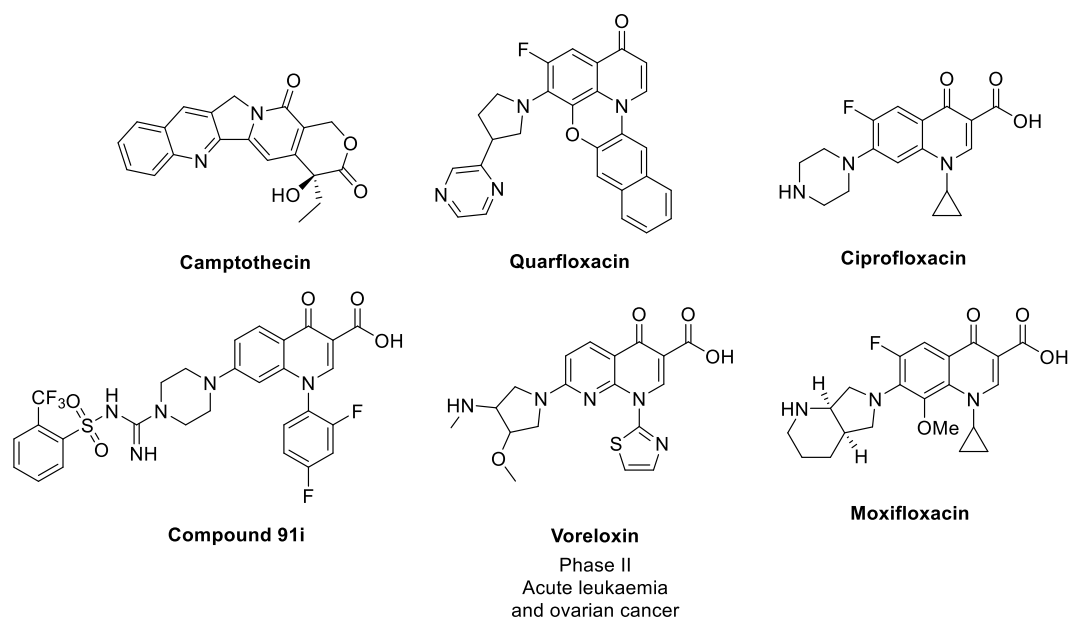
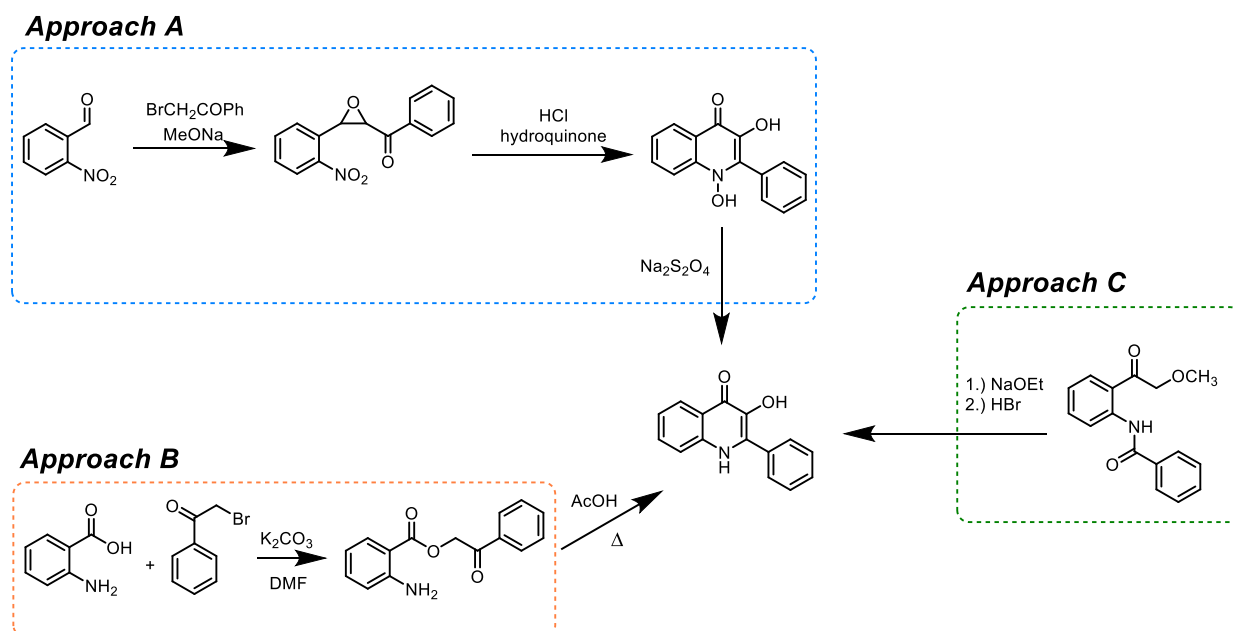


**Figure 2** Quinolones with anticancer activity.

One of the promising structural modifications of 4-(1*H*)-quinolone skeleton is 2-phenyl-3-hydroxy derivatization. Although these compounds are still far away from clinical testing, their activity and molecular action puts them in the role of new promising anticancer agents.

### 1.1.2 Overview of 3-hydroxyquinolones

First 3HQs were synthesized in 1971 by reaction of nitro-benzaldehydes with bromoacetophenones under basic conditions (Scheme 1, Approach A).<sup>28</sup> Since then, several procedures allowing formation of the 3-hydroxy-2-phenyl core were discovered.<sup>29</sup> Throughout my work the synthetic route involving cyclization of phenacylesters<sup>30</sup> (Scheme 1, Approach B) was used. Transformation of this synthetic protocol from the solution to the solid phase synthesis of carboxamide substituted 3HQs developed by Soural et al. allowed the preparation of bigger library of compounds used for biological studies.<sup>31</sup> Another approach demonstrates an alternative way for preparation of 3-hydroxyquinolones by cyclization of alkyl(2-aminophenyl)ketone derivatives under basic conditions and subsequent demethylation of 3-methoxy group by HBr (Scheme 1, Approach C).



Scheme 1 Approaches leading to 3-hydroxyquinolones.

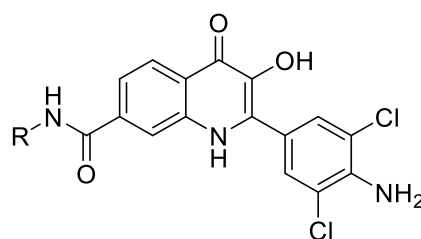
Most of the 3HQs are fluorescent compounds with dual emission character. However, the low maximum excitation wavelength together with often low quantum yield<sup>32–35</sup> limits its use as a fluorescent probe in living organisms.

Biological activity of 3HQs has been studying since the first discovery of 3-hydroxygraveoline isolated from plant *Ruta chalepensis* in 1986. 3HQs were followingly found to possess various activities such as anticancer, antibacterial or immunosuppressive activity.

- **Anticancer activity**

Anticancer activity of numerous derivatives of 3HQs was studied extensively in the past decade. Most of them were synthesized in the Hradil, Soral and Hlavač group.<sup>35–39</sup> Analogues with various substitution at 2-phenyl ring, C-5, C-6, C-7 and C-8 positions were prepared and studied. It was confirmed that the most promising compounds are formed by derivatization with ester or carboxamide group in positions C-8, C-6 or C-7 and with proper substitution at 2-phenyl ring. On the other hand, free carboxylic group at C-7 or other very polar groups in different positions significantly impair its activity, arguably due to the low ability of compounds to penetrate to the cell.<sup>31</sup> The 3-nitro-4-alkylamino and 3,5-dichloro-4-amino substitution on the 2-phenyl ring was studied mostly and thus structure-activity relationship (SAR) studies of these derivatives will be discussed.

SAR studies performed previously revealed some general patterns applicable for 3HQs<sup>28,31</sup>. Compounds were tested on CCRF-CEM (T-lymphoblastic leukaemia), CEM-DNR (T-lymphoblastic leukaemia, daunorubicin resistant), K562 (acute myeloid leukaemia) and K562-TAX (acute myeloid leukaemia, paclitaxel resistant), A549 (human lung adenocarcinoma), HCT116 (human colorectal cancer), HCT116p53 (human colorectal cancer, p53 deficient), U2OS (human osteosarcoma). In general, hydrophobic side chains at carboxamide in position C-7 e.g., alkyl, cycloalkyl or aromatic groups caused improved activity against CEM, K562, HCT116 cell lines (Table 1). Carboxamide in positions C-6 and C-8 was necessary for better activity, but with negligible dependence on hydrophobicity of the side chain as seen for C-7 substitution.

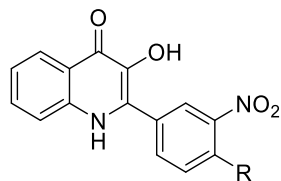


Entry	R	Cell line ( $\mu\text{M}$ )			
		CEM	K562	HCT16	BJ
1	cyclopropyl	3.7	16.9	15.1	-
2	cyclobutyl	1.2	13.6	10.6	-
3	cyclopentyl	1.1	15.3	12.9	-
4	cyclohexyl	1.1	12.6	9.4	-
5	cycloheptyl	1.0	9.5	10.9	-
6	Methyl	3.9	25.8	32.1	-
7	isobutyl	1.8	11.6	8.1	-
8	pentyl	1.0	7.5	5.6	-
9	benzyl	0.94	6.5	6.6	9.6
10	3-Me-Bn	0.75	3.1	4.1	5.0

**Table 1** SAR: C-7 carboxamide side chain hydrophobicity effect on toxicity of 3HQ.

Similar pattern was observed in the case of substitution on 2-phenyl ring where longer, more hydrophobic side chains at amino group of 3-hydroxy-2-(4-amino-3-nitrophenyl)-4-(1*H*)quinolones exhibited better activity also on multidrug resistant cell lines CEM-DNR-BULK or K562-TAX. (Table 2). It was suggested, based on enzyme inhibition studies and SAR studies that 2-phenyl-3-hydroxyquinolinones may function via topoisomerase II inhibition which was previously reported<sup>19</sup> as a molecular target of quinolinone derivatives. However,

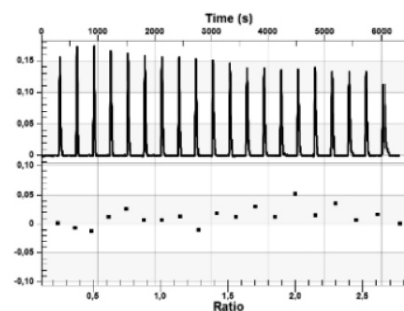
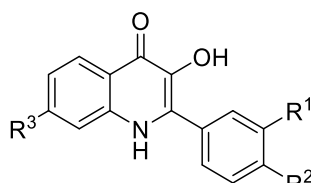
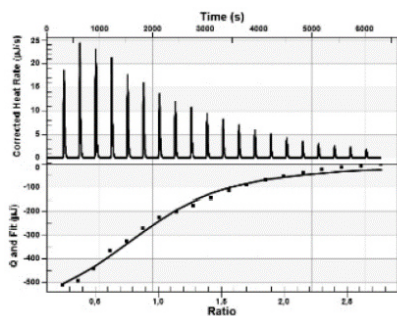
unlike CEM cells, CEM-DNR cells lack topoisomerase II $\alpha$  gene and therefore the activity was probably caused by interaction with different targets.<sup>28,31</sup>



Entry	R	Cell line ( $\mu\text{M}$ )			
		CEM	CEM-DNR	K562	K562-TAX
1	-NH(CH <sub>2</sub> ) <sub>2</sub> OH	2.7	98.8	7.3	44.9
2	-NH(CH <sub>2</sub> ) <sub>3</sub> OH	1.4	46.3	6.2	12.9
3	-NH(CH <sub>2</sub> ) <sub>4</sub> OH	0.7	15.1	1.8	8.6
4	-NH(CH <sub>2</sub> ) <sub>5</sub> OH	1.0	10.8	2.8	5.7
5	-NHCH <sub>2</sub> (CH <sub>3</sub> ) <sub>2</sub>	1.6	6.8	2.1	3.0
6		6.5	2.5	0.6	0.93
7	-N(CH <sub>2</sub> CH <sub>2</sub> CH <sub>3</sub> ) <sub>2</sub>	0.7	2.2	0.6	1.2
8	-N(CH <sub>2</sub> CH <sub>2</sub> OH) <sub>2</sub>	0.3	143	187	198

**Table 2** SAR: Effect of different substitution at 4-amino group of 3-hydroxy-2-(4-amino-3-nitro-phenyl)-4-(1*H*)quinolone.

Recently, the elongation factor eEF1A1 was revealed as a new molecular target for 3HQs that exhibit anticancer activity by pull-down assay.<sup>40</sup> eEF1A1 is responsible for the enzymatic delivery of aminoacyl tRNAs to the ribosome and is associated with the development of various cancers.<sup>41</sup> Therefore, it has been suggested as a potential target for anticancer therapy, but only a few compounds have been confirmed to interact with it. Some tested 3HQs demonstrated strong binding constants, as determined by isothermal titration calorimetry (Entry 3 in the Table 3 corresponds to the left diagram) and docking studies and therefore proving as effective eEF1A1 inhibitors. Unsubstituted, biologically inactive 3HQ (Entry 6, Table 3) showed no interaction with elongation factor (diagram on the right, Table 3), proving the proposed theory.<sup>40</sup>



N°	R <sup>1</sup>	R <sup>2</sup>	R <sup>3</sup>	Cell lines (µM)								
				A549	U2OS	CEM	CEM - DNR	HCT-116	K562	K562-TAX	BJ	
1	-CO <sub>2</sub> H		-H	50	50	49.56	50	50	50	50	50	50
2	-CO <sub>2</sub> H		-H	50	50	50	50	50	50	50	50	50
3	-CONH <sub>2</sub>		-H	9.96	26.0	3.34	21.43	4.46	7.10	6.41	48.92	
4	-CONH <sub>2</sub>		-H	44.37	50	16.24	50	30.6	50	50	50	50
5	-CONH <sub>2</sub>		C <sub>5</sub> H <sub>11</sub> CON H	1.89	0.56	1.73	8.03	0.64	2.39	32.71	10.24	
6	-H	-H	-H	50	46.96	26.74	22.49	44.20	47.96	27.44	50	

**Table 3** SAR: Activities of compounds with different substitutions at position C-7 and 2-phenyl ring. Left and right diagrams correspond to the Entry 3 and Entry 6, respectively.<sup>40</sup>

It is noteworthy to mention that many 3HQ derivatives suffer from poor water solubility, oxidative instability, poor bioavailability and high systemic toxicity against BJ - normal healthy cells as shown in the Table 1 and Table 3. Several modulations were attempted in order to avoid these adverse effects such as liposomal modulations or complexation with  $\beta$ -cyclodextrin and incorporation into antioxidative micelles but only some of them brought partially desired result.<sup>42,43</sup> Another possibility that puts forward to avoid abovementioned unfavorable effects would be attachment of 3HQs to water soluble polymeric carrier such as PEG, PLA or HPMA copolymer or incorporation of 3HQs in targeted drug delivery systems. The latter option is discussed in this work.

#### • Antimicrobial activity

As shown in the previous chapter, quinolones are well known for their antibacterial properties with carboxylic acid substitution being common for most of them. Replacement by 3-hydroxy group leads only to inhibition of DNA gyrase. Based on the study of several 3HQs

on gram-negative and gram-positive strains of bacteria the majority of them exhibit no or only low activity.<sup>28</sup>

## 1.2 Fluorescent dyes

In general, small fluorescent dyes conjugated with relevant molecules are used in numerous areas of research such as biological labelling, development of fluorescence sensors for various analytes such as metals<sup>44</sup>, enzymes<sup>45</sup>, gases or pH sensors<sup>46</sup>, laser dyes<sup>47</sup>, organic photovoltaic devices<sup>48</sup> and light emitting devices<sup>49</sup>, photocatalytic reactions<sup>50</sup>, photoinduced hydrogen generation<sup>51</sup>, light harvesting systems<sup>52</sup>, photodynamic therapy<sup>53</sup> or bioimaging<sup>54</sup>. Development of specific areas led to discovery and tuning of rich variety of fluorescent dyes so far. Most common fluorescent dyes used include xanthene derivatives – fluorescein, rhodamine or eosine, squaraines, coumarines, tetrapyrrole derivatives – porphin or phthalocyanines, 1,8-naphthalimides, cyanines or dipyrromethene derivatives – BODIPY or aza-BODIPY (

Figure 3). The ideal organic fluorophore should possess desirable chemical and physical properties such as high quantum yield, high absorption coefficient, emission at longer wavelengths (near infrared region, NIR), sharp emission profile, chemical stability e.g., against oxidation or photobleaching, solubility in water and pH stability.<sup>55</sup>

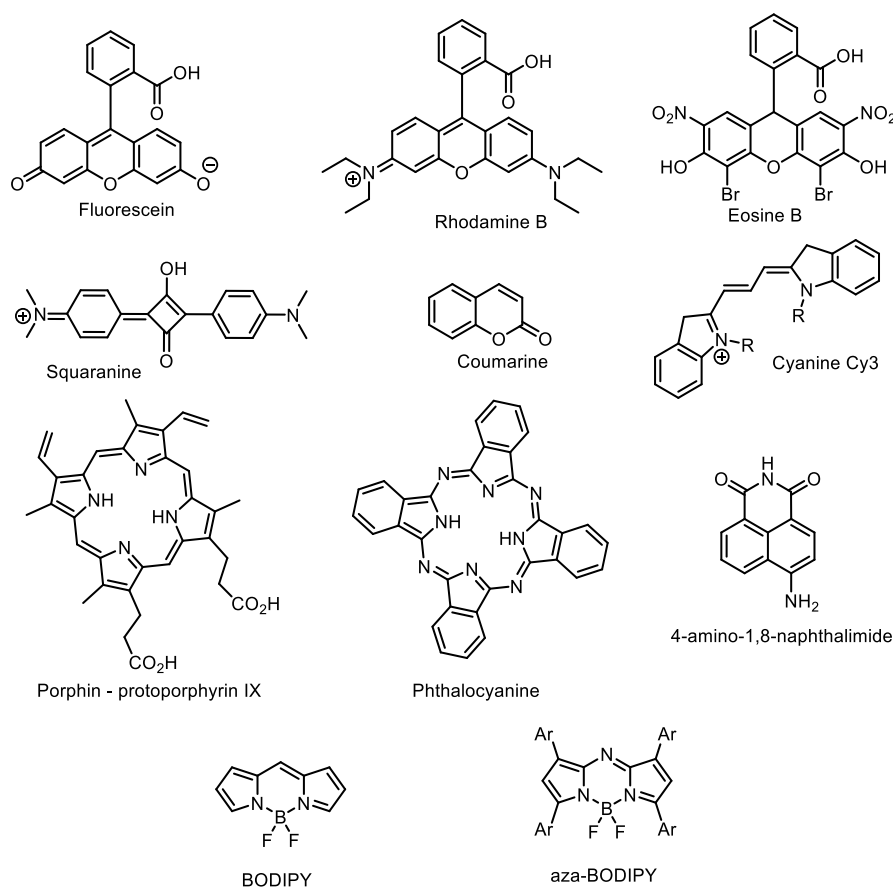


**Figure 3** Commonly used fluorescent dyes.



## 1.2.1 Synthesis of BODIPY dyes and their application in chemical biology

Boron difluoride complexes of dipyrromethenes, 4,4-difluoro-4-bora-3a,4a-diaza-s-indacene or abbreviated BODIPYs are among the most intensively studied dyes recently and thanks to their outstanding properties they have become extremely valuable fluorophores. BODIPYs are hydrophobic dyes with neutral overall charge despite bearing formal charges on boron and nitrogen (Figure 4). They usually tend to absorb strongly in the visible range, thus having high absorption coefficient ( $\epsilon$ ), emit sharp fluorescence bands with high quantum yield ( $\Phi$ ) and high brightness ( $\epsilon \times \Phi$ ). Common feature of BODIPY dyes is also relatively small Stoke's shift, insensitivity to polarity and pH of the solvent and stability in under physiological conditions. However, many BODIPY dyes show emission at low wavelengths ( $<600$  nm), poor solubility in water or low absorption coefficients ( $\epsilon$ ).<sup>56</sup>

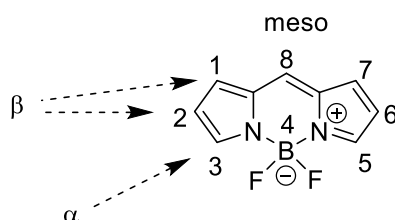


**Figure 4** BODIPY dye structure.

Arguably, the major advantage of BODIPY dyes is their extremely high spectral tunability and structure diversification. For example, fluorescein or rhodamine dyes have also sharp fluorescence bands similar to BODIPYs, but derivatization of their core in order to shift absorption and emission either hypsochromically or bathochromically is often very challenging. The facile and flexible functionalization of BODIPY core is unique in comparison to any other type of dyes.<sup>57</sup> To demonstrate this fact, it is worth to analyze the group of BODIPY dyes called Keio Fluors that were designed to overcome some drawbacks of BODIPY dyes such as decreased quantum yield and absorption coefficient upon extension of  $\pi$ -conjugation by introduction of aryl in  $\alpha$ - positions of BODIPY core. These heteroaryl fused BODIPYs (Figure 5) possess sharp emission spectra, high quantum yields and molar extinction coefficients over a wide spectral range. Introduction of one furane ring in tetramethyl-BODIPY (TM-BDP) resulted in significant bathochromic shift to observe yellow light emitting dye KFL-11 with  $\lambda_{em} = 549$  nm. Additional furane ring (KFL-1) caused shift to  $\lambda_{em} = 583$  nm and further modification with one or two phenyl rings (KFL-12 and KFL-5) increased emission wavelength to 620 nm or 661 nm, respectively.<sup>58</sup>

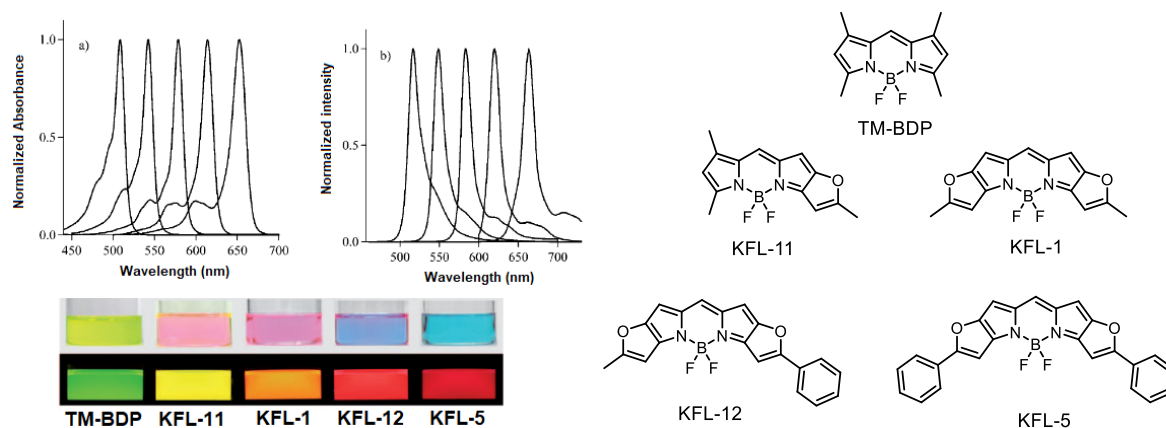
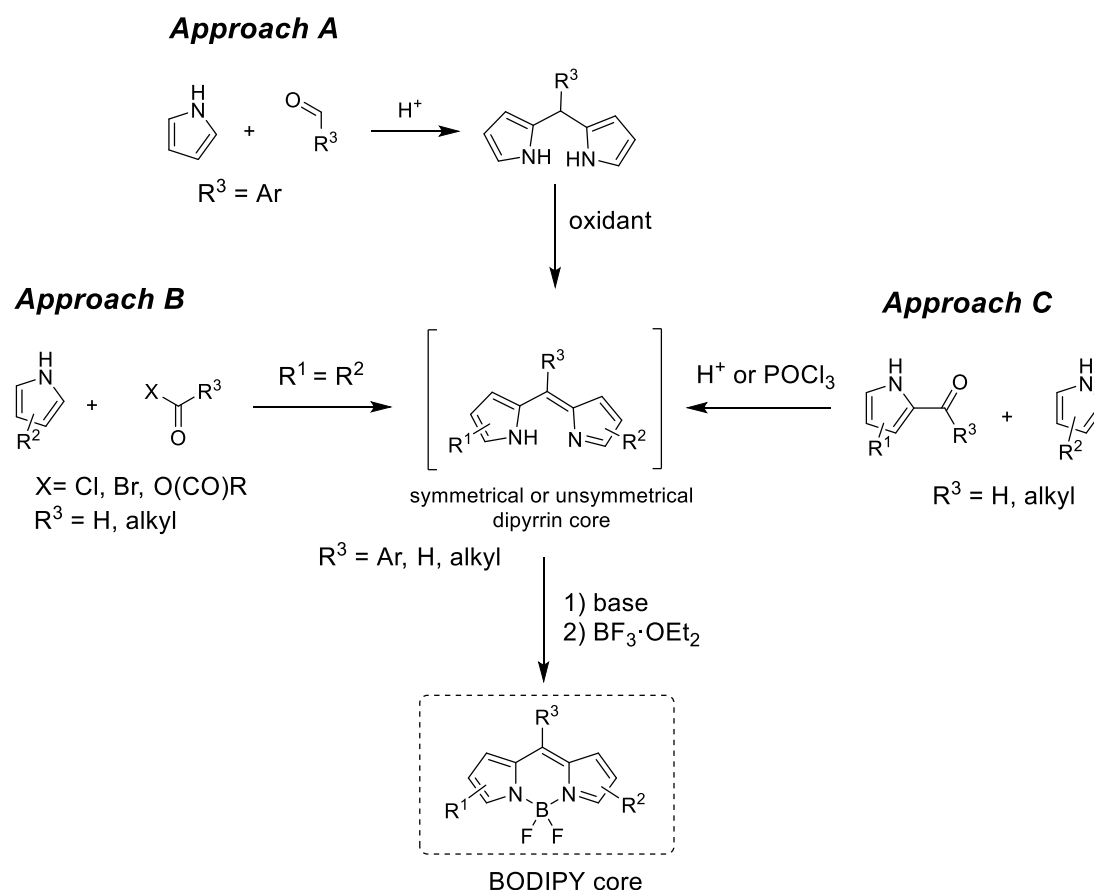


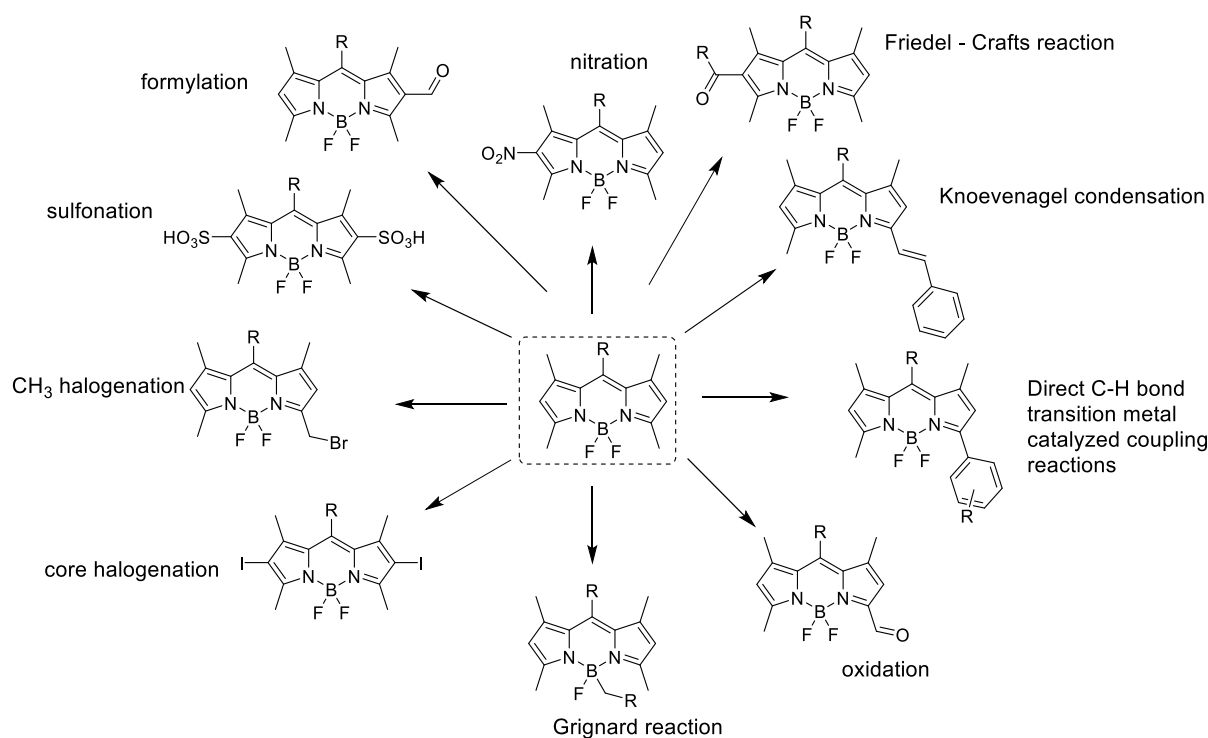
**Figure 5** Example of spectral modification of BODIPY dyes - Keio Fluors.<sup>58</sup>

As mentioned above, synthesis of BODIPYs offer many variations that could be characterized generally in two groups: pre- and post-functionalization.<sup>57</sup> As the synthesis is generally based on reaction of aldehyde and pyrrole the core of BODIPY may be pre-functionalized by introduction of range of substituents either on pyrrole or aldehyde moiety (Scheme 2). The first step of the BODIPY synthesis thus begins with the formation of corresponding dipyrromethene usually under acid-catalyzed reaction conditions. Two possible approaches to obtain dipyrromethane involve reaction of 2-unsubstituted pyrrole with aromatic aldehyde (Approach A), reaction of 2-unsubstituted pyrrole with activated carbonyl (Approach B) or acid-catalyzed condensation of 2-acylpyrrole or 2-formylpyrrole with 2-unsubstituted pyrrole (Approach C). In the first approach the resulting dipyrromethane is firstly oxidized to dipyrromethene with DDQ or chloranil A and subsequently complex with  $\text{BF}_3 \cdot \text{OEt}_2$  under basic conditions is formed to obtain desired boron dipyrin dye. Approach B and C yields the dipyrinium salt in the first step and further deprotonation and fluoroboration leads to BODIPY dye. In contrast with Approach A, the substituent that ends up in meso position is not limited only to aryls thus a broader scope of dyes may be prepared this way.



**Scheme 2** Synthetic approaches towards BODIPY dyes.

Post-modification of BODIPY dyes concisely summarized in Scheme 3 is crucial for development and preparation of larger range of BODIPYs with different properties or systems with moieties that would be hard to construct by other means. Wide scope of reactions may be applied to functionalize BODIPY core.<sup>57</sup> For instance, 1-3 and 5-7 carbons bear the most positive charge thus nucleophilic substitution reaction may be applied involving soft nucleophiles<sup>59</sup>, Pd-catalyzed reaction are also popular for introduction of  $\alpha$ -aryl substitution<sup>60</sup>. On contrary, positions C-2 and C-6 are characterized by aromatic electrophilic substitution reactions  $\text{S}_{\text{E}}\text{Ar}$  such as halogenation<sup>61</sup>, sulfonation<sup>62</sup>, formylation<sup>63</sup> or Friedel-Crafts acylation<sup>64</sup> and Pd-catalyzed cross-coupling reactions. Methyl groups located at 1,3,5 and C-7 are relatively acidic allowing for Knoevenagel condensation reaction with aromatic aldehydes which is popular way to enlarge  $\pi$ -conjugation and shift absorption to higher wavelengths.<sup>65</sup> Meso, or C-8 position may be derivatized when starting from suitably substituted pyrroles and benzaldehydes, but may be accessed also using post-functionalization strategy from 8-methyl, 8-methylsulfanyl or 8-halogenated BODIPYs<sup>66</sup>.



**Scheme 3** Post-modification approaches of tetramethyl BODIPY.

### 1.2.2 BODIPY fluorescent probes

The proper selection of the fluorophore is mandatory with respect to any biological application. Ideal fluorophore must meet some requirements such as good penetration through cell membrane, limited non-specific binding, NIR fluorescence for deeper tissue penetration of the light, prevention from background interference caused by tissue autofluorescence and higher in vivo spatial resolution. Negatively charged dyes, such as fluorescein often suffer from low cell permeability. On the other hand, positively charged rhodamine easily penetrates into the cells but often shows non-specific binding to proteins or lipids and is prone to localize in the mitochondria.<sup>67</sup> Cyanines, having NIR absorption, penetrate well into the cells, however their drawback is typically lower photostability<sup>68</sup>. At this point BODIPY offers as an ideal choice for bioimaging thanks to its already mentioned properties – high photostability, neutral charge or high quantum yield<sup>55</sup>. Although, its hydrophobicity is often problematic and may cause drastic drop in e.g., quantum yield, the versatility of functionalization might overcome these challenges too. BODIPYs are used for imaging of the target proteins, membranes, organelles, antibodies, enzymes, as chemosensors for detection of metals, gases, ROSs, thiols, as pH and hypoxia indicators<sup>69</sup> or as agents in fluorescence guided drug delivery and precision therapy<sup>70</sup>. Generally, the principle of such fluorescent probes is quite straightforward - attachment of microenvironment responsive moiety – linker, chelator or protein to fluorescent

dye. Moreover, PeT or FRET effects are often applied to control fluorescent properties resulting in activatable fluorescent probes.

### 1.2.2.1 Membrane and organelle staining

BODIPY dyes with suitable scaffold modification and low cytotoxicity are valuable tools for specific imaging of cell organelles. BODIPYs for colocalization of lysosomes<sup>71</sup>, ER<sup>72</sup>, Golgi apparatus or mitochondria<sup>73</sup> have been developed and are sold under their trademark (LysoTracker Green DND-26, ER-Tracker Red, Figure 6). Some reports indicate that efficient targeting for particular organelle is achieved by introduction of corresponding targeting hydrophilic moiety (e.g. mitochondria – phosphonium, pyridinium salts and quarternary amines, membranes – fatty acids, lysosomes – tertiary amines).<sup>54</sup>

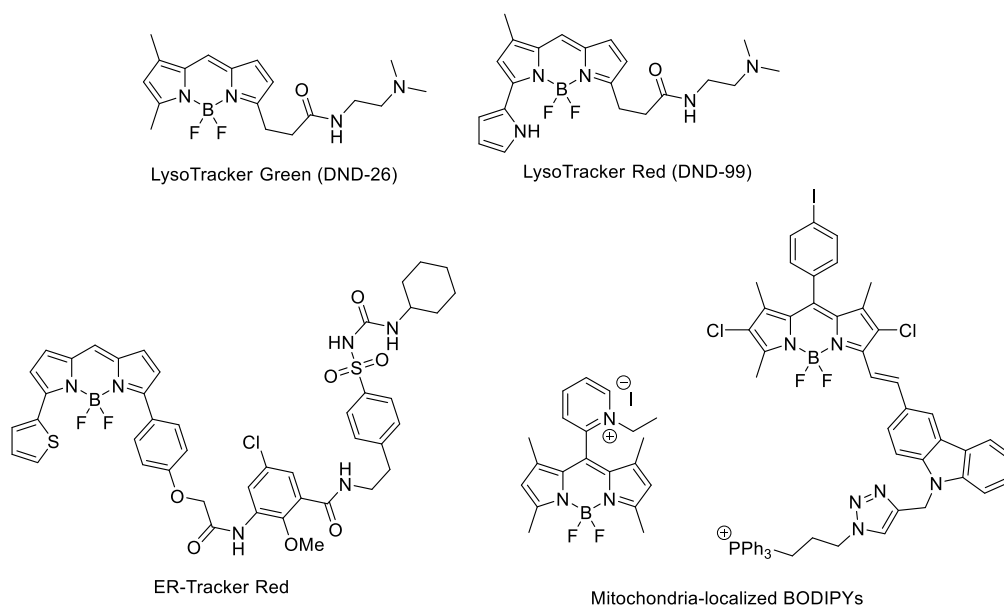


**Figure 6** BODIPY dyes used in cell organelles staining.

### 1.2.2.2 Enzymatically activatable probes

Enzymatically activatable probes represent interesting approach towards targeting and detection of various enzymes such as proteases cathepsins<sup>74</sup>,  $\beta$ -lactamases<sup>75</sup>, nitro-reductases<sup>76</sup> or oxidases and have been rapidly developing in the past decades.<sup>77</sup> Usually quenching by PeT effect, nitroaryl (Figure 7, left probe) and diazo motifs or FRET to another dye (Figure 7, right probe) is employed in order to facilitate the activation of fluorescent response (turn “ON”) after the enzymatic reaction (reduction of nitro group, resp. cleavage of cathepsin specific linker). By eradication of levels of some enzymes typically overexpressed in tumors it may provide valuable insight into detection of cancer biomarkers and diagnosis thanks to its non-invasive character.

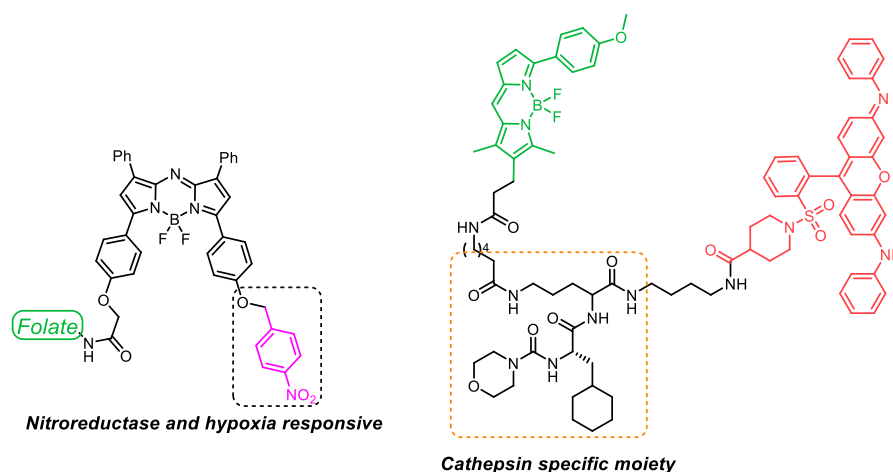


**Figure 7** Examples of enzymatically activatable BODIPY probes.

Recently, very interesting approach towards activatable and tunable BODIPY-based NIR fluorescent probes for *in vitro* and *in vivo* optical imaging of certain enzymes in cancer cells was developed by Zhao (Figure 8). NIR fluorescence response ensures less autofluorescence response, lower tissue absorption and higher penetration of light through tissues. Compared to other NIR fluorescent probes, these probes offer larger Stokes shifts that avoids usually non-desirable cross-talk between excitation and emission spectra that significantly worsens detection and accurate imaging. They employed BODIPY platform connected with various enzyme substrates (NTR - nitroreductase, NQO - NAD(P)H:quinone acceptor oxidoreductase, ALP - alkaline phosphatase) via self-immolative thioether linker (Figure 8). This unit serves as a trigger that after enzymatic reaction activates BODIPY dye towards fluorescence (turn „ON“).<sup>78</sup>

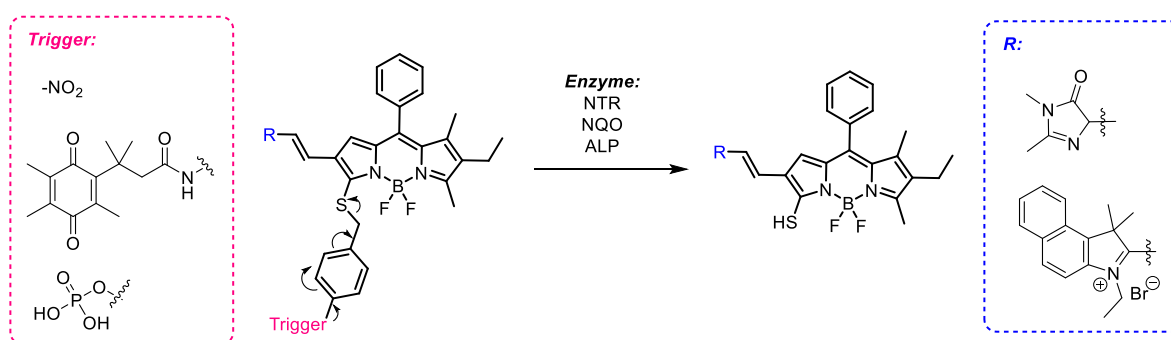


**Figure 8** Enzymatically activatable and tunable NIR-BODIPY probe. NTR - nitroreductase, NQO - NAD(P)H:quinone acceptor oxidoreductase, ALP - Alkaline phosphatase.

## 1.2.2.3 pH sensors

Introduction of pH sensitive moiety such as dialkylamine or aniline on specific position of BODIPY core results in pH responsive probes (Figure 9).<sup>79</sup> Photoinduced electron transfer (PeT) is usually employed in quenching of the fluorescence in the way that the energy gap between orbitals in non-protonated species facilitates electron transfer and thus blocks fluorescence. Protonation then leads to energy gap widening and cancellation of PeT what subsequently triggers the fluorescence (Figure 9). In this fashion pH changes may be visualized in biological organelles e.g., lysosomes or endosomes that possess pH around 4.7 and 5.5-6.3, respectively. As the pKa of fluorescent probes depends on substitution at amino or aniline moiety it may be fine-tuned to access particular target.

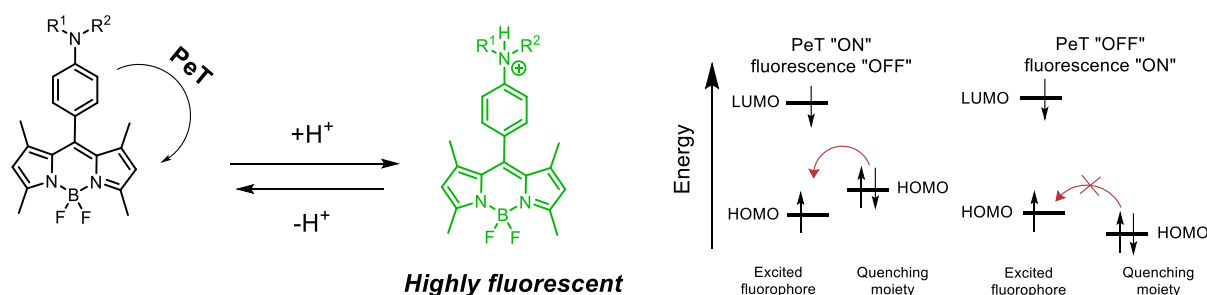


**Figure 9** pH-dependent OFF-ON switching of BODIPY.

Tunability of BODIPY pH responsive probes may be demonstrated by the work of Overkleeft et al.<sup>80</sup> who prepared various BODIPY based pH-dependent dyes by introduction of various substituents in meso position of BODIPY core such as dimethyl, diethyl or piperidinyl. Synthesized probes differed in pKa's and ranged from 2 to 4 as Figure 10 shows.

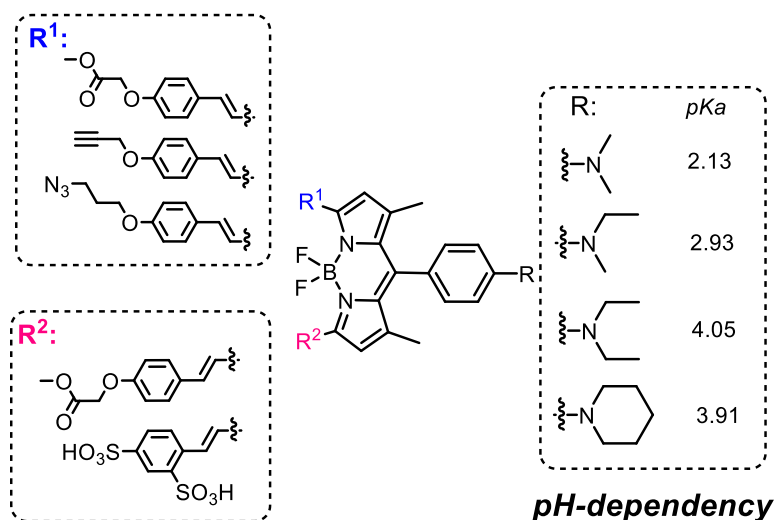


**Figure 10** Tunable pH-activatable BODIPY dyes.

Interesting approach was applied by Kikuchi et al.<sup>81</sup> to image bone-resorbing osteoclasts in live mice. Since osteoclasts create acidic environment during bone resorption administration of BODIPY modified with bisphosphonate group resulted in intense fluorescent signal between osteoclasts and bone tissues (Figure 11).

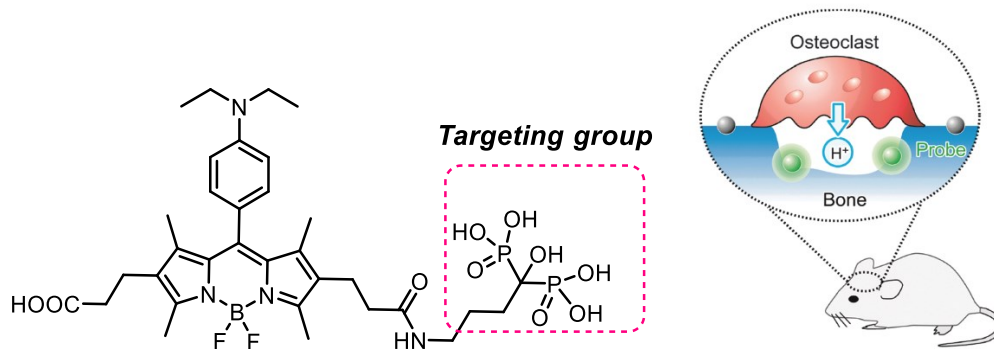


**Figure 11** pH dependent in vivo imaging of osteoclasts.

#### 1.2.2.4 Detection of thiols

Intracellular thiols e.g., glutathione, homocysteine or cysteine have plenty of functions in living organism from maintenance of higher-order structure of proteins to prevention of important cellular components from reactive oxygen species. Their detection is generally based on their nucleophilicity. 2,4-Dinitrobenzylsulfonyl (DNBS) group is popular for its reactivity towards nucleophilic thiols and effective quenching of fluorescence due to the presence of nitro groups. Several BODIPY systems based on DNBS group were synthesized utilizing “OFF-ON”<sup>82</sup> and FRET<sup>83</sup> approach (Figure 12). Compounds showed significant increase of fluorescence response upon reaction with thioglycolic acid and glutathione.

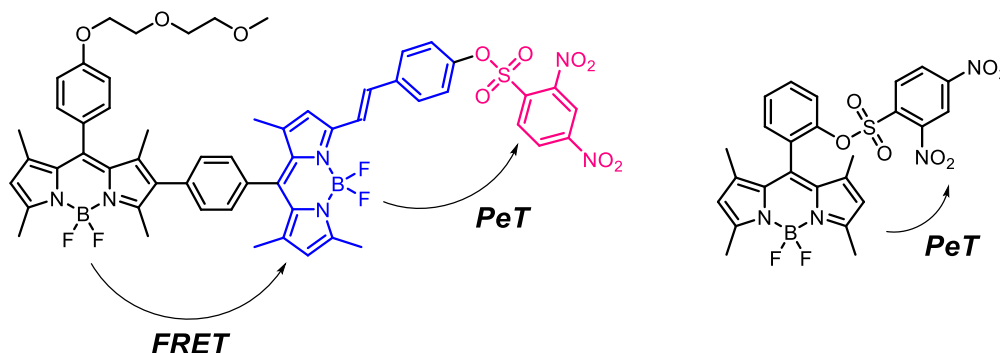
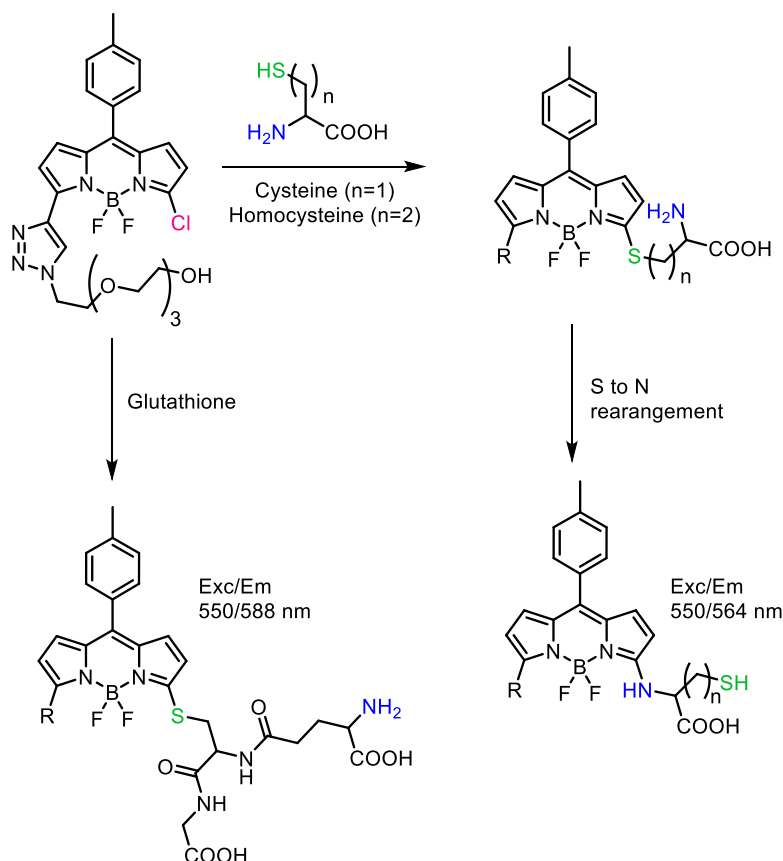


**Figure 12** Thiol sensitive probes with DNBS group.



Ratiometric system for discrimination of glutathione from cysteine and homocysteine was developed by Yang et.al.<sup>84</sup> As monochlorinated BODIPY reacts with thiols to form thioethers the wavelength of emitted light is changing (Scheme 4). In case of reaction with Cys or hCys the S-to-N rearrangement occurs and the yellow emission at 564 nm is increasing. However, glutathione does not provide such reaction due to missing adjacent amino group and the emission of BODIPY thioether at 588nm appears. The sensor was used for detection of GSH in living cells.

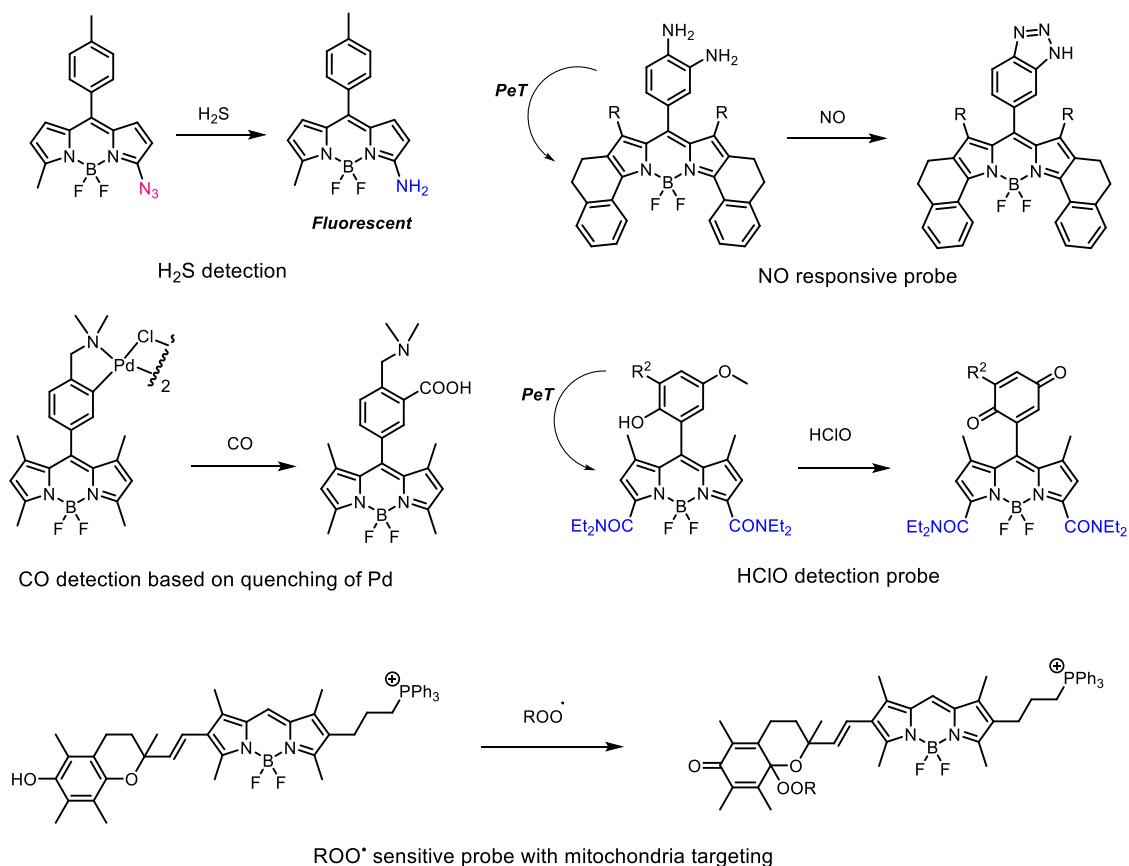


**Scheme 4** Discrimination between thiols – glutathione and cysteine/homocysteine.<sup>84</sup>

#### 1.2.2.5 Sensors for gases, ROS and RNS

Scheme 5 shows the summary of some gas molecules – H<sub>2</sub>S<sup>85</sup>, NO<sup>86</sup>, CO<sup>87</sup> sensors as well as example probes used for detection of ROS and RNS species such as hypochlorous acid<sup>88</sup>, peroxy-radical ROO<sup>•</sup><sup>89</sup> or peroxyxynitrite<sup>90</sup> ONOO<sup>-</sup>. Incorporation of quenching moiety such as DNB or azide group for H<sub>2</sub>S detection, o-phenylenediamine for NO detection and palladium complexes in case of CO recognition are applied. Since these gaseous molecules are endogenously produced in living cells their levels can be studied in e.g. lung tissue inflammation, presence of tumor<sup>91</sup> or gives information about real-time spatial and temporal abundance of CO in live cells. Targeting ROS/RNS provides information about e.g.

intracellular signaling, regulation of gene expression and host defense from microbial infection where ROS/RNS are usually involved.<sup>92</sup>



**Scheme 5** BODIPY-based sensors for gases – NO, CO, H<sub>2</sub>S and ROS.

### 1.3 Targeting cancer cells

Traditional cancer chemotherapy uses most typically small-molecule agents that disrupt normal functioning of a cell by inhibiting replication or causing apoptosis. It is mostly based on preferential killing of rapidly proliferating cancer cells and usually does not discriminate other rapidly proliferating cells in the body including hair, intestinal epithelial cells or bone marrow cells.<sup>93</sup> The most broadly used agents in the treatment of various cancer and probably the most effective chemotherapeutics available such as daunorubicin, doxorubicin, paclitaxel or cisplatin cannot distinguish cancer cells from normal cells what leads to undesirable severe side effects of systemic toxicity – nausea, fatigue, cardiotoxicity or liver damage. Moreover, in order to efficiently eradicate the tumor, higher doses of chemotherapeutic agents are required because of non-specific accumulation in the body what may subsequently lead to patient's lower ability to tolerate the medication and increased risk of systemic failure.<sup>94</sup>

Therefore, it is suggesting that the use of targeting techniques represents logical, smart and more effective way to deliver the therapeutic agents selectively to the place of action. In addition, targeted delivery of therapeutic agents may overcome some difficulties generally connected with conventional free anticancer drugs including insolubility in aqueous medium, rapid clearance from body, low bioavailability and most of all lack of selectivity.<sup>95</sup> The most prominent and recently thoroughly studied strategies for cancer targeting involve (i) passive targeting by enhanced permeability and retention (EPR) effect mainly applicable for nanoparticles (NPs)<sup>96</sup>, (ii) active targeting by incorporation of targeting moiety to cargoes such as peptides, antibodies, aptamers or small-molecule ligands<sup>97</sup>, (iii) introduction of the cell penetrating peptides (CPPs)<sup>98</sup> or (iv) conjugation of drugs with delivery vehicles via cleavable linkers responsive to tumor microenvironment (glutathione, pH, hypoxia or temperature)<sup>99</sup>.

### 1.3.1 Passive targeting

To clearly introduce the passive targeting mechanism of molecules to tumors it is suitable first to describe briefly the generalized tumor physiology. Once a single cell undergoes mutation and blocks apoptotic signaling pathway it starts to divide in uncontrollable fashion.<sup>100</sup> During the first stage when the size of tumor is lower than 2 mm<sup>3</sup> it relies solely on diffusion to obtain nutrients necessary for its growth. In order to overcome diffusion-limited size the tumor undergoes the process called angiogenesis in which it recruits new blood vessels and start to build unorganized and aberrant vasculature.<sup>101</sup> This results in heterogenous blood flow, leaky membranes and incomplete endothelial linings causing higher permeability of tumors. Moreover, due to poorly defined lymphatic system caused by fast proliferation of cells macromolecules (<50kDa) accumulate and retain in tumors for longer time. These features together with presence of vascular endothelial growth factor (VEGF) which increases permeability of blood vessels, basic fibroblast growth factor (bFGF) and nitric oxide result in enhanced permeability and retention effect (EPR) (Figure 13).<sup>102</sup>

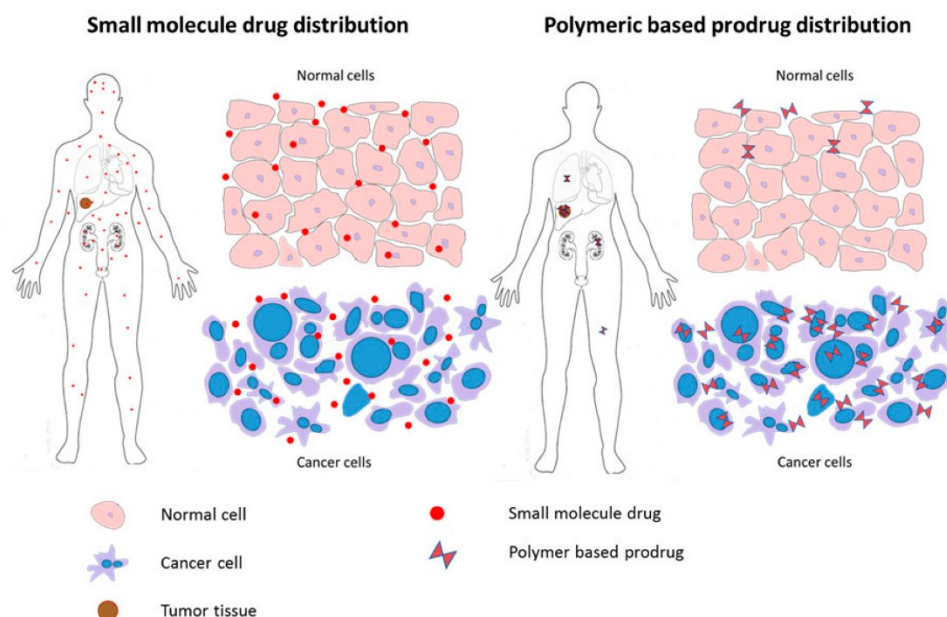


**Figure 13** EPR effect.

The permeability of the vasculature and retention by an insufficient lymphatic system can passively accumulate macromolecules or polymers and increase their tumor concentration by 70-fold<sup>103</sup>. The ideal size of polymeric NPs was determined to be 10-150 nm as molecules smaller than 10 nm are subject for first renal pass filtration and thus have significantly lower circulation time in the body and bigger molecules are cleared by mechanisms involving reticuloendothelial system (RES) and mononuclear phagocytic system (MPS).

Efficiency of passive targeting can be modulated by the size, shape, and surface characteristics of the nanoparticle drug carriers.<sup>94</sup> However, passive targeting suffers from several limitations similarly as traditional chemotherapeutics - mainly the inability of active distinguishing between healthy and cancer cells. Additionally, it is not feasible in all tumors due to varying degree of vascularization and porosity in different tumor types and may lead to uneven distribution and thus lowered efficiency.<sup>104</sup>

### 1.3.2 Active targeting

The drawbacks of passive targeting and classical small-molecule drugs may be overcome by introduction of affinity targeting moiety that actively binds to specific receptor located on the cancer cell surface. Various actively targeting moieties that can promote selective binding to specific receptors on cancer cells have been discovered so far (Figure 14). Ranging from short peptide sequences – cell targeting peptides (CTPs), small molecule ligands or vitamins<sup>105</sup>, to bigger and more complex moieties such as antibodies and aptamers.<sup>106</sup> This

chapter will mainly focus on peptides and some small molecule targeting units since other systems are far beyond the scope of our research and purpose of this work.

Cancer cells overexpress plentiful of tumor-specific receptors that can be used for targeted delivery of active chemotherapeutics such as folic acid receptor, transferrin (TfR) receptor, epidermal growth receptor (EGFR), somatostatin, bombesin, lectins, hyaluronic acid receptor, integrins etc.<sup>107</sup> Suitable, specific and actively targeting drug delivery systems (DDS) must preferentially bind to the target receptor overexpressed by tumor cells and the target receptor must be homogeneously expressed on surface of all target cells. For targeted tumor delivery it is also necessary that resulting conjugate is non-toxic to healthy cells and accumulates preferentially in tumor tissues, where it liberates the active form of the drug.<sup>108,109</sup>

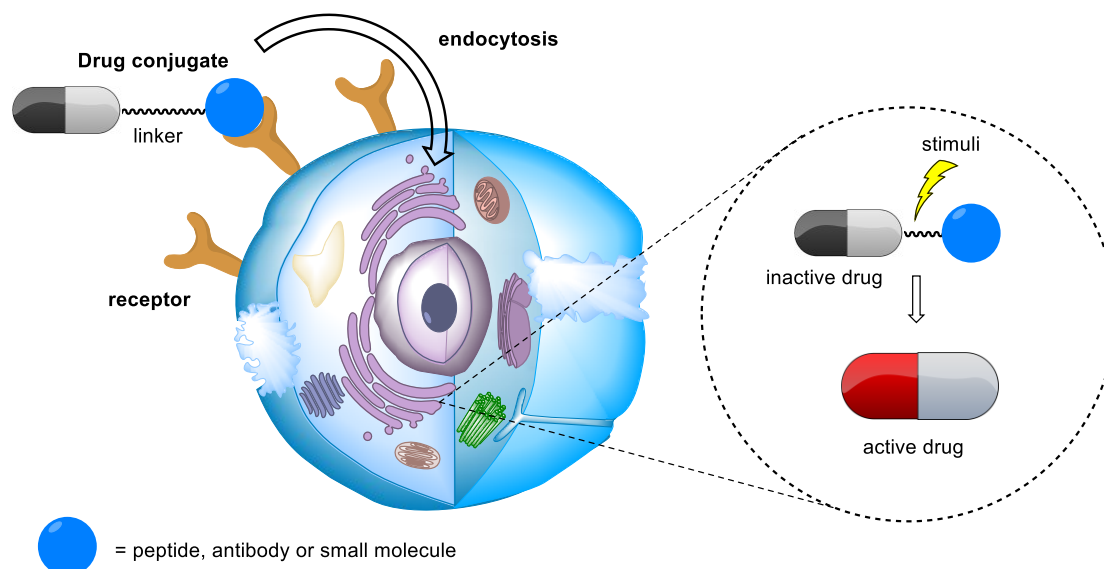


**Figure 14** Active targeting.

### 1.3.2.1 Cell-targeting peptides

With the discovery of targeting ability of some peptides in the last decades they have become an attractive option for specific targeting of various cancers and cancer imaging due to their small size, low immunogenicity and ease of synthesis.<sup>110</sup> Moreover, they are much less expensive than development of antibodies and easier to screen against potential ligands using combinatorial phage display. This way numerous peptides with specificity to various targets were discovered (Table 4). Among them, peptides with RGD structural motif were extensively studied as they demonstrated strong affinity against integrin receptor family.<sup>111</sup>

Peptide	Drug	Type	Target	Status
Tyr3-octreotide	Lutetium-177	peptide-radioisotope	Somatostatin receptor	Phase I/II
Bombesin	Docetaxel	DTX loaded NPs	Bombesin receptor	- <sup>112</sup>
PEN-221	DM1	peptide-drug conjugate	Somatostatin receptor	Phase I/IIa
Angiopep-1	paclitaxel	peptide-drug conjugate	LRP-1 expressing in glioma cells	Phase II
cRGD	P53 gene	peptide-conjugated adenovirus	Recurrent glioblastoma	Phase I
BT-1718	DM1	peptide-drug conjugate	Metalloproteinase MT1-MMP in solid tumors	Phase I
iRGD	Gemcitabine and paclitaxel	peptide-drug conjugate	Pancreatic cancer	Phase I
NGR	Daunorubicin	peptide-drug conjugate	Amino-peptidase N	- <sup>113</sup>

**Table 4** Targeted peptide-drug systems.<sup>114</sup>

Integrins are a family of cell adhesion receptors that are involved in tumor-induced angiogenesis, vascularization and metastasis. Integrin  $\alpha_v\beta_3$  is highly expressed on activated endothelial cells and new-born vessels, but is absent in resting endothelial cells and most normal organ systems, making it a suitable target for anti-angiogenic cancer therapy.<sup>115</sup> In 1984, peptides with minimal sequence consisting of linear arginine-glycine-aspartic acid (RGD) were firstly described for its high affinity recognition integrins.<sup>116</sup> However, RGD triple peptide as well as other peptide based cell targeting peptides (CTPs) has limited *in vivo* use due to its short circulation half-life. Further chemical modification including conformational restriction by ring closure or use of D-amino acids resulted not only in higher stability and bioavailability but also in higher binding affinity.<sup>117</sup> Cilengitide, a cyclic pentapeptide c(RGDf[NMe]V) has become the most advanced integrin binding ligand in clinical development and reached Phase III for treatment of several types of glioblastoma progressive tumors (Figure 15).<sup>118</sup>

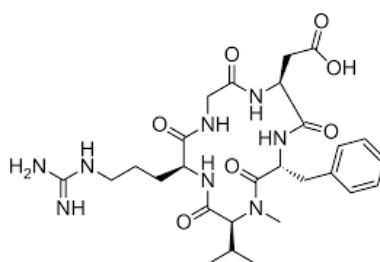


**Figure 15** Cilengitide – cRGD peptide-based drug.

Currently, several peptide-targeted systems are undergoing various phases of clinical trials. **ANG1005**, paclitaxel conjugate with angiopep-2 targeting peptide designed to treat brain tumors has completed Phase II clinical trials. It acts through selective binding to low-density-lipoprotein receptor (LRP-1) which is upregulated in some types of cancer and thus enhances delivery of paclitaxel approximately 70-times to brain compartments compared to free PTX (Figure 16).<sup>114</sup> **PEN-221**, is maytansinoid (DM-1) drug conjugate with peptide ligand highly selective in targeting somatostatin receptor 2 (SSTR 2) connected through disulfide cleavable linker. SSTR2 is typically overexpressed on the cell surface of neuroendocrine tumors, small cell lung cancers (SCLC) and metastatic prostate cancers. PEN-221 is currently under Phase II clinical trials (Figure 16).

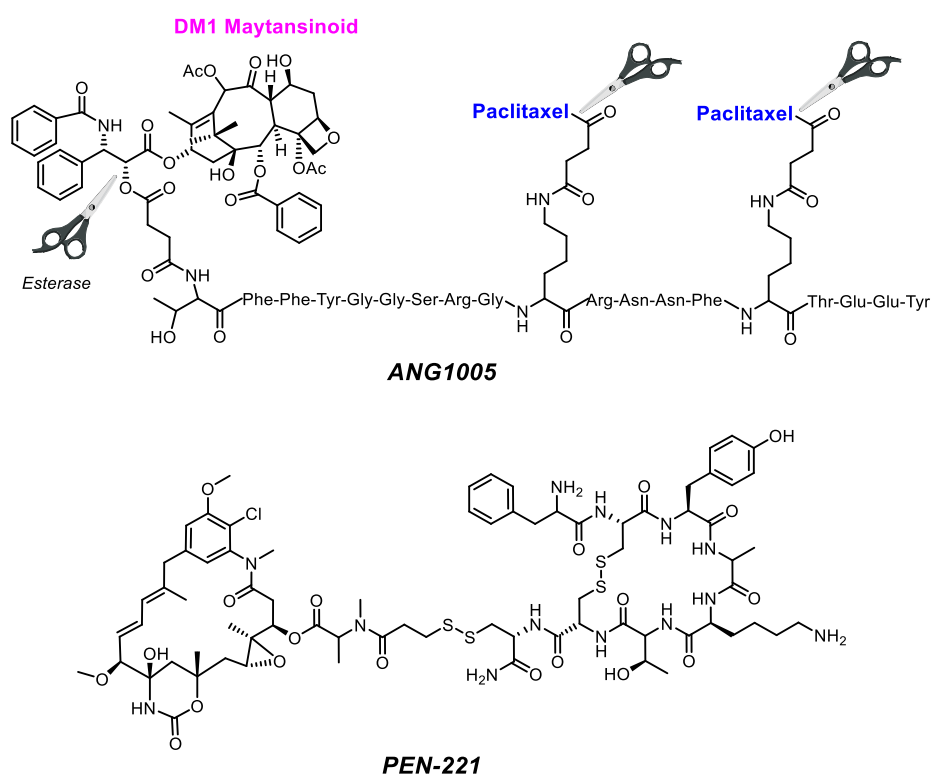


**Figure 16** Examples of cell targeting peptide - drug conjugates.

#### 1.3.2.2 Small molecule targeting vs antibodies

Active targeting with monoclonal antibodies (mAbs) is currently far more common in clinical practice (Figure 17) than targeting with small molecules that are relatively minor group with only few ligands showing suitable properties.<sup>105</sup> Although, mAbs are widely used they have serious limitations such as low penetration into solid tumors due to its size, and moreover slow clearance from the body resulting in high exposure to normal tissues. mAbs can also induce immunogenic reaction in the body even though they are humanized and may cause

hypersensitivity and low efficiency. On the other hand, small molecules offer fast penetration, accumulation and saturation ability together with rapid clearance and thus shorter exposure to normal cells. Furthermore, they are non-immunogenic, chemically modifiable, cheaper than mAbs and have superior shelf lives. However, application of many commonly used small molecules is limited since not all tumor types overexpress receptors on their surface in sufficient amount and some ligands possess lower than suitable affinity.<sup>105</sup>

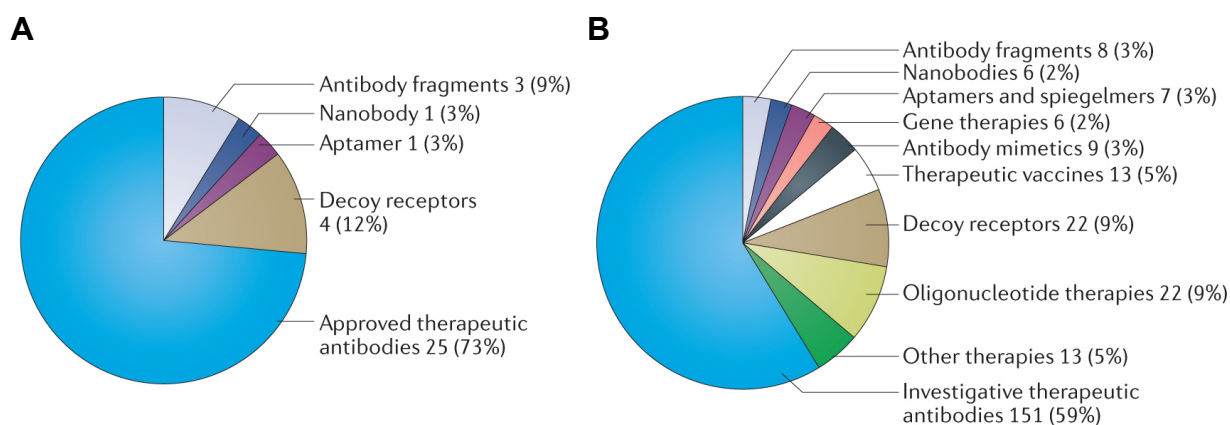


**Figure 17** (A) Proportion of FDA approved therapies and (B) investigative clinical therapies.<sup>120</sup>

Among the most used small molecule targeting ligands such as prostate-specific membrane antigen (PSMA) and vitamins – folic acid, biotin, riboflavin or B12 (Figure 18) play the most significant role because of simple reason – cancer cells need higher amount of vitamins than normal cells to sustain their rapid growth.<sup>121</sup>

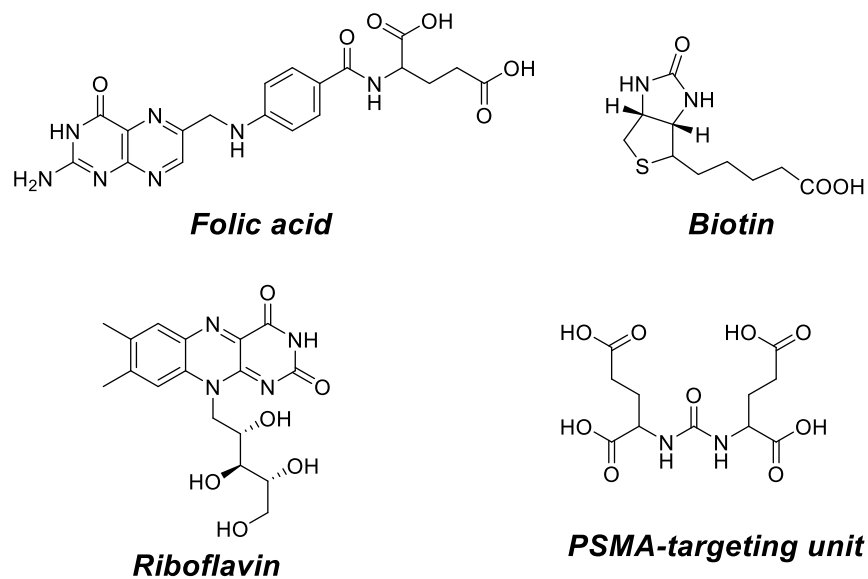


**Figure 18** Small-molecule targeting ligands.



Biotin, or the vitamin B7 is an essential growth promoter at cellular level and acts as a co-enzyme for carboxylase enzymes in the synthesis of fatty acids, amino acids and participates in gluconeogenesis.<sup>122</sup> Biotin binding site in avidin is characterized by a very high affinity to biotin ( $K_D \sim 10^{-15}$  M), the strongest known among the naturally occurring, non-covalent, protein-ligand interactions.<sup>122</sup> Biotin uptake proceeds in two ways – through high-affinity biotin transporter and a sodium-dependent multivitamin transporter (SMVT) with latter being responsible for biotin uptake in cancer cells. Enhanced uptake of biotin was observed in many cancer cell-lines e.g., leukemia, ovarian, colon, mastocytoma, lung, renal, and breast cancer cell lines.<sup>105</sup>

Numerous conjugates with biotin targeting unit were prepared and tested for interactions with cancer cells and further for uses in cancer imaging and diagnostics. However, no biotin targeted compounds have reached clinical trials, yet.

Ojima et al. synthesized tumor targeted biotinylated dual warhead conjugates consisting of taxoid maytansinoid and camptothecin as active drugs connected via cleavable disulfide linker (Figure 19). These compounds exhibited significantly higher accumulation and activity against biotin receptor positive cells ( $IC_{50} = 3.22-9.80$  nM) while the toxicity against normal lung fibroblast cells WI38 was two orders higher - 705 nM.<sup>123</sup>

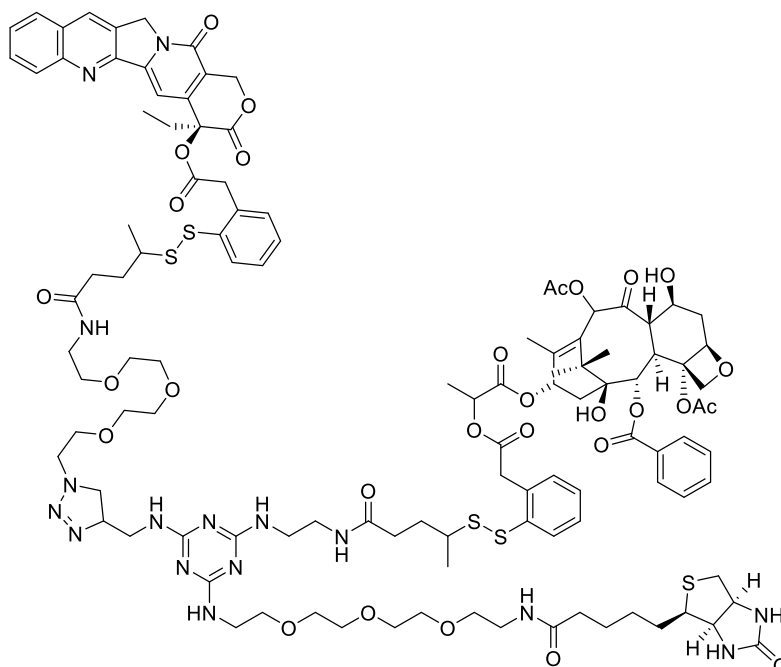


**Figure 19** Biotin targeted CPT-taxol dual warhead conjugate.<sup>123</sup>

## 1.4 Cell-penetrating peptides

Generally, cell-penetrating peptides (CPPs) are usually short oligopeptides consisting of 5-30 amino acids that enhance the cellular uptake of various cargoes that do not penetrate easily or possess poor water-solubility. They are chemically and structurally highly variable compounds with one common feature which is energy-independent membrane penetration. Its main drawbacks are lack of cell-type selectivity, impossibility of oral administration, short duration of action due to enzymatic degradation and renal clearance. CPPs are the most exploited cargos for efficient intracellular delivery of nucleic acids, proteins, anticancer agents or small molecules. Many of these conjugates have entered clinical trials.<sup>98,124-126</sup>

Appropriately designed CPPs directly transport cargoes to cell organelles through recognition of specific localization sequences inside the cell.<sup>127</sup> Although the exact mechanism of CPPs internalization is still argued the most recent works point to mainly endocytosis-mediated uptake<sup>128</sup>. Generally, CPPs can be divided into three groups according to their net charge as cationic, amphipathic and hydrophobic. Cationic CPPs usually contain more than five arginine or lysine units and show excellent affinity to the cell membrane thanks to the presence of negatively charged glycoproteins.<sup>98</sup> The first CPP discovered was cationic and was derived from the HIV-1 protein Tat RKKRRQRRRA (Table 5).<sup>124</sup> Special case of cationic CPPs are nuclear localization sequences (NLSs) derived from minimal sequence of PKKKRKV originated from simian virus 40. These peptides are able to deliver cargoes to the cell nucleus using specific nuclear transportation processes.<sup>127</sup> Amphipathic CPPs consist usually of arginine/lysine rich part, such as PKKKRKV NLS with covalently bound hydrophobic domain for more effective cell uptake. They account for the most used CPPs. On the other hand, hydrophobic CPPs represent the smallest group with only few examples shown in .

Peptide	Sequence	Length	Origin
<i>Cationic CPPs</i>			
TAT	RKKRRQRRR	9	Protein derived
R8	RRRRRRRR	8	Synthetic
Penetratin	RQIKIWFQNRRMKWKK	16	Protein derived
NLS	PKKKRKW	7	Protein derived
<i>Amphipathic CPPs</i>			
pVEC	LLIILRRRIRKQAAHASK	18	Protein derived
Transportan	GWTLNSAGYLLGKINLKALAALAKKIL	27	Protein derived
MAP	KLALKLALKALKAAALKLA	18	Synthetic
<i>Hydrophobic CPPs</i>			
Bip4	VSALK		Protein derived
C105Y	CSIPPEVKFNPFVYLI	16	Protein derived

**Table 5** Classification of CPPs and some examples.

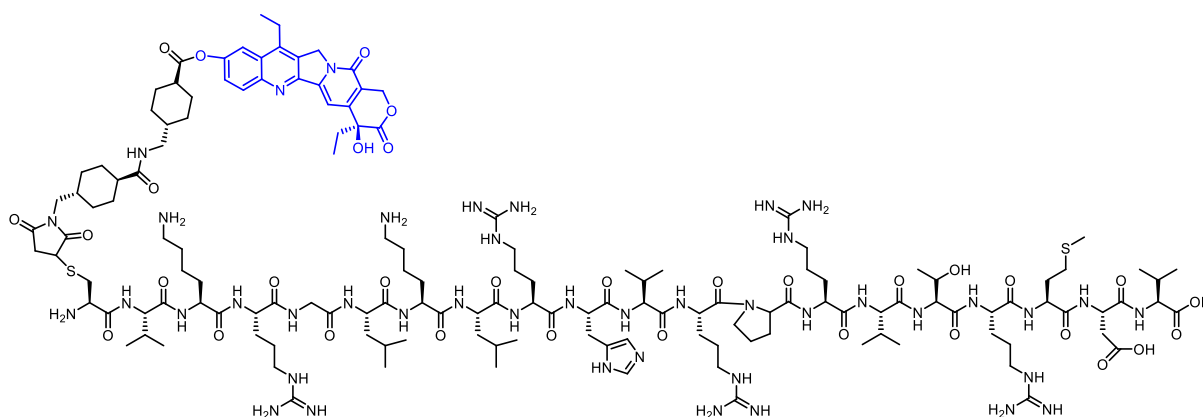


**Figure 20** The DTS-108 conjugate - SN38 drug conjugated with cell-penetrating Vectocell<sup>®</sup> peptide DPV1047.<sup>129</sup>

CPP-drug conjugates show versatile utilization and several of them proceeded into clinical trials for e.g. keloid scarring (AZX100, Phase II), wrinkling skin (RT001, Phase II) or cancer (DTS-108, Phase I, Figure 20).<sup>129</sup> The conjugation of various cytotoxic drugs including Doxorubicin or Taxol to CPPs such as Tat or R8 peptide through disulfide linker resulted in improved aqueous solubility, localized biodistribution, ability to overcome MDR, lengthened pharmacokinetics and significantly lower side effects.<sup>130–132</sup>

## 1.5 Linkers for stimulus responsive targeting

Linkage between a therapeutic drug and moiety such as targeting unit or diagnostic label is of tremendous importance. Non-cleavable linkers are typically preferred when the payload is an imaging agent and such molecule should retain unchanged in order to track the distribution within the cell or tissues, but has no influence on active targeting of the whole molecule. On the other hand, covalently bound therapeutics via cleavable linkers, when designed appropriately contribute to targeting to the desired site and thus reduce off-target adverse effects of cytotoxic drugs. Special attention is paid to drug-carrier linkages (Figure 21) which are responsive to /activated by physiological or biochemical features of the destination site (stimuli responsive linkers)<sup>133</sup> exhibiting abnormalities compared to healthy tissues. Stimuli that may be used for such responsive release are for instance low pH, overexpressed enzymes or proteins, elevated levels of ROS or GSH<sup>134</sup>, hypoxia<sup>135</sup> or higher temperature.<sup>136</sup> For effective delivery, linker must be stable in circulation and rapidly cleavable upon the cell uptake while the released cargo should be free, unmodified therapeutic. Cleavable linkers have been applied in drug conjugation of various antibodies, nanoparticles and small molecule systems.<sup>99</sup>

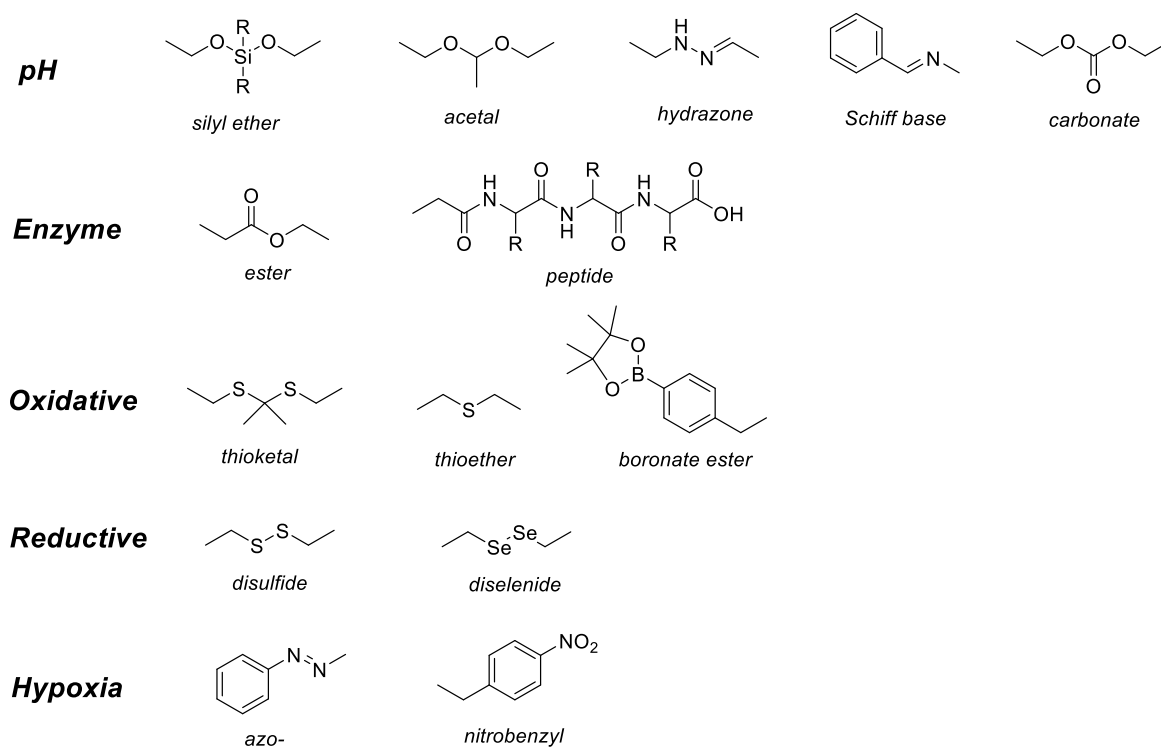
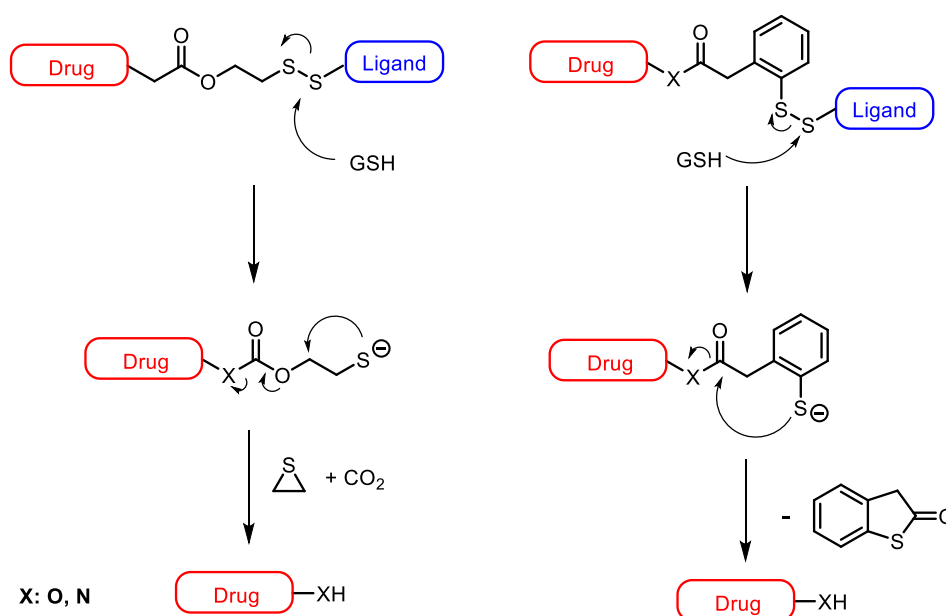


**Figure 21** Linkers for stimulus responsive cleavage.

Reductively cleavable linkers such as disulfide or diselenide linkers offer an attractive concept for targeting cancer cells via glutathione mediated cleavage (Scheme 6).<sup>137</sup> Glutathione is responsible for damage prevention of cells due to the presence of reactive oxygen species

such as free radicals, peroxides etc. and is found in 100-1000 times higher concentration in intracellular compartments than in plasma and blood. Moreover, in some tumor cells GSH is overexpressed and found in concentrations 2-10 mM allowing a cancer targeted delivery with good stability of the conjugates in bloodstream.<sup>138</sup> Disulfide linkers were broadly explored in conjugation to numerous drugs, nanoparticles or mAbs. Drugs containing disulfide linkers such as Vintafolide or Epopolate reached clinical studies. Antibody containing conjugates Gemtuzumab or Mirvetuximab soravtansine were approved by FDA.<sup>134</sup>

Disulfide linker was employed by Zhu et al.<sup>139</sup> who prepared NIR fluorescent activatable prodrug with camptothecin and polyethylene glycol (PEG) - polylactic acid (PLA) loaded nanoparticles (Figure 22). Their platform can be assessed as a **theranostic** – combination of diagnostic tool and therapeutic. In terms of diagnostic properties, treatment with GSH resulted in cleavage of disulfide bond and huge increase of fluorescence intensity occurred (turn ON of the fluorescence). Moreover, they demonstrated that the cytotoxicity of dicyanomethylene-4H-pyran disulfide conjugate with camptothecin (DCM-S-CPT) is effectively quenched by conjugation and proved it by synthesizing the non-cleavable DCM-C-CPT conjugate. This molecule showed significantly lower toxicity *in vitro* (>50uM) and *in vivo* compared to cleavable conjugate DCM-S-CPT.



**Scheme 6** Cleavage of disulfide linker by GSH.

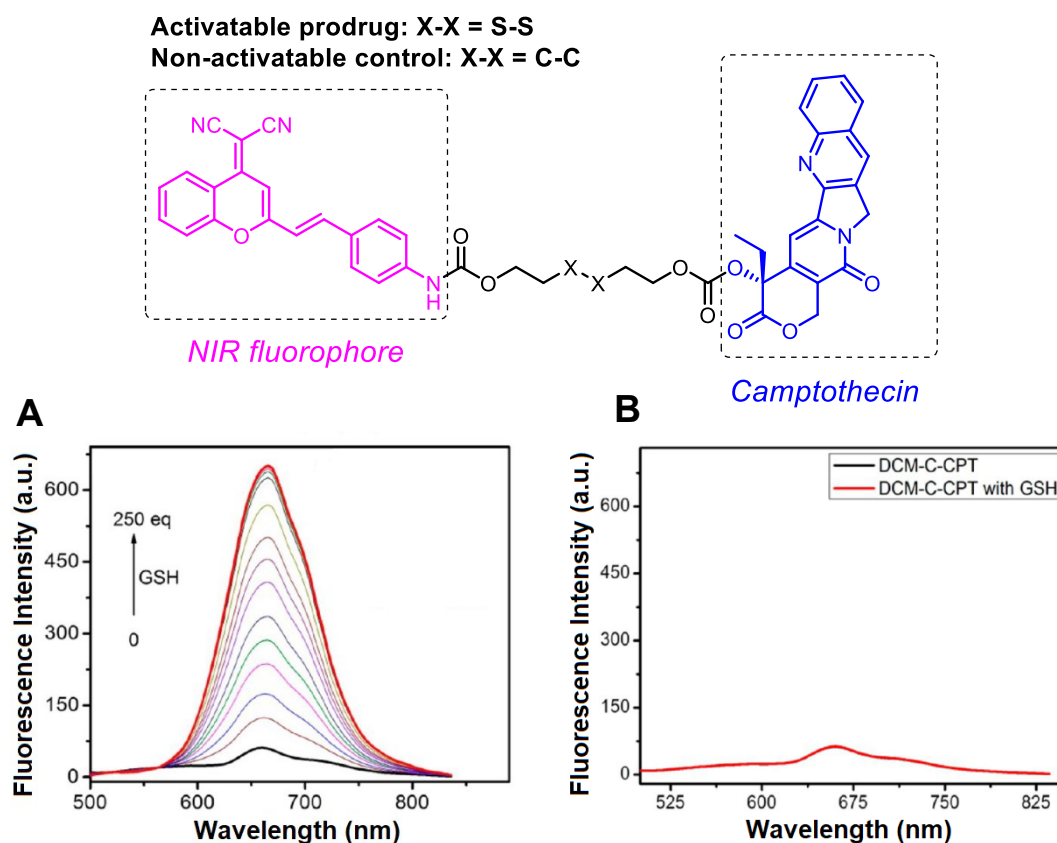
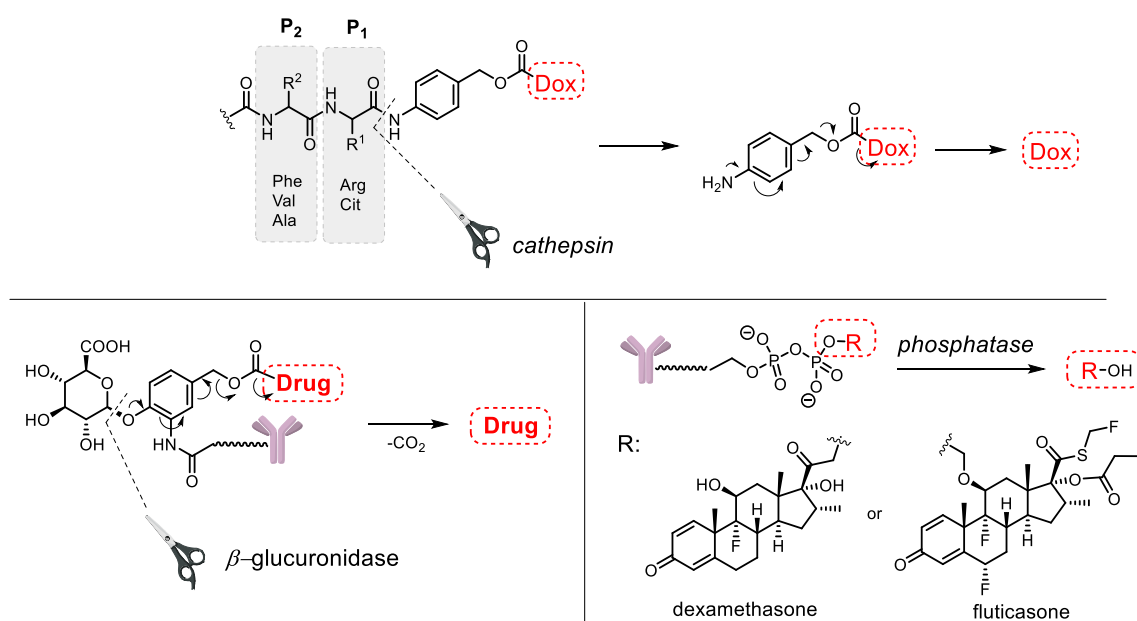


**Figure 22** Activatable disulfide CPT-DCM theranostic prodrug. (A) Change of the fluorescence response of the cleavable DCM-SS-CPT and (B) non-cleavable DCM-C-CPT conjugate in the presence of GSH.<sup>139</sup>

Since many proteolytic enzymes are overexpressed or activated inside the diseased cells (cancer, arthritis, ulcerative colitis etc.) but not in healthy cells they can be also used for selective drug release.<sup>45</sup> Typically, enzymes employed in such way are proteases, cathepsins<sup>140</sup>,  $\beta$ -glucuronidase<sup>141</sup>,  $\beta$ -galactosidase<sup>142</sup>, matrix metalloproteinases (MMPs)<sup>143</sup> or phosphatases (Scheme 7).<sup>144</sup>

Enzymatically cleavable linkers with antibodies produce drug conjugates (ADCs) with improved plasma stability comparable to that of non-cleavable linkers while having more controlled method of drug release. There are numerous ADCs in clinical trials that use enzymatically cleavable linkers, such as dipeptide-based linkers Val-Cit and Phe-Lys. Poly-L-glutamic acid was employed in pioneering protease-reactive drug Xyotax, releasing paclitaxel, and was approved by FDA.<sup>108</sup>



**Scheme 7** Example of enzymatically activatable prodrugs based on cathepsin B (top)<sup>140</sup>,  $\beta$ -glucuronidase (left)<sup>141</sup> and phosphatase<sup>144</sup> (right) selective linkers.

pH stimulus driven cleavable linkers such as hydrazones or carbonates (Figure 21) were explored and used in many FDA approved antibody drug conjugates (Mylotarg, Besponsa etc.). However, the requirement for pH labile linkers to strictly discriminate between pH 5 (endosomes 5.5-6.2, lysosomes 4.5-5.0) and pH 7.4 is inherently difficult and because discrepancies in the stability in the bloodstream circulation occur, mainly the development of ADCs has rather focused on more stable linkers such as linkers described previously.<sup>144</sup>

## 2 Results and discussion



The motivation of the main project of my thesis was to prepare fluorescent conjugates with 3HQs with a possibility to monitor their penetration into the cells as well as to study the liberation to the free 3HQ drug. The choice of 3HQ derivatives as conjugated drugs was based on thorough experience with their synthesis and properties in our group together with their potential to become a hit molecule in the cancer or antimicrobial research in the future. However, 3HQs possess some undesirable properties. Their insolubility in aqueous media and high polarity causes significant disadvantages for advanced biological testing. Moreover, 3HQs are generally highly toxic not only to cancer cells but also show unfavorable toxicity to normal healthy cells.<sup>31,35</sup> Despite their native fluorescence around 540 nm, they can't be used alone as molecular fluorescent probes for cell imaging because excitation wavelength around 350 nm is usually in the window where ever-present cofactors such as NAD/NADH are excited as well. Therefore, we chose fluorescent BODIPY dye for further conjugation and improvement of the spectral properties. As described above, BODIPYs are great fluorophores - mainly high quantum yield, stability against photobleaching and ease of chemical modification. Additionally, the hydrophobic character of BODIPY dyes could increase penetrating ability of 3HQs into the cells. Moreover 3HQ-BODIPY conjugation via disulfide cleavable linker could preferentially release the 3HQs in the cancer cells due to higher concentration of glutathione.

In the early phase of my work on this project, I focused on synthesis of simple 3HQ-SS-BODIPY conjugates and study of their fluorescent properties in order to effectively follow their cleavage in the living cells. This led to development of the first generation of 3HQ conjugates (Figure 23). The conjugates were potent against cancer cells but lacked the

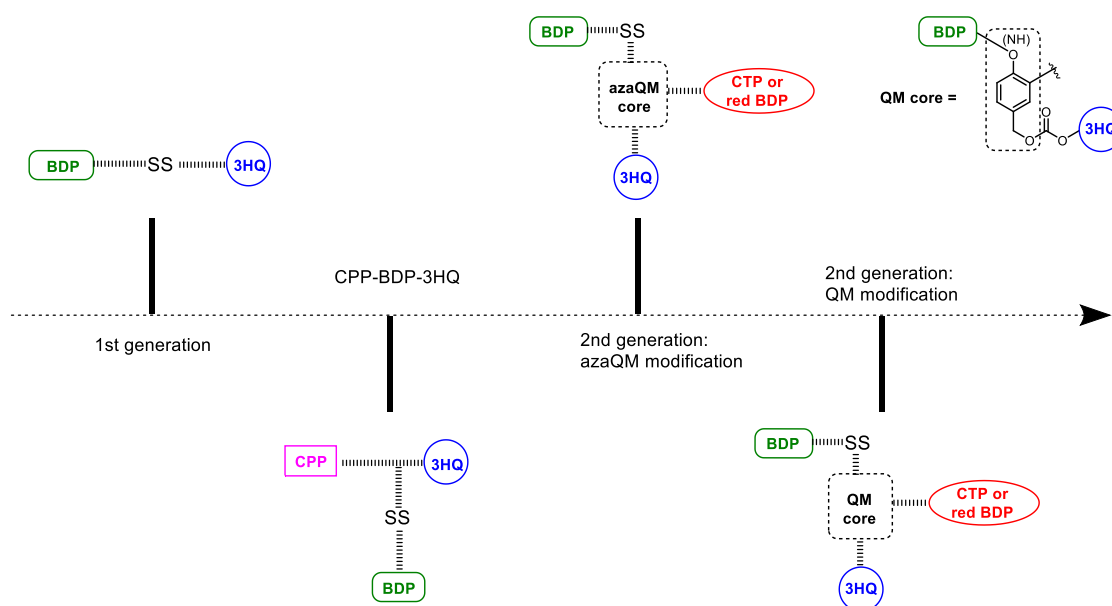
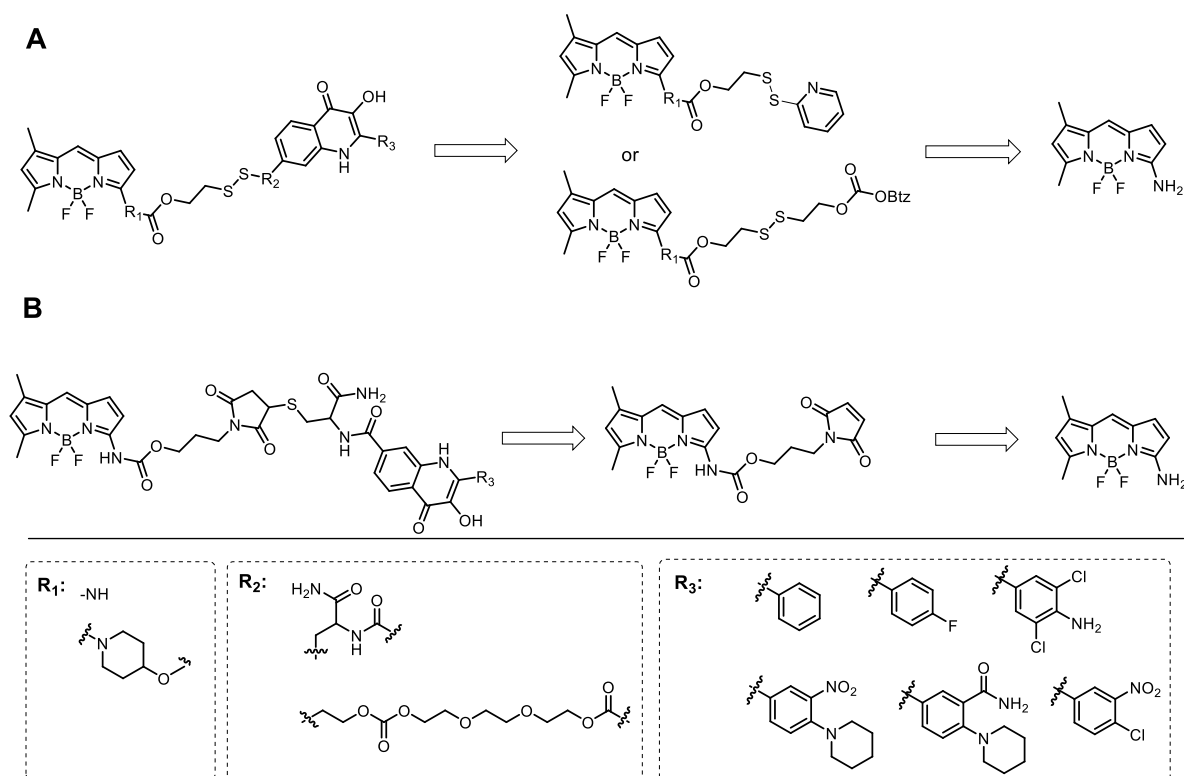


**Figure 23** Timeline of 3HQ-BODIPY conjugates development.

possibility of active targeting to cancer cells resulting in lower selectivity and better fluorescent resolution towards real-time monitoring for bioimaging. Thus, next steps in the synthesis resulted in the attempts to synthesize conjugates decorated with CPPs and finally second generation with cell targeting peptide (CTP) - cRGD peptide as an effective cell targeting moiety together with smart quinone methide central core and redBODIPY with higher absorption for FRET monitoring (Figure 23). This approach represented current trends for development of novel theranostics as diagnostic and therapeutic tools.

## 2.1 1<sup>st</sup> generation of 3HQ conjugates

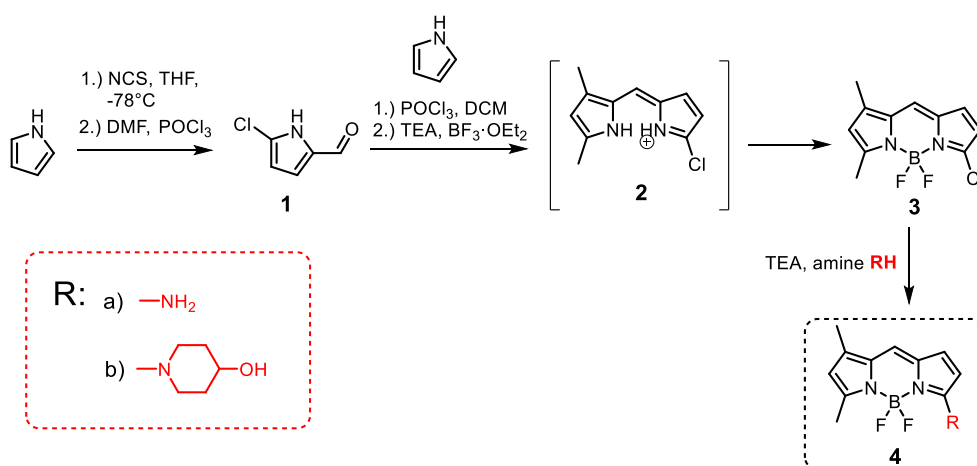
As depicted in the Figure 23 the first generation of 3-HQ-BODIPY conjugates represents the connection of 3HQ drug with BODIPY dye through disulfide cleavable linker or maleimide non-cleavable linker. Synthesis of 3HQ-BODIPY conjugates begins with appropriate modification of BODIPY dye (Scheme 8) followed by introduction of cleavable disulfide or non-cleavable maleimide linker. Attachment of 3HQ drugs was carried out through amino, hydroxy and thiol group (Scheme 8 A, R<sub>3</sub> substitution) to investigate the cleavage efficiency of final conjugates. Non-cleavable conjugates (Scheme 8 B) were synthesized in order to monitor the role of disulfide bond in cleavable conjugates and their cytotoxicity.



**Scheme 8** Retrosynthetic approach towards (A) cleavable conjugates and (B) non-cleavable maleimide conjugates of 1<sup>st</sup> generation.

## 2.1.1.1 Synthesis of BODIPY dyes

As stated before, BODIPY dyes are beneficial for their spectroscopical properties and ease of modification. We therefore designed small BODIPY dye with green emission – aminoBODIPY (**4a,b**, Scheme 9). For the synthesis of the aminoBODIPY dye the Approach B (see Introduction, Scheme 2) was used in which generally 2-formyl pyrrole reacts with pyrrole unsubstituted in the position 2 according to the Scheme 9. The synthesis starts with the preparation of 5-chloropyrrole-2-carbaldehyde **1** prepared from pyrrole in two step one-pot synthesis. The first step – chlorination was accomplished with use of NCS as the chlorinating agent followed by Vilsmeier-Haack formylation reaction described previously by Reynolds et al.<sup>145</sup>. In the next step precursor **1** was condensed with pyrrole to dipyrromethene **2** using POCl<sub>3</sub> and complexed with BF<sub>3</sub>.OEt<sub>2</sub> to give 3-chloro-BODIPY **3** (Scheme 9). Further modification of BODIPY core with ammonia and 4-hydroxy piperidine resulted in substitution of chlorine in the position C-3. However, the reaction with aqueous ammonia solution led to decomposition of the BODIPY core and therefore using water-free conditions was necessary to obtain the desired aminoBODIPY **4a**. Both BODIPY dyes showed slightly different spectroscopic properties as will be discussed in the next chapters.

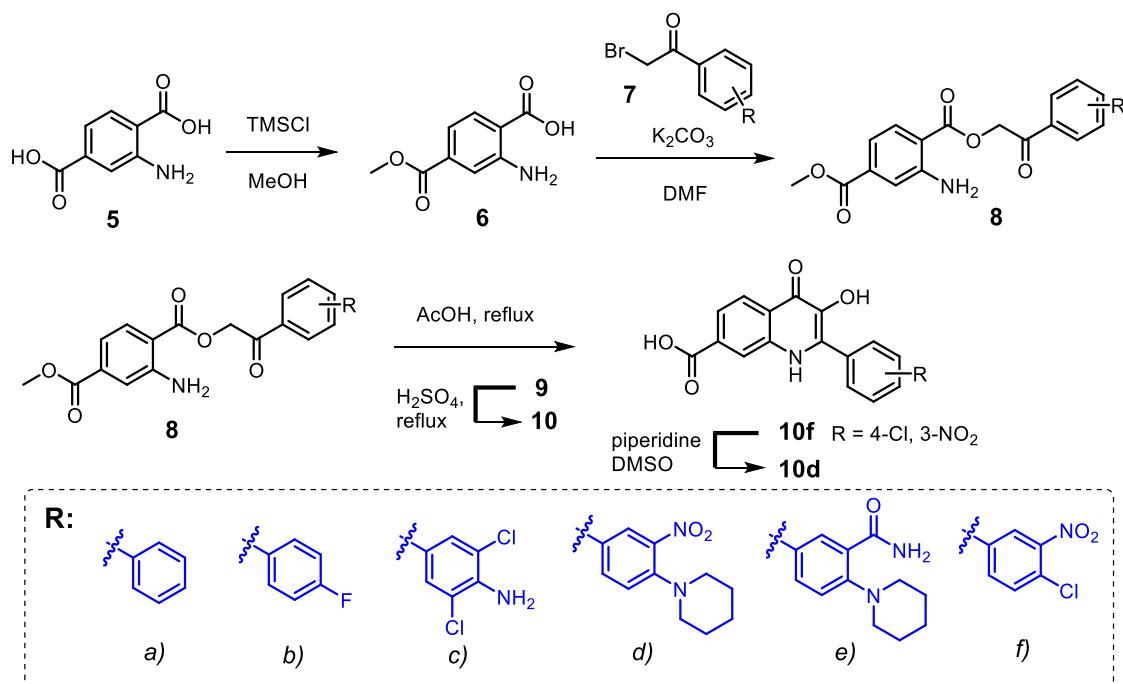


**Scheme 9** Synthesis of aminoBODIPY **4a** and **4b**.

## 2.1.1.2 Synthesis and modification of 3HQs

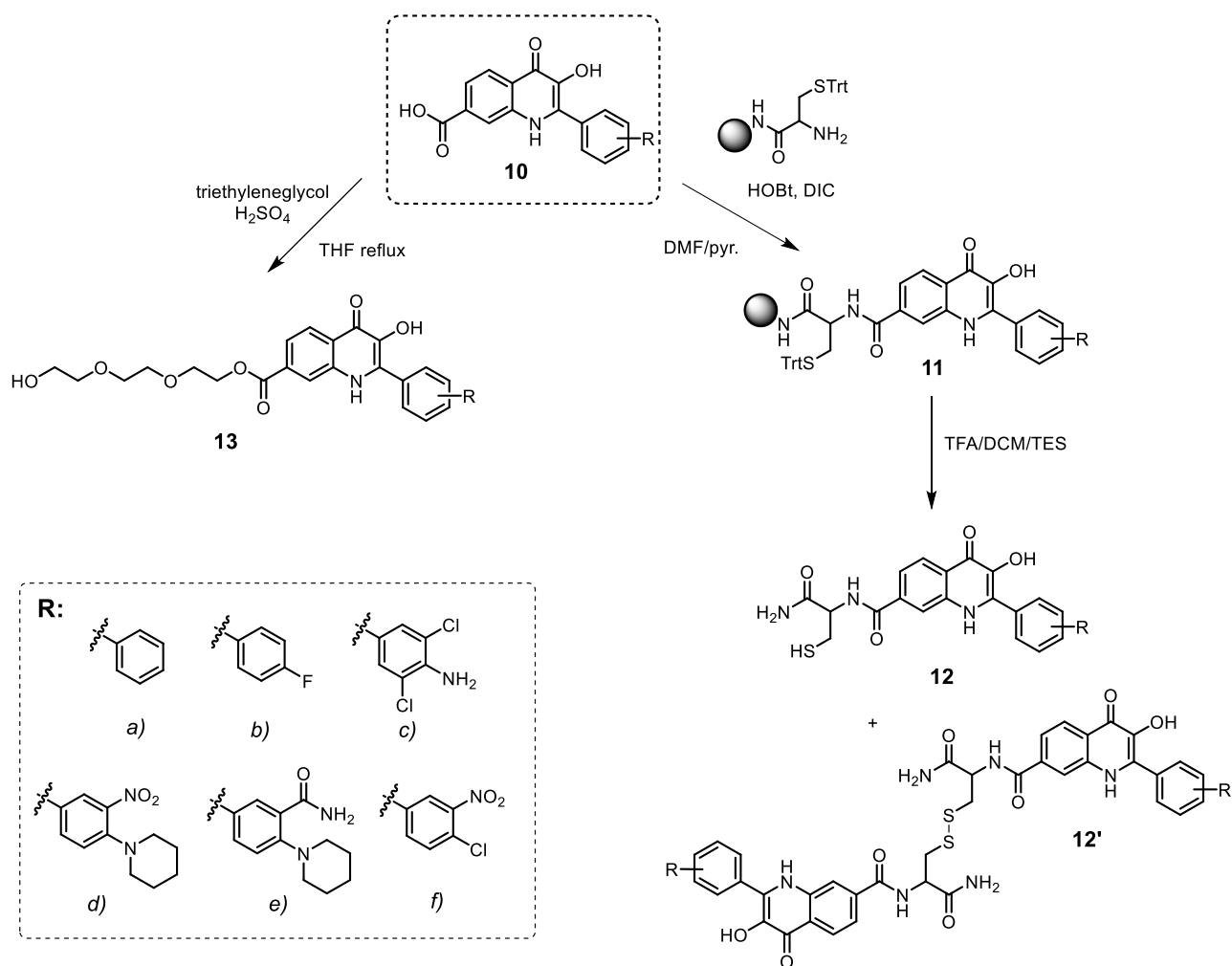
As mentioned previously, 3HQ became the drug of our choice on which we demonstrated functionality of the proposed system. In the first step aminoterephthalic acid **5** was converted to monomethyl ester **6** with use of TMSCl in MeOH (Scheme 10). Following reaction with the correspondingly substituted bromoacetophenones **7** afforded appropriate phenacylestere **8**. Acid catalyzed reaction of phenacyl estere **8** led to cyclization to 3HQ-ester

**9a-e** and the final hydrolysis by sulfuric acid afforded free 3-hydroxy-2-phenylquinolinone-7-carboxylic acid **10a-e**.



**Scheme 10** Synthesis of 3HQs **10a-f**.

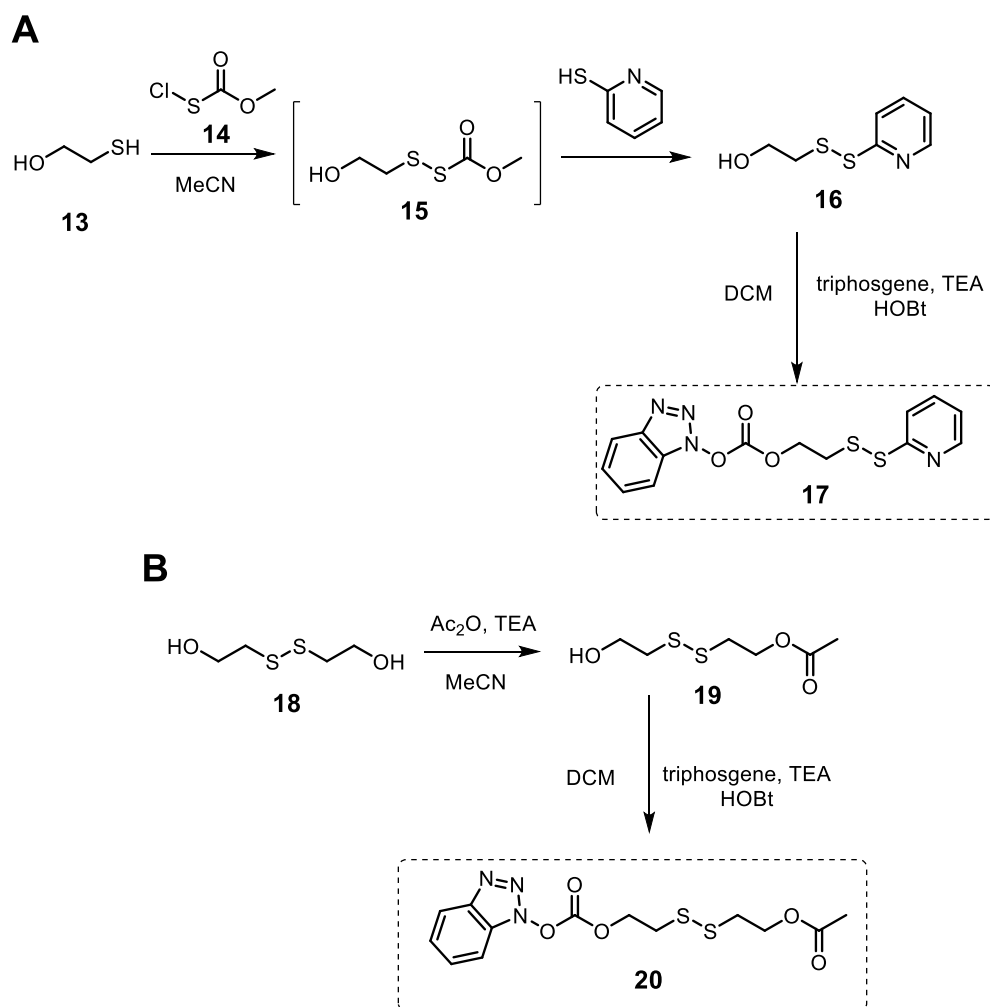
For the further attachment of 3HQs to the self-immolative linker or maleimide linker 3HQs **10a-e** had to be pre-modified. Two different auxiliary moieties were chosen – triethyleneglycol ester and cysteine amide (Scheme 11). 3HQs **12** derivatized by cysteine were synthesized by solid phase chemistry approach, by firstly immobilization of the Fmoc-Cysteine(Trt)-OH on Rink amide resin followed by deprotection of Fmoc protecting group and acylation with 7-COOH-3HQ **10** using DMF/pyridine as solvent mixture. Resulting Cys(Trt)-HQs **11** were cleaved from resin by TFA/DCM/TES mixture (1:1:0.05), and triturated with Et<sub>2</sub>O to get rid of trityl residue. Obtained solid compounds **12a-e** were contaminated by certain amount of disulfide dimeric product **12'** and were further purified by HPLC. Triethyleneglycol ester derivatives **13a-e** were prepared by acid catalyzed esterification of carboxylic group in the position C-7 of HQs **10a-e** according to the Scheme 11. In such fashion ten different 3HQ derivatives were prepared and used in further synthesis and biological screening.



**Scheme 11** Modification of 3HQs with cysteine and triethyleneglycol.

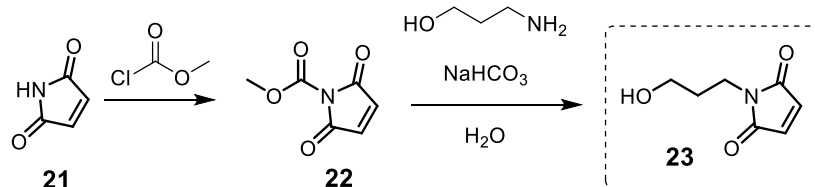
### 2.1.3 Synthesis of linkers

Cleavable disulfide self-immolative linkers and non-cleavable maleimide linker played key role in connecting the BODIPY and 3HQ parts together and maintained the cytotoxicity of resulting conjugates as well. Two types of disulfide linkers were proposed for conjugation – non-symmetrical and symmetrical linker (Scheme 12). Non-symmetrical linker was synthesized according to procedure described in literature<sup>146</sup> in two steps. Reactive methoxycarbonyl sulfonyl chloride **14** reacts in the first step with mercaptoethanol **13** to form disulfide intermediate **15** which is converted to asymmetric linker precursor **16** by treatment with 2-mercaptopyridine. For further attachment of BODIPY dye, the OH group on linker **16** was converted to activated carbonate **17** using triphosgene and HOBT (Scheme 12 A). Symmetrical linker was prepared from 2-hydroxyethyl disulfide **18** in two steps – protection of one hydroxy group with acetic anhydride to yield intermediate **19** and subsequent conversion of other OH group to activated carbonate **20** with triphosgene and HOBT.



**Scheme 12** Synthesis of (A) non-symmetrical linker **17** and (B) symmetrical disulfide linker **20**.

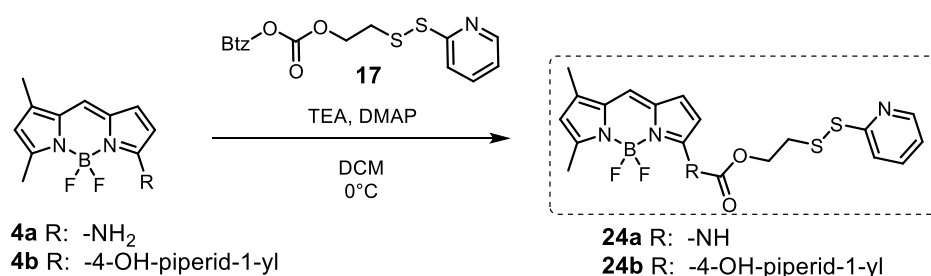
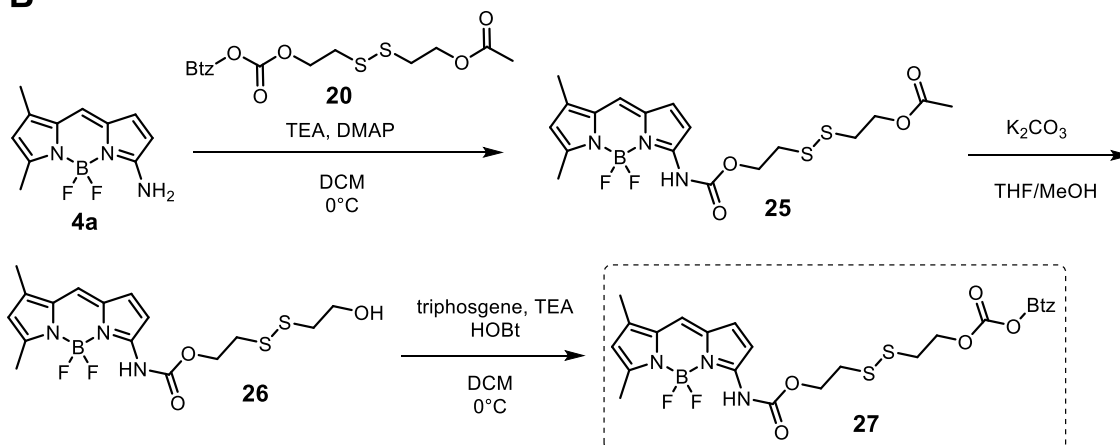
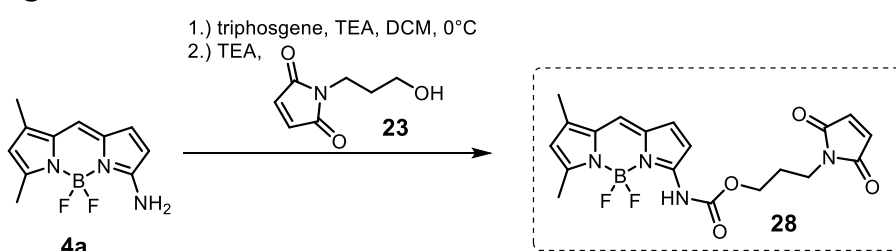
To demonstrate that biological activity of conjugates was caused due to cleavage of disulfide linker and liberation of the free 3HQ non-cleavable counterpart linker **23** was synthesized as well (Scheme 13). The synthesis of maleimide linker **23** starts with conversion of maleimide **21** to methylcarbamate **22** reacting with methylchloroformate. Further treatment with 3-aminopropanol in aqueous  $\text{Na}_2\text{CO}_3$  led to the desired 3-hydroxypropyl maleimide **23**.



**Scheme 13** Synthesis of non-cleavable maleimide linker.

## 2.1.4 Synthesis of conjugates

After preparing all the three parts – BODIPY dyes, linkers and 3HQs the next step was the conjugation – connecting the parts together. The first step involved derivatization of BODIPY dyes with linkers (Scheme 14). This was accomplished by reacting amino-BODIPY **4a,b** with HOBt-activated disulfide linkers **17** or **20** using TEA and DMAP in dry DCM to afford intermediates **24**, resp. **25**. Dry solvent generally increased purity and yield of this reaction. In the case of symmetrical linker intermediate **25**, removal of acetyl protecting group by  $K_2CO_3$  in THF/MeOH to obtain intermediate **26** followed by activation of newly formed OH group by triphosgene/HOBt resulted in activated carbonate BODIPY-SS-OBtz **27** (Scheme 14 B).

**A****B****C**

**Scheme 14** Modification of BODIPY dyes **4a,b** with (A) non-symmetrical disulfide linker **17**, (B) symmetrical disulfide linker **20** and (C) non-cleavable maleimide linker **23**.

Non-cleavable linker was installed to aminoBODIPY **4a** in reversed fashion as disulfide linkers (Scheme 14 C). Firstly, aminoBODIPY **4a** was transformed to reactive isocyanate intermediate by triphosgene in the presence of TEA and treated after 1 hour in one pot fashion with 3-hydroxypropyl maleimide **23** to obtain BODIPY-maleimide pro-linker **28**.

The final incorporation of 3HQs **12**, **13** and **29** (Figure 24) as the representative compounds having thiol, amino and hydroxyl group, respectively, was accomplished generally in three ways according to the used linker and the reactive group on 3HQ – disulfide exchange reaction in case of non-symmetrical linker **24**, substitution of activated carbonate (symmetrical linker **27**) and Michael addition to double bond (maleimide linker **28**) (Scheme 15). Thiol disulfide exchange reaction was utilized in the preparation of BDP-SS-Cys-3HQ conjugates **30** and **31** with non-symmetrical cysteine linker, while mercaptopyridine acted as an effective leaving group (Scheme 15 A). The reaction proceeded under heating smoothly and provided products in good crude purity which were further purified by preparative HPLC to obtain pure final conjugates. This way five aminoBODIPY conjugates **30a-e** and two hydroxypiperidine-BODIPY conjugates **31a,d** varying by the substitution on 3HQ phenyl ring were prepared.

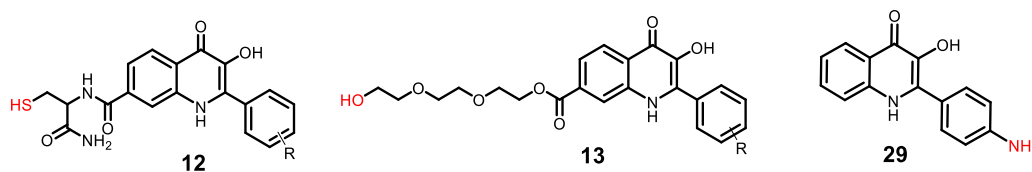


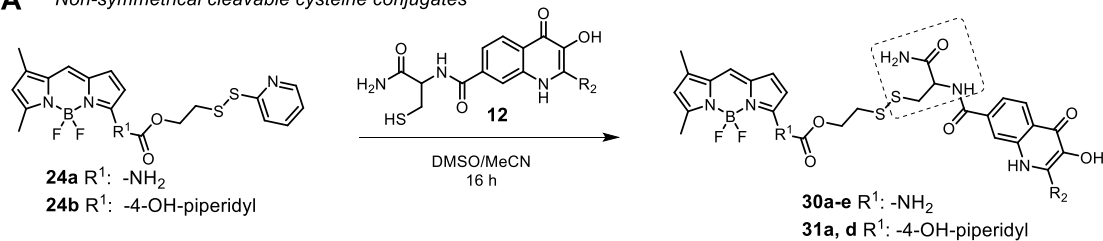
**Figure 24** Three types of 3HQs used in the conjugation step.

The preparation of conjugates with **symmetrical** cleavable linker was accomplished by substitution of HOBt activated carbonate by hydroxy-3HQ **13** or amino-3HQ **29** in the presence of the base TEA and DMAP in DMF. In overall, five carbonate bound symmetrical conjugates **32a-e** and one carbamate bound conjugate **33** were prepared (Scheme 15 B and C). Lastly, maleimide linker was used to synthesize **non-cleavable** (negative control) conjugates by Michael addition reaction of cysteine-3HQs **12** with maleimide BODIPY linker **28**. However, maleimide linker together with cysteine in enantiopure L-configuration installed on 3HQ provided mixture of diastereomers **34a-e** clearly detectable by LC/MS as two distinct signals with different retention times. The mixture of diastereomers was not separable by standard preparative HPLC and thus was purified and used in further biological experiments only as a diastereomeric mixture. Together five derivatives **34a-e** with maleimide non-cleavable linker were prepared and characterized by NMR, HRMS and their spectroscopical properties were reviewed (Scheme 15). Conjugate **35** with cysteamide attached to the aminoBODIPY via

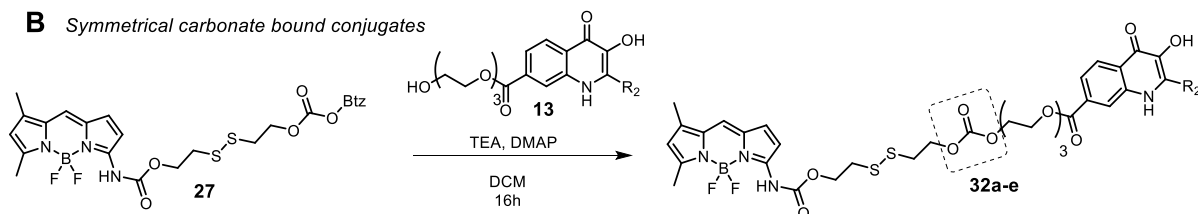


disulfide linker was prepared in order to monitor the influence of 3HQ on fluorescent properties of aminoBODIPY **4a**.

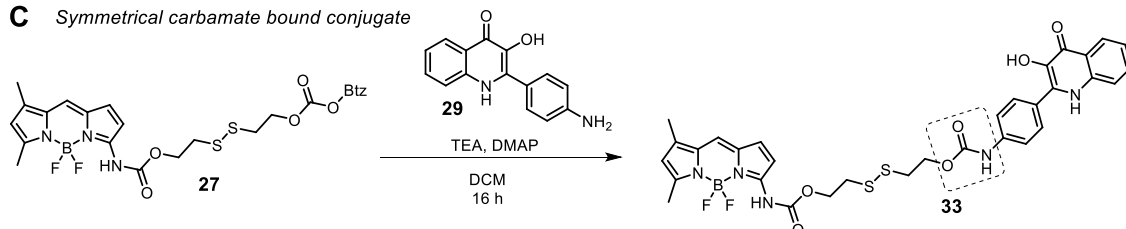
**A** Non-symmetrical cleavable cysteine conjugates



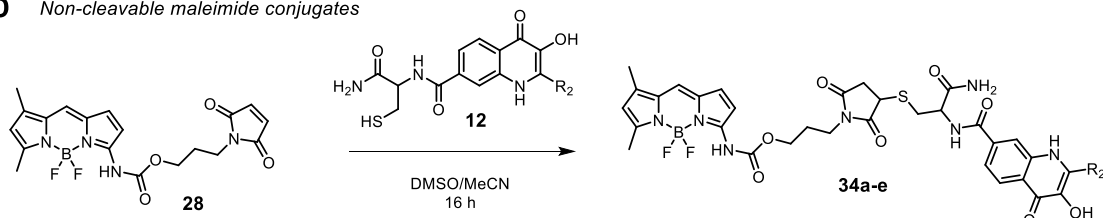
**B** Symmetrical carbonate bound conjugates



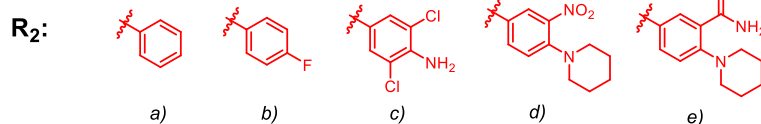
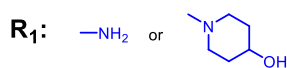
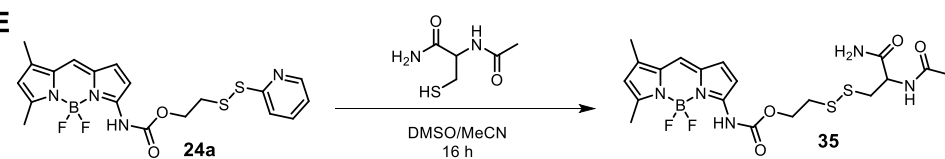
**C** Symmetrical carbamate bound conjugate



**D** Non-cleavable maleimide conjugates



**E**



**Scheme 15** Synthesis of (A) cysteine cleavable conjugates **30** and **31**, (B) cleavable carbonate bound conjugates **32**, (C) cleavable carbamate bound conjugate **33** and (D) non-cleavable maleimide conjugates **34**. (E) Synthesis of cysteamide-BODIPY **35**.

## 2.1.5 Fluorescent properties of BODIPY dyes and its conjugates

After preparation of proposed compounds, they were subjected to cleavage experiments with triscarboxyethyl phosphine (TCEP) and glutathione (GSH) to test the cleavability and change of fluorescent properties. The cleavage experiments served as a first preliminary guidance for several reasons – (i) how effective and rapid is the cleavage, (ii) what are the intermediates that are forming during the cleavage, (iii) how does the fluorescent and absorption profile changes during the cleavage and (iv) what are the limitations or applicability for biological imaging. As described in literature chapter, disulfide bonds in self-immolative linkers are prone to disruption under reductive conditions. Therefore, TCEP was used in the first experiments and later was replaced by GSH to simulate conditions in cancer cells. which plays a key role in capturing radicals, expulsion of xenobiotics from living cells and is overexpressed in some cancer cells.

Compound	Solvent	$\lambda_{exc}$ (nm)	$\lambda_{em}$ (nm)	$\Delta\lambda$ (nm)	QY (%)
<b>30d</b>	HEPES	515	527	12	1.4
	DMSO/HEPES	517	531	14	7.7
<b>32a</b>	HEPES	516	525	9	14
	DMSO/HEPES	520	530	10	58
<b>33</b>	HEPES	517	525	8	32
	DMSO/HEPES	521	532	11	53
<b>4a</b>	HEPES	480	523	43	77
	DMSO/HEPES	496	523	40	95
<b>32d</b>	DMSO/HEPES	521	549	28	23
<b>35</b>	DMSO/HEPES	520	531	11	95
<b>4b</b>	DMSO/HEPES	521	550	29	48

**Table 6** Spectral properties of some prepared conjugates.

However, at first the optical properties of free BODIPY dyes and conjugates were measured (Table 6). AminoBODIPY **4a** showed an interesting feature – in the bound/acylated form (conjugates **30**) the BODIPY core has an excitation maximum at  $\lambda_{exc.} = 515$  nm, while in the free form (**4a**, BODIPY-NH<sub>2</sub>) the excitation wavelength is significantly shifted to the lower wavelengths with maximum at  $\lambda_{exc} = 480$  nm. Interestingly, the emission maximum remained approximately the same 523 nm and 527 nm, respectively (Figure 25 A). The shift of the excitation maxima is caused probably due to alteration of electronical properties at the amino

group that is bound directly to the BODIPY core. Free amino group is good electron donor, but turning it to carbamate group results in formation of electron more deficient structure. This fact can be supported by optical properties of piperidineBODIPY **4b** which has its binding site attached not directly to the core of BODIPY. No such shift of excitation maxima was observed and thus conjugates **31** have the same excitation and emission as the free BODIPY **4b** (Figure 25 B). Moreover, the excitation wavelength shift in the case of aminoBODIPY **4a** is universal - it does not depend on the conjugated counterpart and is not typical only for 3HQs as was confirmed by the preparation and measurement of optical properties of cysteamide-BODIPY conjugate **35**.

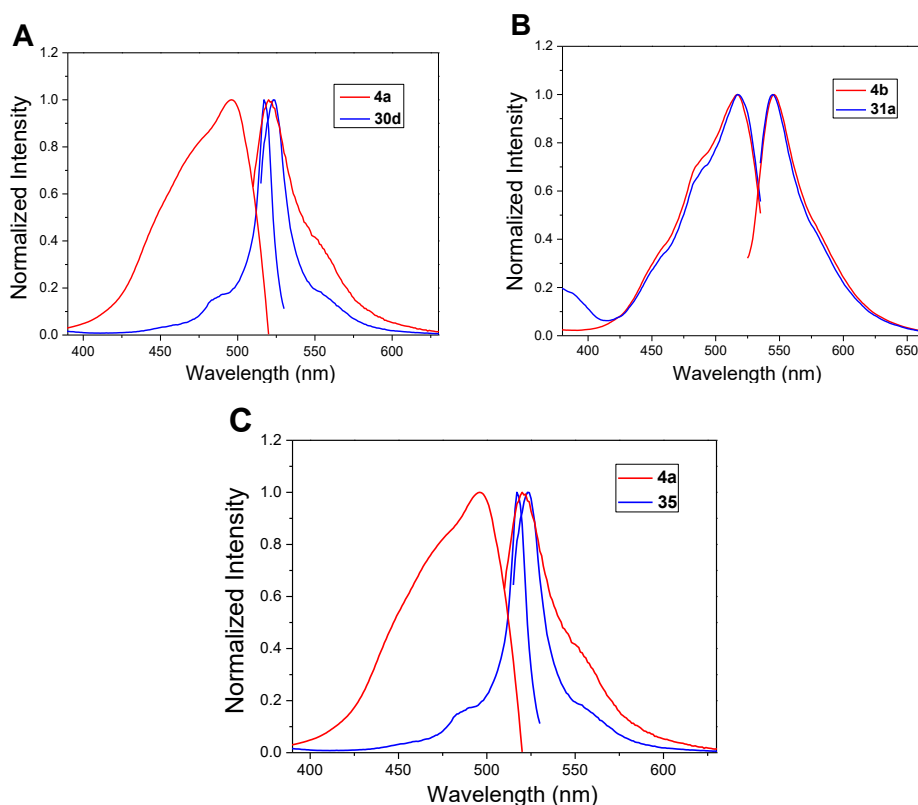
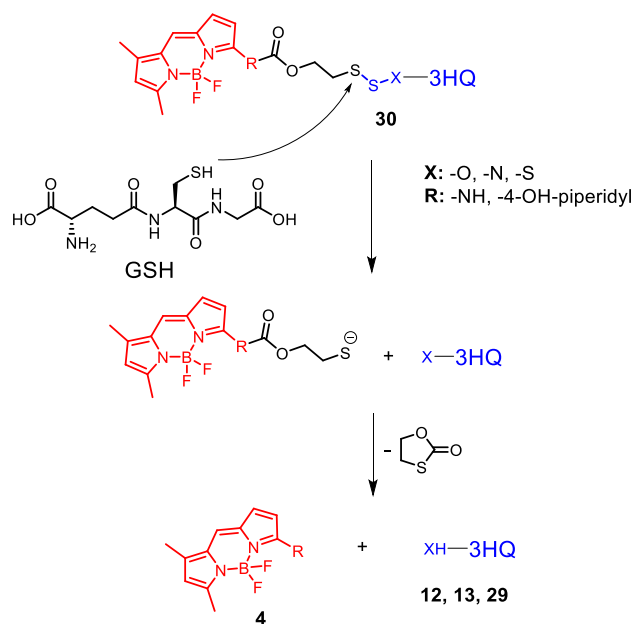


**Figure 25** Normalized excitation and emission spectra of (A) aminoBODIPY **4a** and 3HQ conjugate **30d**, (B) BODIPY **4b** and 3HQ conjugate **31a** and (C) aminoBODIPY **4a** comparison with cysteamideBODIPY **35**. Measured in DMSO/HEPES 2:1.

#### 2.1.6 GSH-mediated cleavage

Bathochromic shift in excitation maximum of aminoBODIPY conjugates enabled us to apply so called “OFF-ON” monitoring and further ratiometric monitoring of GSH-mediated cleavage (Scheme 16). Since conjugates themselves have only little absorption at 480 nm at the beginning of cleavage there is only weak fluorescence at 525 nm (OFF state). As the cleavage proceeds aminoBODIPY **4a** is liberated and strong green fluorescence appears (ON state)

(Scheme 16, Figure 26 A). On the other hand, when the emission intensity upon excitation at maximum absorption of conjugate - 510nm is followed we observe strong emission at 525 nm at the beginning of the cleavage (compound is in conjugated form) and as the cleavage continues the increase of fluorescence is lower or even in some cases the fluorescence decreases as the conjugate disappears (Figure 26 B). This fact was utilized in ratiometric determination of cleavage extent as ratiometric systems are beneficial for several reasons mentioned in the introduction chapter. Therefore, the ratio of fluorescence intensity after excitation at 480 nm and 510 nm was used for the cleavage monitoring. Supported by the significant difference in quantum yields (Table 6) between the free BODIPY dyes (**4a,b**) and some conjugates containing fluorescence quenching -NO<sub>2</sub> group (e.g. conjugate **32d**) the change of fluorescence intensity during the GSH-mediated cleavage was observed to be 4-5 fold what was acceptable for further cleavage experiments.



**Scheme 16** GSH-mediated cleavage of disulfide 3HQ-BODIPY conjugates.

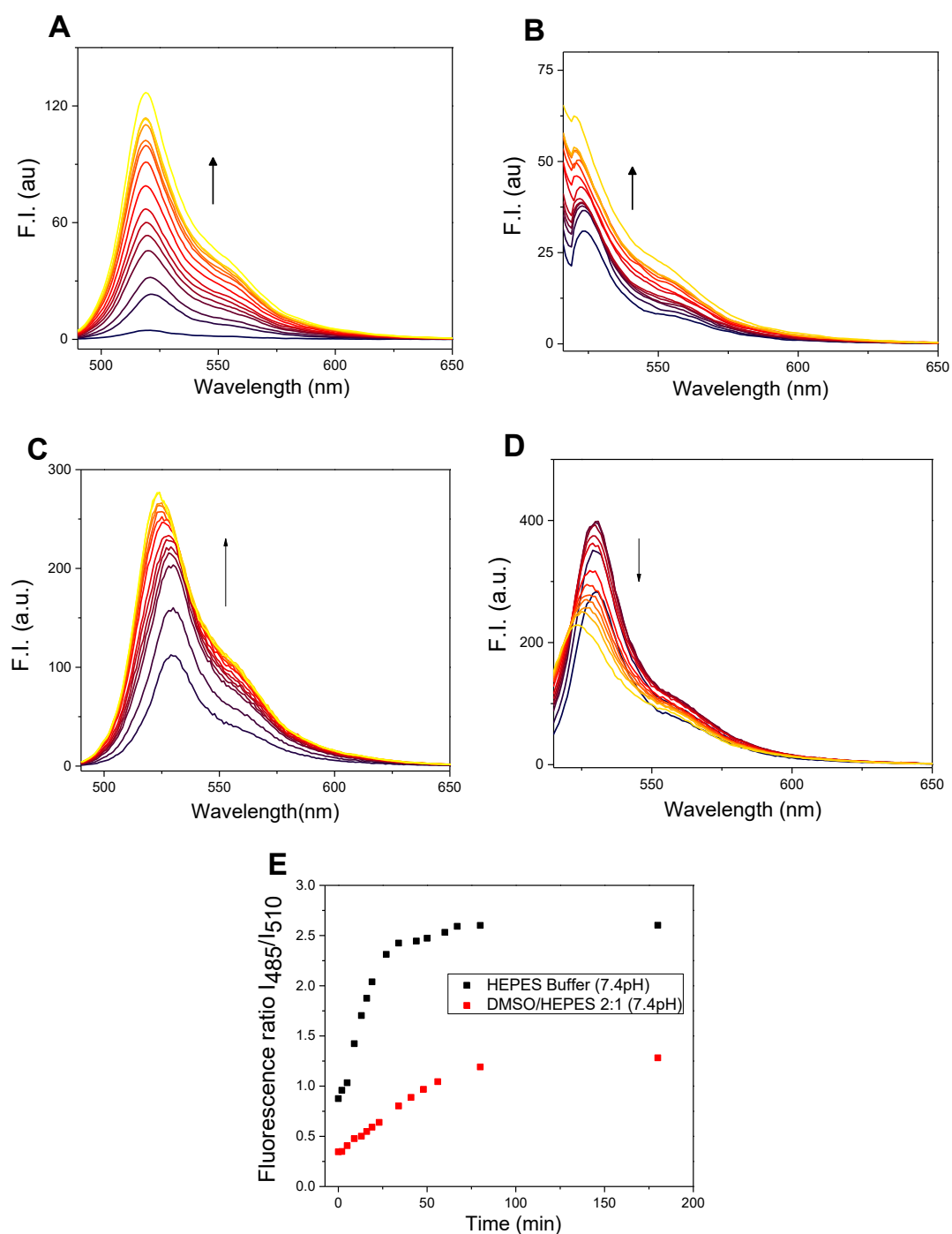
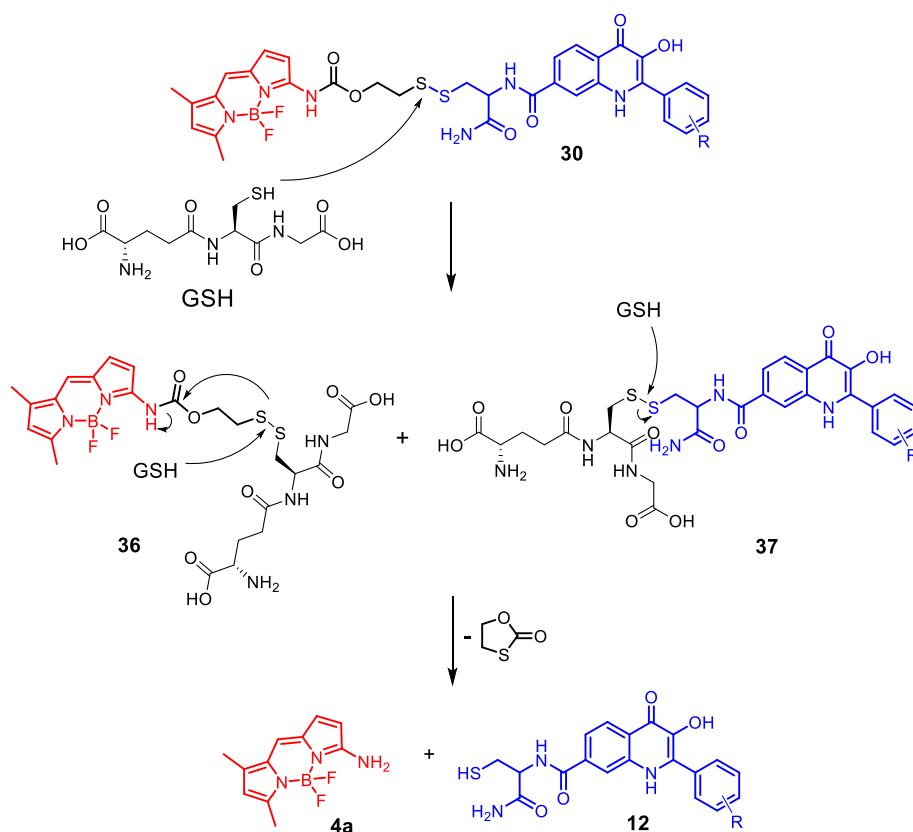


**Figure 26** GSH-mediated cleavage of probe **30d** in HEPES buffer monitored within 180 min by fluorescence emission at 525 nm after excitation at (A) 480 nm and (B) 510 nm (5  $\mu$ M probe **30d**, 5 mM GSH). (C) GSH-mediated cleavage of probe **30d** in DMSO/HEPES buffer monitored within 180 min by fluorescence emission at 525 nm after excitation at 480 nm and (D) 510 nm (5  $\mu$ M probe **30d**, 5 mM GSH). (E) Time dependent change of fluorescence ratio  $I_{485}/I_{510}$ .

To confirm the ability of disulfide linker to release the amino-BODIPY **4a** or **4b** and the model drugs **12**, **13** and **29** by thiols according to the , conjugates **30-35** were treated with 5 mM glutathione at physiological conditions (37 °C, pH 7.4) and monitored by LC/MS (Figure 27). Because of the necessity to use a high concentration of the probes for UV detection, the present study was performed only in DMSO/HEPES buffer (2:1). As shown in Scheme 17 and Figure 27 A, the treatment of prodrug **30d** with GSH resulted in four products detected by LC/MS. According to mass spectrometry, the presence of the expected released drug **12d** and amino-BODIPY **4a** indicating complete cleavage of the conjugate was detected, as well as the formation of GSH adducts **36** and **37** derived from the BODIPY dye and 3-HQ, respectively. Interestingly, the concentration of the adduct **37** increases in a time-dependent manner, which might be attributed to the equilibrium between **37** and **12**. Conversely, the concentration of adduct **36** decreased with time due to the presence of self-immolative disulfide linker that prevents such equilibrium (Figure 27).



**Scheme 17** Example of GSH-mediated cleavage of conjugate **30d** and formed GSH by-products.

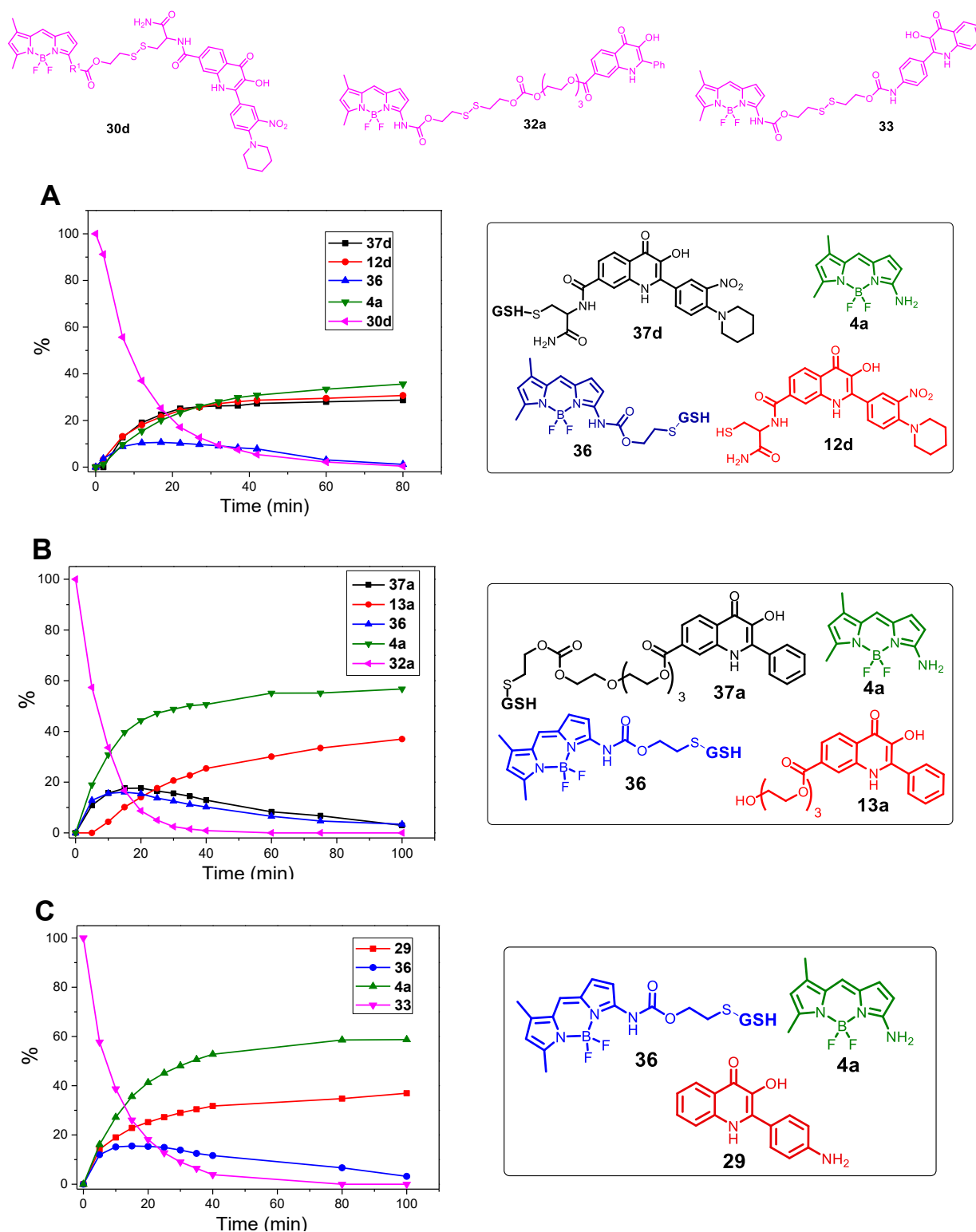


**Figure 27** Monitoring of the drug release from conjugates (A) **30d**, (B) **32a**, and (C) **33** (5  $\mu$ M; DMSO/HEPES buffer 2:1, 0.1M; pH 7.4; 37  $^{\circ}$ C) after treatment with GSH (5 mM) by HPLC/MS.

The cleavage of the conjugates **32a** and **33**, where 3HQ is bound via carbonate and carbamate bonds, afforded the corresponding 3HQs **13a** and **29**, respectively (Figure 27 B, C).

Although the GSH adducts **36** and **37** were also observed, these were subsequently converted to the final free 3HQ derivatives and amino-BODIPY **4a**.

As mentioned previously, the difference in excitation spectra of free aminoBODIPY enabled us to monitor cleavage of conjugates in “OFF-ON” and in ratiometric fashion. Therefore, we focused mainly on experiments with fluorescence detection of cleavage using the ratio of emission intensity at 530 nm upon excitation at 480 nm and 510 nm ( $I_{480}/I_{510}$ ) which allowed for measurement independently of conjugate concentration. The rate of the GSH-mediated cleavage of disulfide bridge depends on the concentration of GSH (Figure 28). While 5 mM GSH normally present in some cancer cells was sufficient for full cleavage of conjugate **30d** within 50 min and within 120 min in case of conjugates **32a** and **33**, low concentrations of GSH caused only partial cleavage during the same period. In addition, the cleavage is pH dependent and proceeds rapidly under basic conditions whereas in acidic medium, none or only little conjugate is cleaved (Figure 29). As expected, conjugates with maleimide non-cleavable linker were completely stable in the presence of 5 mM GSH as indicated by no change in ratio  $I_{485}/I_{510}$  over 16 h (Figure 28 D).

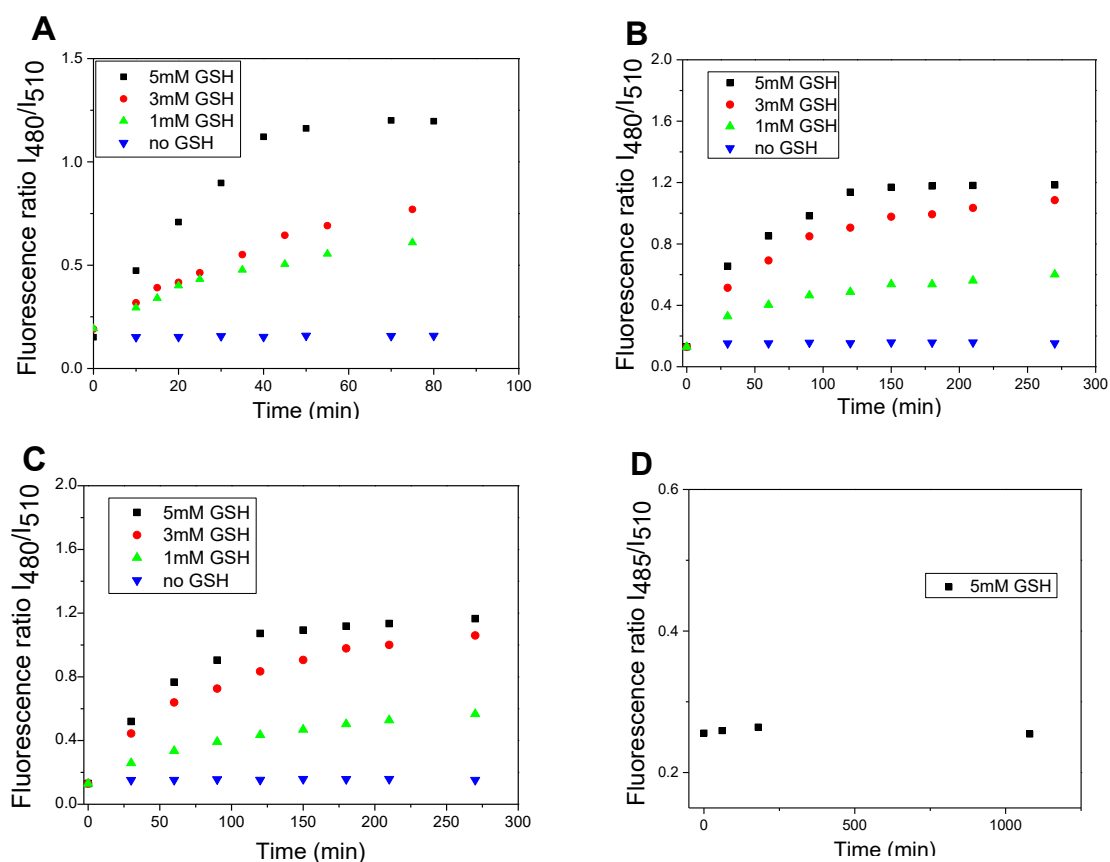


**Figure 28** Ratio of emission intensities at 525 nm upon excitation at 480 and 510 nm in time after treatment with different concentrations of GSH (5, 3, 1, 0 mM). (A) Probe **30d**, (B) probe



**32a**, (C) probe **33** and (D) non-cleavable probe **34c**. (5  $\mu$ M probes; DMSO/HEPES buffer 2:1, 0.1M, pH 7.4, 37  $^{\circ}$ C).

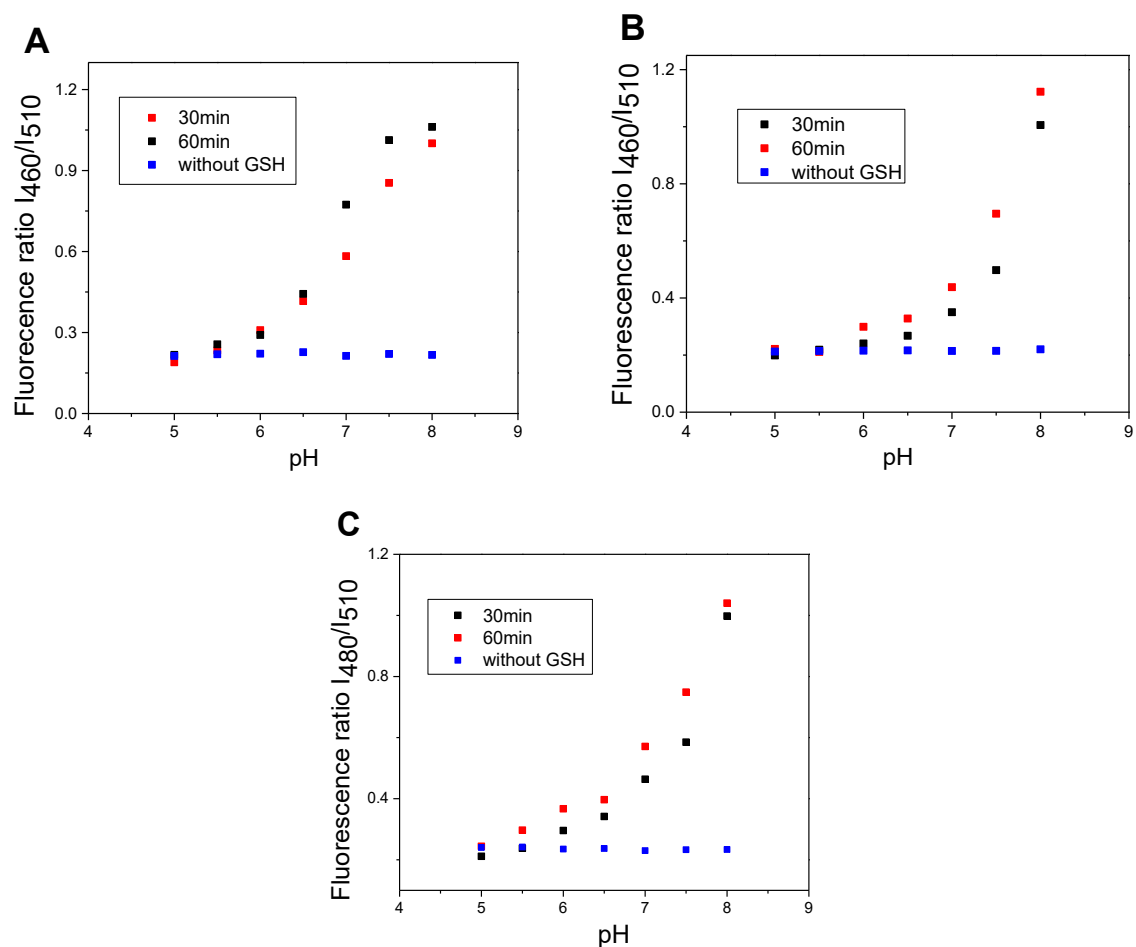


**Figure 29** Ratio of emission intensities at 525 nm upon excitation at 480 and 510nm after 30 and 60 minutes of incubation of probes **30-33** with GSH at various pH (5.0 - 8.0) and without GSH after 60 minutes. (A) Probe **30d**, (B) probe **32a** and (C) probe **33** (5  $\mu$ M probes, 5 mM GSH, DMSO/HEPES buffer 2:1, 0.1M, 37 $^{\circ}$ C).

As exemplified on the probe **30d**, not only GSH but also cysteine, commonly present in proteins, can cause the aminoBODIPY to release. The Figure 30 shows stability of the conjugate **30d** against the cleavage in presence of various amino acids as well.

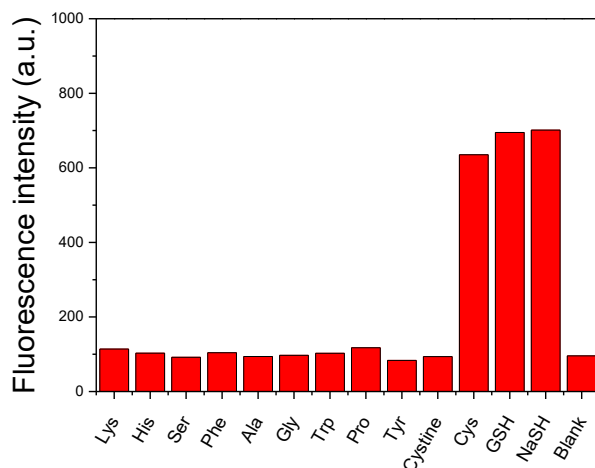


**Figure 30** Fluorescence intensity enhancement upon incubation of probe **30d** (5  $\mu$ M) with various amino acids (100 mM, DMSO/HEPES buffer 2:1, 0.1M, pH 7.4) after 60 min. ( $\lambda_{\text{exc}} = 480$  nm,  $\lambda_{\text{em}} = 525$  nm).

Furthermore, we explored monitoring of cleavage by UV/VIS spectroscopy which resulted in the hyperchromic as well as hypochromic shift with an isosbestic point at approximately 490 nm (Figure 31). As the absorption profile of 3HQs bound in conjugates **30-34** did not interfere with this wavelength, the isosbestic point was connected with the change of acylamino-BODIPY to amino-BODIPY regardless of the bound drug and stage of the cleavage, thus can be used for independent quantification of the initial conjugate quantification. This phenomenon could be supported by the same results obtained from UV/VIS-based monitoring of cleavage of conjugate **35** bearing cysteamide and having no absorption in the UV/VIS region (Figure 31 B).

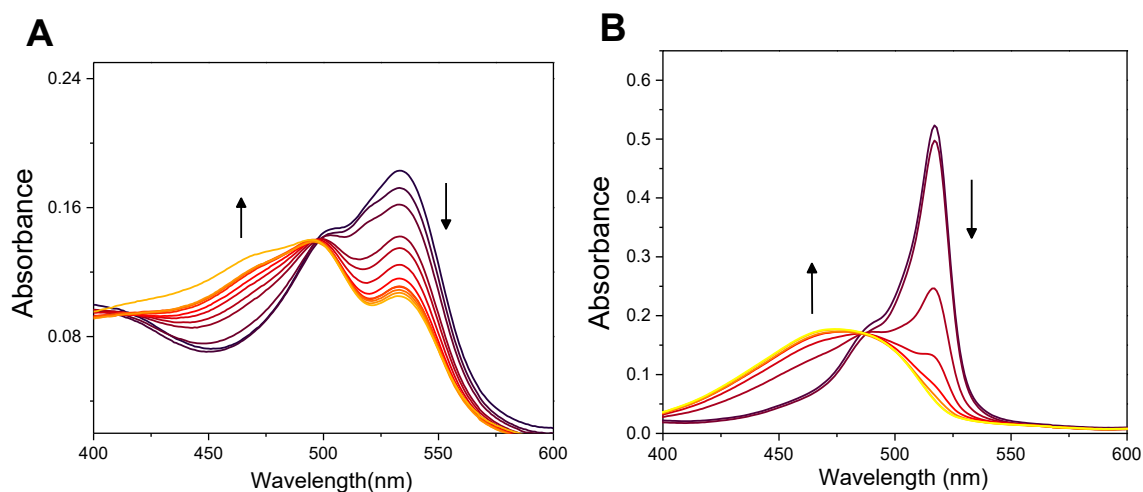


**Figure 31** Monitoring of cleavage of probes **30d** (A) and (B) **35** by UV/VIS spectroscopy. (5  $\mu$ M probes; 5 mM GSH, 0.1M HEPES buffer, pH 7.4, 37  $^{\circ}$ C).

## 2.1.7 Biology

To prove the real functioning of the system, we performed the cleavage experiment of conjugates **30-34** in HeLa cells. Due to the instrumental limitation, excitation at 485 nm was used instead of  $\lambda_{\text{exc}} = 480$  nm. Although the inherent concentration of GSH in the cells was sufficient to cleave the disulfide conjugates **30-33**, the cleavage was more efficient when conjugates were added to the cells preincubated with additional 20mM GSH (Figure 32, Figure 33 B). However, conjugate **32a** with the most susceptible carbonate linker was cleaved efficiently inside native cells without preincubation with GSH. Arguably, the GSH concentration in the HeLa cells is sufficiently high for maximal cleavage of the linker, and the preincubation with GSH does not further accelerate the disruption of the disulfide bond.

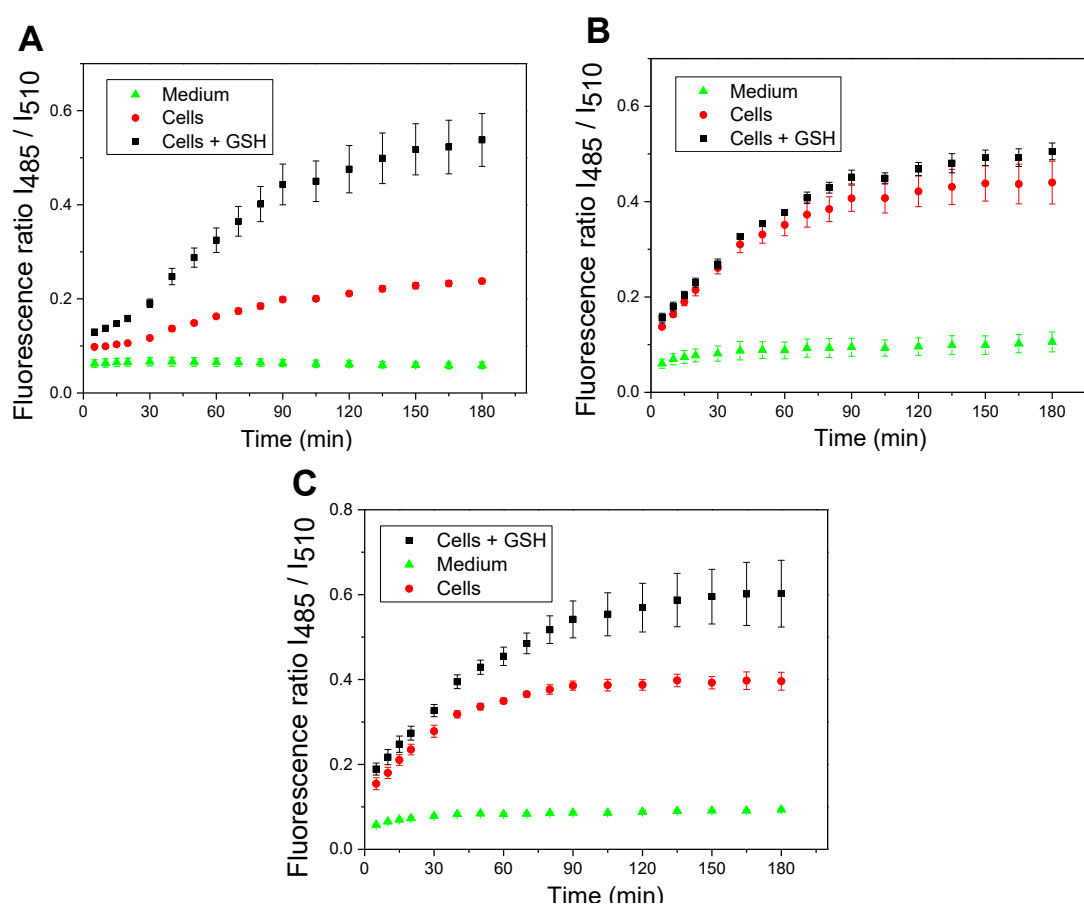


**Figure 32** Ratio of emission intensities at 525 nm upon excitation at 485 nm and 510 nm inside HeLa cells corresponding to the cleavage of conjugate (A) **30d**, (B) **32a**, and (C) **33** within 3 h period.

Additionally, microscopy images of cellular internalization of conjugates **30-33** before and after treatment with GSH (20 mM) were recorded. It is apparent that after GSH treatment,

the green fluorescence of released aminoBODIPY **4a** has appeared and “OFF-ON” effect is observed as exemplified in Figure 33 C, D.

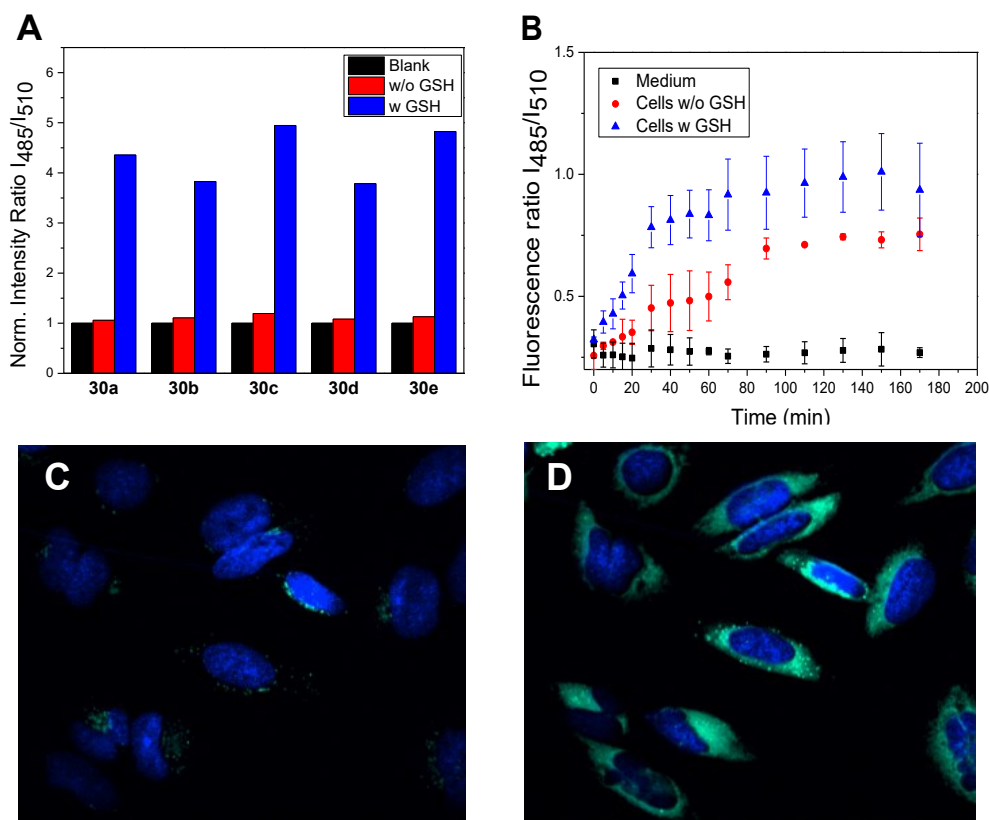


**Figure 33** (A) Schematic representation of the ratiometric change of fluorescence intensities at 530 nm after excitation at 485 nm and 510 nm (fluorescence ratio  $I_{485}/I_{510}$ ) for conjugates **30a-e** incubated in HEPES Buffer and measured at 0 h (black columns), HEPES buffer without GSH for 3 h (red columns) and in HEPES buffer with GSH (5 mM) for 3 h at 37°C (blue columns). (B) Time monitored cleavage of conjugate **30d** in medium without GSH (black), after treatment of the HeLa cells (red marks) or HeLa cells pretreated by 20 mM GSH (blue spots) with conjugate **30d**. (C) The microscopy images of the internalization of conjugate **30d** inside the HeLa cells before treatment and (D) 2h after treatment with GSH (20 mM).

Similarly, fluorescence ratio  $I_{485}/I_{510}$  of non-cleavable conjugates **34a-e** was monitored in DMSO/HEPES buffer (2:1) as well as in HeLa cells after treatment with GSH (Figure 34). In this case, no significant changes were observed, confirming the stability of conjugates towards thiols and GSH.

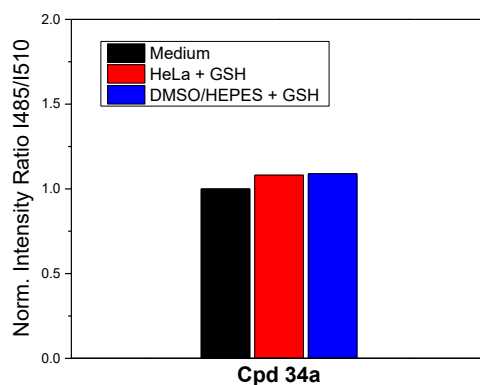
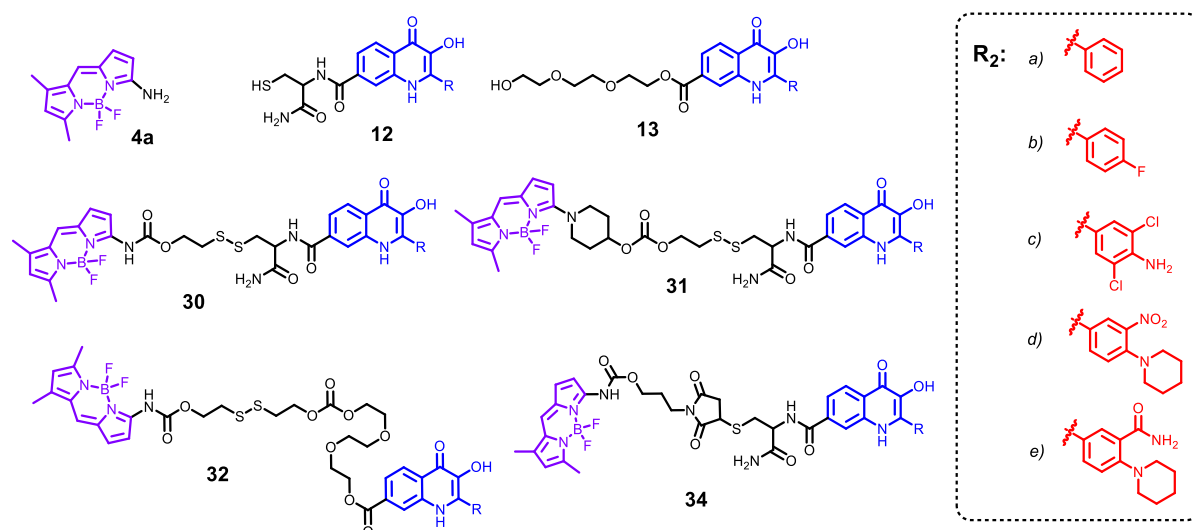


**Figure 34** Fluorescence ratio  $I_{485}/I_{510}$  monitoring after incubation of non-cleavable conjugate **34a** (5  $\mu$ M) in free medium (black column), HeLa cells with additional GSH (20 mM) (red column) and in the presence of GSH (5 mM) in DMSO/HEPES Buffer 2:1 (0.1 M, pH 7.4, 37  $^{\circ}$ C) (blue column) for 180 min.

In collaboration with the Institute of molecular and translational medicine (IMTM) and biological screening department, the disulfide compounds **30-33** and non-cleavable maleimide conjugates **34** were tested for their cytotoxicity and  $IC_{50}$  values were determined (Table 7). Cancer cell lines involved in the screening were derived from solid tumors as well as hematological malignancies: CCRF-CEM (acute lymphoblastic leukemia), K562 (chronic myeloid leukemia), A549 (lung adenocarcinoma), colorectal carcinoma cell lines HCT116 with and without functional p53 protein HCT116p53, respectively. The panel also included chemo-resistant subclone CCRF-CEM-DNR (resistant to daunorubicin) overexpressing P-glycoprotein and/or lung resistance-related protein (LRP), which are pumps or detoxifying systems responsible for the most common forms of clinical resistance. To evaluate non-tumor cell toxicity, we used human skin fibroblast cell line BJ and lung fibroblast cell line MRC-5.

In general, free cysteine-3HQs **12a-e** exhibited no toxicity whatsoever probably due to their high polarity and impaired cell uptake. However, conjugation to aminoBODIPY **4a** or **4b** led to the increased toxicity mainly in case of cleavable conjugates Cys-3HQ **30** and **31** and PEG-3HQ conjugates **32**. Cys-3HQ conjugates **30a-e** and **31a,d** showed moderate activity against CEM cells but only subtly increased toxicity to other cell lines compared with non-cleavable conjugates **34**. Non-cleavable conjugates exhibit only certain inherent toxicity to CCRF-CEM cells, arguably as a result of insufficient rendering of 3HQ toxicity, but exhibit completely no toxicity to other cell lines. The highest toxicity was exhibited by triethyleneglycol (peg) derivatives of 3HQs **13a-e** and their conjugates **32a-e**. Although, peg-3HQ derivatives showed micromolar and in case of derivative **13d** sub-micromolar activity against CEM cells and good-to-moderate toxicity against other cell types (HCT116, K562 and

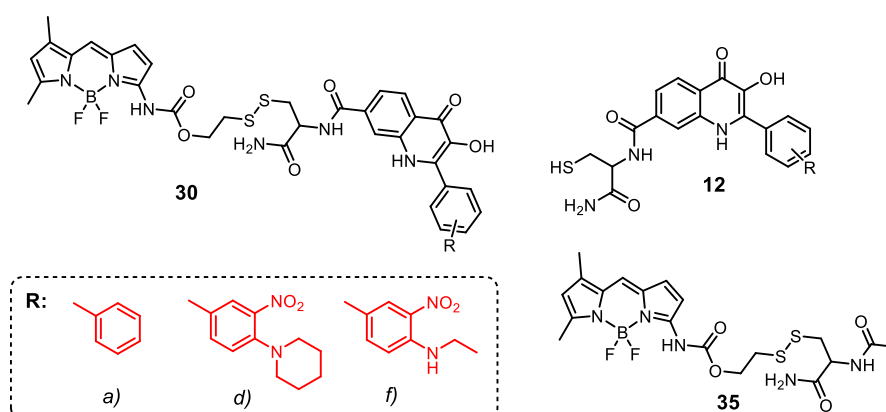
U2OS) they showed also substantial toxicity to healthy cell line MRC-5. The only exception was the compound **13e** which showed no toxicity probably due to its very low solubility. On the contrary, aminoBDP-peg-3HQ conjugates **32** retained the toxicity of peg-3HQs against cancer cells (CEM, K562, U2OS) and even demonstrated improved cytotoxicity to resistant cell lines (CEM-DNR, K562-TAX or HCT116-p53). Moreover, the toxicity to normal cell line MRC-5 was significantly lower. The higher toxicity of aminoBODIPY-peg-3HQ conjugates **32** corresponds with the previously obtained data from monitoring of GSH mediated cleavage inside the cells where these compounds were cleaved effectively even in the presence of native GSH concentrations (Figure 32). However, it is important to mention that unexpectedly also aminoBODIPY **4a** exhibited significant, non-specific toxicity to cancer cells (Table 7) and subtle toxicity to healthy MRC-5 cell line.



Code	IC50 (μM)									
	A549	BJ	CCRF-CEM	CEM-DNR	HCT116	HCT116 p53	K562	K562-TAX	MRC-5	U2OS
<b>12a</b>	50	50	50	50	50	50	50	50	50	50
<b>12b</b>	50	50	50	50	50	50	50	50	50	50
<b>12c</b>	50	50	50	50	50	50	50	50	50	50
<b>12d</b>	50	50	50	50	50	50	50	50	50	50
<b>12e</b>	50	50	50	50	50	50	50	50	50	50
<b>13a</b>	9.27	46.84	6.21	23.55	8.17	13.37	5.55	22.13	24.07	12.81
<b>13b</b>	50	50	9.1	45.19	32.31	33.71	50	43.49	41.79	50
<b>13c</b>	8.64	50	1.00	30.91	5.95	6.56	5.95	27.7	17.09	6.15
<b>13d</b>	13.13	50	0.39	7.6	3.35	3.55	4.55	7.04	7.62	13.06
<b>13e</b>	50	50	24.02	50	50	50	50	50	50	50
<b>32a</b>	11.55	50	1.99	15.3	10.39	9.66	6.83	19.23	43.31	8.69

<b>32b</b>	7.56	50	1.70	5.22	6.56	6.21	6.1	6.36	41.1	6.7
<b>32d</b>	3.2	50	0.45	7.97	2.85	2.07	1.94	9.79	50	2.41
<b>32e</b>	10.17	50	1.43	8.54	7.54	8.09	5.52	8.5	50	3.64
<b>30a</b>	50	50	19.73	34.42	50	50	49.82	39.77	50	50
<b>30b</b>	46.43	50	8.14	26.51	50	49.79	44.65	33.59	50	42.3
<b>30c</b>	50	50	2.59	40.09	50	50	41.43	41.83	50	50
<b>30d</b>	46.27	50	1.52	37.91	39.71	42.6	29.91	40.61	50	44.15
<b>30e</b>	50	50	50	46.25	50	50	50	46.16	50	50
<b>34a</b>	50	50	14.6	50	50	50	50	50	50	50
<b>34b</b>	50	50	6.37	50	50	50	50	50	50	50
<b>34c</b>	50	50	12.7	50	50	50	50	50	50	50
<b>34d</b>	50	50	50	50	50	50	50	50	50	50
<b>34e</b>	50	50	5.1	50	50	50	50	49.55	50	50
<b>31a</b>	50	50	3.01	50	12.9	9.76	7.09	50	50	48.98
<b>31c</b>	50	50	5.88	50	50	43.02	41.67	50	50	50
<b>4a</b>	47.2	50	4.25	5.08	11.56	12.74	3.29	6.41	40.11	19.8

**Table 7** IC<sub>50</sub> values of the prepared conjugates **30-32**, **34** and free 3HQs **12** and **13**.



Compound	$\Delta_r H_m^\circ$ (kJ mol <sup>-1</sup> )	$K_a^\circ$ (M <sup>-1</sup> )	n	$\Delta_r S_m^\circ$ (J mol <sup>-1</sup> K <sup>-1</sup> )	$\Delta_r G_m^\circ$ (J mol <sup>-1</sup> )
<b>12a</b>	-7997	4,722x10 <sup>6</sup>	0,981	-26696	-37587
<b>12f</b>	-9119	4,437x10 <sup>6</sup>	1,131	-30458	-37947
<b>12d</b>	-8247	4,199x10 <sup>6</sup>	1,221	-27536	-37141
<b>30a</b>	-15846	2,844x10 <sup>6</sup>	0,911	-53025	-36596
<b>30d</b>	-11378	5,373x10 <sup>6</sup>	1,378	-38035	-37864
<b>30f</b>	-15108	6,317x10 <sup>6</sup>	1,292	-50543	-38604
<b>35</b>	-4198	6,442x10 <sup>6</sup>	1,672	-13949	-39106

**Table 8** Determination of interaction of selected 3HQ conjugates with elongation factor eEF1A1 by ITC.

Some of the prepared Cys-3HQs and aminoBODIPY-3HQ conjugates were subjected for determination of interaction affinity to eukaryotic translation elongation factor eEF1A1 as a potential molecular target by isothermal titration calorimetry. The results shown in Table 8 suggest that free Cys-3HQs **12** and conjugates **30** strongly bind to elongation factor (high values of  $\Delta H$  and  $\Delta S$ ) whereas the compound **35** with N-acetyl cysteamide instead of 3HQ showed no or very little affinity to protein (small values  $\Delta H$  and  $\Delta S$ ).

## 2.2 Second generation conjugates

Next aim of the project was to develop such compounds that would bear multiple moieties including drug, fluorescent dyes and/or targeting moieties (CPPs, CTPs) connected with aminoBODIPY by disulfide bond for GSH responsive system and “OFF-ON” fluorescence monitoring. Various approaches to prepare such conjugates were attempted as depicted in Figure 35. As a logical continuation of the first generation of conjugates, simple prolongation of peptide chain on 3HQs seemed to be the most straightforward route (Approach A, Figure 35).

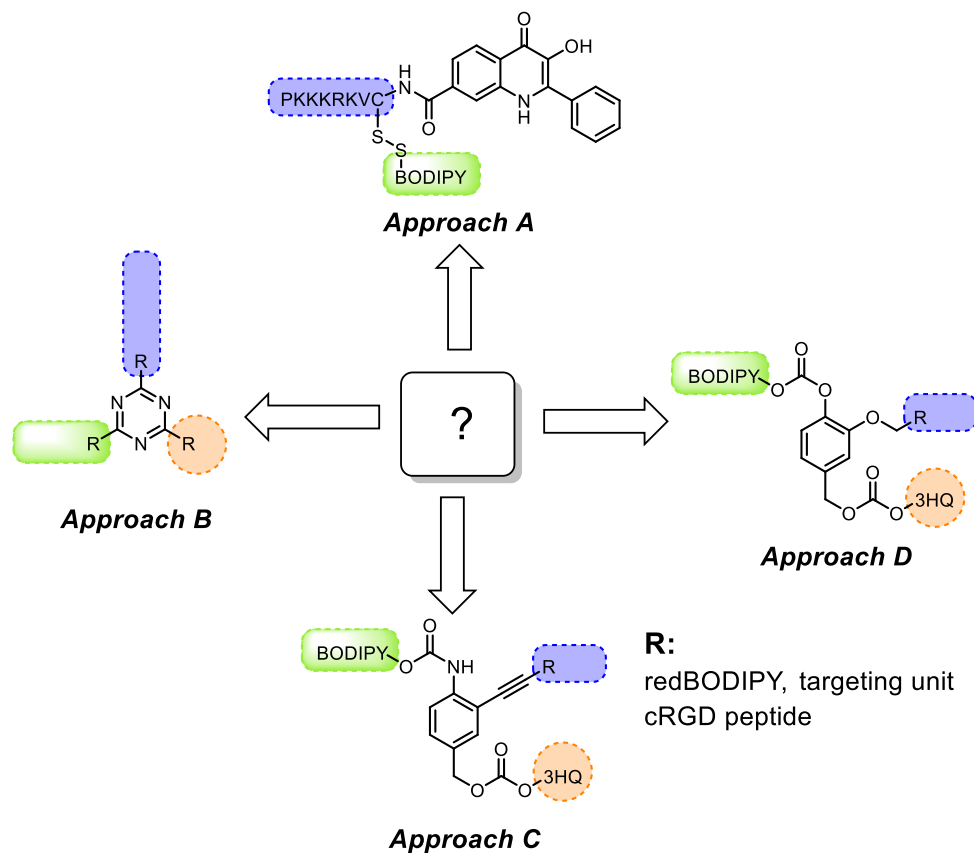


**Figure 35** Approaches towards conjugates with three-component central unit.



By the **Approach A** several compounds with PKKKRKV cell penetrating peptide and different spacers were synthesized and tested for cytotoxicity. However, these compounds lacked the central unit capable of simultaneous releasing of the free drug. As a consequence, the CPP-SS-BDP-3HQ conjugates **38a-d** exhibited only poor toxicity against CEM, CEM-DNR, K562 and K562-TAX cell lines (Table 10, Biology chapter). Therefore, this approach was abandoned and more emphasis was focused on finding suitable “smart” central unit.

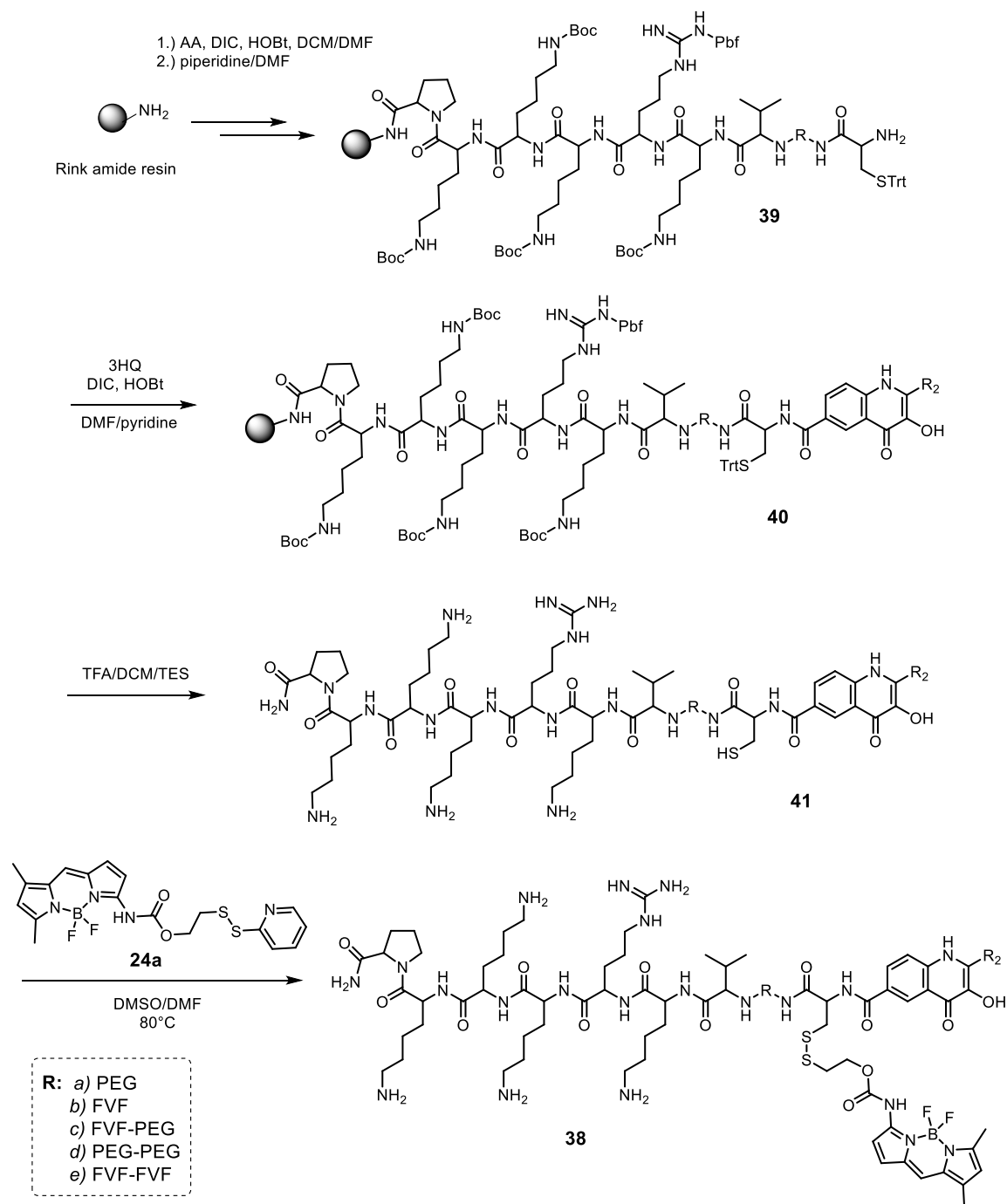
**Approach B** in which derivatization of cyanuric chloride with various amines results in branched scaffolds has been employed previously in numerous research items e.g., by Ojima.<sup>147</sup> This system would potentially offer feasible way for incorporation of three components – a drug, BODIPY dyes or targeting unit. However, preliminary unsuccessful modifications of cyanuric chloride with disulfide linkers and poor design of the final conjugates - two equal disulfide linkers had to be used in order to cleave both BODIPY dye and 3HQ discouraged us from further continuation of this route. Moreover, overwhelmed by the beauty and simplicity of azaquinone-methide central unit (aQM) we invested effort in synthesis of such “smart” central unit which would be “triggered” by stimulus event and electron push would finish the release of the free, unchanged drug (**Approach C and D**). **Approach C** involved modification of central unit by Heck or Sonogashira coupling reactions in which only latter led to efficient synthesis of the final molecule. Despite the synthetic success of the **Approach C**, we continued in the synthesis due to very slow cleavage and subsequent slow liberation of 3HQ in the presence of GSH as demonstrated by LCMS analysis (see chapter 2.2.4). The final conjugates with higher cleavage rate of 3HQ were then synthesized via **Approach D** with use of quinone-methide central core (Figure 35).

### 2.2.1 Synthesis

#### ***Approach A***

Synthesis of the compounds CPP-(BODIPY)-3HQ **38** (Scheme 18) was mainly based on the previous synthesis of BODIPY-3HQ conjugates **30**. Peptides **39** of the sequence PKKKRKV with different hydrophobic (FVF) and hydrophilic (PEG) spacers with the cysteine ending were synthesized by solid phase chemistry approach on Rink amide resin using DIC/HOBt protocol. 3HQs were attached to the peptide on the resin by DIC/HOBt in the solvent mixture DMF/pyridine (1:1) affording resins **40**. After the cleavage and deprotection of trityl group by TFA/DCM/TES mixture the peptide-3HQ **41** was isolated by precipitation and repeated

trituration in Et<sub>2</sub>O. AminoBODIPY was attached to the peptide-3HQ in disulfide exchange reaction with the linker **24a** to obtain the final conjugates **38** (Scheme 18). In some cases, optimization of reaction conditions was necessary as the reaction in PBS/DMF mixture led to high extent of side product with mercaptopyridine attached instead of aminoBODIPY. Water-free solvent DMF/DMSO afforded the desired products and only low extent of mentioned side product. All compounds were purified by preparative HPLC with acidic mobile phase (0.1% TFA/MeCN).



**Scheme 18** Synthesis of PPKKRKV-aminoBODIPY-3HQ conjugates **38a-e**.

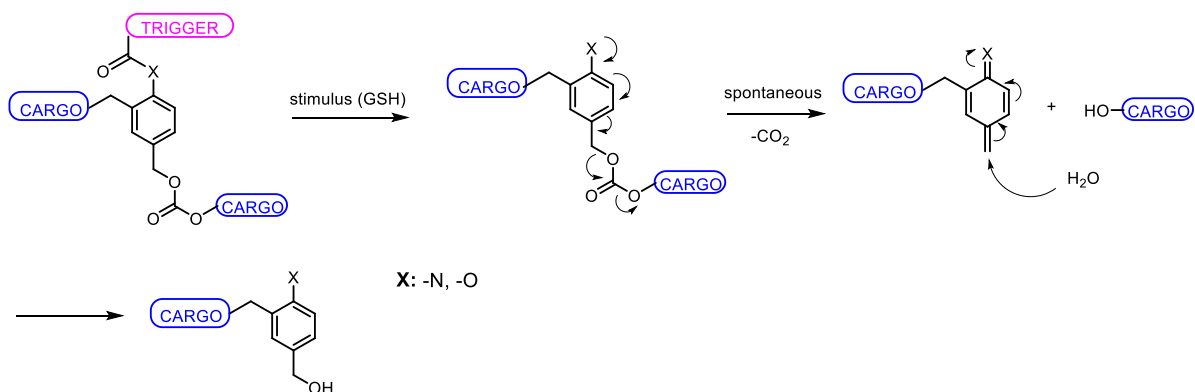
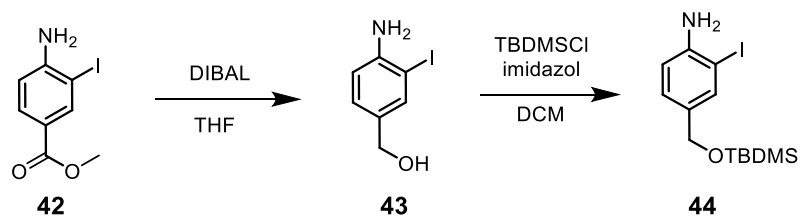


**Figure 36** Quinone-methide elimination.

### Approach C

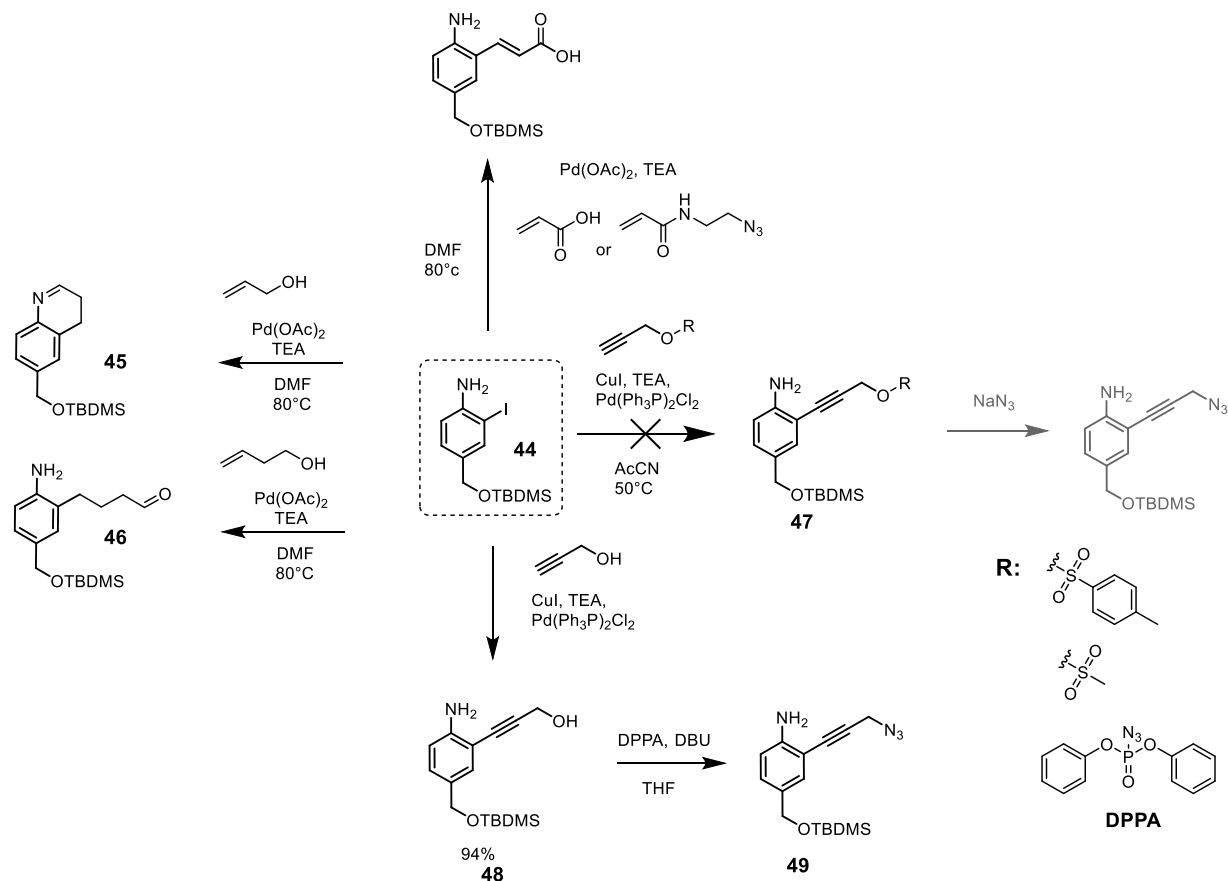
Aza-quinone methide (Approach C) and quinone methide linkers (Approach D) function as stable spacers between an enzyme- or reagent- responsive group and a reporter moiety, drug molecule and can undergo 1,4-, 1,6-, or 1,8-type elimination reactions after cleavage of the triggering group (Figure 36). Such reactivity results in the release of the reporter group through formation of a quinone-methide species. This approach has been applied in the development of multiple self-immolative dendrimers and molecular amplifiers, fluorescent turn-on probes etc.<sup>148–150</sup> We designed system utilizing this scaffold in order to prepare targeted, self-immolative and fluorescent theranostic compounds. Synthesis starts with already described preparation of compound **44** in two step synthesis – first step involved reduction of ester **42** to the primary benzylalcohol **43** which was protected by TBDMS group in the second step to obtain compound **44** (Scheme 19).<sup>151,152</sup>



**Scheme 19** Synthesis of central unit intermediate **44**.

The following coupling reaction with intermediate **44** was attempted by Heck or Sonogashira coupling reaction. Sonogashira coupling proved to be more feasible as complications in the Heck pathway occurred in the following incorporation of aminoBODIPY disulfide linker **27**. Heck coupling with allyl alcohol and 4-butenol resulted in formation of cyclized product **45** or aldehyde **46**, respectively (Scheme 20). Sonogashira coupling with tosyl or mesyl propargyl alcohol to intermediate **47** did not proceed, resp. decomposition of starting material was observed. Therefore, synthesis of the compound **49** was accomplished by

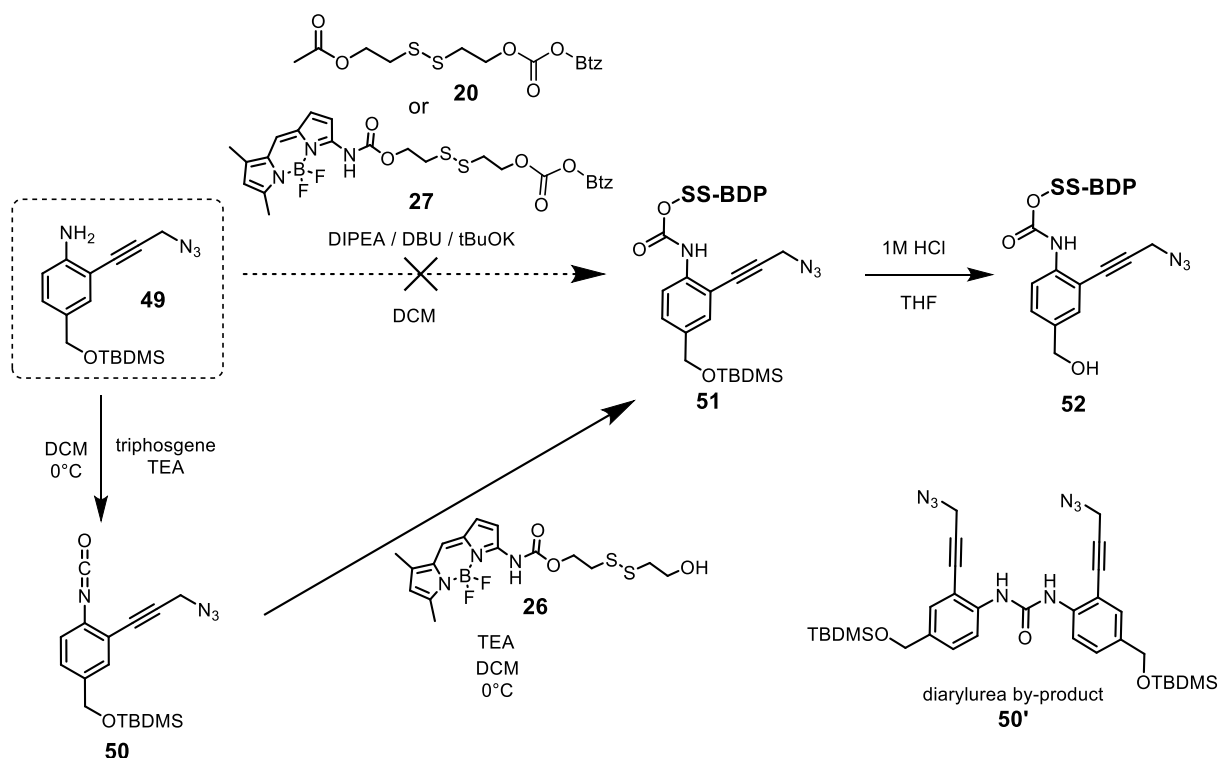
Sonogashira coupling of non-protected propargylalcohol with the intermediate **44** followed by the reaction with 1.0 equivalent of diphenyl phosphoryl azide (DPPA) with alcohol **48** in the presence of excess of DBU (Scheme 20) which gave desired product in excellent yield (93 %) and purity.



**Scheme 20** Modification of central unit via Heck or Sonogashira coupling.

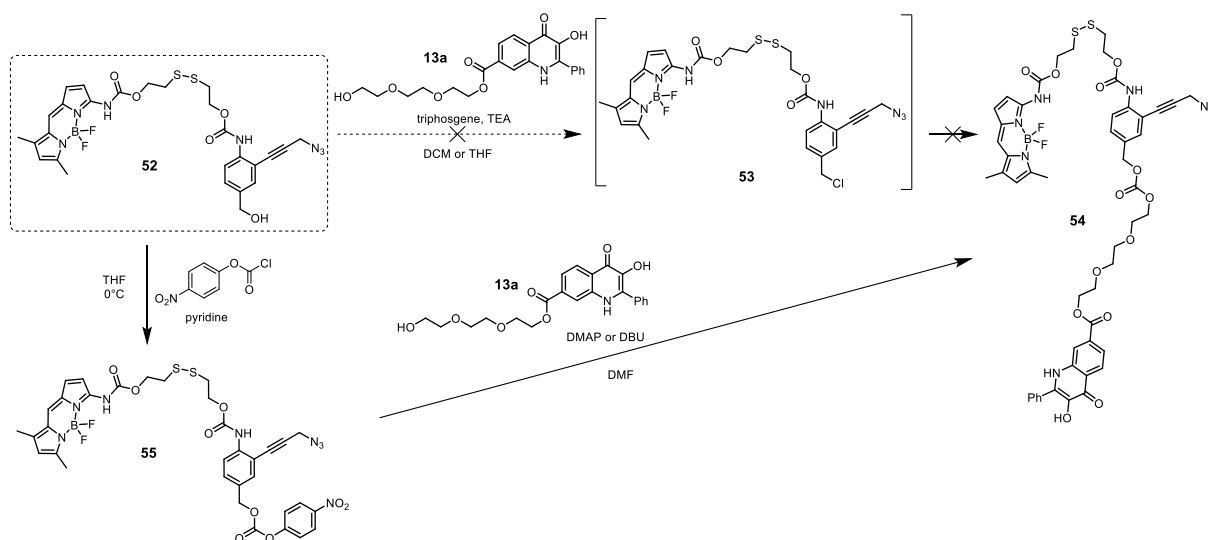
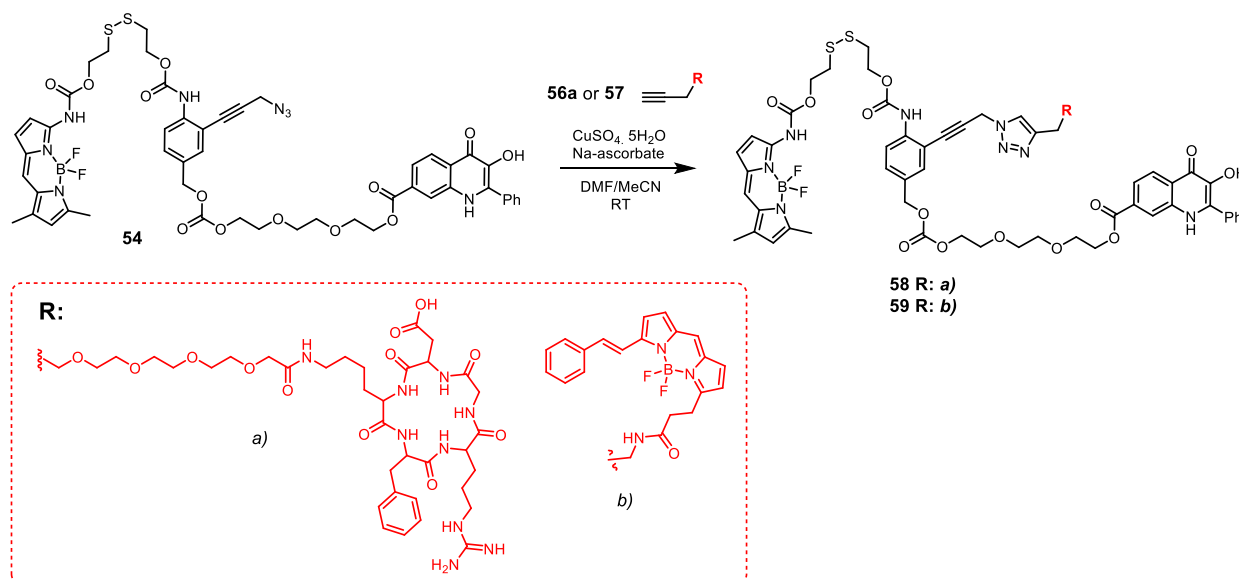
In the next step amino-BODIPY with disulfide linker was attached to the amino group of the compound **49** to form „triggering unit“ for GSH-mediated cleavage. As a first choice, reaction of modified aminoBODIPY linker **27** or acetyl-disulfide linker **20** were attempted. However, after many unsuccessful attempts with different bases (DIPEA, NaHCO<sub>3</sub>, DBU, *t*-BuOK) we switched the strategy and firstly reacted the intermediate **49** with triphosgene to obtain isocyanate **50**. Addition of the solution of starting amine **49** together with the base (TEA) slowly to the cooled solution of triphosgene was absolutely necessary to prevent the formation of diarylurea. Subsequent reaction with BDP-SS-OH **26** may be performed as a one pot two-step reaction without previous isolation of isocyanate **50**. However, in both cases the formation of product **51** was incomplete and addition of excess of isocyanate was necessary. However, yields of this reaction after purification by column chromatography were usually low between 25-42 %. Subsequent deprotection of TBDMS protecting group was accomplished by stirring

the solution of **51** in THF with 1M HCl and reaction was usually complete in 2 h with good yields (69 %) of benzylalcohol **52** after isolation (Scheme 21).



**Scheme 21** Installation of aminoBODIPY to central unit via disulfide linker.

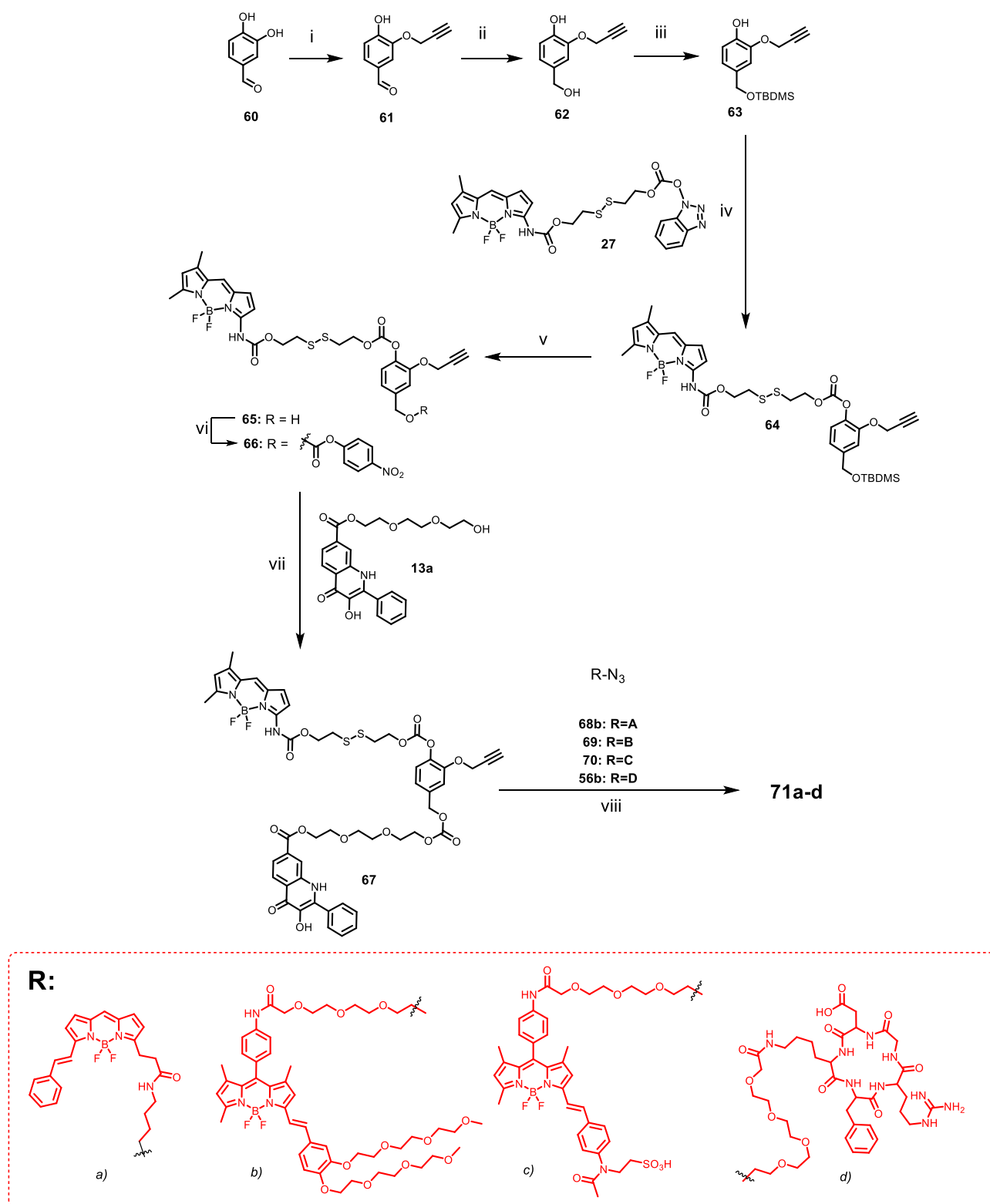
Implementation of PEG-3HQ **13a** to the central aza-quinone methide core was performed by the two-step protocol (Scheme 22). Firstly, utilizing triphosgene to form carbonate bond was attempted but led only to formation of benzylchloride **53** if triphosgene was added to benzylalcohol **52**. Very low conversion to the desired product **54** was obtained when triphosgene was added to the solution of 3HQ-peg-OH **13a** and then treated with benzylalcohol **52**. Second protocol involved firstly activation of benzyl alcohol **52** with 4-nitrophenylchloroformate to 4-nitrophenylcarbonate **55** followed by substitution with 3HQ-peg-OH **13a** in the presence of DMAP and furnished desired product **54** in approximately 25% yield over two steps after purification by column chromatography (Scheme 22). In the last step of the synthesis the azide intermediate **54** was decorated by cRGD peptide **56** or redBODIPY **57** in the Cu(I) catalyzed click reaction to obtain the final products **58** or **59** (Scheme 23) This approach allows simple and efficient decoration of the final compounds by various targeting, fluorescent or other moieties in the last step. However, it is important to mention that both starting compounds had to be purified prior to click reaction as the possible impurities from previous reaction blocked the click reaction completely.

Scheme 22 Synthesis of aminoBODIPY-3HQ intermediate **54**.Scheme 23 Synthesis of alkynyl aminoBODIPY-3HQ conjugates **58** and **59**.

### Approach D

This approach utilized similar chemistry as the previous Approach C but uses quinone methide instead of aza-quinone methide as a central core to provide a comparison of the GSH-mediated cleavage rate. The synthesis starts with preparation of compound **63** from 3,4-dihydroxybenzaldehyde **60** by recently published procedure<sup>153</sup> in the three step synthetic pathway (Scheme 24). The first step involves attachment of propargyl group by reacting with propargyl bromide with NaH to afford intermediate **61** followed by reduction of aldehyde with NaBH<sub>4</sub> to obtain benzylalcohol **62**. Treatment with TBDMSCl led to the protection of hydroxy group to afford intermediate **63**. The next incorporation of aminoBODIPY disulfide linker with

BDP-SS-OBtz activated carbonate **27** worked smoothly and afforded the intermediate **64** in 85 % yield. Subsequent deprotection of TBDMS under acidic conditions worked quantitatively to afford benzyl alcohol **65** which was further transformed to activated 4-nitrophenylcarbonate **66**. Similarly to the previous approach, intermediate **66** was treated with 3HQ-peg-OH **13a** in the presence of excess of DIPEA to afford intermediate **67** in moderate yields after purification by column chromatography. Lastly, Cu(I) catalyzed click reaction with various redBODIPY **68-70** and cRGD peptide **56b** led to final compounds **71a-d** typically in full conversion and good-to-moderate yields on 10-40 mg scale after purification by preparative HPLC. RedBODIPYs **68-70** were designed to bear groups with different hydrophilicity increasing in order: phenyl < PEGchains < SO<sub>3</sub>H (**68** < **69** < **70**). Different BODIPYs were introduced in order to increase the water solubility of final conjugates as well as to study the influence on FRET efficiency and fluorescence monitoring.



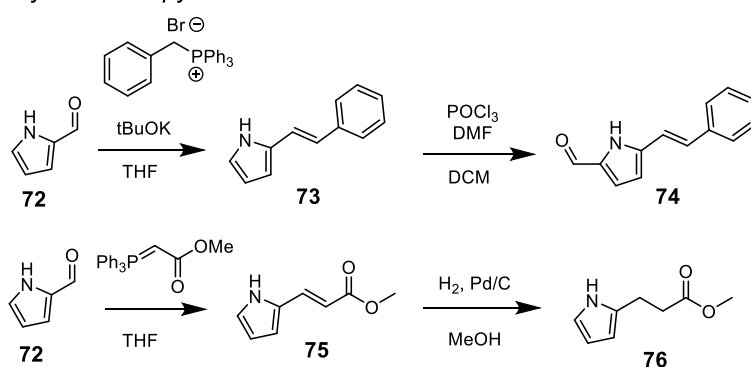
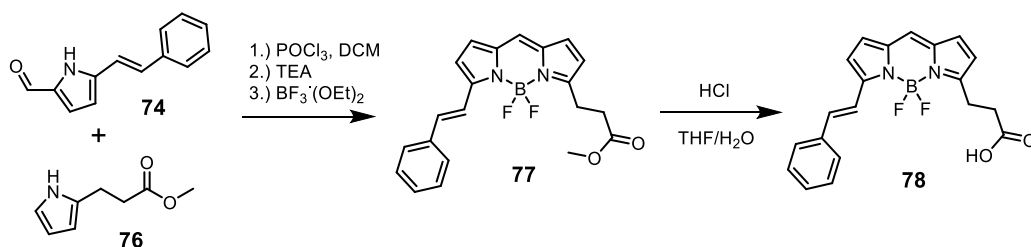
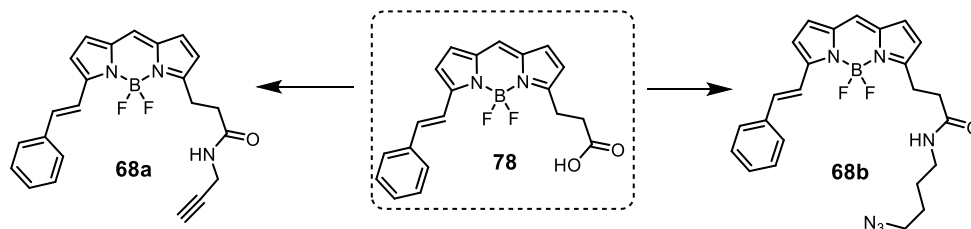
Scheme 24 Synthesis of conjugates 71a-d.

## 2.2.1.1 RedBODIPY synthesis

In order to shift the excitation and emission of BODIPY core to establish efficient FRET pair the  $\pi$ -conjugation was enlarged by introducing additional phenyl ring in the position C-3.



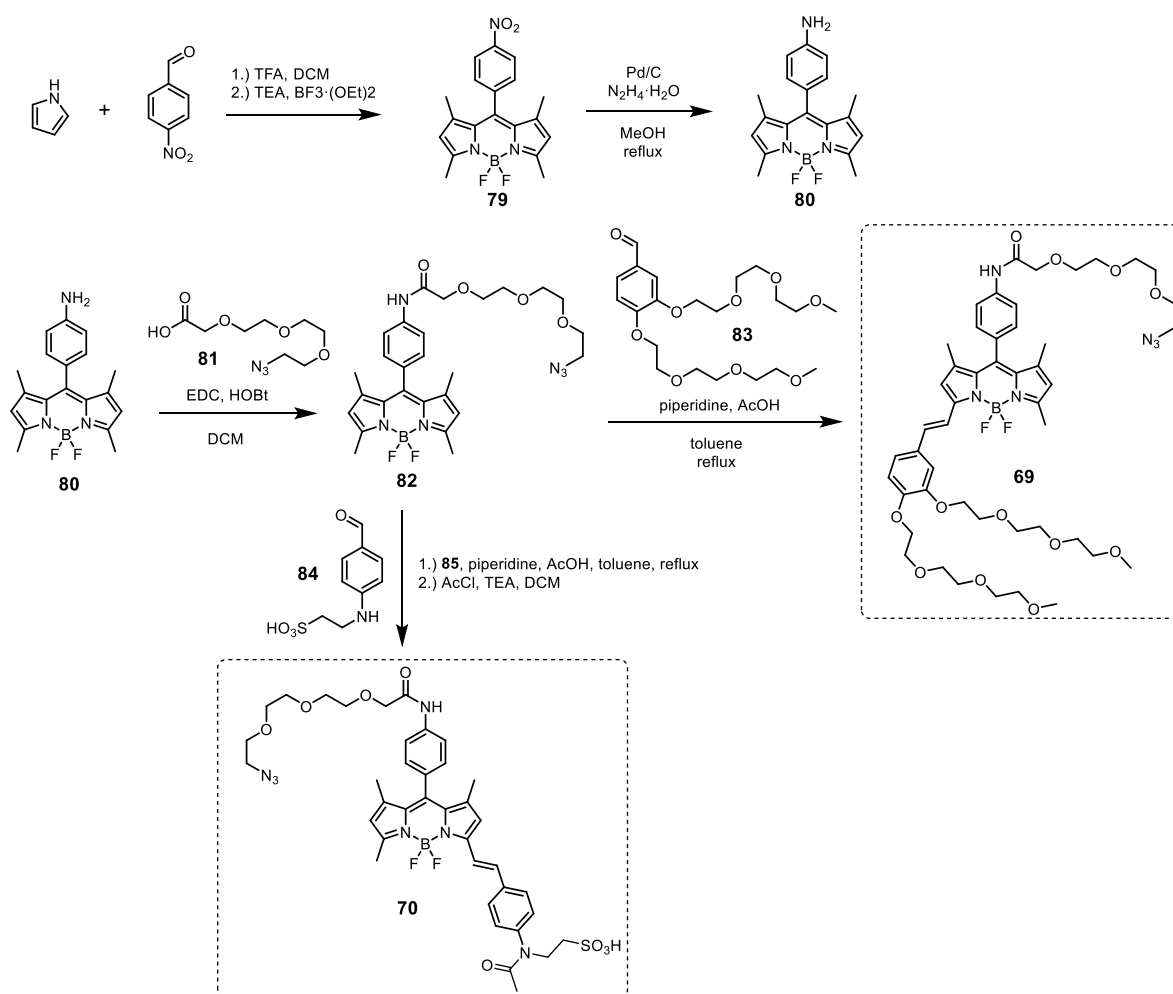
Corresponding pyrroles **74** and **76** were synthesized by previously described procedures in two step syntheses starting from pyrrole-2-carboxaldehyde **72** via Wittig reaction to afford intermediates **73** or **75** (Scheme 25).<sup>154</sup> Further Vilsmeier-Haack formylation of intermediate **73** provided aldehyde **74**. Reduction of double bond in intermediate **75** by Pd/C catalyzed hydrogenation afforded pyrrole **76**. Pyrroles **74** and **76** were subsequently condensed in the presence of POCl<sub>3</sub> and complexed with BF<sub>3</sub>·OEt<sub>2</sub> to the desired redBODIPY methylester **77**. Followingly the intermediate **77** was hydrolyzed under acidic conditions to the free acid of redBODIPY **78** and modified by propargylamine or 4-azidobutanamine to amides **68** and **69** for further click reaction (Scheme 25 C).

**A Synthesis of pyrroles****B Synthesis of redBODIPY 78****C Modification of red BODIPY**

**Scheme 25** Synthesis and modification of redBODIPY **78**.

Other two BODIPY dyes **69** and **70** used in the preparation of the conjugates **71** were synthesized by the different approach summarized in the Scheme 26. Synthesis started with the preparation of BODIPY-NH<sub>2</sub> **80** according to the literature in the two-step synthesis starting

with the condensation of pyrrole and 4-nitrobenzaldehyde to obtain BODIPY **79**. Following Pd/C catalyzed reduction of nitro group by hydrazine afforded intermediate **80**. In the next step azidoPEG chain was introduced on amino group and the resulting intermediate **82** was further modified by Knoevenagel condensation with corresponding benzaldehydes **83** or **84** affording redBODIPYs **69** and **70**. Typically, this reaction proceeded slowly and always mono and di-alkylated products were obtained in moderate yields. In the case of redBODIPY **70** further acylation of aminogroup with AcCl of amino group was necessary to block the pH influence on the fluorescence.

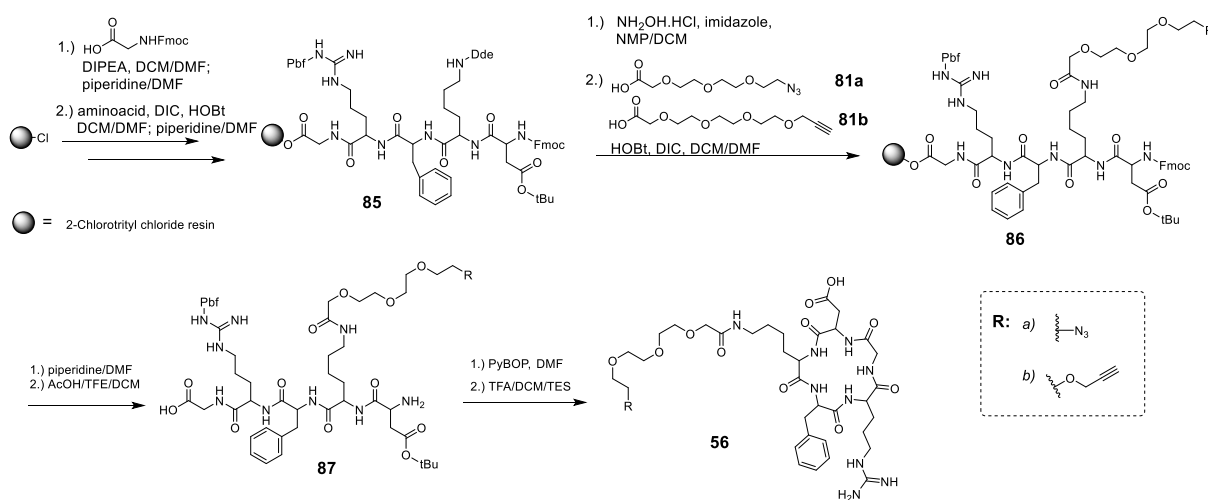


**Scheme 26** Synthesis of hydrophilic redBODIPYs **69** and **70**.

### 2.2.2 cRGD synthesis

Integrin targeting cRGD peptides **56a,b** were synthesized by the slightly modified literature procedure on 2-chlorotrityl resin (Scheme 27). The first amino acid – Fmoc-Gly-OH was immobilized on the resin in the presence of the base DIPEA for 16 h. Next amino acids Arg, D-Phe, Lys and Asp were introduced by the standard DIC/HOBt protocol using 50%

piperidine in DMF for the Fmoc deprotection to afford resin **85**. Following, the Dde protecting group on lysine was deprotected by  $\text{NH}_2\text{OH}/\text{imidazole}$  mixture in NMP orthogonally to Fmoc group and the resulting amino group was acylated by the azido-PEG chain **81** to obtain intermediate resin **86**. Further deprotection of the Fmoc and cleavage of the protected peptide chain from the resin by  $\text{AcOH}/\text{Trifluoroethanol}/\text{DCM}$  mixture gave the linear peptide **87** which in the next reaction was intramolecularly cyclized and deprotected by  $\text{TFA}/\text{DCM}/\text{TES}$  mixture to free cyclic RGD peptide **56**. cRGD peptides **56a** and **56b** were purified by preparative HPLC prior to use.



**Scheme 27** cRGD peptide synthesis and modification.

### 2.2.3 Fluorescent properties and GSH-cleavage

According to the previously described results, the acylaminoBODIPY in conjugates **71a-d** and the released aminoBODIPY **4a** should differ significantly in excitation wavelengths, while the emission maxima should remain almost identical (see chapter 2.1.5). To demonstrate this feature, we compared the excitation and emission spectra of the cRGD-aminoBODIPY-3HQ conjugate **71d** and aminoBODIPY **4a**. As shown in Figure 37 A, the spectral properties are expectedly similar to the previously described 1<sup>st</sup> generation system, allowing the “OFF-ON” ratiometric drug release monitoring.

In the case of conjugates **59** and **71a-c** (aza-QM and QM conjugates), the emission of aminoBODIPY is expectedly transferred to redBODIPY, and the emission at approximately 595 nm is observed (Figure 37 B) in DMSO/HEPES buffer. However, arguably due to the hydrophobic character and low water solubility, despite the attached ethyleneglycol chains on redBODIPY **69** or  $-\text{SO}_3\text{H}$  group on **70**, the FRET efficiency drastically dropped in HEPES buffer. The effect of hydrophobicity of redBODIPY dyes is demonstrated in the Figure 37 C-E. Incremental addition of DMSO into the HEPES buffer (pH 7.4) solution of conjugates **59**

and **71-b,c** with different redBODIPY dyes **68a**, **69** and **70** respectively, probably resulted in better solvation and increased efficiency of FRET fluorescence. Conjugate **71c** with redBODIPY decorated with presumably more hydrophilic SO<sub>3</sub>H group showed at least two times higher efficiency compared to the conjugate **71b** with PEG decorated redBODIPY **69** in the same media (e.g. 50% DMSO). However, we did not continue further cleavage and biological experiments with conjugate **71c** due to low amount of compound available and difficulties in its synthesis. FRET efficiency of conjugate **71b** was determined as 72 % in DMSO/HEPES (2:1) buffer.

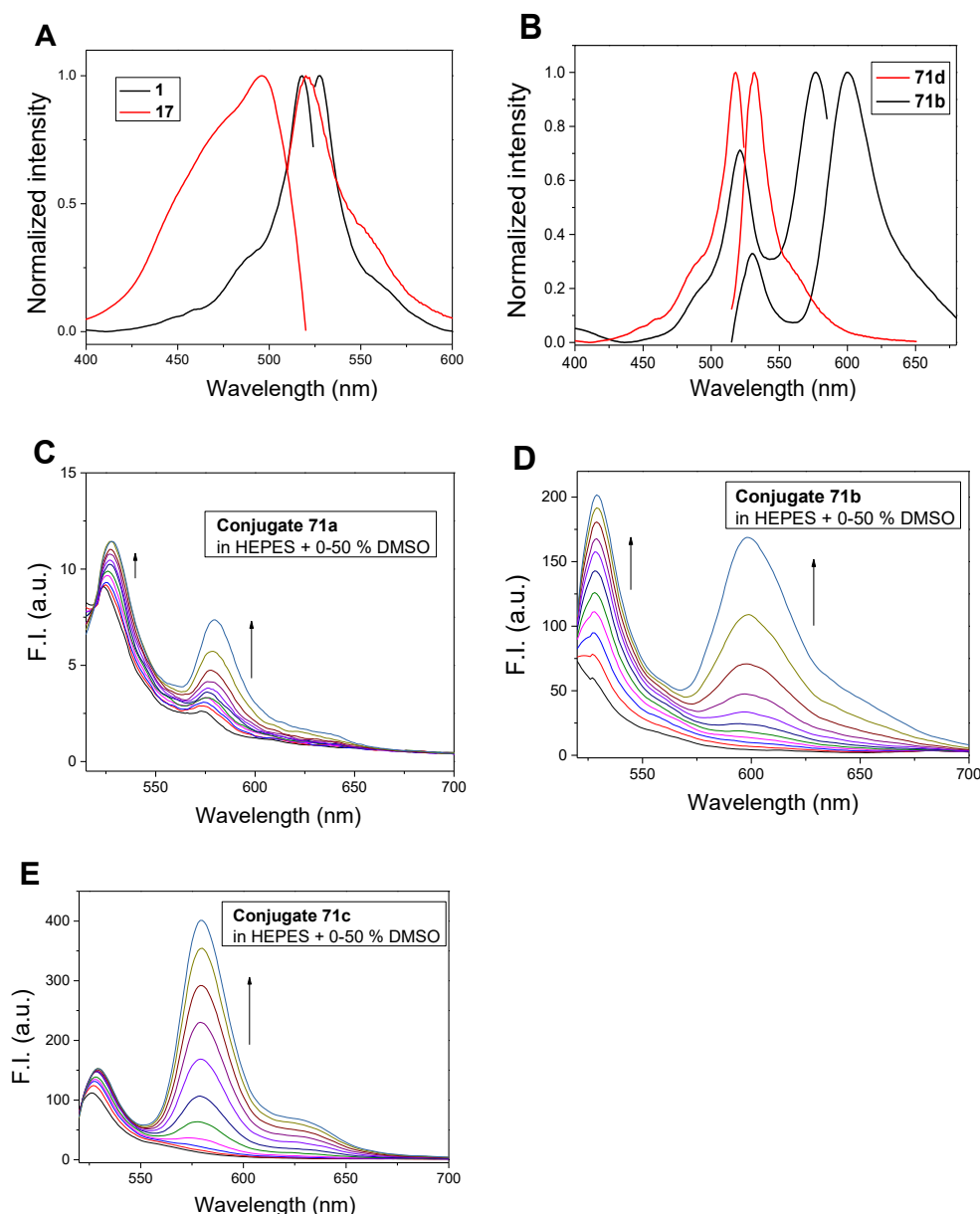
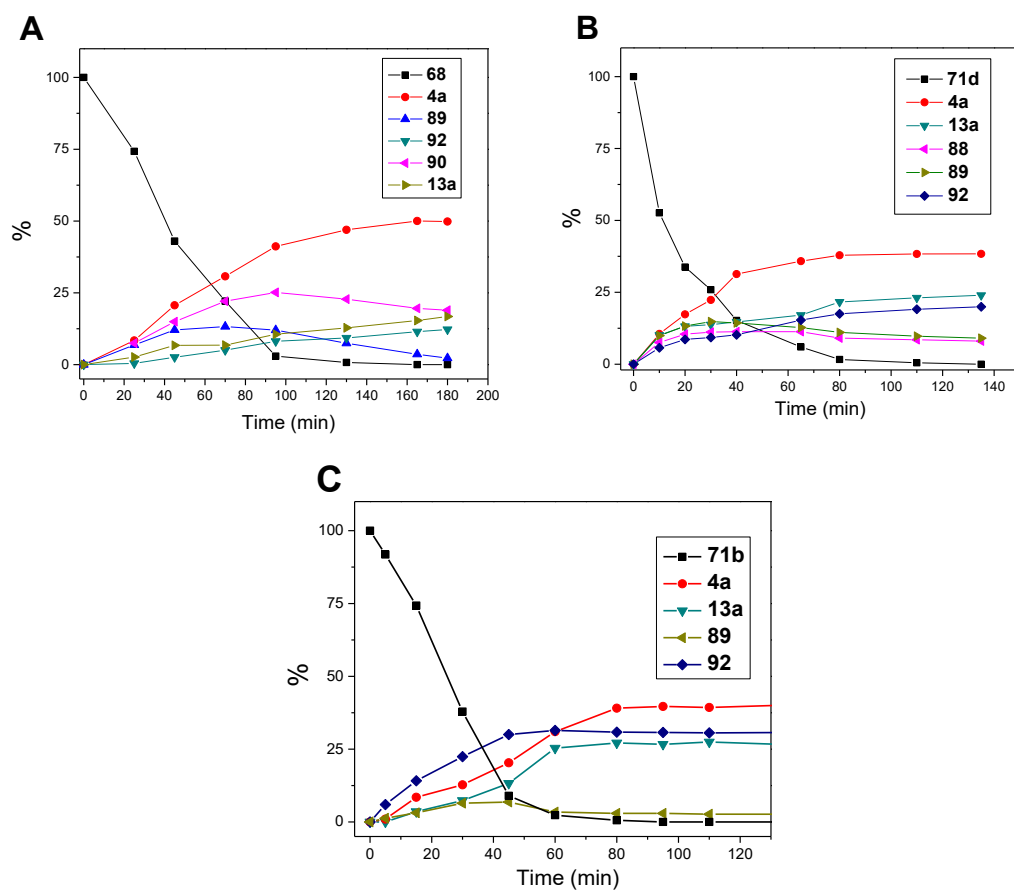
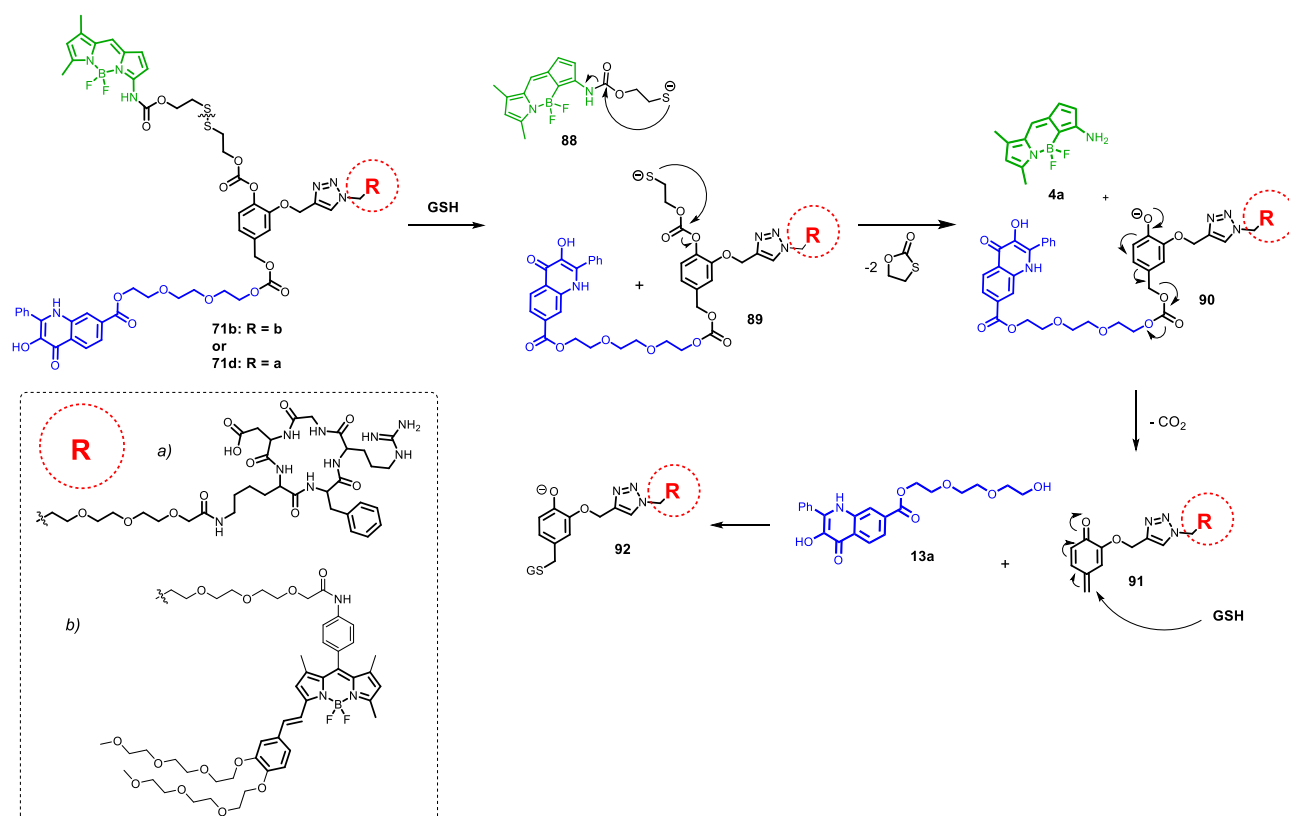


**Figure 37** (A) Normalized excitation and emission spectra of conjugate **71d** and aminoBODIPY **4a** (HEPES buffer, 0.1 M, pH 7.4), (B) conjugate **71b** and conjugate **71d** (DMSO/HEPES buffer 0.1 M, 2:1, pH 7.4). Change of FRET efficiency by incremental addition

of DMSO to HEPES solution of (C) conjugate **71a**, (D) conjugate **71b** and (E) conjugate **71c**. Excitation wavelength  $\lambda_{\text{exc}} = 510$  nm.

To prove the ability of a fluorescence monitoring of the prepared conjugates **58**, **59** and **71a-d** GSH-mediated cleavage and the rate of subsequent liberation of the drug we performed GSH cleavage experiments with LC/MS and fluorescence detection in HEPES buffer and DMSO/HEPES buffer (2:1), in which conjugate **71b** exhibits adequate FRET. GSH concentration used in our experiments was in the range normally found in cancer cells (up to 5mM).<sup>155,156</sup>

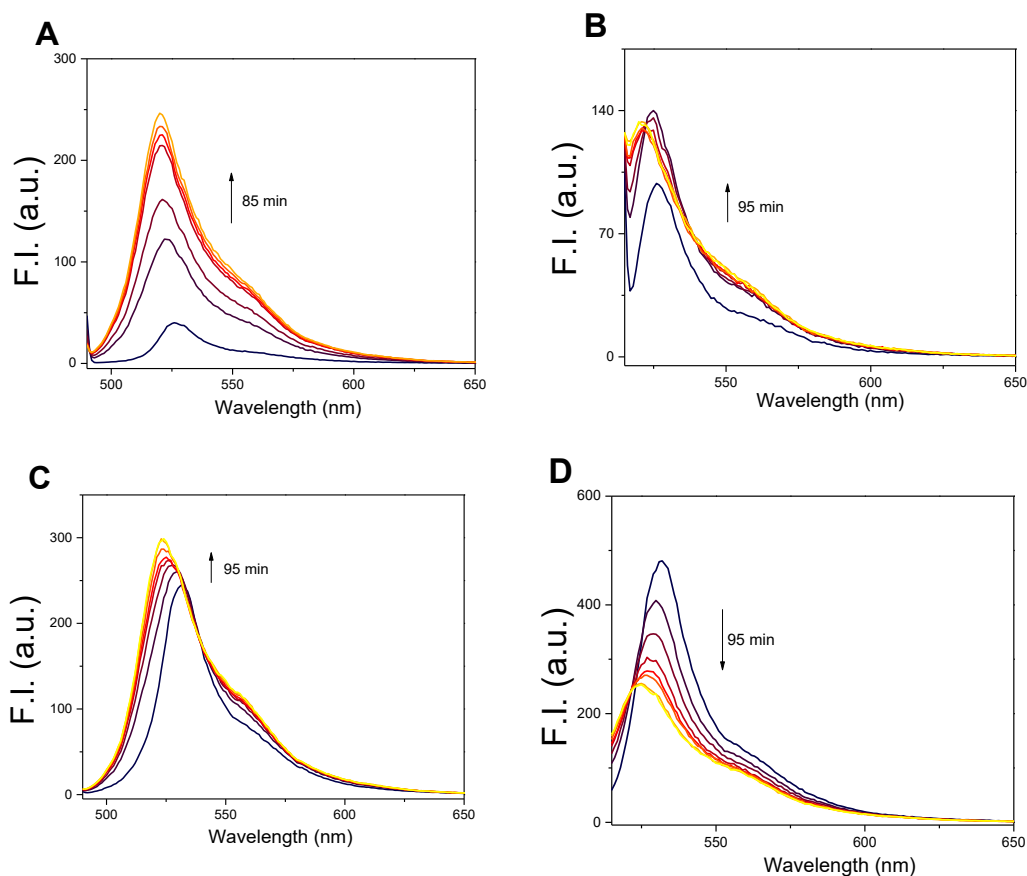
The data from LC/MS (Figure 38) show the full cleavage of conjugates **68** and **71b,d** within 100, 80 and 60 minutes, respectively, along with the formation of the aminoBODIPY **4a**. Intermediates **89** that formed during the cleavage were common for all three conjugates. In the case of conjugate **68** with aza-QM central core the cleavage was the slowest, high quantity of intermediate **89a** and **90a** was formed and only slow transformation to the final cleaved product **92a** was observed. Cleavage of the conjugates **71d** and **71b** led also firstly to the detectable quantity of the intermediate **89** which was almost fully converted to final products in both cases during the cleavage time 3 h. Therefore, we assume that the rate determining step – linker self-immolation, electron shift and subsequent elimination of 3HQ is slowed down in the aza-QM central core and thus we expected lower cytotoxicity during biological screening.



**Figure 38** Mechanism of GSH cleavage of conjugate **71b,d**. GSH-mediated cleavage of the conjugate (A) **68** (0.5 mM, 5 mM GSH, DMSO/HEPES buffer 0.1 M, 2:1, 37 °C), (B) conjugate

**71b** and (C) **71d** (0.5 mM, 2 mM GSH, DMSO/HEPES buffer 0.1 M, 2:1, 37 °C), with the detection of resulting products by LC/MS.

Upon subjecting conjugate **71d** to 5 mM GSH, the rapid liberation of aminoBODIPY **4a** via disrupting of the disulfide bond and the self-immolative elimination of thiolactone caused the increase of the fluorescence intensity at 530 nm after excitation at 485 nm in HEPES as well as HEPES/DMSO (2:1) mixture (Figure 39 A and C). In contrast, the emission intensity at 530 nm after excitation at 510 nm, belonging to the conjugate, slightly increases with time in HEPES but decreases in DMSO/HEPES mixture 2:1 (Figure 39 B and D). When the ratio of the emission intensities at 530 nm after excitation at 485 nm and 510 nm (herein  $I_{485}/I_{510}$ ) is followed in time, it is possible to detect that the conjugate is fully cleaved. In HEPES buffer conjugate **71d** is cleaved within approximately 50 minutes, as indicated by reaching the plateau formation. The cleavage in DMSO/HEPES (2:1) mixture is slightly slower. In addition, the cleavage is accompanied by significant 6-fold change in the  $I_{485}/I_{510}$  ratio in HEPES buffer or smaller 2.5-fold change in DMSO/HEPES (2:1) mixture (Figure 39 E).



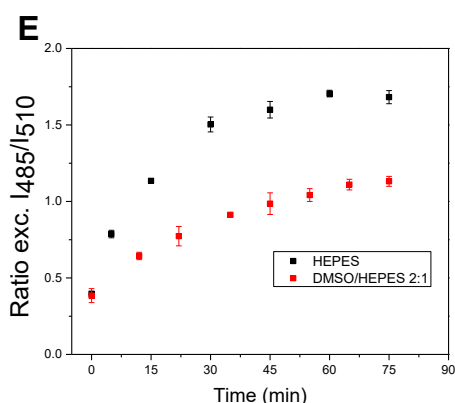


**Figure 39** (A) Fluorescence spectra of GSH-mediated cleavage (5 mM GSH) of conjugate **71d** (5  $\mu$ M) upon excitation at 485 nm or (B) 510 nm in HEPES buffer (0.1 M, pH 7.4). (C) Fluorescence spectra of GSH-mediated cleavage (5 mM GSH) of conjugate **71d** (5  $\mu$ M) upon excitation at 485 nm and (D) 510 nm in DMSO/HEPES buffer (0.1 M, 2:1, 37  $^{\circ}$ C). (E) Schematic representation of ratiometric change of fluorescence intensities at 530 nm after excitation at 485 nm and 510 nm ( $I_{485}/I_{510}$  ratio). Slit widths 2.5, 2.5.

Apart from the aminoBODIPY conjugate **71d** the conjugates **71a-c** carry the additional dye – red BODIPY – designed for efficient FRET. As demonstrated on conjugate **71b** in Figure 40, before the GSH-mediated cleavage of conjugate **71b** the system affords the fluorescence of the redBODIPY ( $\lambda_{em} = 595$  nm) upon the excitation of aminoBODIPY ( $\lambda_{exc} = 510$  nm) due to the effective FRET transfer. During the cleavage, the green emission (530 nm) of the released aminoBODIPY **4a** appears and increases with time (A). When the ratio of both emissions at 530 nm and 595 nm (herein  $I_{530}/I_{595}$ ) upon excitation at 510 nm is followed within the time, the plateau is achieved in approximately 30 minutes. The fluorescence response (emission ratio  $I_{530}/I_{595}$ ) enhancement in this case is particularly higher than in the case of conjugate **71d** and stands for almost one order increase (B).

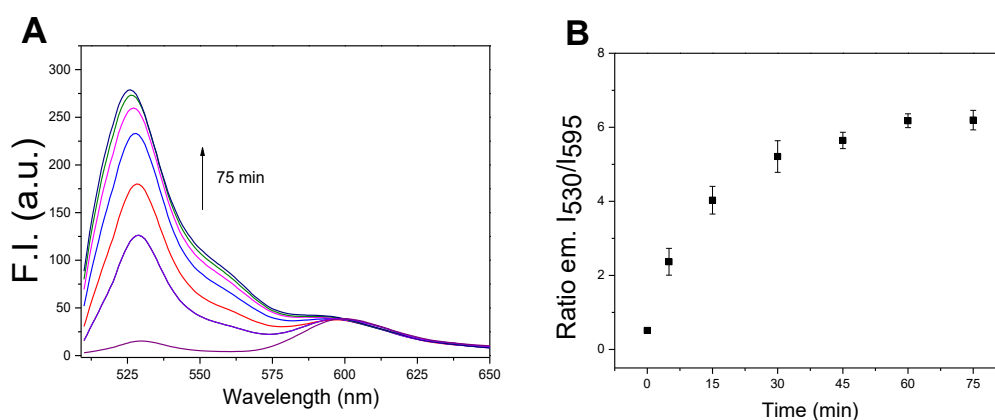


**Figure 40** (A) Fluorescence spectra of conjugate **71b** (1  $\mu$ M) during GSH-mediated cleavage (3 mM GSH) upon excitation at 510 nm and (B) schematic representation of the ratiometric change of  $I_{530}/I_{595}$  emissions ratio (3 mM GSH, DMSO/HEPES buffer 0.1 M, 2:1, 37  $^{\circ}$ C).



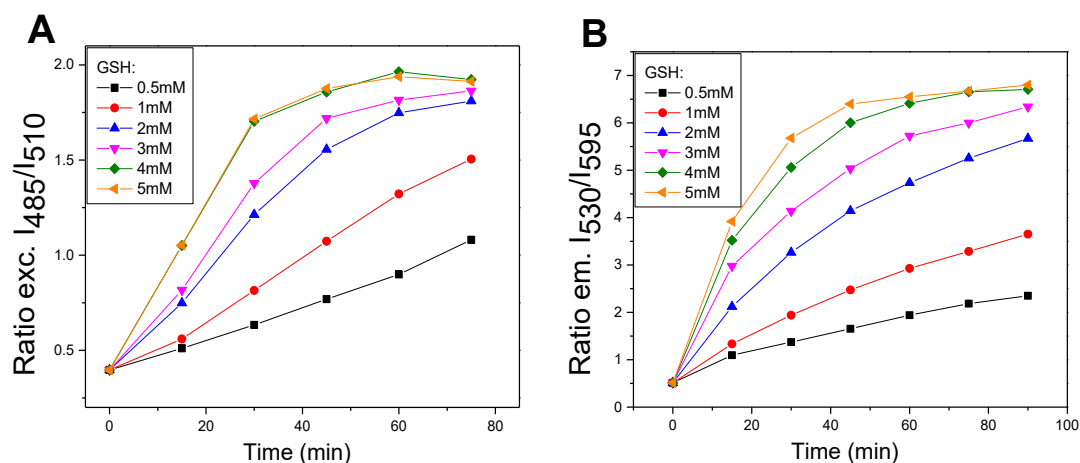


**Figure 41** (A) GSH concentration influence on the rate of the cleavage of conjugate **71d** (1  $\mu$ M, HEPES buffer, 0.1 M, pH 7.4, 37  $^{\circ}$ C) demonstrated by the ratio of the emission intensities at 530 nm after excitation at 485 nm and 510 nm ( $I_{485}/I_{510}$ ) and (B) conjugate **71b** (1  $\mu$ M, DMSO/HEPES buffer 0.1 M, 2:1, 37  $^{\circ}$ C) demonstrated by the ratio of the fluorescence intensities at 530 nm and 595 nm ( $I_{530}/I_{595}$ ) after excitation at 510 nm. All data points were measured in 3 replicates with SD ranging up to 5 %.

Figure 41 together with Table 9 summarize the GSH concentration and rate of the cleavage relationship followed by above mentioned fluorescence intensities ratios. Half-life of the conjugate **71d** was significantly longer at 5mM GSH concentration compared to conjugate **71b** but  $t_{1/2}$  at lower GSH concentrations were similar. The fluorescence quantum yield ( $\Phi_f$ ) of compound **71d** in HEPES was calculated to be 0.15, taking fluorescein as a reference. The quantum yield of the aminoBODIPY dye released after conjugate disruption was previously calculated as 0.77 (in HEPES buffer).<sup>157</sup>

Conjugate	GSH conc.	Buffer	$t_{1/2}$ (min) <sup>c</sup>
<b>71b</b>	5 mM	DMSO/HEPES <sup>b</sup>	18.4
<b>71b</b>	4 mM	DMSO/HEPES <sup>b</sup>	23.6
<b>71b</b>	3 mM	DMSO/HEPES <sup>b</sup>	32.7
<b>71b</b>	2 mM	DMSO/HEPES <sup>b</sup>	51.5
<b>71d</b>	5 mM	HEPES <sup>a</sup>	22.3
<b>71d</b>	4 mM	HEPES <sup>a</sup>	23.1
<b>71d</b>	3 mM	HEPES <sup>a</sup>	38.2
<b>71d</b>	2 mM	HEPES <sup>a</sup>	54.6

**Table 9** Summary of half-lives of conjugates **71d** and **71b** (5  $\mu$ M) after treatment by various concentrations of GSH. All measurements were performed in 3 repetitions; <sup>a</sup> HEPES, 0.1M, pH

7.4; <sup>b</sup> DMSO/HEPES 2:1, 0.1M, pH 7.4. <sup>c</sup>  $T_{1/2}$  were determined by ExpDecay function in OriginLab software.

Next, we examined the stability of conjugates **71b** and **71d** at various pH and the rate of cleavage by 5 mM GSH at 37 °C in the pH range of 5-8. It is known that the disulfide bond is stable in presence of thiols at lower pH, and at higher pH the linker is readily cleaved. The same pH stability is observed for both conjugates, as shown in the Figure 42 and Figure 43. Both conjugates **71b** and **71d** were stable in the presence of GSH (3 mM) at acidic pH (5-5.5) and were readily cleaved at higher pH (7-8).

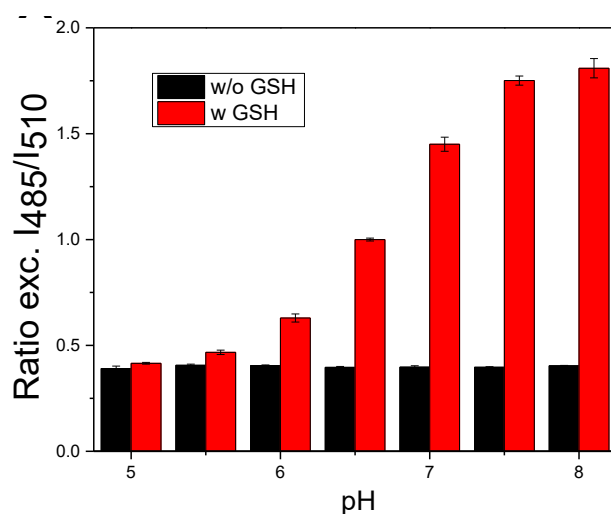


**Figure 42** Stability of conjugate **71d** (1  $\mu$ M) at various pH 5-8 in HEPES buffer (0.1 M, 37 °C) in the absence of GSH (black bars) and with 3 mM GSH (red bars) upon irradiation for 1 hour. All datapoints were acquired upon irradiation at 485 nm and 510 nm with the following emission at 530 nm and were performed in 3 repetitions.

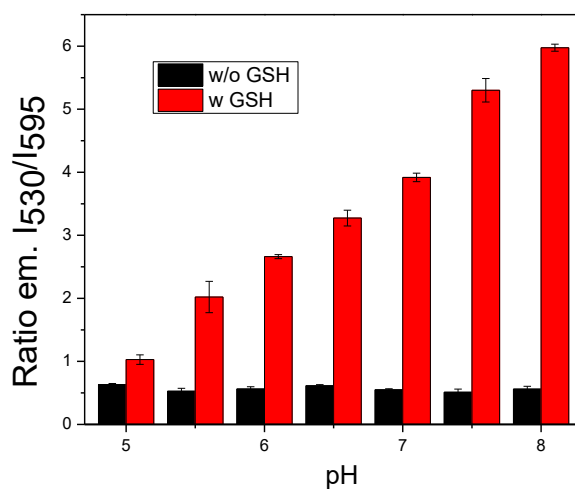


**Figure 43** Stability of conjugate **71b** (1  $\mu$ M) at various pH (pH 5-8) (DMSO/HEPES buffer 0.1 M, 2:1, 37 °C) without GSH and cleavage of conjugate **71b** in the presence of GSH (3 mM)

upon incubation for 1 hour. All datapoints were acquired upon irradiation at 510 nm with the following emissions at 530 nm and 595 nm and were performed in 3 repetitions.

As expected, the cleavage of both conjugates increases with increasing pH for both conjugates. For conjugate **71d**, the cleavage rate in the range of 5-6.5 pH is significantly slower than that for conjugate **71b**. When the emission ratio  $I_{530}/I_{595}$  of conjugate **71b** without the presence of GSH ( $I_{530}/I_{595} = 0.50$ ) is compared to the value obtained after the incubation of conjugate **71b** with GSH at pH 5 for 1 h ( $I_{530}/I_{595} = 1.32$ ) and considering a value of  $I_{530}/I_{595} = 6.7$  as the full cleavage (Figure 44), we can estimate that the conjugate is cleaved from 13 % at pH 5. In addition, both conjugates proved to be stable in the selected pH range without the presence of reduced GSH.

#### 2.2.4 Biology

The cleavability and efficiency of conjugate **71b** and **71d** was tested on a series of experiments on HeLa cells, with and without pre-incubation with additional glutathione. The pretreatment with the N-ethylmaleimide (NEM) was used for the total inhibition of thiol activity in the assay.

The images from confocal fluorescence microscopy on HeLa cells show that our model system **1** emit a green light at the beginning of experiment as well as after two hours (Figure 44 A). This corresponds to the assumption that the active thiols in the cells are depleted by NEM, so that the conjugate **71d** is not cleaved and no or only little change in fluorescence intensity is observed. Additionally, from microscopy images an altered distribution of compound **71d** inside the NEM treated cells and slightly higher green emission intensity at the beginning of experiment was observed compared to untreated cells (Figure 44 A, B, C). Arguably, this behavior may be explained by the fact that SH groups play key role in the regulation of the permeability transition pores. NEM is a membrane-permeant alkylating agent and by binding to cysteine residues may affect transition pores in membranes as previously confirmed that high concentrations of NEM (0.5–1.0 mM) induce pore opening.<sup>158,159</sup>

When the cells without NEM pretreatment were incubated with the conjugate **71d** the increase of the fluorescence in 2 hours is evident (Figure 44 B) as the conjugate is cleaved by native GSH to release the drug. Moreover, the emission intensity is significantly enhanced in 2 hours when the cells are treated with GSHEt (Figure 44 C), and greater amount of the aminoBODIPY and drug is released. Thus, the drug release can be easily detected by “OFF-ON” effect as also confirmed by the results of real-time monitoring of cleavage in cells by EnVision plate reader (Figure 45). Cleavage of conjugate **71b** (Figure 45 B) inside the HeLa

cells was not well reproducible with high error and did not correspond with images from fluorescence microscopy arguably because of its low solubility and dependence on environment solvation.

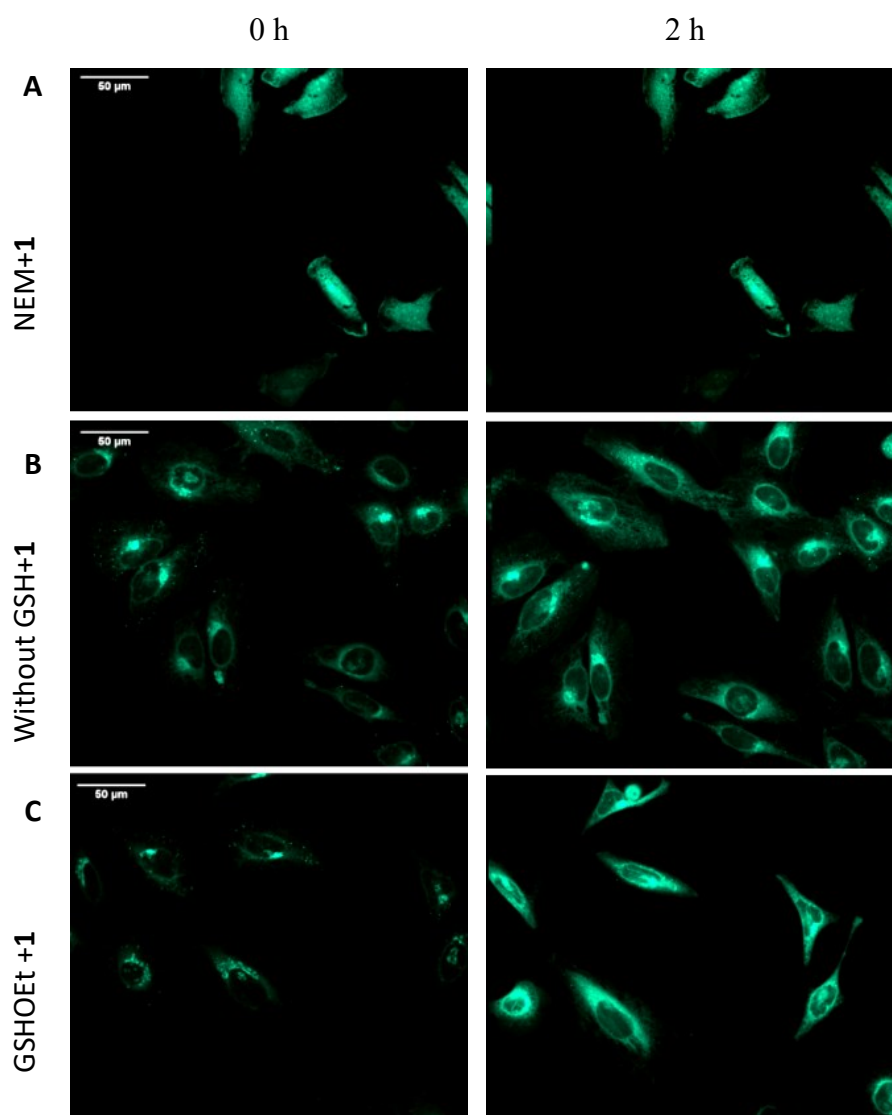


**Figure 44** (A) Microscopy images of the conjugate **71d** internalization inside the HeLa cells after pretreatment with 1mM NEM, (B) without any pretreatment and (C) after pretreatment with 20 mM GSHOEt. (D) Quantification of fluorescence intensity in HeLa cells. Excitation/emission wavelength 488/515-530 nm.

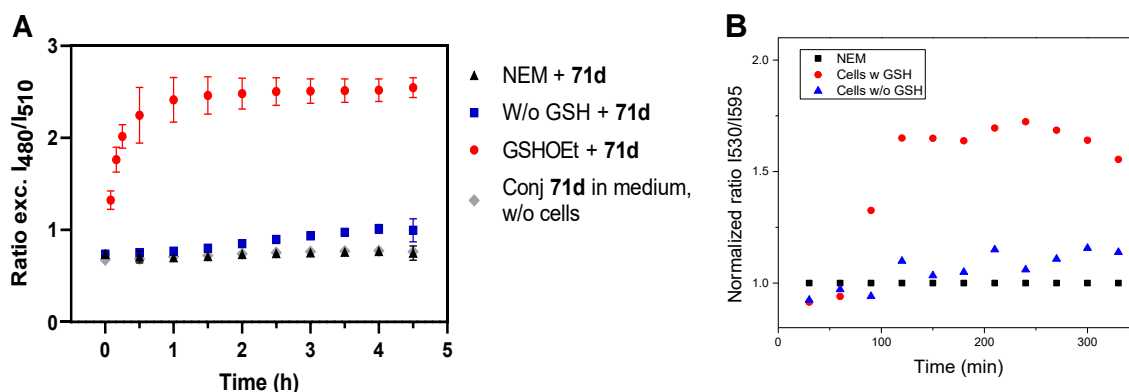


**Figure 45** (A) Monitoring of time-dependent cleavage of conjugate **71d** and (B) **71b** inside HeLa cells pretreated with NEM (1 mM, 30min) and HeLa cells with or without treatment with GSHOEt (20mM). Excitation/emission wavelengths for conjugate **71d** were 485/530 and 510/530 and for conjugate **71b** 500/530 and 500/595 nm.

Enhanced uptake of the cRGD conjugate **71d** by HeLa cells which possess overexpressed levels of  $\alpha_v\beta_3$  integrins<sup>160,161</sup> was proven by cRGD binding assay performed similarly to the described protocol<sup>162</sup>. Cells were pre-incubated with various cRGD peptide **56a** concentrations (0-100  $\mu\text{M}$ ) and then treated with conjugate **71d** (10  $\mu\text{M}$ ). As Figure 46 depicts, fluorescence response decreased with higher concentrations of cRGD peptide suggesting that binding sites at  $\alpha_v\beta_3$  integrins were occupied by free cRGD peptide and thus less conjugate **71d** penetrated into the cells. Pre-incubation with 100  $\mu\text{M}$  cRGD **56a** led approximately to 53 % reduction in the cell uptake of conjugate **71d** according to fluorescence intensity at 530 nm.

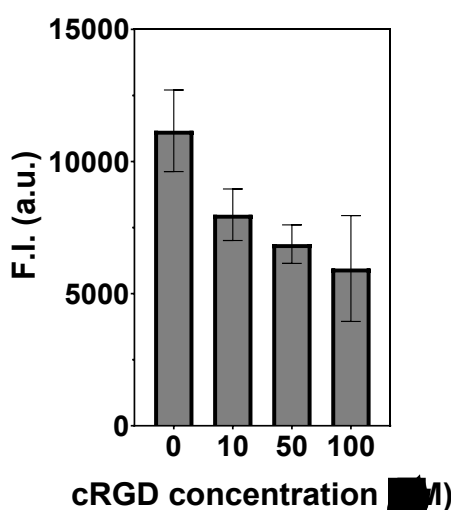


**Figure 46** Uptake of the conjugate **71d** (10  $\mu\text{M}$ ) by HeLa cells pre-incubated with cRGD peptide (0-100  $\mu\text{M}$ ). Fluorescence was measured at  $\lambda_{em} = 530\text{nm}$  upon excitation by  $\lambda_{exc} = 485\text{nm}$ . All measurements were performed in at least 5 repetitions.

Cytotoxicity of prepared CPP-3HQ-BDP compounds **38a-e**, aza-quinone methide conjugates **58** and **59** and quinone methide conjugates **71a-d** are summarized in the Table 10. Conjugates with PKKKRKV cell penetrating peptide **38a-e** showed only poor activity against CEM and K562 cell lines with no or only little effect of the PEG or Phe spacer. Arguably, this inactivity could be caused by inability of the conjugates to release free 3HQ drug or low penetration into the cells. In general, drug releasable conjugates **59** and **71a-c** with redBODIPY dye showed no activity regardless of the aza-quinone or quinone methide central unit. On the other hand, both conjugates **58** and **71d** with cRGD targeting peptide exhibited cytotoxic activity comparable with the free 3HQ-PEG model drug **13a**. This activity was probably the result of either effective targeting and penetration to cells or enhanced water solubility of the compounds. Moreover, the toxicity of compounds **58** and **71d** against normal cells (MRC-5) was reduced.

Compound	Cell line/IC <sub>50</sub> (μM)									
	A549	BJ	CCRF-CEM	CEM-DNR	HCT116	HCT116 p53	K562	K562-TAX	MRC-5	U2OS
<b>38a</b>	50	50	50	50	50	50	50	50	50	50
<b>38b</b>	50	50	41.33	37.74	50	50	36.19	35.73	50	50
<b>38c</b>	50	50	29.53	32.85	50	50	31.96	31.32	50	50
<b>38d</b>	50	50	39.81	37.03	50	50	37.95	34.46	50	50
<b>38e</b>	50	50	34.21	50	50	50	50	43.66	50	50
<b>59</b>	50	50	50	50	50	50	48.68	50	50	50
<b>58</b>	8.62	50	6.23	30.75	7.43	8.22	7.08	36.06	50	8.01
<b>71a</b>	50	50	46.35	50	50	50	49.84	50	50	50
<b>71d</b>	8.50	42.02	6.06	17.89	7.22	7.48	7.98	22.42	45.82	8.80
<b>71b</b>	50	50	50	50	50	50	50	50	50	50
<b>71c</b>	50	50	50	50	50	50	50	32.74	50	50
<b>13a</b>	9.27	46.84	6.21	23.55	8.17	13.37	5.55	22.13	24.07	12.81

**Table 10** IC<sub>50</sub> values of 2<sup>nd</sup> generation conjugates.

### 2.3 Conclusion

To summarize, in this project we successfully prepared and optimized synthetic route leading to two generations of BODIPY-3HQ conjugates. These potential theranostics were then evaluated through GSH-mediated cleavage and fluorescence monitoring of the drug release in

glass cuvettes as well as inside the HeLa cells. In collaboration with cell biology department at IMTM we tested cytotoxicity of all final compounds on cancer cell lines and normal cell lines. Firstly, simple conjugation of aminoBODIPY **4a** and **4b** with various 3HQs as model drugs *via* disulfide cleavable or maleimide non-cleavable linkers resulted in the first generation of conjugates **30-34**. During the studies on fluorescent monitoring of drug release we discovered an interesting feature of aminoBODIPY dye **4a** – significantly different excitation maximum in the acylated form of aminoBODIPY (515 nm) compared to the free aminoBODIPY dye (480 nm) while emission spectra remained very similar (525 nm). Moreover, quantum yields of fluorescence of conjugates bearing nitro group were significantly lower. Followingly, we utilized this behavior to develop ratiometric and “OFF-ON” system based on dual excitation and single emission wavelength. We proved the universality of this system by attaching the drug part by three different disulfide cleavable linkages – cysteine (thiol), carbonate (-OH group) and carbamate (-NH group) linkers. In all cases, the drug and free aminoBODIPY dyes were efficiently released and monitored by fluorescence spectroscopy and LC/MS detection. In general, conjugates with more labile carbonate linker **32a-e** were more susceptible for nucleophilic attack and were strongly cytotoxic against cancer cell lines with IC<sub>50</sub> in sub-micromolar concentration in some cases, but not toxic to normal healthy cells. Conjugates with cysteine disulfide linker **30a-e** and **31a,c** possessed improved cytotoxicity and penetration ability in comparison to free Cys-3HQ **12a-e**. On the other hand, non-cleavable maleimide conjugates **34a-e** exhibited no toxicity with IC<sub>50</sub> >50 μM. Therefore, this demonstrates that cytotoxic effect is mainly based on the cleavage of disulfide linker and liberation of free 3HQs and BODIPY dye.

Furthermore, BODIPY-3HQ conjugates **38a-e** with cell penetrating sequence – PKKKRQV nuclear localization sequence with various hydrophobic or hydrophilic spacers were prepared. However, these conjugates exhibited no cytotoxic activity probably due to the fact that cleavage of such conjugates resulted only in 3HQ-CPP molecule which could not reach its active site or because of low cellular uptake. Therefore, in further efforts to prepared 2<sup>nd</sup> generation of conjugates we focused on systems that would be able to release the drug in the free form.

The main intention of second generation of conjugates was to develop GSH responsive system with possibility to introduce three parts: (i) cancer cell targeting moiety or second redBODIPY to provide FRET monitoring of drug release, (ii) 3HQ model drug and (iii) aminoBODIPY connected to central unit via disulfide linker. From various attempted synthetical approaches quinone methide and aza-quinone methide approach matched the requirements for central unit – one event (disulfide bond cleavage by GSH) triggers the cleavage of both aminoBODIPY dye

and the free drug. Conjugates with quinone methide **71a-d** and aza-quinone methide central unit **58** and **59** decorated with either cRGD peptide, for targeting integrins overexpressed in cancer cells, or redBODIPY for more effective drug release monitoring via FRET were synthesized and tested. Aza-quinone methide conjugates showed slower rate of GSH cleavage compared to quinone methide conjugates **71**. However, FRET conjugates equipped with redBODIPY dyes showed no cytotoxicity probably as a result of low solubility or insufficient penetration into the cells. Conjugates **58** and **71d** equipped with integrin targeting cRGD peptide exhibited moderate cytotoxicity against cancer cells with improved toxicity to normal healthy cells.

**Published articles:**

Porubský, M.; Gurská, S.; Stanková, J.; Hajdúch, M.; Džubák, P.; Hlaváč, J. *RSC Adv.* **2019**, *9*, 43, 25075–25083.

Porubský, M.; Gurská, S.; Stanková, J.; Hajdúch, M.; Džubák, P.; Hlaváč, J. *Molecular Pharmaceutics.* **2021**, *18*, 6, 2385–2396.

Porubský, M.; Vychodilová, K.; Miličević, D.; Buděšinský, M.; Stanková, J.; Džubák, P.; Hajdúch, M.; Hlaváč, J. *ChemistryOpen.* **2021**, *10*, 1-8.



## Part II:

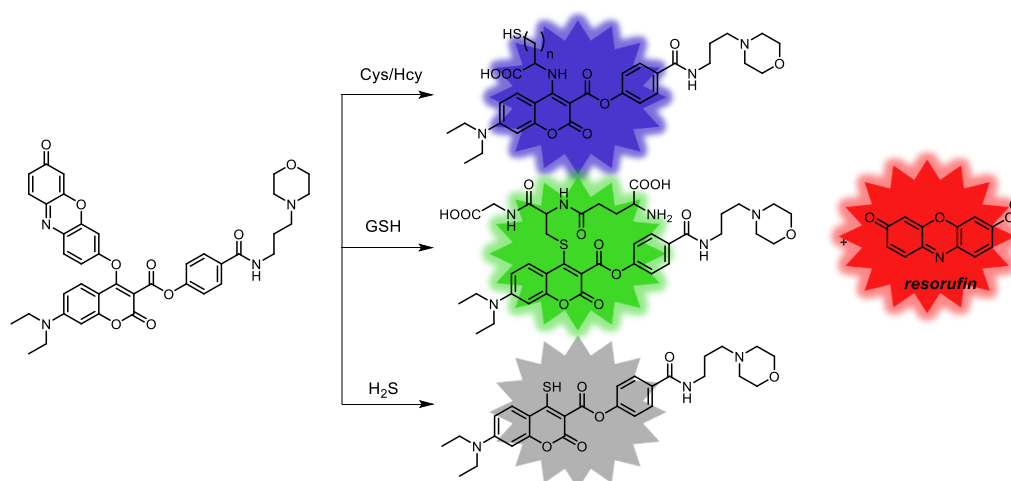
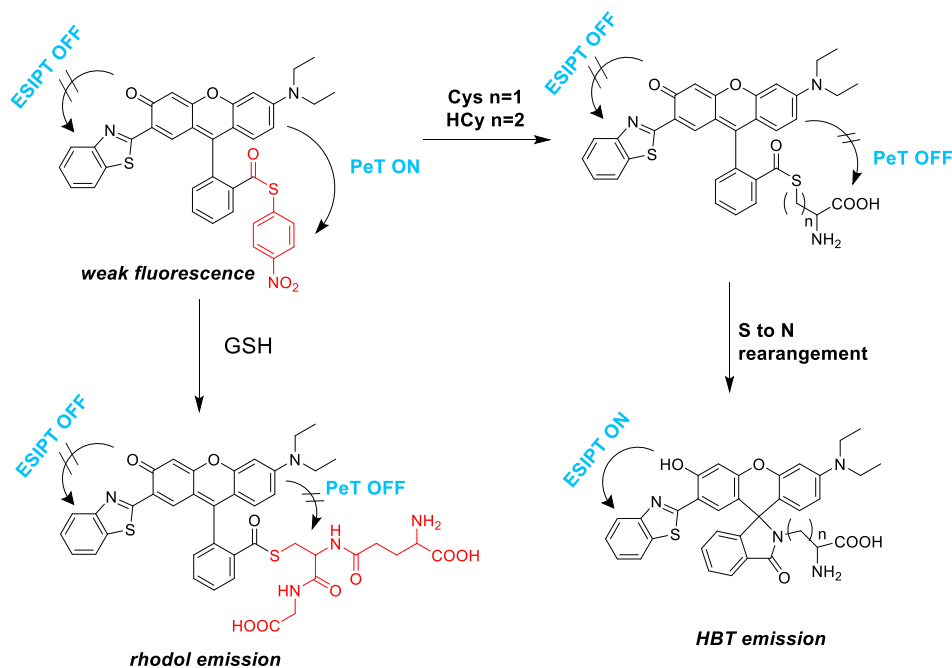
Development of dual FRET probes for detection and  
quantification of caspases -8 and -9

### 3 Introduction

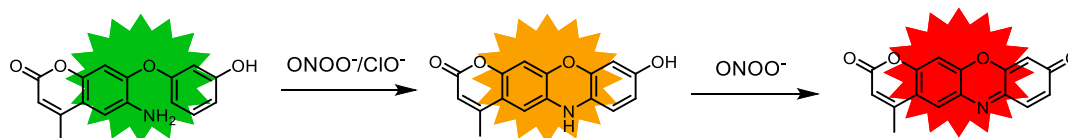
As mentioned also in the previous part, fluorescent probes are powerful tools that have brought revolution to our ability to monitor biochemical processes and detect bioactive molecules.<sup>163</sup> Recently, many fluorescent probes based on simple or functionalized small organic dyes, fluorescent proteins, and nanoparticles have been developed.<sup>101,164–167</sup> Many of them enable a determination of biological and environmental molecules and ions with high sensitivity and selectivity and some of them even in the real-time manner. Moreover, fluorescence is widely used for single-analyte or multi-analyte probes being often superior to other techniques such as mass spectrometry, electrophoresis or other biochemical methods due to its high sensitivity, simplicity, tunability and cost of instrumental equipment.<sup>168</sup>

#### 3.1 Multi-analyte detection probes

Recently, multiple-analyte probes have attracted increasing attention thanks to addressing the challenges of selectivity among structurally similar targets and the visualization of the interactions in the complex mixture of the analytes.<sup>169,170</sup> Probes for differentiation among multiple small-molecule analytes have been synthesized but are usually limited only to thiols, ROS/RNS (H<sub>2</sub>O<sub>2</sub>, HClO etc.), ATP sensing and few enzymes such as phosphodiesterase/ $\beta$ -D-glucosidase<sup>171</sup>, MMP-2/caspase-3<sup>172</sup>, cathepsin B<sup>173</sup> or trypsin/chymotrypsin<sup>174</sup>. Some of plentiful probes for differentiation of thiols - H<sub>2</sub>S, GSH, Cys and HCys were mentioned in the previous part. For completeness, some thiols sensitive multi-analyte probes based on other dyes than BODIPY are listed in the Scheme 28 and Scheme 29.

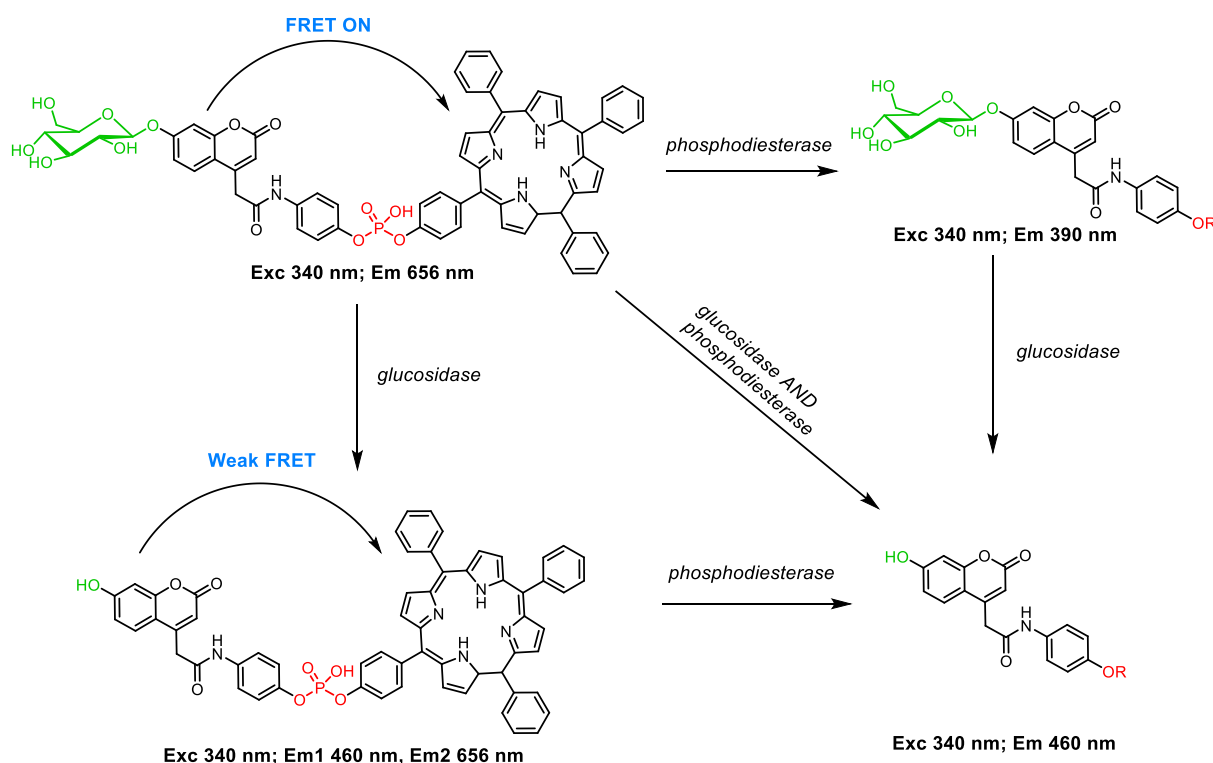


Oxidation-induced fluorophore assembly approach led to development for detection of non-thiol analytes such as peroxynitrite ( $\text{ONOO}^-$ ) and hypochlorite ( $\text{ClO}^-$ ) which can be detected over other ROSs or RNSs ( $\text{H}_2\text{O}_2$ ,  $^1\text{O}_2$ ,  $\text{O}_2^{\cdot-}$ ). Reaction with  $\text{ClO}^-$  produces green to orange fluorescence change while reaction with  $\text{ONOO}^-$  causes red fluorescence via the cyclic intermediate (middle structure, ). The disadvantage of this system is three excitations – three emissions non-ratiometric measurement resulting in concentration dependent quantification of ROS/RNS (Scheme 30).<sup>176</sup>



**Scheme 30** Probe for detection of  $\text{ClO}^-$  and  $\text{ONOO}^-$  over other ROS/RNS and excitation/emission spectra.<sup>176</sup>

The first fluorescent probe for dual enzyme simultaneous detection was mentioned by Yang et.al in 2011. They synthesized FRET system based on glucose modified coumarin dye (donor) that was attached via phosphoester bond to meso-tetraphenylporphyrin (acceptor). Upon  $\beta$ -D-glucosidase cleavage of glucose, FRET partially disappeared and red shifted emission of coumarin was observed. Treatment by phosphodiesterase I afforded emission of coumarin (390nm). If both enzymes were present, single red shifted emission of coumarin (460nm) was detected (Scheme 31).



**Scheme 31** Probe for simultaneous intracellular  $\beta$ -D-glucosidase and phosphodiesterase signaling.<sup>177</sup>

Zhang et.al. reported a probe for detection of extracellular metalloproteinase-2 (MMP-2) and intracellular caspase-3 as cancer related biomarkers.<sup>172</sup> Their approach was based on one quencher (DABCYL) and two dyes (fluorescein, Rhodamine B) connected with enzyme specific peptide linkers forming a ratiometric FRET system. Single enzyme (MMP-2 or

caspase-3) cleavage led to the increased emission at the wavelength 520 nm or 570 nm, respectively. If both enzymes were present, dual excitation/emission measurement was necessary (Exc/Em 465/520 and 540/656) (Figure 47). Moreover, this system is probably significantly pH dependent due to unblocked xanthene ring closing/opening.

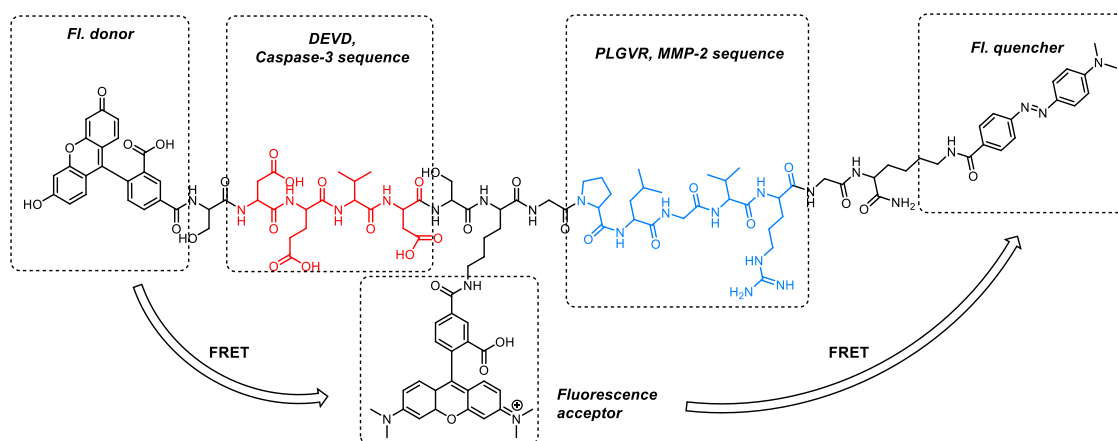


**Figure 47** Probe for simultaneous detection of MMP-2 and caspase-3.<sup>172</sup>

Lastly, in our group the model dual-FRET system based on three dyes (coumarine, fluorescein, Rhodamine B) connected by corresponding cleavable peptide linkers capable of simultaneous differentiation of single enzymes trypsin and chymotrypsin or their mixture was developed.<sup>174</sup> The system works by one wavelength excitation (435 nm) and three emissions monitoring. Emission changes arising upon enzymatic cleavage of linkers were used for enzymes detection with application of developed mathematical model (Figure 48) based on ratio  $X = E_{mDEAC}/E_{mFI}$  and  $Y = E_{mRhB}/E_{mDEAC}$  upon excitation of DEAC ( $\lambda_{exc} = 430$  nm). The measurement within the time affords the values  $X_t$  and  $Y_t$ . The change of these parameters from time 0 can be expressed as  $X_0/X_t$  or  $Y_0/Y_t$  respectively. Treatment with trypsin led to cleavage of the linker between DEAC and FI resulting in FRET disappearance and displayed as a decrease of  $X_0/X_t$  and increase of  $Y_0/Y_t$  ratio. The appropriate curve is reaching point A, where the trypsin linker is totally cleaved. (green curve, Figure 48). Chymotrypsin cleaved the linker between FI and RhB what resulted in disruption of second FRET in cascade and caused the increase of fluorescein emission (520 nm). This resulted in the rise of  $X_0/X_t$  ratio while  $Y_0/Y_t$  parameter stayed approximately at the same value as demonstrated by the blue curve in Figure 48. The time curve is reaching point B demonstrating total cleavage of the chymotrypsin linker. Treatment by both enzymes simultaneously resulted in expected increase of both DEAC and Fluorescein emissions. The curve is finally turned toward point C characteristic for total cleavage of both linkers. This system was able to distinguish three scenarios: (i) presence of

trypsin, (ii) presence of chymotrypsin and (iii) presence of mixture of both enzymes. However, it was unable to determine the relative activity of enzymes in various mixtures.

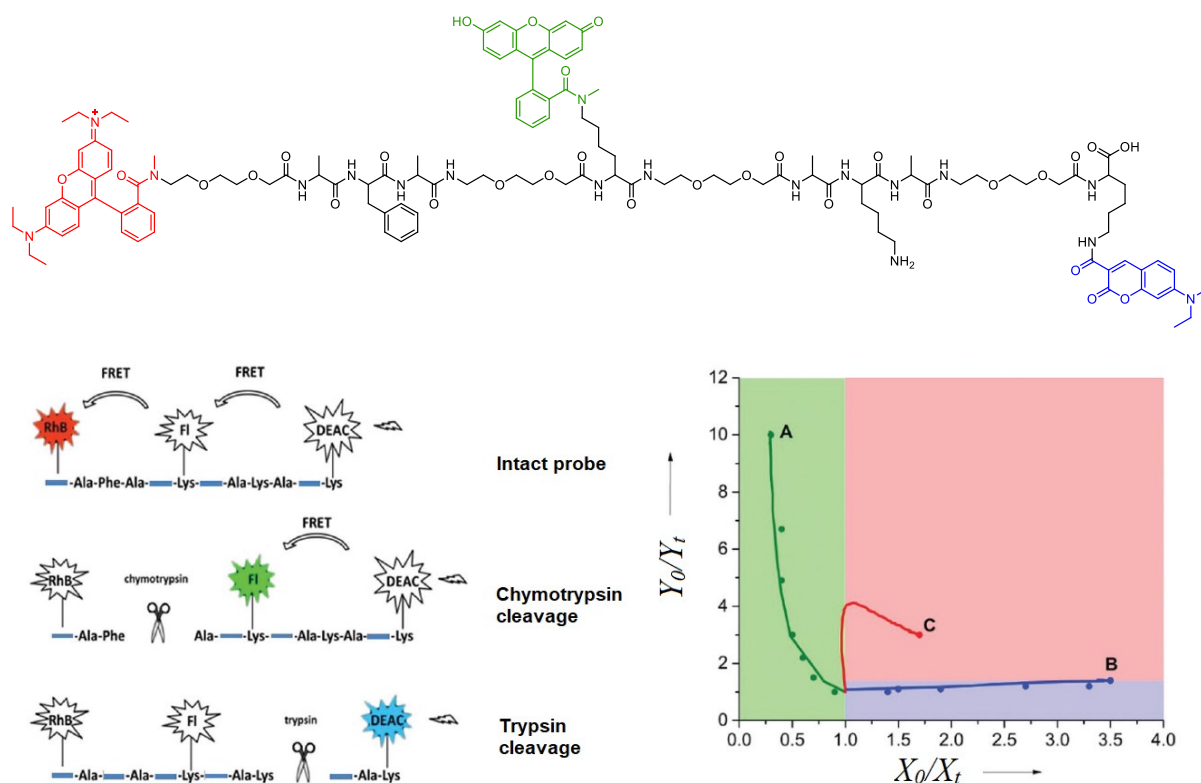


**Figure 48** Chymotrypsin-trypsin dual-FRET model system.<sup>174</sup>

### 3.2 Caspases

Caspases (**cysteine-aspartic proteases**) are a family of endo-proteases playing key role in maintaining homeostasis through programmed cell death and inflammation regulation during development and throughout life of the cell. Caspases hydrolyze peptide bonds in a reaction that depends on catalytic cysteine residues in the caspase active site and occurs only after certain aspartic acid residues in the substrate. To date there are 14 confirmed caspases and are generally classified by their known roles in apoptosis (caspase-3, -6, -7, -8, and -9 in mammals), and in inflammation (caspase-1, -4, -5, -12 in humans and caspase-1, -11, and -12 in mice). The functions of caspase-2, -10, and -14 are less easily categorized. Caspases involved in apoptosis have been subclassified by their mechanism of action and are either initiator caspases (caspase-8 and -9) or executioner caspases (caspase-3, -6, and -7).

Apoptosis, programmed cell death involves the controlled dismantling of intracellular components while avoiding inflammation and damage to surrounding cells. Initiator caspases activate executioner caspases that subsequently coordinate their activities to demolish key structural proteins and activate other enzymes. The initiator caspases-8 and -9 normally exist

as inactive procaspase monomers that are activated by dimerization and not by cleavage. Inappropriate activation of the executioner caspases-3, -6, and -7 is prevented by their presence as inactive procaspase dimers that must be cleaved by initiator caspases.

Simultaneous detection of more caspases can serve for elucidation of various metabolic pathways.<sup>178</sup> Usually the initiator caspases, caspases-8, -9, and -10 are overexpressed due to action of xenobiotics or other stimuli and they activate the downstream executioner caspases in a proteolytic cascade to start the apoptotic process.<sup>179</sup> In mammals, it is well known that drug mediated apoptosis proceeds by two major signaling pathways. One of these, the extrinsic apoptotic pathway, is initiated by binding to the cell surface “death receptors” such as Fas.<sup>180</sup> In this pathway, apoptotic signals are mediated through the caspase cascade in association with the activation of the initiator caspase-8 and executioner caspases such as caspase-3 and caspase-7. Intrinsic pathway is also known as mitochondrial apoptosis because it depends on factors released from the mitochondria. This pathway is activated by a cellular stresses, including growth factor deprivation, cytoskeletal disruption, DNA damage, accumulation of unfolded proteins or hypoxia and results in the activation of initiator caspase-9.<sup>179,181</sup> In some cases the cross pathway, in which both initiator caspases are activated can proceed (Figure 49).

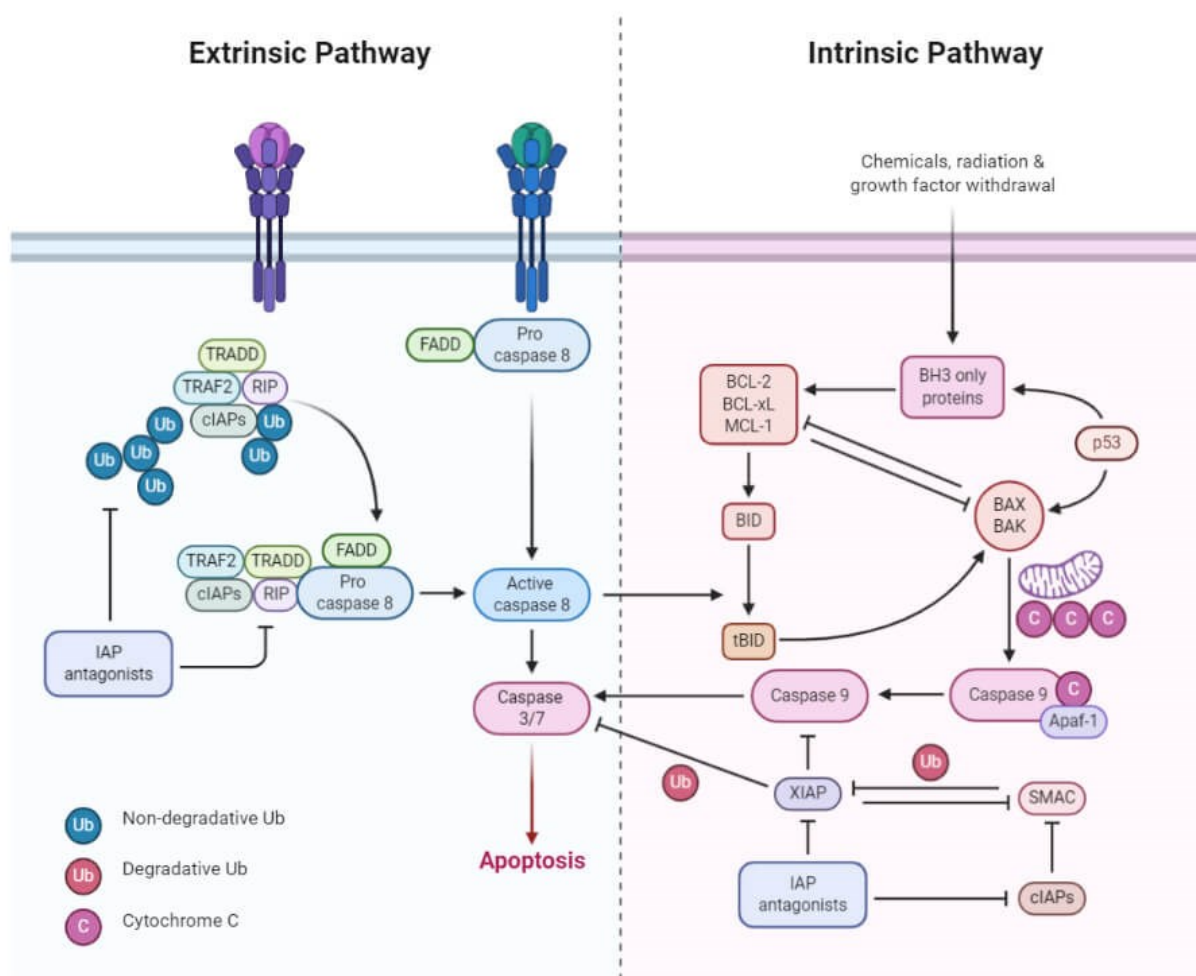


**Figure 49** Extrinsic and intrinsic caspase pathway.<sup>182</sup>

Thornberry et al. summarized preferred caspase cleavage sequences for all caspases as depicted in the Figure 50.<sup>180</sup> This may serve as a guideline for design of caspase probes and prediction of selectivity of caspases. In general, caspases can recognize distinct four amino acid sequences in the peptide substrate with one crucial requirement – aspartic acid residue at position P1. Both caspases of interest – caspase-8 and caspase-9 have preference for leucine and glutamic acid in the position P4 and P3, respectively. However, the greatest difference occurs at position P2 at which the presence of tyrosine favors the cleavage by caspase-8 and on the other hand caspase-9 has selective preference for substrates with histidine at P2. Other caspases such as caspase-2, -6 may participate in cleavage of both substrates for casp-8 and -9 while caspases -5, -4, and -1 have similar substrate sequences as casp-9 and may interfere unless inhibited.

Both caspases -8 and -9 can be activated through the action of variety of small molecule compounds such as dinaciclib, doxorubicin, taxol,  $\alpha$ -cycloheximide (CHX) or protein ligands based on tumor necrosis factor (TNF) related apoptosis-inducers such as TRAIL. Activation of



initiator caspases is rarely selective and is usually accompanied by the activation of other caspases.<sup>183</sup>

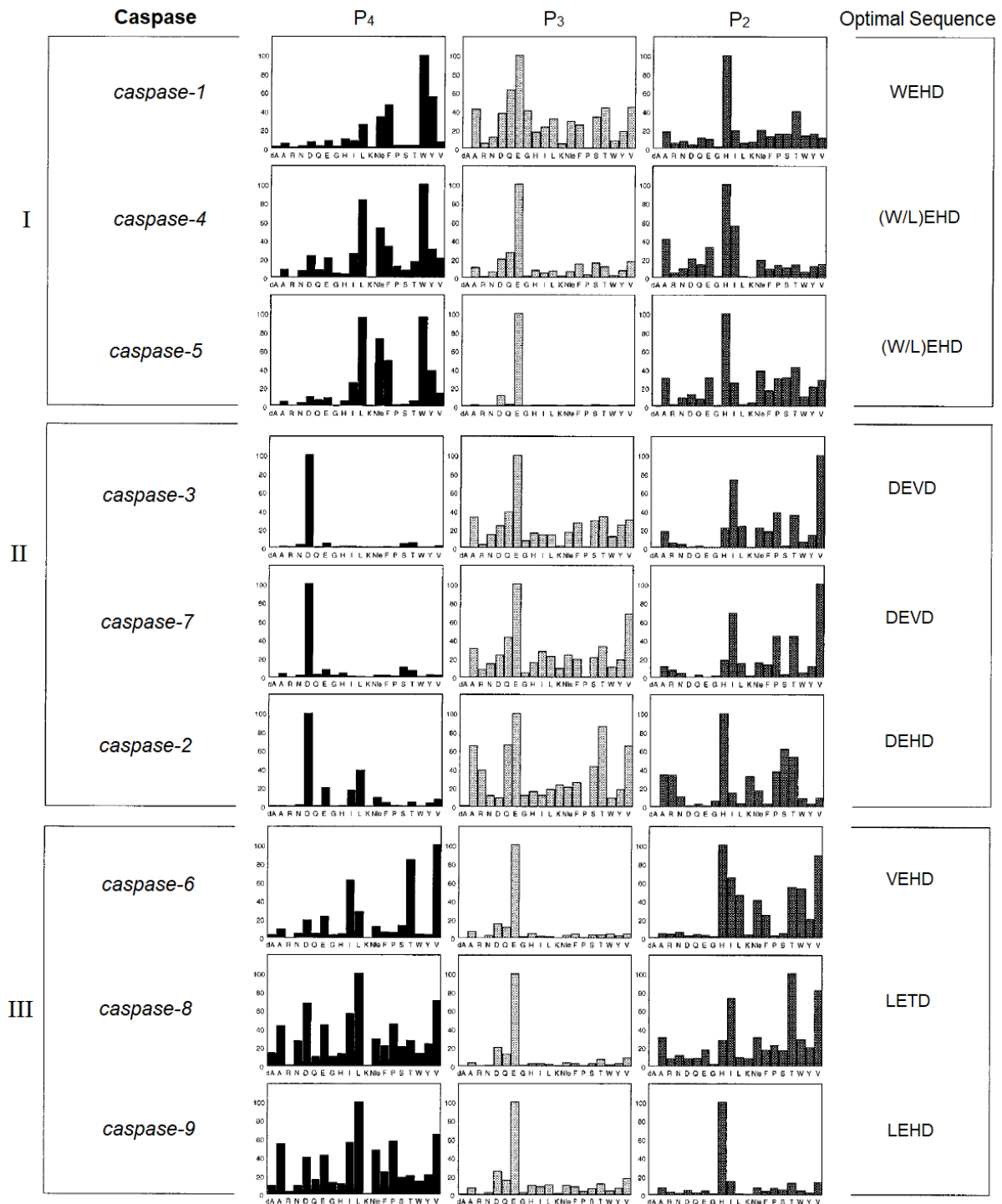
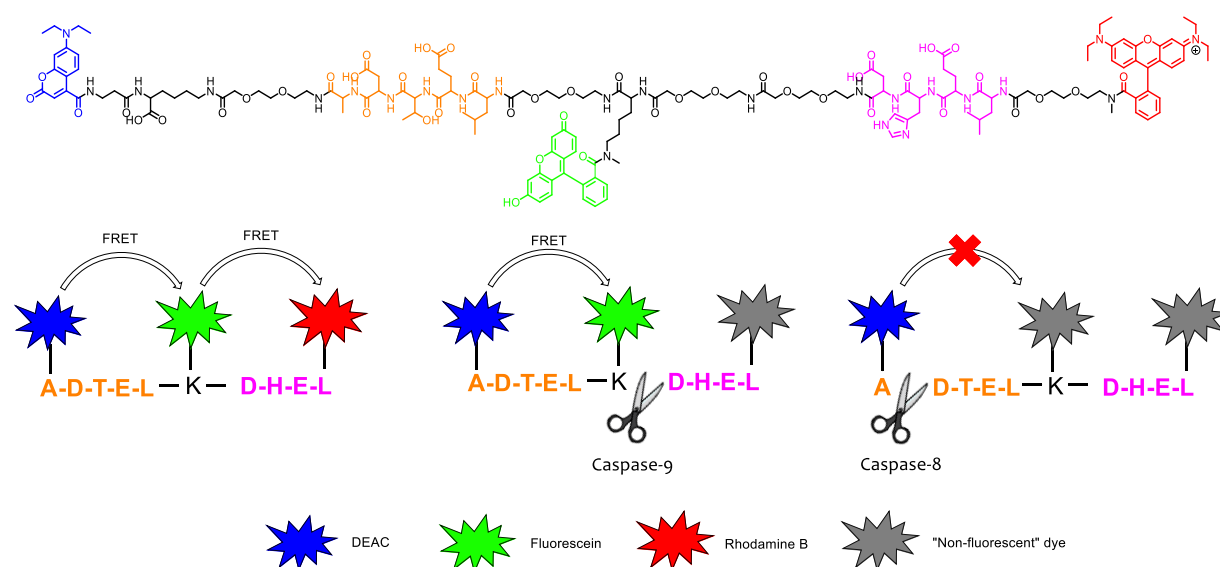


Figure 50 Preferred peptide sequences for caspases -1 to -9.<sup>180</sup>

## 4 Results and discussion

Herein, we describe three-fluorophore system containing coumarine, fluorescein and rhodamine B dyes connected with two peptide-like sequences that are recognized and cleaved by caspase-8 and caspase-9 (Figure 51). Cleavage of the caspase-9 peptide linker should lead to disappearance of the FRET between fluorescein and rhodamine (Figure 51, middle structure) and cleavage of the caspase-8 peptide linker should similarly result in total vanishing of the FRET (Figure 51, structure on the right). This system should provide simple FRET-based detection of caspase-8 and -9 and resolution of extrinsic and intrinsic mechanism of action of drugs together with relative quantification of caspase-8 and -9 activity in simple mixtures. For this purpose a mathematical model was used for data interpretation in order to validate detection and quantification of the activity of selected caspases in model samples as well as in cell lysates.



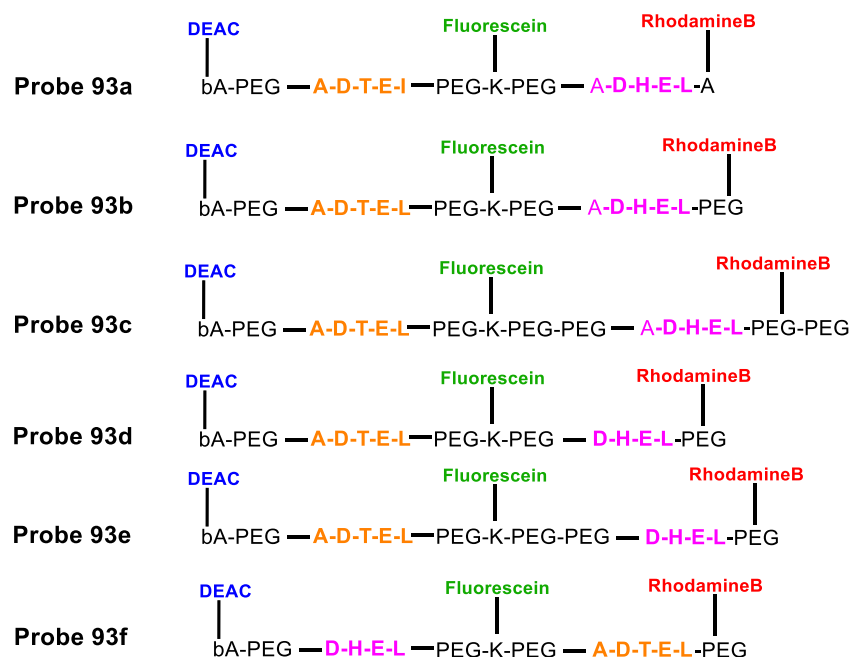
**Figure 51** Dual-FRET Probe **93e** and basic principle of cleavage mechanism by caspase-8 and caspase-9.

We chose DEAC, fluorescein and Rhodamine B based on our previous experience with the model chymotrypsin-trypsin system as fluorophores capable to serve as donor, acceptor/donor and acceptor of energy, respectively. Fluorophores are located at the beginning, in the middle and at the end of linear peptide backbone. The backbone itself consists of two specific sequences (I)LETD and LEHD which are according to literature and previous studies cleaved with sufficient selectivity by caspase-8 and -9, respectively.

Firstly, it is important to mention that for efficient FRET in such dual-FRET systems even small changes in the structure or distance between dyes or polarity of linkers may be

critical and sometimes misleading. Efficient FRET is then absolutely essential for successful monitoring of both caspases.

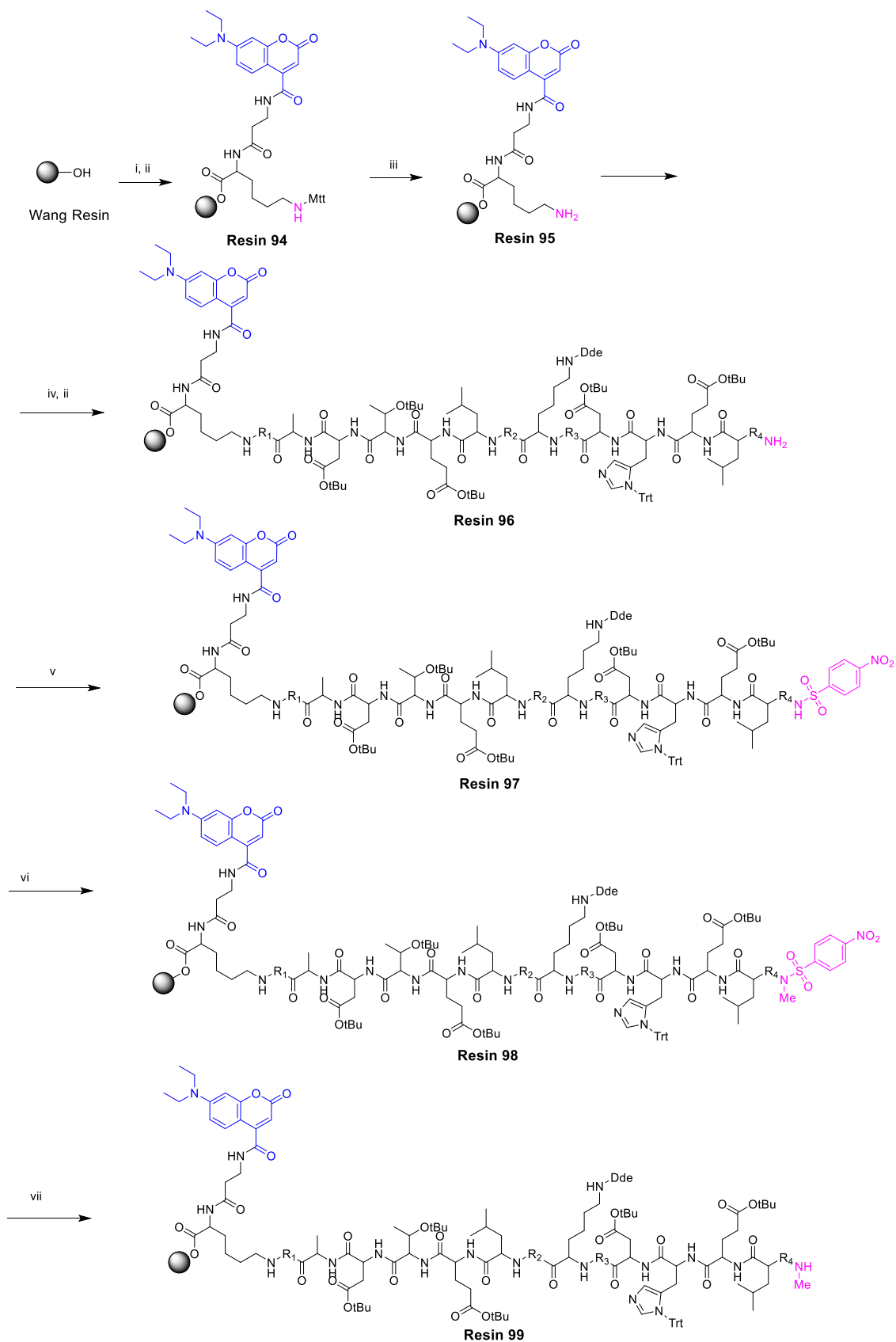
#### 4.1 Synthesis of dual-FRET probes

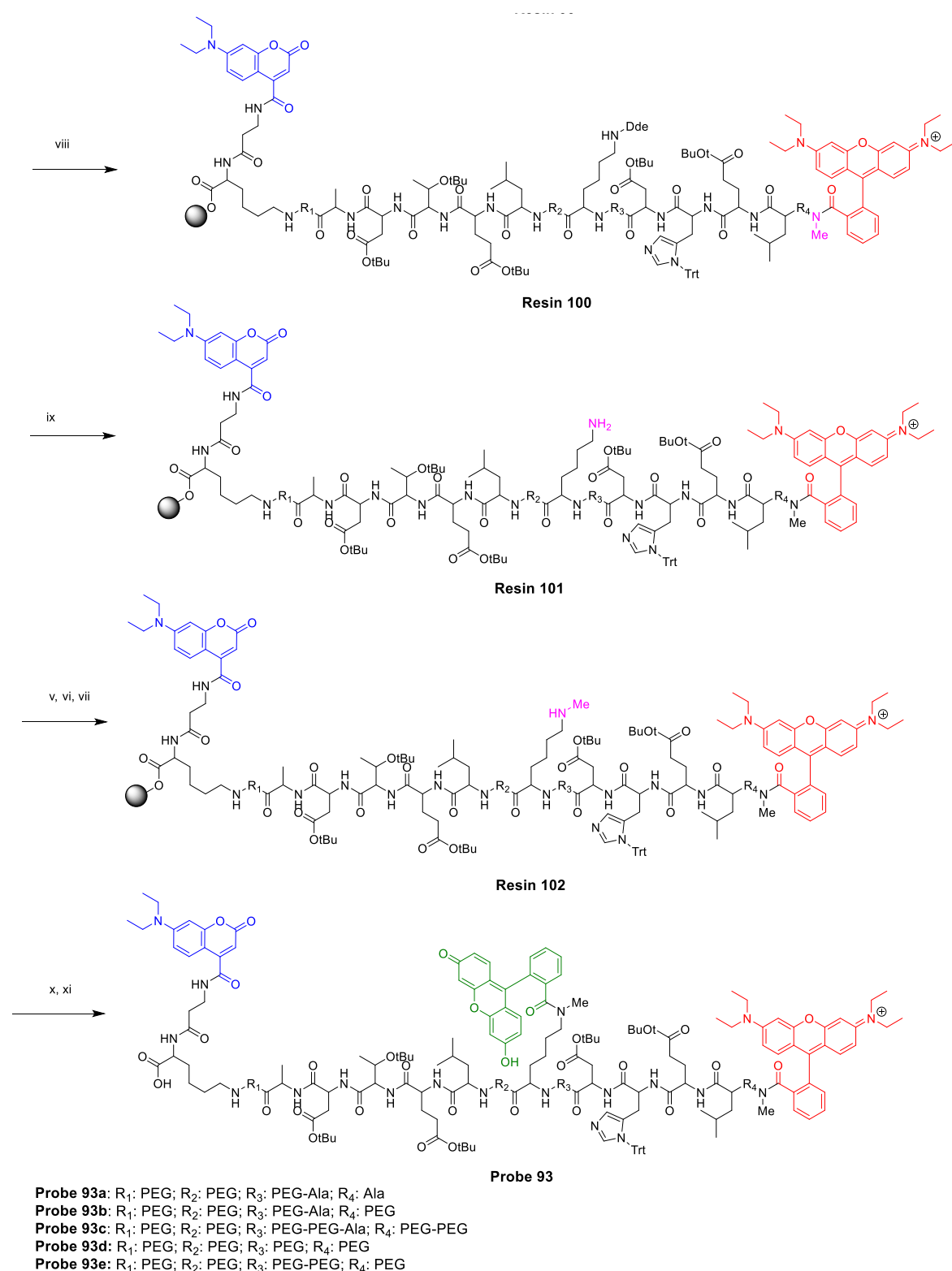


**Figure 52** Structures of the Probes **93a-f** (one letter code refers to individual amino acid).

Synthesis of the probes **93a-f** (Scheme 32) was performed by standard solid phase chemistry using Fmoc-based protocol. First amino acid Fmoc-Lys(Mtt)-OH was immobilized on Wang Resin, followed by attachment of Fmoc-bAla-OH and 7-diethylaminocoumarine-3-carboxylic acid (DEAC) to obtain Resin **94**. Then the peptide backbone was built by incorporation of individual amino acids, ethyleneglycol spacers and suitably protected Fmoc-Lys(Dde)-OH for appending of the middle fluorophore, what was done as a last step of synthesis. Based on our previous experience, the modification of amides of xanthene dyes (fluorescein and RhB) at the 2'-position provides derivatives with increased photostability and reduced pH dependence. Therefore, methyl groups were introduced to the amino groups of Resins **96** and **101** prior to their coupling with RhB and Fl by sequence of three consecutive reactions – protection with 4-nitrosulfonyl chloride (Nosyl-Cl, Resin **97**), Mitsunobu reaction (Resin **98**) and deprotection of nosyl group (Resin **99**). Coupling of the secondary amine **99** with RhB worked smoothly using DIC/HOBt and DMAP, however, in the case of amide formation from amine **102** with fluorescein an excess of DIPEA base had to be used along with heating to 60 °C for 16 h. The cleavage of final peptides **93a-f** was performed by mixture of TFA/DCM/TES for 2-3 h. The crude purity of cleaved products was usually poor and precise

HPLC purification was necessary. By this approach several compounds with various peptide linker length and orientation were prepared. Some of them are depicted in the .

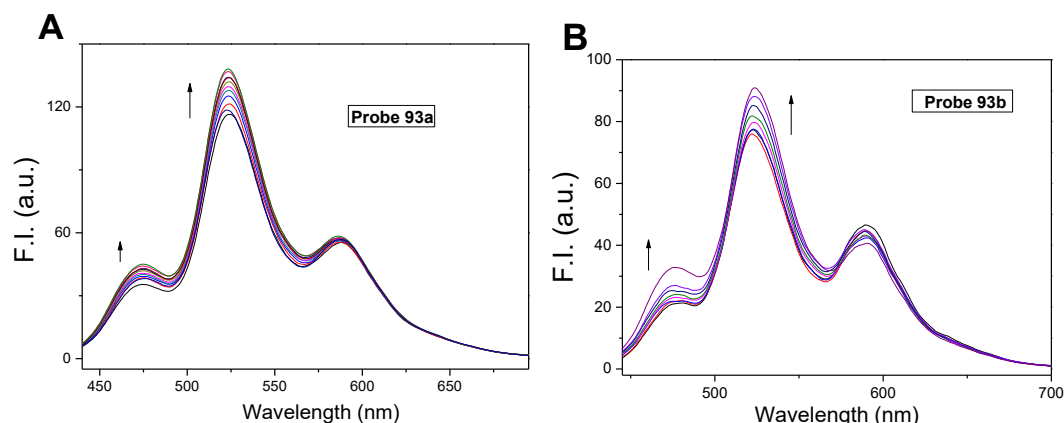




**Scheme 32** Synthesis of dual-FRET probes **93a-e** for caspase-8 and -9 detection. *Conditions and reagents:* i) Fmoc-Lys(Mtt)-OH; Fmoc-βAla-OH; DEAC; HOBt, DIC, DMAP, DCM/DMF 1:1, rt, 16 h; ii) 50% piperidine/DMF, rt, 30 min; iii) TES/HFIP/TFE/DCE 20:10:5:65, 60°C, 24 h; iv) aminoacid, DIC, HOBt, DCM/DMF 1:1, rt, 2 h; v) NsCl, 2,6-lutidine, DCM, rt, 1 h; vi) MeOH, PPh<sub>3</sub>, DIAD, THF, -20°C to rt, 3 h; vii) 2-mercaptoethanol, DBU, DMF, rt, 1 h; viii) rhodamine B, HOBt, DIC, DMAP, DMF 1:1, rt, 16 h; ix) MeOH, PPh<sub>3</sub>, DIAD, THF, -20°C to rt, 2 h; x) fluorescein acid, DIPEA, HOBt, DIC, DMF, 50°C, 16 h; xi) TFA/DCM/TES (50:50:3), rt, 2 h.

## 4.2 Caspase cleavage studies

To test functionality of prepared probes we firstly measured emission spectra upon excitation of the first dye DEAC at wavelength 425 nm (Figure 53) to evaluate the efficiency of FRET. The bottom spectrum in each figure demonstrates the spectral profile of each native probe in the aqueous buffer mixture used for caspase cleavage experiments. Firstly, the cleavage by caspase-9 was tested to see the expected increasing of fluorescein emission after cleavage of LEHD linker causing the termination of energy transfer between fluorescein and rhodamine. In other words, Figure 53 demonstrates the sensitivity of the probes **93a-f** to the presence of caspase-9 in the model analyte. Probes **93a-d** (Figure 53 A-D) possessed only very low FRET efficiency that led to weak response during caspase cleavage as the most energy is emitted by fluorescein and only little is passed to Rhodamine B. Probe **93e** showed satisfying response (almost 2-fold increase) during caspase-9 cleavage and superior FRET efficiency as well. The Probe **93f** bearing reversed peptide sequences (caspase-8 linker instead of caspase-9 linker and vice versa) but the same order of fluorophores showed unexpected and significant increase of fluorescein emission during the treatment by caspase-9 (Figure 53 F). This behaviour indicates complete lack of selectivity of caspase-9 against the probe **93f**. From the structural difference between the probes some hypothetical conclusions can be drawn upon our observations: (i) presence of Alanine or other hydrophobic amino acid such as Gly before the caspase-9 specific DHEL sequence is unfavorable, (ii) replacement of amino acid residue with less rigid PEG chain accelerates rate of cleavage, (iii) optimal length of linker should be kept between 34-44 atoms and (iv) the order of fluorophores and peptide sequences should be kept as follows: (DEAC)-casp8 linker-(FL)-casp9 linker-(RhB).



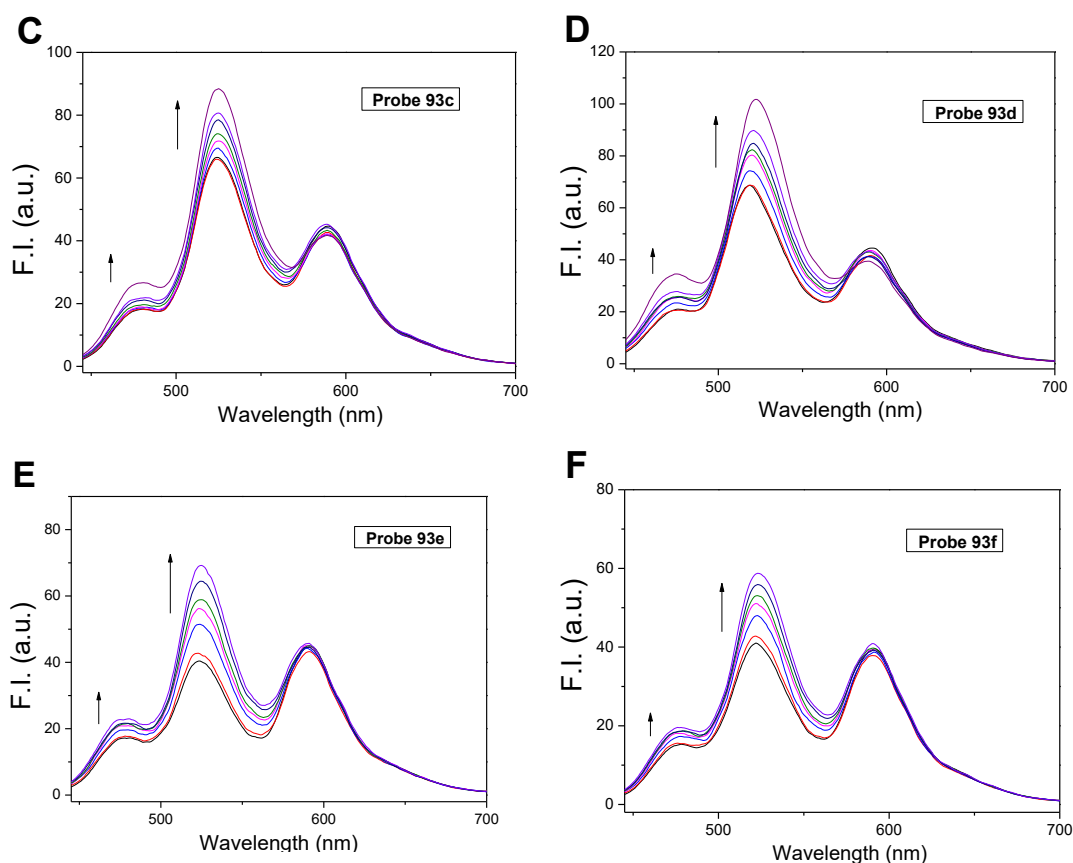


**Figure 53** Emission spectra of probes **93a-f** (2  $\mu\text{M}$ , A-E) after treatment with active caspase-9 for 2 h (6 U/mL, HEPES Buffer, NaCl, EDTA, DTT, 5% glycerol).

As a result of abovementioned experiments, we chose Probe **93-e** for further studies due to its moderate FRET efficiency and the best rate of cleavage by caspase-9 that was observed among tested probes. Figure 54 summarizes data for cleavage of this probe by caspase-8, caspase-9 and both caspases simultaneously. As expected, cleavage by caspase-8 is considerably faster and emission of coumarine is rising significantly (almost 6-fold). According to LC/MS analysis the probe **93e** (2  $\mu\text{M}$ ) is fully cleaved after 180 min in the presence of 20 Units/mL of caspase-8 yielding to cleavage products depicted in Figure 55. In the presence of 40 Units/mL of caspase-9 the increase in fluorescein emission is up to 5-fold.

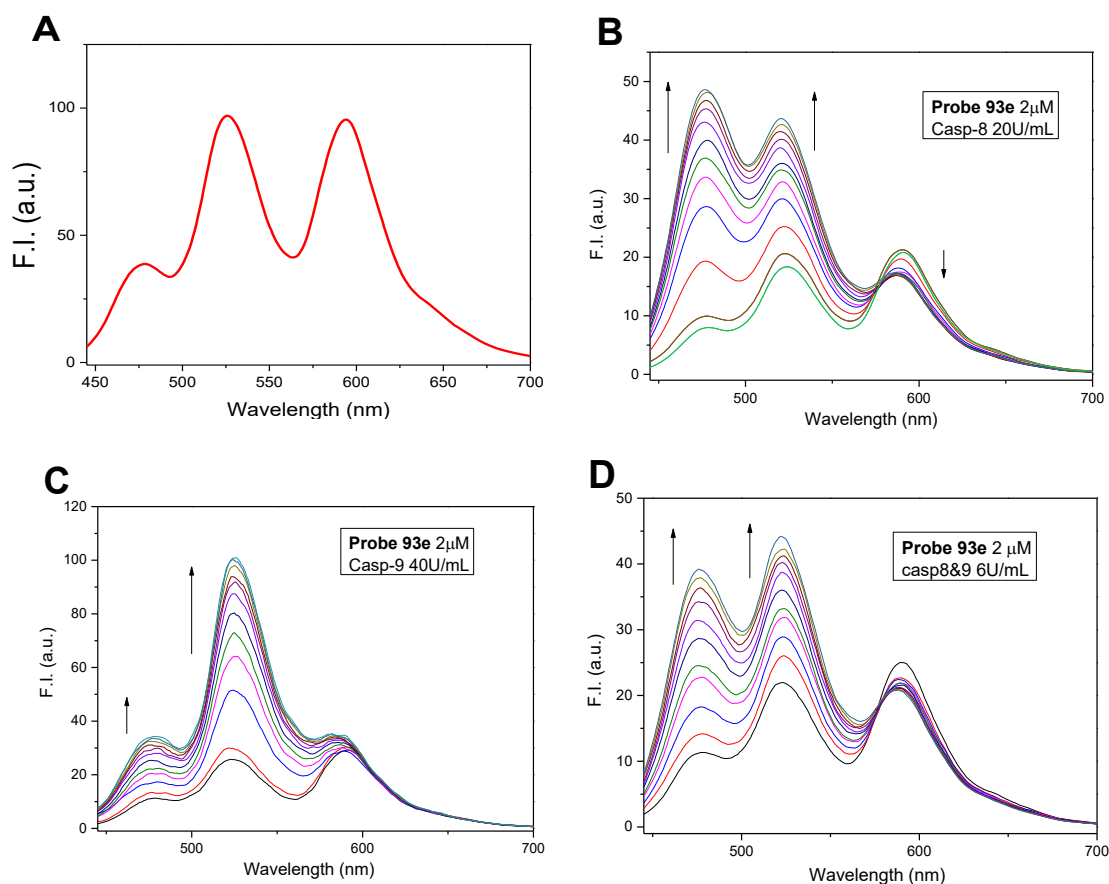


**Figure 54** (A) Emission profile of intact Probe **93e** (50mM HEPES, pH 7.2, 50mM sodium chloride, 10mM EDTA, 5% glycerol, 10mM DTT; 37 °C), (B) after treatment with caspase-8 (2 μM probe, 20 U/mL), (C) caspase-9 (2 μM probe, 40 U/mL) and (D) mixture of both caspases-8 and -9 (2 μM probe, 6 U/mL each caspase). Excitation wavelength 425nm.

However, according to LC/MS analysis cleavage by caspase-8 or -9 is usually incomplete after 3 h in concentration range that was used (up to 20 U/mL and 40 U/mL for caspase-8 and -9, respectively) and products of cross linker cleavage are formed due to non-selectivity of caspases to its substrate linker and different cleavage rates. Non-selectivity of the cleavage is more significant in the case of caspase-9 as the Figure 55 shows. Treatment by caspase-9 leads to formation of expected cleavage products **105** and **106** and cross linker cleavage by-products **103** and **104**. Treatment by caspase-8 was accompanied only with slight non-selective cleavage of caspase-9 linker to obtain main cleavage products **103** and **104** as demonstrated by Figure 56.



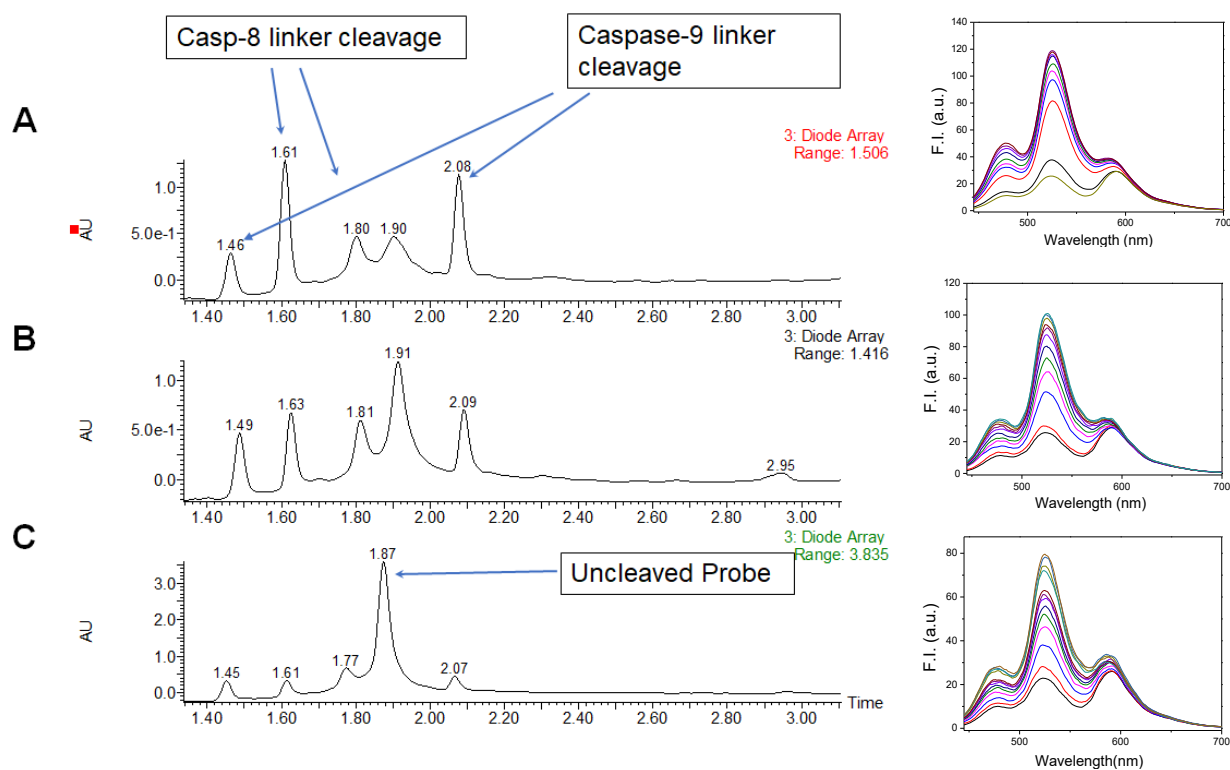
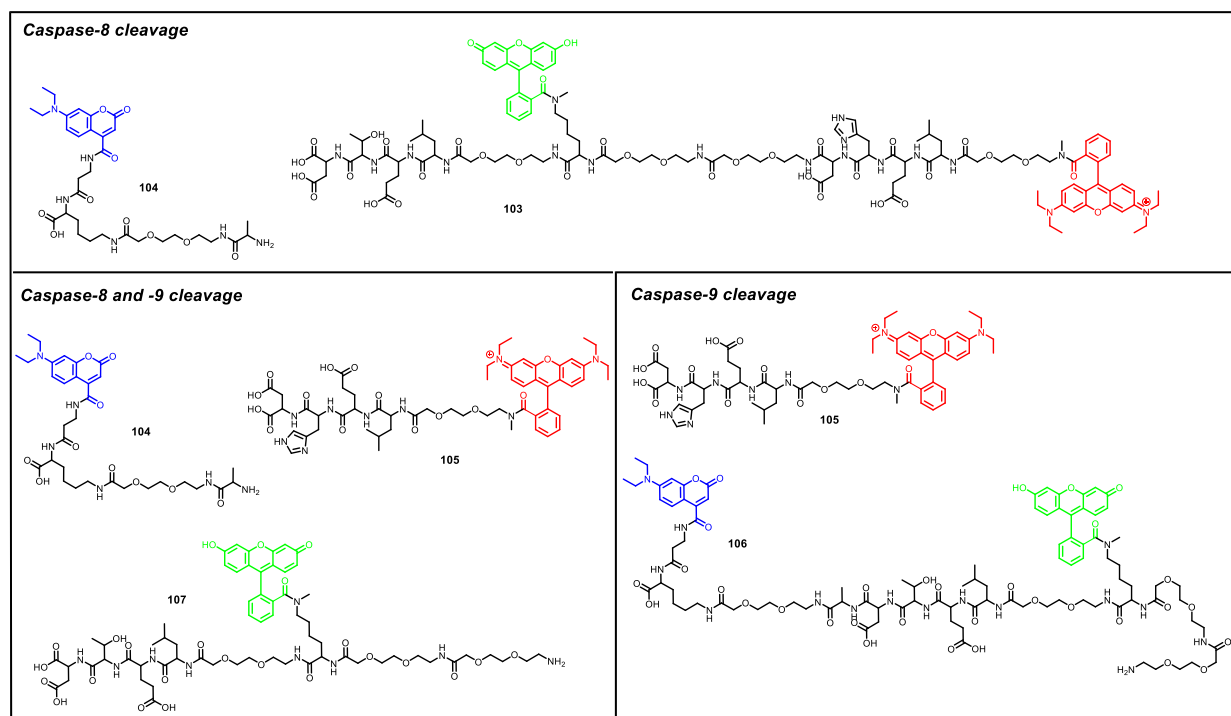


**Figure 55** LC/MS analysis of cleavage products after cleavage by caspase-9 (left) and fluorescence response upon excitation at 425 nm (right). Caspase-9 concentration: (A) 80 U/mL, (B) 40 U/mL and (C) 20 U/mL.

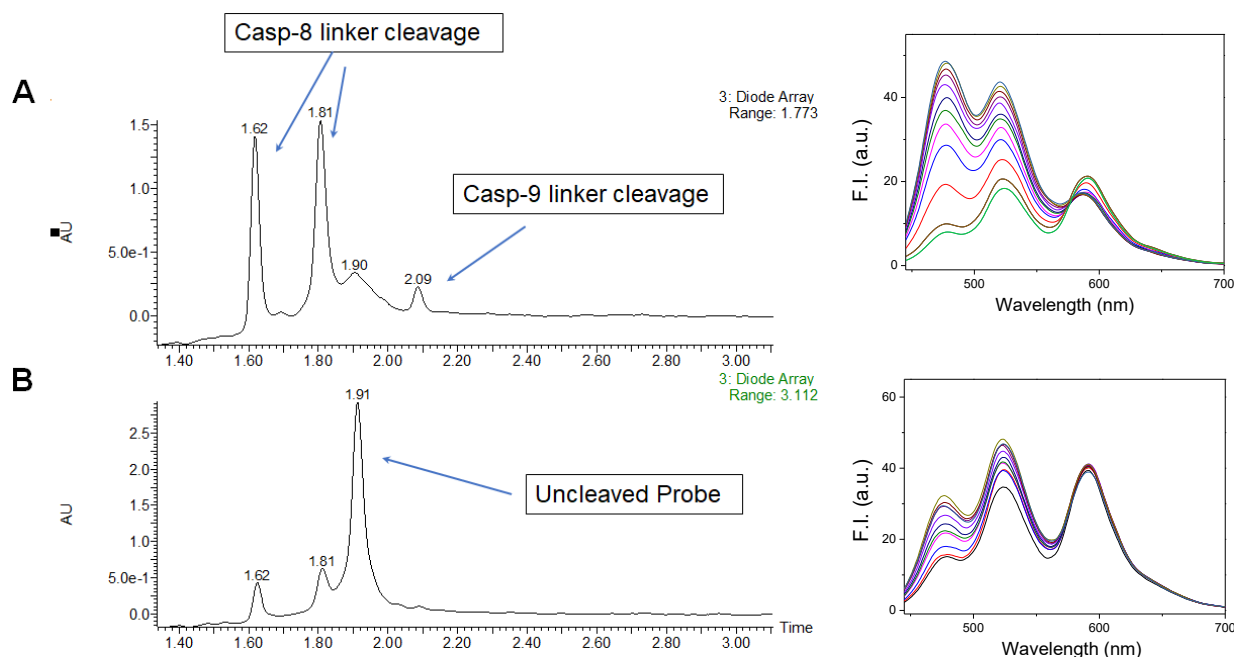


**Figure 56** LC/MS analysis of cleavage products after cleavage of the Probe **93e** (2  $\mu$ M) by caspase-8 (left) and fluorescence response upon excitation at 425 nm (right). Caspase-8 concentration: (A) 2 U/mL and (B) 0.5 U/mL.

#### 4.3 Mathematical “sun watch” model

To unambiguously distinguish between presence of any caspase solely or in their mixture we had to develop reliable mathematical model. The model used for previous model trypsin/chymotrypsin probe<sup>184</sup> we found insufficient mainly because of non-selectivity of caspase-9.<sup>174</sup> Therefore, in this case we applied new model where we used  $X = \text{Em}_{\text{DEAC}} / \text{Em}_{\text{FI}}$  against  $Y = \text{Em}_{\text{RhB}} / \text{Em}_{\text{FI}}$ . When we plot ratio  $X_0 / X_t$  ( $X_0$  is value in time = 0 min;  $X_t$  is value in appropriate time interval) against  $Y_0 / Y_t$  in Cartesian coordinate system, we obtained curve that starts from point [1,1] (as the  $X_t = X_0$  and  $Y_t = Y_0$ ) and is linear in adequately broad interval. These lines obtained from cleavage of probe **93e** by individual caspases-8 and-9 intersect at an angle approximately  $80^\circ$  (Figure 57, black and left red line) to make an appropriate sector in coordinate system. The lines corresponding to any mixture of both enzymes in various concentrations lies inside this sector.

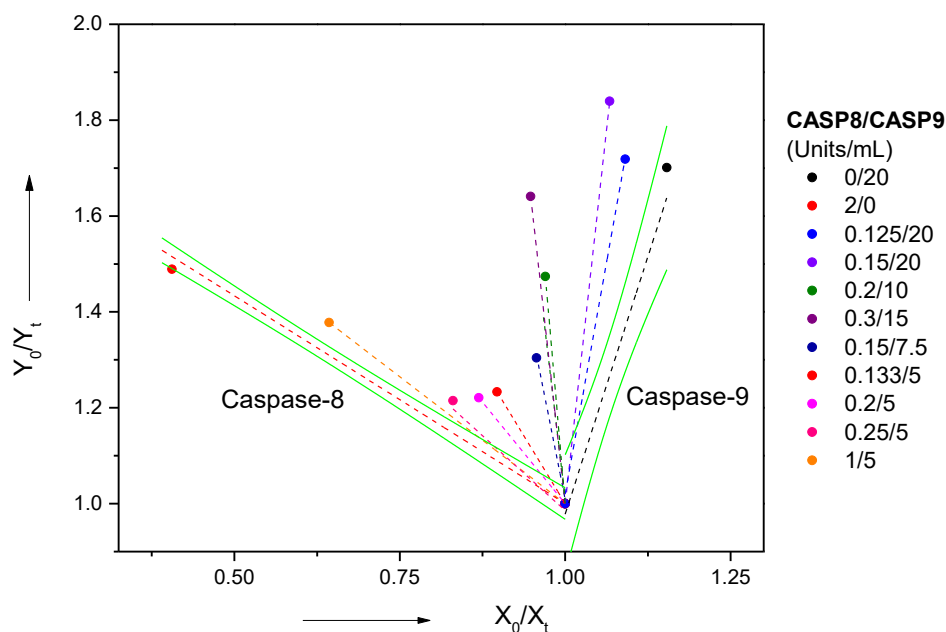


**Figure 57** “Sun watch” model for detection and quantification of caspases-8 and -9. All data points acquired after 120 min on incubation with corresponding caspase mixture.

Multiple mixtures with various relative and absolute concentration of caspase-8 and -9 were measured as Figure 57 summarizes. The measurement had to be performed strictly at the 37°C as even slight changes of sample temperature caused fluctuation of emission intensity, mainly of RhB. Usually, the probe in buffer was incubated for 10-15 min and the emission upon excitation at 425 nm was measured ( $t_0$ ). Then corresponding amount of enzyme was added and emission was measured in time intervals (up to 120 min). Interestingly, linear curves were obtained in appropriate individual enzyme concentration range – 0.125 – 2 U/mL and 2.5 - 20 U/mL for caspase-8 and -9, respectively, during incubation for 120 min (Figure 58 A, B). Detection and quantification limits were determined as 10xSD (error bars) of blank samples measured after 120 min incubation at 37°C without enzyme as depicted in Figure 58. Higher than upper limit concentrations of enzymes caused loss of linearity and bending of curves towards the central axis probably due to lower selectivity of enzymatic cleavage and rapid non-distinguishing consumption of substrate (Figure 58 C, D). Therefore, we specify the operational region for guidance purposes as depicted by the red boxes in Figure 58 C and D where valid datapoints should be located within limit of quantification and are defined as 0.125-2 U/mL and 5-20 U/mL for **individual** caspase-8 and -9, respectively. Detection limits for **mixtures** of enzymes were slightly different to those determined for individual enzymes and were set as concentrations of enzymes in mixture distinguishable from the single enzyme curve (e.g. orange curve for 1u5u mixture is recognizable from red CASP-8 curve, Figure 57) based on 95%

probability curve (green solid curves). Combination of CASP-8 and CASP-9 clearly distinguishable from individual enzymes were determined as 1 U/mL and 5 U/mL of caspase-8 and caspase-9, respectively ( $X_{\text{casp8}} = 17\%$ ) and 0.125 U/mL and 20 U/mL of caspase-8 and caspase-9, respectively ( $X_{\text{casp8}} = 0.6\%$ ), while all mixtures in this interval should be located inside the sector.  $X_{\text{casp8}}$  refers to relative molar concentration of caspase-8 in the sample. According to this model we are limited to determination of relative enzyme concentration and not absolute concentration of enzymes in the sample. Mixtures with the same relative concentration (ratio; e.g. CASP-8/CASP-9 0.15u7.5u, 0.2u10u, 0.3u15u, Figure 57) showed approximately the same angle.

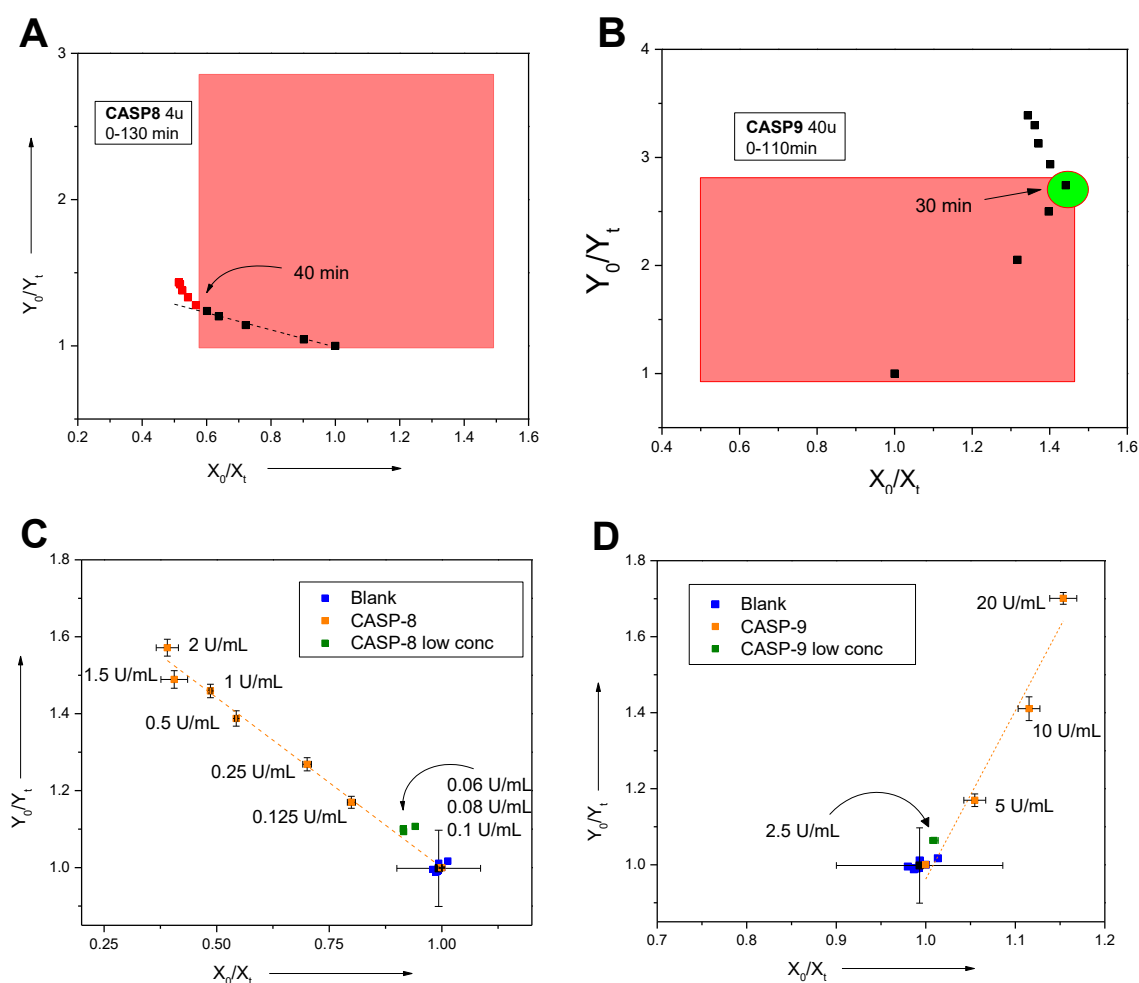


**Figure 58** Determination of linear region (red box) and overconcentrated non-linear region in samples containing (A) 4 U/mL of caspase-8 and (B) 40 U/mL of caspase-9 together with the Probe **93e** (2  $\mu\text{M}$ ). Determination of LOD and LOQ for (C) caspase-8 and (D) caspase-9. Data points were measured in at least 3 repetitions after 120 min of incubation at 37  $^\circ\text{C}$  with corresponding enzyme concentration.

Since the process of apoptosis is accompanied by activation of other caspases than caspase-8 or -9, mainly executioner caspase-3 and caspase-7 we investigated also the selectivity

of recombinant caspases -3 and -7 towards the probe **93e**. Probe **93e** was treated with 1, 3, 6 U/mL of caspase-3 and -7 in similar fashion as for the previous experiments with caspase-8 and -9 summarized in Figure 59. In the case of caspase-3, significant cleavage of caspase-8 linker (LETD) was observed resulting in the green data points following the trend of caspase-8 curve (red). Caspase-7 did not significantly cleave any of the peptide linkers in Probe **93e** what is demonstrated by blue points close to or within standard deviation (error bars) of blank measurements (Figure 59).

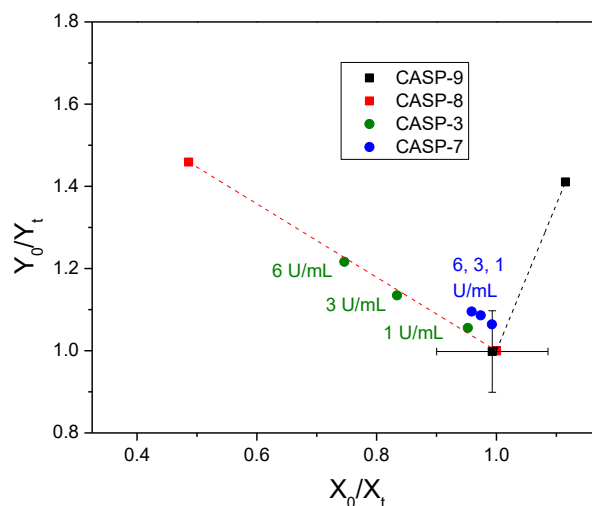


**Figure 59** Cleavage selectivity of caspase-3 and -7. Caspase-3 and -7 cleavage of the Probe **93e** measured in concentration 1, 3, 6 Units/mL after 120 min of incubation at 37°C (pH 7.2, HEPES Buffer, NaCl, EDTA, DTT, 5% glycerol).

#### 4.4 Biology

To demonstrate the functionality of the proposed system and mathematical model on cell culture we established a collaboration with the group of Vladimir Kryštof from Laboratory of Growth Regulators (LGR, Palacky University Olomouc). Cell lysates of various cancer cell lines – MV4-11, MINO, REC-1 and JURKAT wild-type (WT) and special caspase-8 deficient and caspase-9 deficient types were prepared by treatment with several known agents inducing apoptosis including caspase-9 selective inducers doxorubicin (DOXO) and taxol (TAX) and caspase-8 selective inducer - tumor necrosis factor/cycloheximide (TNF/CHX).

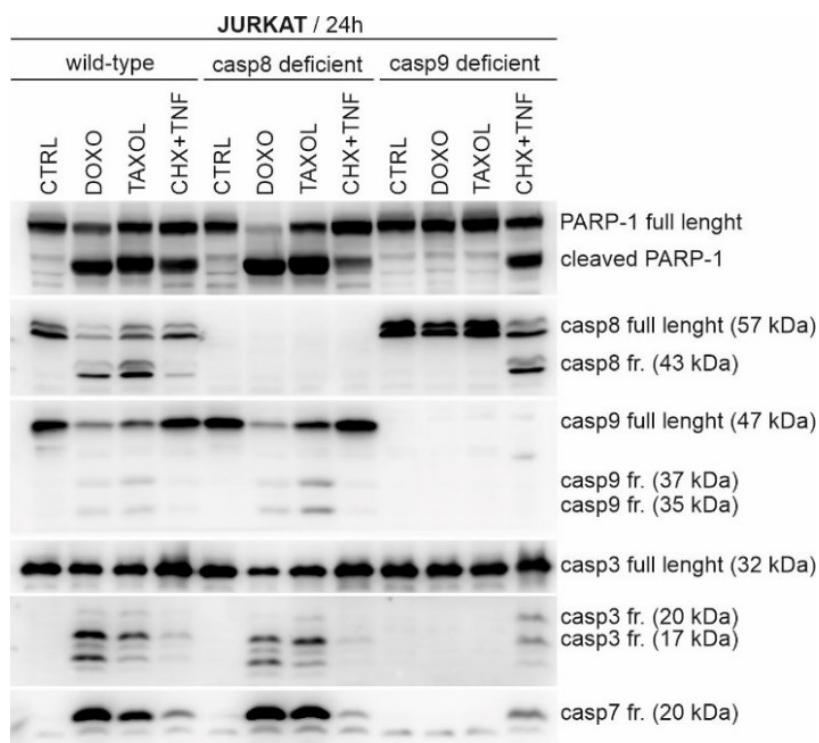


**Figure 60** Western blot analysis of JURKAT cell lysates of WT, casp-8 and casp-9 deficient cell lines with activation by DOXO, TAX and CHX/TNF.

Treatment of selected cell lines by some caspase inducers initiated the programmed cell death – apoptosis as indicated by cleaved PARP-1 (Figure 60). PARP-1 is one of few known cellular substrates of caspases and acts as a mediator of apoptotic cell death. Cleavage of PARP-1 is therefore considered as a hallmark of apoptosis.<sup>185,186</sup> In western blot analysis we used inactive caspase-8 57kDa and inactive caspase-9 47kDa as the references. These inactive procaspases can be transformed to their active forms – caspase-8 (43kDa) and caspase-9 (35 or 37 kDa) possibly detectable in western blot.

a) Testing of the probe on wild type cell line

In wild type cell line (WT) both caspase-8 and caspase-9 can be activated from their inactive forms. After treatment of these cells by doxorubicin, taxol or CHX/TNF the apoptosis occurred as indicated by the higher abundance of cleaved PARP-1. In case of doxorubicin and taxol treatment the procaspase-8 is diminished and active caspase-8 is in higher extent in comparison to the control experiment. Similarly, the active caspase-9 is generated from its procaspase, although less significantly. In case of CHX/TNF treatment caspase-8 is activated only slightly, while caspase-9 almost not at all. When we compare the observations of western blot results with our sun-watch model, we can observe a very good agreement. The lines for DOXO and

TAX treatment responded to a mixture of caspase-8 and caspase-9, while no significant response was observed for CHX/TNF treatment.

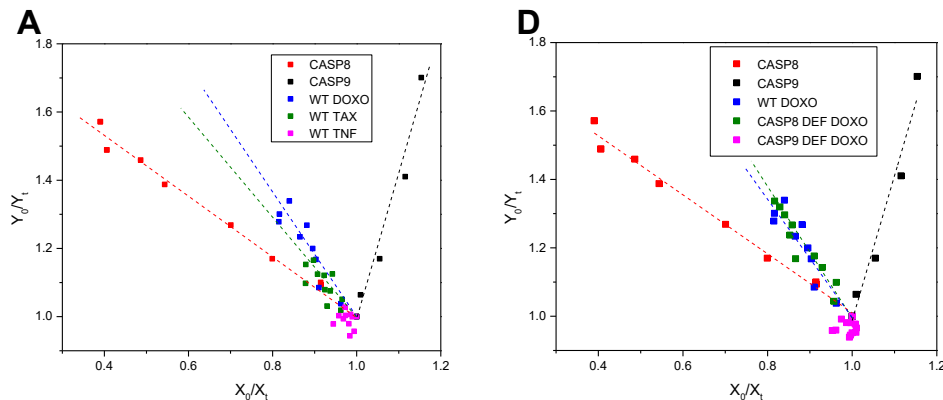
b) Testing of the probe on caspase-8 deficient cell line

Significant cleavage of PARP-1 was observed in JURKAT caspase-8 deficient cells after treatment with DOXO and TAXOL as indicated by western blot Figure 60. However, treatment of caspase-8 deficient cells with CHX-TNF led only to insignificant PARP-1 cleavage and thus small amounts of activated caspases. DOXO and TAX activation in caspase-8 deficient cells led also to generation of high amount of caspase-7 and caspase-3 besides desired caspase-9 initiator caspase. Arguably, the presence of mixture of caspases caused the lower angle of the curves in model representation (Figure 61 A) mainly due to the presence of caspase-3 which causes false positive results for caspase-8 as demonstrated in the Figure 59. However, small change of angle may be observed when results of WT and casp-8 deficient cells are compared, suggesting the presence of higher amount of caspase-8 and/or caspase-3/7 in WT cell lysate (light blue vs dark blue in DOXO and TAX graphs).

c) Testing of the probe on caspase-9 deficient cell line.

Based on the western blot analysis, only treatment of caspase-9 deficient cells with TNF-CHX resulted in apoptosis and cleavage of PARP-1 while activation of caspase-8, no caspase-9 and little amount of casp-3/7 occurred. This observation is in accordance with our model where the curve (CASP-9 DEF TNF/CHX, Figure 61) runs alongside with the pure recombinant caspase-8 line (marked as red points).

Cell lysates in which the apoptosis was not effectively induced and PARP-1 cleavage did not occur possessed only caspases in their native concentrations. In our caspase model it is translated as data points within the standard deviation of blank measurement (around point [1,1]) and is in accordance with western blot experiment (Figure 61).



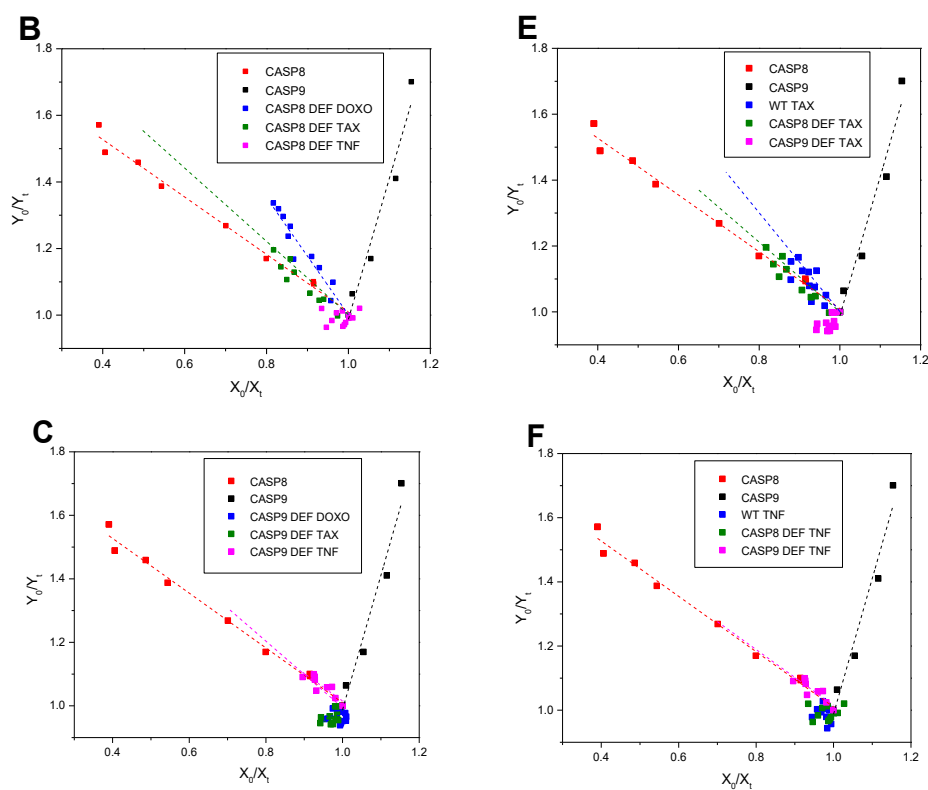


**Figure 61** Incubation of the probe **93e** with cell lysates from WT and caspase-8 and caspase-9 deficient cell lines treated with DOXO, TAX or TNF/CHX. Each figure A-C represents comparison of various treatments in the same line while each figure D-F represents comparison of the same treatment in various cell lines

Since the generation of executioner caspases-3 and -7 in cell lysates was not negligible and contributed to a false response we considered also the use of caspase-3/7 inhibitor – the peptide sequence Ac-DEVD-CHO as their preferred substrate.<sup>180</sup> However, we found out that not only desired inhibition of caspase-3/7 occurs but the inhibitor blocks also activity of caspase-8 in the various concentrations (10, 50, 100  $\mu$ M) as demonstrated in Figure 62.



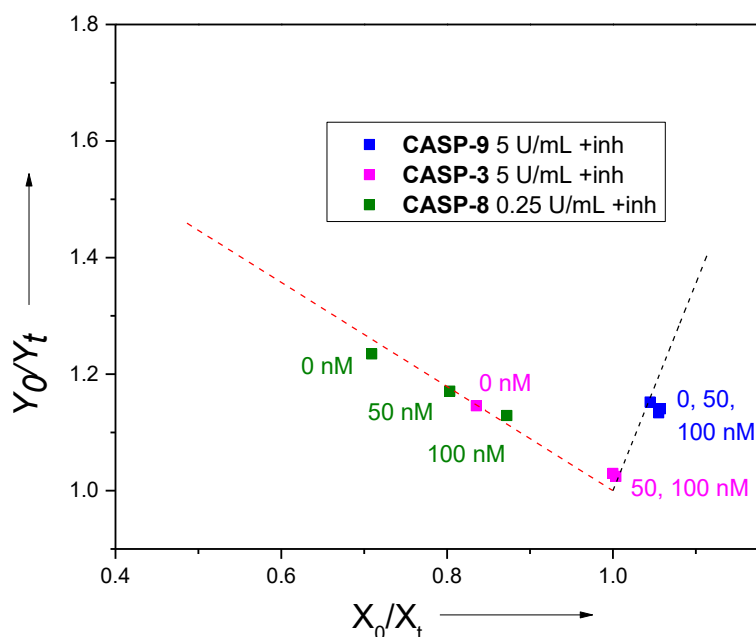


**Figure 62** Inhibition of caspase-3, -8, -9 by caspase-3 selective inhibitor Ac-DEVD-CHO in concentrations 0, 50, 100 nM (50mM HEPES buffer, 50mM NaCl, 10mM EDTA, 10mM DTT, 5% glycerol, pH 7.2, 37 °C) in presence of the Probe **93e** (2  $\mu$ M). Concentration of caspases: caspase-8 0.25 U/mL, caspase-9 5 U/mL, caspase-3 5 U/mL.

To rule out the caspase-3 cleavage of the Probe **93e** in the cell lysates, mainly caspase-8 DEF cells which gave positively false results because of presence of caspase-3 we carried out series of inhibition experiments. As demonstrated by Figure 62, caspase-9 was not inhibited in chosen concentration range (0-100 nM), caspase-8 exhibited only partial inhibition and caspase-3 was effectively inhibited at 50nM and higher concentration of caspase-3 inhibitor. Treatment of JURKAT CASP-8 DEF cell lysates with various concentrations of caspase-3 inhibitor Ac-DEVD-CHO led to gradual shift of the curves (Figure 63 C, D) towards caspase-9 line (to the right) in the sun-watch model representation as expected. However, currently we are not able to credibly quantify activity of caspase-8 vs caspase-9 due to partial inhibition of caspase-8 by Ac-DEVD-CHO inhibitor. Therefore, arguably the proposed model would be valid for relative quantification in cell lysates in combination with more selective inhibitor of caspase-3. One of such inhibitors proposed by Wolan et al. could be of a good choice.<sup>187</sup>

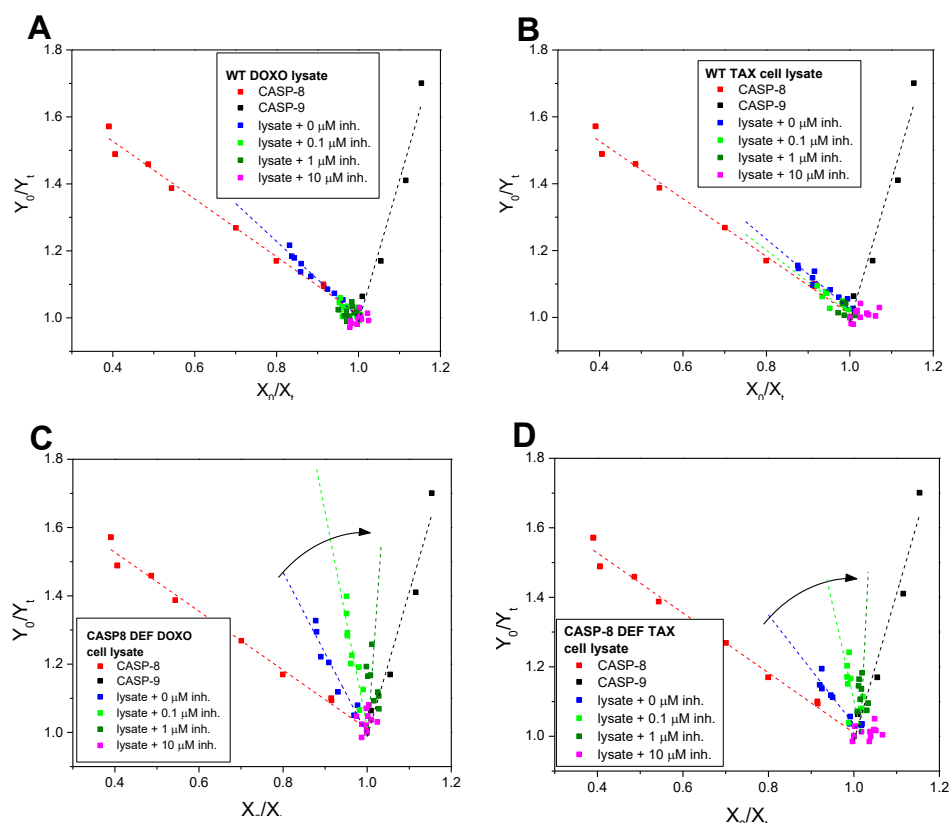


**Figure 63** Treatment of WT and CASP8-DEF cell lysates with caspase-3 selective inhibitor Ac-DEVD-CHO in concentrations 0, 0.1, 1 and 10  $\mu\text{M}$ .

#### 4.5 Conclusion

In summary, we prepared a series of three fluorophore multi-FRET probes for caspase-8 and -9 detection and relative quantification by solid phase chemistry approach. Peptide substrates - LETD and LEHD served as linkers and preferred cleavage sites for caspase-8, resp. caspase-9. Prepared compounds exhibited different FRET efficiencies and selectivity towards caspase cleavage and for further studies we chose the probe **93e** with moderate FRET efficiency and the best selectivity towards caspase-9 among tested probes. Mathematical "sun-watch" model was developed in order to evaluate the activity of caspase-8 and -9 in cell lysates simultaneously. However, we found that executioner caspase-3 also cleaves the probe **93e** selectively at LETD (caspase-8) linker and the use of Ac-DEVD-CHO inhibitor was necessary in the cell lysates where whole cascade of caspases was activated. Inhibition of caspase-3 led to significant shift of the curve in mathematical model representation towards caspase-9 content in caspase-8 Def cell lysate and no shift was observed in WT cell lysates. This means that caspase-8 was activated in much higher extent in wild type cells than caspase-9 or caspase-9 was activated in amount lower than detection limit (2.5 U/mL). On the other hand, since

caspase-8 could not be activated in caspase-8 deficient cells apoptosis was triggered by activation of caspase-9 according to western blot and confirmed also by our model.

**Submitted articles:**

Porubský, M.; Řezníčková, E.; Kryštof, V.; Hlaváč, J. Development of fluorescent dual-FRET probe for simultaneous detection and relative quantification of caspase-8 and caspase-9. (*submitted*).

## 5 Literature

- (1) Panche, A. N.; Diwan, A. D.; Chandra, S. R. *J. Nutr. Sci.* **2016**, *5*.
- (2) Castañeda-Ovando, A.; Pacheco-Hernández, M. de L.; Páez-Hernández, M. E.; Rodríguez, J. A.; Galán-Vidal, C. A. *Food Chem.* **2009**, *113* (4), 859–871.
- (3) Pietta, P. G. *J. Nat. Prod.* **2000**, *63* (7), 1035–1042.
- (4) Si, H.; Liu, D.; Si, H.; Liu, D. *Curr. Med. Chem.* **2007**, *14* (24), 2581–2589.
- (5) Choy, K. W.; Murugan, D.; Leong, X. F.; Abas, R.; Alias, A.; Mustafa, M. R. *Front. Pharmacol.* **2019**, *10* (OCT), 1–8.
- (6) Lee, J. Y.; Jeong, K. W.; Shin, S.; Lee, J. U.; Kim, Y. *Bioorganic Med. Chem.* **2009**, *17* (15), 5408–5413.
- (7) Emmerson, A. M.; Jones, A. M. *J. Antimicrob. Chemother.* **2003**, *51* (SUPPL. 1), 13–20.
- (8) Oliphant, C. M.; Green, G. M. *Am. Fam. Physician* **2002**, *65* (3), 455–464.
- (9) Pham, T. D. M.; Ziora, Z. M.; Blaskovich, M. A. T. *Medchemcomm* **2019**, *10* (10), 1719–1739.
- (10) Sparano, J. A.; Moulder, S.; Kazi, A.; Coppola, D.; Negassa, A.; Vahdat, L.; Li, T.; Pellegrino, C.; Fineberg, S.; Munster, P.; Malafa, M.; Lee, D.; Hoschander, S.; Hopkins, U.; Hershman, D.; Wright, J. J.; Kleer, C.; Merajver, S.; Sebti, S. M. *Clin. Cancer Res.* **2009**, *15* (8), 2942–2948.
- (11) Ni, Z. J.; Barsanti, P.; Brammeier, N.; Diebes, A.; Poon, D. J.; Ng, S.; Pecchi, S.; Pfister, K.; Renhowe, P. A.; Ramurthy, S.; Wagman, A. S.; Bussiere, D. E.; Le, V.; Zhou, Y.; Jansen, J. M.; Ma, S.; Gesner, T. G. *Bioorganic Med. Chem. Lett.* **2006**, *16* (12), 3121–3124.
- (12) Cheng, P.; Zhang, Q.; Ma, Y. B.; Jiang, Z. Y.; Zhang, X. M.; Zhang, F. X.; Chen, J. J. *Bioorganic Med. Chem. Lett.* **2008**, *18* (13), 3787–3789.
- (13) Upadhyay, K. D.; Dodia, N. M.; Khunt, R. C.; Chaniara, R. S.; Shah, A. K. *ACS Med. Chem. Lett.* **2018**, *9* (3), 283–288.
- (14) Shin, S.; Guerra, D.; Rich, M.; Seung, K. J.; Mukherjee, J.; Joseph, K.; Hurtado, R.; Alcantara, F.; Bayona, J.; Bonilla, C.; Farmer, P.; Furin, J. *Clin. Infect. Dis.* **2003**, *36* (8), 996–1003.
- (15) Lee, G. C.; Reveles, K. R.; Attridge, R. T.; Lawson, K. A.; Mansi, I. A.; Lewis, J. S.; Frei, C. R. *BMC Med.* **2014**, *12* (1).
- (16) Advani, R. H.; Hurwitz, H. I.; Gordon, M. S.; Ebbinghaus, S. W.; Mendelson, D. S.; Wakelee, H. A.; Hoch, U.; Silverman, J. A.; Havrilla, N. A.; Berman, C. J.; Fox, J. A.; Allen, R. S.; Adelman, D. C. *Clin. Cancer Res.* **2010**, *16* (7), 2167–2175.
- (17) Zhou, P.; Huang, L.; Zhou, J.; Jiang, B.; Zhao, Y.; Deng, X.; Zhao, Q.; Li, F. *Bioorganic Med. Chem. Lett.* **2017**, *27* (17), 4185–4189.
- (18) Suthar, S. K.; Jaiswal, V.; Lohan, S.; Bansal, S.; Chaudhary, A.; Tiwari, A.; Alex, A. T.; Joseph, A. *Eur. J. Med. Chem.* **2013**, *63*, 589–602.
- (19) Pommier, Y. *ACS Chem. Biol.* **2013**, *8*, 82–95.
- (20) Uivarosi, V. *Molecules* **2013**, *18* (9), 11153–11197.
- (21) Iv, T.; Marians, K. J.; Hiasa, H. *J. Biol. Chem.* **1997**, *272* (14), 9401–9409.
- (22) Visone, V.; Vettone, A.; Serpe, M.; Valenti, A.; Perugino, G.; Rossi, M.; Ciaramella, M. *Int. J. Mol. Sci.* **2014**, *15* (9), 17162–17187.
- (23) Bau, J. T.; Kang, Z.; Austin, C. A.; Kurz, E. U. *Mol. Pharmacol.* **2014**, *85* (2), 198–207.
- (24) Abdel-Aal, M. A. A.; Abdel-Aziz, S. A.; Shaykoon, M. S. A.; Abuo-Rahma, G. E. D. A. *Arch. Pharm. (Weinheim)*. **2019**, *352* (7).
- (25) Dhiman, P.; Arora, N.; Thanikachalam, P. V.; Monga, V. *Bioorg. Chem.* **2019**, *92* (May),

- 103291.
- (26) Ayadi, A. and; Melard, G. *Nat. Rev. Drug Discov.* **2011**, *10* (4), 261–275.
- (27) Li, J.; Zheng, T. C.; Jin, Y.; Xu, J. G.; Yu, J. G.; Lv, Y. W. *Chem. Pharm. Bull.* **2018**, *66* (1), 55–60.
- (28) Hradil, P.; Hlavac, J.; Soural, M.; Hajduch, M.; Kolar, M.; Vecerova, R. *Mini-Reviews Med. Chem.* **2009**, *9* (6), 696–702.
- (29) Sui, Z.; Nguyen, V. N.; Altom, J.; Fernandez, J.; Hilliard, J. J.; Bernstein, J. I.; Barrett, J. F.; Ohemeng, K. A. *Eur. J. Med. Chem.* **1999**, *34* (5), 381–387.
- (30) Lucie Spáčilová, Jan Hlaváč, Pavel Hradil, Iveta Fryšová, Miroslav Soural, Petr Krejčí, M. M. *J. Heterocycl. Chem.* **2006**, *43*, 1065–1070.
- (31) Soural, M.; Hlaváč, J.; Funk, P.; Džubák, P.; Hajdúch, M. *ACS Comb. Sci.* **2011**, *4*, 39–44.
- (32) Motyka, K.; Hlaváč, J.; Soural, M.; Hradil, P.; Krejčí, P.; Kvapil, L.; Weiss, M. *Tetrahedron Lett.* **2011**, *52* (6), 715–717.
- (33) Motyka, K.; Hlaváč, J.; Soural, M.; Funk, P. *Tetrahedron Lett.* **2010**, *51* (38), 5060–5063.
- (34) Krajčovičová, S.; Stanková, J.; Džubák, P.; Hajdúch, M.; Soural, M. *Chem. - A Eur. J.* **2018**, *24*, 4957–4966.
- (35) Funk, P.; Motyka, K.; Džubák, P.; Znojek, P.; Gurská, S.; Kusz, J.; McMaster, C.; Hajdúch, M.; Soural, M. *RSC Adv.* **2015**, *5* (60), 48861–48867.
- (36) Krajčovičová, S.; Hlaváč, J.; Vychodilová, K. *RSC Adv.* **2021**, *11* (16), 9362–9365.
- (37) Hradil, P.; Jirman, J. *Collect. Czechoslov. Chem. Commun.* **1995**, *60* (8), 1357–1366.
- (38) Hradil, P.; Krejci, P.; Hlavac, J.; Wiedermannova, I.; Lycka, A.; Bertolasi, V. *J. Heterocycl. Chem.* **2004**, *41* (3), 375–379.
- (39) Soural, M.; Hlaváč, J.; Hradil, P.; Fryšová, I.; Hajdúch, M.; Bertolasi, V.; Maloň, M. *Eur. J. Med. Chem.* **2006**, *41* (4), 467–474.
- (40) Burglová, K.; Rylová, G.; Markos, A.; Přichystalová, H.; Soural, M.; Petráček, M.; Medvedíkova, M.; Tejral, G.; Sopko, B.; Hradil, P.; Džubák, P.; Hajdúch, M.; Hlaváč, J. *J. Med. Chem.* **2018**, *61* (7), 3027–3036.
- (41) Tomlinson, V. A. L.; Newbery, H. J.; Wray, N. R.; Jackson, J.; Larionov, A.; Miller, W. R.; Dixon, J. M.; Abbott, C. M. *BMC Cancer* **2005**, *5*, 1–7.
- (42) Cagno, M. Di; Stein, P. C.; Styskala, J.; Hlaváč, J.; Skalko-Basnet, N.; Bauer-Brandl, A. *Eur. J. Pharm. Biopharm.* **2012**, *80* (3), 657–662.
- (43) di Cagno, M.; Styskala, J.; Hlaváč, J.; Brandl, M.; Bauer-Brandl, A.; Skalko-Basnet, N. *J. Liposome Res.* **2011**, *21* (4), 272–278.
- (44) Tang, F. K.; Zhu, J.; Kong, F. K. W.; Ng, M.; Bian, Q.; Yam, V. W. W.; Tse, A. K. W.; Tse, Y. C.; Leung, K. C. F. *Chem. Commun.* **2020**, *56* (18), 2695–2698.
- (45) Chyan, W.; Raines, R. T. *ACS Chem. Biol.* **2018**, *13* (7), 1810–1823.
- (46) Baki, C. N.; Akkaya, E. U. *J. Org. Chem.* **2001**, *66*, 1512–1513.
- (47) Zhang, D.; Martín, V.; García-Moreno, I.; Costela, A.; Pérez-Ojeda, M. E.; Xiao, Y. *Phys. Chem. Chem. Phys.* **2011**, *13* (28), 13026–13033.
- (48) Chen, J. J.; Conron, S. M.; Erwin, P.; Dimitriou, M.; McAlahney, K.; Thompson, M. E. *ACS Appl. Mater. Interfaces* **2015**, *7* (1), 662–669.
- (49) Zampetti, A.; Minotto, A.; Squeo, B. M.; Gregoriou, V. G.; Allard, S.; Scherf, U.; Chochos, C. L.; Cacialli, F. *Sci. Rep.* **2017**, *7* (1), 1–7.
- (50) De Bonfils, P.; Péault, L.; Nun, P.; Coeffard, V. *European J. Org. Chem.* **2021**, *2021* (12), 1809–1824.
- (51) Yang, H.; Wang, J.; Ma, J.; Yang, H.; Zhang, J.; Lv, K.; Wen, L.; Peng, T. *J. Mater. Chem. A* **2019**, *7* (17), 10439–10445.
- (52) Engelhardt, V.; Kuhri, S.; Fleischhauer, J.; García-Iglesias, M.; González-Rodríguez, D.;

- Bottari, G.; Torres, T.; Guldi, D. M.; Faust, R. *Chem. Sci.* **2013**, *4* (10), 3888–3893.
- (53) Kue, C. S.; Ng, S. Y.; Voon, S. H.; Kamkaew, A.; Chung, L. Y.; Kiew, L. V.; Lee, H. B. *Photochem. Photobiol. Sci.* **2018**, *17* (11), 1691–1708.
- (54) Kaur, P.; Singh, K. *J. Mater. Chem. C* **2019**, *7* (37), 11361–11405.
- (55) Kowada, T.; Maeda, H.; Kikuchi, K. *Chem. Soc. Rev.* **2015**, *44* (14), 4953–4972.
- (56) Loudet, A.; Burgess, K. *Chem. Rev.* **2007**, *107* (11), 4891–4932.
- (57) Boens, N.; Verbelen, B.; Ortiz, M. J.; Jiao, L.; Dehaen, W. *Coord. Chem. Rev.* **2019**, *399*.
- (58) Umezawa, K.; Matsui, A.; Nakamura, Y.; Citterio, D.; Suzuki, K. *Chem. - A Eur. J.* **2009**, *15* (5), 1096–1106.
- (59) Rohand, T.; Baruah, M.; Qin, W.; Boens, N.; Dehaen, W. *Chem. Commun.* **2006**, No. 3, 266–268.
- (60) Rurack, K.; Kollmannsberger, M.; Daub, J. *Angew. Chemie - Int. Ed.* **2001**, *40* (2), 385–387.
- (61) Bonardi, L.; Ulrich, G.; Ziesel, R. *Org. Lett.* **2008**, *10* (11), 2183–2186.
- (62) Li, L.; Han, J.; Nguyen, B.; Burgess, K. *J. Org. Chem.* **2008**, *73* (5), 1963–1970.
- (63) Jiao, L.; Yu, C.; Li, J.; Wang, Z.; Wu, M.; Hao, E. *J. Org. Chem.* **2009**, *74* (19), 7525–7528.
- (64) Mirri, G.; Schoenmakers, D. C.; Kouwer, P. H. J.; Veranič, P.; Mušević, I.; Štefane, B. *ChemistryOpen* **2016**, *5* (5), 450–454.
- (65) Buyukcakir, O.; Bozdemir, O. A.; Kolemen, S.; Erbas, S.; Akkaya, E. U. *Org. Lett.* **2009**, *11* (20), 4644–4647.
- (66) Gómez-Durán, C. F. A.; García-Moreno, I.; Costela, A.; Martín, V.; Sastre, R.; Bañuelos, J.; López Arbeloa, F.; López Arbeloa, I.; Peña-Cabrera, E. *Chem. Commun.* **2010**, *46* (28), 5103–5105.
- (67) Johnson, L. V.; Walsh, M. L.; Chen, L. B. *Proc. Natl. Acad. Sci. U. S. A.* **1980**, *77* (2 II), 990–994.
- (68) Bera, A.; Bagchi, D.; Pal, S. K. *J. Phys. Chem. A* **2019**, *123* (35), 7550–7557.
- (69) Wang, S.; Liu, H.; Mack, J.; Tian, J.; Zou, B.; Lu, H.; Li, Z.; Jiang, J.; Shen, Z. *Chem. Commun.* **2015**, *51* (69), 13389–13392.
- (70) Chen, C.; Tian, R.; Zeng, Y.; Chu, C.; Liu, G. *Bioconjug. Chem.* **2020**, *31* (2), 276–292.
- (71) Zhang, J.; Yang, M.; Li, C.; Dorh, N.; Xie, F.; Luo, F. *J. Mater. Chem. B* **2015**, 2173–2184.
- (72) Jiao, L.; Yu, C.; Uppal, T.; Liu, M.; Li, Y.; Zhou, Y.; Hao, E.; Hu, X.; Grac, M. *Org. Biomol. Chem.* **2010**, *8*, 2517–2519.
- (73) Cheng, G.; Fan, J.; Sun, W.; Sui, K.; Jin, X. *Analyst* **2013**, *138*, 6091–6096.
- (74) Watzke, A.; Kosec, G.; Kindermann, M.; Jeske, V.; Nestler, H.; Turk, V.; Turk, B.; Wendt, K. U. *Angew. Chemie Int. Ed.* **2008**, *47*, 406–409.
- (75) Erdem, S. S.; Shazia, K.; Palanisami, A.; Hasan, T. *J. Biomed. Opt.* **2014**, *19*, 105007.
- (76) Karan, S.; Cho, M. Y.; Lee, H.; Lee, H.; Park, H. S.; Sundararajan, M.; Sessler, J. L.; Hong, K. S. *J. Med. Chem.* **2021**, *64*, 2971–2981.
- (77) Drake, C. R.; Miller, D. C.; Jones, E. F. *Curr. Org. Synth.* **2011**, *8* (4), 498–520.
- (78) Wang, R.; Chen, J.; Gao, J.; Chen, J. A.; Xu, G.; Zhu, T.; Gu, X.; Guo, Z.; Zhu, W. H.; Zhao, C. *Chem. Sci.* **2019**, *10* (30), 7222–7227.
- (79) Darst, M. R. T. K. P.; Lee, K. D.; Martin, C. W.; Po, J. *Angew. Chemie Int. Ed.* **1989**, *36*, 1333–1335.
- (80) Hoogendoorn, S.; Blom, A. E. M.; Willems, L. I.; Van Der Marel, G. A.; Overkleeft, H. S. *Org. Lett.* **2011**, *13* (20), 5656–5659.
- (81) Kowada, T.; Kikuta, J.; Kubo, A.; Ishii, M.; Maeda, H.; Mizukami, S.; Kikuchi, K. *J. Am. Chem. Soc.* **2011**, *133* (44), 17772–17776.

- (82) Guo, H.; Jing, Y.; Yuan, X.; Ji, S.; Zhao, J.; Li, X.; Kan, Y. *Org. Biomol. Chem.* **2011**, *9* (10), 3844–3853.
- (83) Scales, S. J.; Tsai, S. P.; Zacharias, N.; Cruz-chuh, J.; Bullen, G.; Velasquez, E.; Chang, J.; Bruguera, E.; Kozak, K. R.; Sadowsky, J. *Bioconjug. Chem.* **2019**, *30*, 3046–3056.
- (84) Niu, L.-Y.; Guan, Y.-S.; Chen, Y.-Z.; Wu, L.-Z.; Tung, C.-H.; Yang, Q.-Z. *J. Am. Chem. Soc.* **2012**, *134* (46), 18928–18931.
- (85) Saha, T.; Kand, D.; Talukdar, P. *Org. Biomol. Chem.* **2013**, *11* (47), 8166–8170.
- (86) Zhang, H. X.; Chen, J. B.; Guo, X. F.; Wang, H.; Zhang, H. S. *Anal. Chem.* **2014**, *86* (6), 3115–3123.
- (87) Michel, B. W.; Lippert, A. R.; Chang, C. J. *J. Am. Chem. Soc.* **2012**, *134* (38), 15668–15671.
- (88) Sun, Z. N.; Liu, F. Q.; Chen, Y.; Tam, P. K. H.; Yang, D. *Org. Lett.* **2008**, *10* (11), 2171–2174.
- (89) Krumova, K.; Greene, L. E.; Cosa, G. *J. Am. Chem. Soc.* **2013**, *135* (45), 17135–17143.
- (90) Yang, D.; Wang, H. L.; Sun, Z. N.; Chung, N. W.; Shen, J. G. *J. Am. Chem. Soc.* **2006**, *128* (18), 6004–6005.
- (91) Wu, J.; Akaike, T.; Maeda, H. *Cancer Res.* **1998**, *58* (1), 159–165.
- (92) Fang, F. C. *Nat. Rev. Microbiol.* **2004**, *2* (10), 820–832.
- (93) Feng, S. S.; Chien, S. *Chem. Eng. Sci.* **2003**, *58* (18), 4087–4114.
- (94) Lin, G. G.; Scott, J. G. **2012**, *100* (2), 130–134.
- (95) Yao, V. J.; D’Angelo, S.; Butler, K. S.; Theron, C.; Smith, T. L.; Marchiò, S.; Gelovani, J. G.; Sidman, R. L.; Dobroff, A. S.; Brinker, C. J.; Bradbury, A. R. M.; Arap, W.; Pasqualini, R. *J. Control. Release* **2015**.
- (96) Matsumura, Y.; Maeda, H. *Cancer Res.* **1986**, *46* (8), 6387–6392.
- (97) Mohanty, C.; Das, M.; R. Kanwar, J.; K. Sahoo, S. *Curr. Drug Deliv.* **2010**, *8* (1), 45–58.
- (98) Xie, J.; Bi, Y.; Zhang, H.; Dong, S.; Teng, L.; Lee, R. J.; Yang, Z. *Front. Pharmacol.* **2020**, *11* (May), 1–23.
- (99) Srinivasarao, M.; Low, P. S. *Chem. Rev.* **2017**, *117* (19), 12133–12164.
- (100) Haley, B.; Frenkel, E. *Urol. Oncol. Semin. Orig. Investig.* **2008**, *26* (1), 57–64.
- (101) Yu, M. K.; Park, J.; Jon, S. *Theranostics* **2012**, *2* (1), 3–44.
- (102) Dragojevic, S.; Ryu, J. S.; Raucher, D. *Molecules* **2015**, *20* (12), 21750–21769.
- (103) Duncan, R. *Nat. Rev. Drug Discov.* **2003**, *2* (5), 347–360.
- (104) Gu, F. X.; Karnik, R.; Wang, A. Z.; Alexis, F.; Levy-Nissenbaum, E.; Hong, S.; Langer, R. S.; Farokhzad, O. C. *Nano Today* **2007**, *2* (3), 14–21.
- (105) Chin S. Kue, Anyanee Kamkaew, Kevin Burgess, Lik V. Kiew, Lip Y. Chung, H. B. L. *Med. Res. Rev.* **2016**, *36* (3), 494–575.
- (106) Arslan, F. B.; Ozturk Atar, K.; Calis, S. *Int. J. Pharm.* **2021**, *596* (October 2020), 120268.
- (107) Hossen, S.; Hossain, M. K.; Basher, M. K.; Mia, M. N. H.; Rahman, M. T.; Uddin, M. J. *J. Adv. Res.* **2019**, *15*, 1–18.
- (108) Morales-Cruz, M.; Delgado, Y.; Castillo, B.; Figueroa, C. M.; Molina, A. M.; Torres, A.; Milián, M.; Griebenow, K. *Drug Des. Devel. Ther.* **2019**, *13*, 3753–3772.
- (109) Wang, S.; Yu, G.; Wang, Z.; Jacobson, O.; Tian, R.; Lin, L.; Zhang, F.; Wang, J.; Chen, X. *Adv. Mater.* **2018**, *30* (40), 1–8.
- (110) Wang, A. Z.; Gu, F.; Zhang, L.; Chan, J. M.; Radovic-Moreno, A.; Shaikh, M. R.; Farokhzad, O. C. *Expert Opin. Biol. Ther.* **2008**, *8* (8), 1063–1070.
- (111) Danhier, F.; Breton, A. Le. *Mol. Pharm.* **2012**, *9*, 2961–2973.
- (112) Kulhari, H.; Pooja, D.; Singh, M. K.; Kuncha, M.; Adams, D. J.; Sistla, R. *Nanomedicine* **2015**, *10* (18), 2847–2859.
- (113) Tripodi, A. A. P.; Randelović, I.; Biri-Kovács, B.; Szeder, B.; Mező, G.; Tóvári, J.

- Pathol. Oncol. Res.* **2020**, *26* (3), 1879–1892.
- (114) Zhao, Z.; Ukidve, A.; Kim, J.; Mitragotri, S. *Cell* **2020**, *181* (1), 151–167.
- (115) Zhao, Z.; Liu, Fan Wang, Xiaoyuan Chen. *DRUG Dev. Res.* **2008**, *69*, 329–339.
- (116) Pierschbacher, M. D.; Ruoslahti, E. *Nature* **1984**, *309* (5963), 30–33.
- (117) Eble, J.; Haier, J. *Curr. Cancer Drug Targets* **2006**, *6* (2), 89–105.
- (118) Mas-Moruno, C.; Beck, J. G.; Doedens, L.; Frank, A. O.; Marinelli, L.; Cosconati, S.; Novellino, E.; Kessler, H. *Angew. Chemie - Int. Ed.* **2011**, *50* (40), 9496–9500.
- (119) Teesalu, T.; Sugahara, K. N.; Kotamraju, V. R.; Ruoslahti, E. *Proc. Natl. Acad. Sci. U. S. A.* **2009**, *106* (38), 16157–16162.
- (120) Attwood, M. M.; Jonsson, J.; Rask-Andersen, M.; Schiöth, H. B. *Nat. Rev. Drug Discov.* **2020**, *19* (10), 695–710.
- (121) Russell-Jones, G.; McTavish, K.; McEwan, J.; Rice, J.; Nowotnik, D. *J. Inorg. Biochem.* **2004**, *98* (10 SPEC. ISS.), 1625–1633.
- (122) Ren, W. X.; Han, J.; Uhm, S.; Jang, Y. J.; Kang, C.; Kim, J. H.; Kim, J. S. *Chem. Commun.* **2015**, *51* (52), 10403–10418.
- (123) Vineberg, J. G.; Zuniga, E. S.; Kamath, A.; Chen, Y. J.; Seitz, J. D.; Ojima, I. *J. Med. Chem.* **2014**, *57* (13), 5777–5791.
- (124) Milletti, F. *Drug Discov. Today* **2012**, *17* (15–16), 850–860.
- (125) Derakhshankhah, H.; Jafari, S. *Biomed. Pharmacother.* **2018**, *108* (September), 1090–1096.
- (126) Tripathi, P. P.; Arami, H.; Banga, I.; Gupta, J.; Gandhi, S. *Oncotarget* **2018**, *9* (98), 37252–37267.
- (127) Böhmová, E.; Machová, D.; Pechar, M.; Pola, R.; Venclíková, K.; Janoušková, O.; Etrych, T. *Physiol. Res.* **2018**, *67*, s267–s279.
- (128) Duchardt, F.; Fotin-Mleczek, M.; Schwarz, H.; Fischer, R.; Brock, R. *Traffic* **2007**, *8* (7), 848–866.
- (129) Coriat, R.; Faivre, S. J.; Mir, O.; Dreyer, C.; Ropert, S.; Bouattour, M.; Desjardins, R.; Goldwasser, F.; Raymond, E. *Int. J. Nanomedicine* **2016**, *11*, 6207–6216.
- (130) Sun, L. *Res Rev Drug Deliv* **2016**, *1* (1), 8–20.
- (131) Dubikovskaya, E. A.; Thorne, S. H.; Pillow, T. H.; Contag, C. H.; Wender, P. A. *Proc. Natl. Acad. Sci. U. S. A.* **2008**, *105* (34), 12128–12133.
- (132) Vivès, E.; Schmidt, J.; Pèlegri, A. *Biochim. Biophys. Acta - Rev. Cancer* **2008**, *1786* (2), 126–138.
- (133) Taresco, V.; Alexander, C.; Singh, N.; Pearce, A. K. *Adv. Ther.* **2018**, *1*, 1–14.
- (134) Wang, Q.; Guan, J.; Wan, J.; Li, Z. *RSC Adv.* **2020**, *10* (41), 24397–24409.
- (135) Amit Sharma, Jonathan F. Arambula, Seyoung Koo, Rajesh Kumar, Hardev Singh, Jonathan L. Sessler, J. S. K. *Chem. Soc. Rev.* **2019**, *48* (3), 771–813.
- (136) Pillai, G. *SOJ Pharm. Pharm. Sci.* **2014**, *1*, 1–13.
- (137) Santra, S.; Kaittanis, C.; Santiesteban, O. J.; Perez, J. M. *J. Am. Chem. Soc.* **2011**, *133* (41), 16680–16688.
- (138) Balendiran, G. K.; Dabur, R.; Fraser, D. *Cell Biochem. Funct.* **2004**, *22*, 343–352.
- (139) Wu, X.; Sun, X.; Guo, Z.; Tang, J.; Shen, Y.; James, T. D.; Tian, H.; Zhu, W. *J. Am. Chem. Soc.* **2014**, *136* (9), 3579–3588.
- (140) Vandooren, J.; Opendakker, G.; Loadman, P. M.; Edwards, D. R. *Adv. Drug Deliv. Rev.* **2016**, *97*, 144–155.
- (141) Tranoy-Opalinski, I.; Legigan, T.; Barat, R.; Clarhaut, J.; Thomas, M.; Renoux, B.; Papot, S. *Eur. J. Med. Chem.* **2014**, *74*, 302–313.
- (142) Chiba, M.; Kamiya, M.; Tsuda-Sakurai, K.; Fujisawa, Y.; Kosakamoto, H.; Kojima, R.; Miura, M.; Urano, Y. *ACS Cent. Sci.* **2019**, *5* (10), 1676–1681.
- (143) Vartak, D.; Gemeinhart, R. *J. Drug Target.* **2007**, *15* (1), 1–20.



- (144) Bargh, J. D.; Spring, D. R.; Isidro-llobet, A.; Parker, J. S. *Chem. Soc. Rev.* **2019**.
- (145) Kancharla, P.; Kelly, J. X.; Reynolds, K. A. *J. Med. Chem.* **2015**, *58* (18), 7286–7309.
- (146) Roy, J.; Nguyen, T. X.; Kanduluru, A. K.; Venkatesh, C.; Lv, W.; Reddy, P. V. N.; Low, P. S.; Cushman, M. *J. Med. Chem.* **2015**, *58* (7), 3094–3103.
- (147) Vineberg, J. G.; Wang, T.; Zuniga, E. S.; Ojima, I. **2015**.
- (148) Polaske, N. W.; Kelly, B. D.; Ashworth-Sharpe, J.; Bieniarz, C. *Bioconjug. Chem.* **2016**, *27* (3), 660–666.
- (149) Luo, C. Q.; Zhou, Y. X.; Zhou, T. J.; Xing, L.; Cui, P. F.; Sun, M.; Jin, L.; Lu, N.; Jiang, H. L. *J. Control. Release* **2018**, *274* (September 2017), 56–68.
- (150) Gnaim, S.; Shabat, D. *Acc. Chem. Res.* **2014**, *47*, 2970–2984.
- (151) Weinstain, R.; Sagi, A.; Karton, N.; Shabat, D. *Chem. - A Eur. J.* **2008**, *14* (23), 6857–6861.
- (152) Kumar, V.; Munkhbat, O.; Secinti, H.; Thayumanavan, S. *Chem. Commun.* **2020**, *56* (60), 8456–8459.
- (153) Shin, W. S.; Han, J.; Verwilt, P.; Kumar, R.; Kim, J. H.; Kim, J. S. *Bioconjug. Chem.* **2016**, *27* (5), 1419–1426.
- (154) Hansen, A. M.; Sewell, A. L.; Pedersen, R. H.; Long, D. L.; Gadegaard, N.; Marquez, R. *Tetrahedron* **2013**, *69* (39), 8527–8533.
- (155) Britten, R. A.; Green, J. A.; Warenius, H. M. *Int. J. Radiat. Oncol.* **1992**, *24* (3), 527–531.
- (156) Gamcsik, M.; Kasibhatla, M.; Teeter, S.; Colvin, O. *Biomarkers* **2012**, *17* (8), 671–691.
- (157) Porubský, M.; Gurská, S.; Stanková, J.; Hajdúch, M.; Džubák, P.; Hlaváč, J. *RSC Adv.* **2019**, *9* (43), 25075–25083.
- (158) Costantini, P.; Colonna, R.; Bernardi, P. *Biochim. Biophys. Acta - Bioenerg.* **1998**, *1365* (3), 385–392.
- (159) García, N.; Pavón, N.; Chávez, E. *Cell Biochem. Biophys.* **2008**, *51* (2–3), 81–87.
- (160) Liu, Y.; Zhao, F.; Gu, W.; Yang, H.; Meng, Q.; Zhang, Y.; Yang, H.; Duan, Q. *J. Biomed. Biotechnol.* **2009**, *2009*.
- (161) Orgovan, N.; Peter, B.; Bosze, S.; Ramsden, J. J.; Szabó, B.; Horvath, R. *Sci. Rep.* **2014**, *4*, 1–8.
- (162) Jang, J. H.; Kim, W. R.; Sharma, A.; Cho, S. H.; James, T. D.; Kang, C.; Kim, J. S. *Chem. Commun.* **2017**, *53* (13), 2154–2157.
- (163) Ueno, T.; Nagano, T. *Nat. Methods* **2011**, *8* (8), 642–645.
- (164) Elmes, R. B. P. *Chem. Commun.* **2016**, *52* (58), 8935–8956.
- (165) Jo, S. D.; Ku, S. H.; Won, Y.; Kim, S. H.; Kwon, I. C. *Theranostics* **2016**, *6* (9), 1362–1377.
- (166) Wang, R.; Wang, R.; Ju, D.; Lu, W.; Jiang, C.; Shan, X.; Chen, Q.; Sun, G. *Analyst* **2018**, *143* (23), 5834–5840.
- (167) Chabok, A.; Shamsipur, M.; Yeganeh-Faal, A.; Molaabasi, F.; Molaei, K.; Sarparast, M. *Talanta* **2019**, *194*, 752–762.
- (168) Vendrell, M.; Zhai, D.; Er, J. C.; Chang, Y. T. *Chem. Rev.* **2012**, *112* (8), 4391–4420.
- (169) Yue, Y.; Huo, F.; Cheng, F.; Zhu, X.; Mafireyi, T.; Strongin, R. M.; Yin, C. *Chem. Soc. Rev.* **2019**, *48* (15), 4155–4177.
- (170) Kolanowski, J. L.; Liu, F.; New, E. J. *Chem. Soc. Rev.* **2018**, *47* (1), 195–208.
- (171) Li, Y.; Wang, H.; Li, J.; Zheng, J.; Xu, X.; Yang, R. *Anal. Chem.* **2011**, *83*, 1268–1274.
- (172) Li, S. Y.; Liu, L. H.; Cheng, H.; Li, B.; Qiu, W. X.; Zhang, X. Z. *Chem. Commun.* **2015**, *51* (77), 14520–14523.
- (173) Xu, J.; Fang, L.; Shi, M.; Huang, Y.; Yao, L.; Zhao, S.; Zhang, L.; Liang, H. *Chem. Commun.* **2019**, *55* (11), 1651–1654.
- (174) Okorochenkova, Y.; Porubský, M.; Benická, S.; Hlaváč, J. *Chem. Commun.* **2018**, *54*

- (55).
- (175) Zhang, H.; Xu, L.; Chen, W.; Huang, J.; Huang, C.; Sheng, J.; Song, X. *Anal. Chem.* **2019**, *91* (3), 1904–1911.
- (176) Zhang, Q.; Zhu, Z.; Zheng, Y.; Cheng, J.; Zhang, N.; Long, Y. T.; Zheng, J.; Qian, X.; Yang, Y. *J. Am. Chem. Soc.* **2012**, *134* (45), 18479–18482.
- (177) Li, Y.; Wang, H.; Li, J.; Zheng, J.; Xu, X.; Yang, R. *Anal. Chem.* **2011**, *83* (4), 1268–1274.
- (178) Shalini, S.; Dorstyn, L.; Dawar, S.; Kumar, S. *Cell Death Differ.* **2015**, *22* (4), 526–539.
- (179) Kominami, K.; Nagai, T.; Sawasaki, T.; Tsujimura, Y.; Yashima, K.; Sunaga, Y.; Tsuchimochi, M.; Nishimura, J.; Chiba, K.; Nakabayashi, J.; Koyamada, K.; Endo, Y.; Yokota, H.; Miyawaki, A.; Manabe, N.; Sakamaki, K. *PLoS One* **2012**, *7* (11).
- (180) Thornberry, N. A.; Rano, T. A.; Peterson, E. P.; Rasper, D. M.; Timkey, T.; Garcia-Calvo, M.; Houtzager, V. M.; Nordstrom, P. A.; Roy, S.; Vaillancourt, J. P.; Chapman, K. T.; Nicholson, D. W. *J. Biol. Chem.* **1997**, *272* (29), 17907–17911.
- (181) Shi, Y. *Protein Sci.* **2004**, *13* (8), 1979–1987.
- (182) <https://microbenotes.com/apoptosis/>.
- (183) Palchaudhuri, R.; Lambrecht, M. J.; Botham, R. C.; Partlow, K. C.; van Ham, T. J.; Putt, K. S.; Nguyen, L. T.; Kim, S. H.; Peterson, R. T.; Fan, T. M.; Hergenrother, P. J. *Cell Rep.* **2015**, *13* (9), 2027–2036.
- (184) Okorochenkova, Y.; Porubský, M.; Benická, S.; Hlaváč, J. *Chem. Commun.* **2018**, *54* (55), 7589–7592.
- (185) Kaufmann, S. H.; Desnoyers, S.; Ottaviano, Y.; Davidson, N. E.; Poirier, G. G. *Cancer Res.* **1993**, *53* (17), 3976–3985.
- (186) Chaitanya, G. V.; Alexander, J. S.; Babu, P. P. *Cell Commun. Signal.* **2010**, *8* (1), 31.
- (187) Solania, A.; E. González-Páez, G.; W. Wolan, D. *ACS Chem. Biol.* **2019**, *14* (11), 2463–2470.
- (188) Leen, V.; Leemans, T.; Boens, N.; Dehaen, W. *European J. Org. Chem.* **2011**, No. 23, 4386–4396.
- (189) Azéma, L.; Lherbet, C.; Baudoin, C.; Blonski, C. *Bioorganic Med. Chem. Lett.* **2006**, *16* (13), 3440–3443.
- (190) Sun, C.; Aspland, S. E.; Ballatore, C.; Castillo, R.; Smith, A. B.; Castellino, A. J. *Bioorganic Med. Chem. Lett.* **2006**, *16* (1), 104–107.
- (191) Krajčovičová, S.; Gucký, T.; Hendrychová, D.; Kryštof, V.; Sural, M. *J. Org. Chem.* **2017**, *82* (24), 13530–13541.
- (192) Gießler, K.; Griesser, H.; Göhringer, D.; Sabirov, T.; Richert, C. *European J. Org. Chem.* **2010**, No. 19, 3611–3620.
- (193) Aydın Tekdaş, D.; Viswanathan, G.; Zehra Topal, S.; Looi, C. Y.; Wong, W. F.; Min Yi Tan, G.; Zorlu, Y.; Gürek, A. G.; Lee, H. B.; Dumoulin, F. *Org. Biomol. Chem.* **2016**, *14* (9), 2665–2670.
- (194) Sang Won Jeong; O'Brien, D. F. *J. Org. Chem.* **2001**, *66* (14), 4799–4802.
- (195) Poolman, J. M.; Maity, C.; Boekhoven, J.; Van Der Mee, L.; Le Sage, V. A. A.; Groenewold, G. J. M.; Van Kasteren, S. I.; Versluis, F.; Van Esch, J. H.; Eelkema, R. *J. Mater. Chem. B* **2016**, *4* (5), 852–858.

## 6 Appendices

## List of publications

### Appendix A

Porubský, M.; Gurská, S.; Stanková, J.; Hajdúch, M.; Džubák, P.; Hlaváč, J. *RSC Adv.* **2019**, 9 (43), 25075–25083.

### Appendix B

Porubský, M.; Vychodilová, K.; Miličević, D.; Buděšinský, M.; Stanková, J.; Džubák, P.; Hajdúch, M.; Hlaváč, J. *ChemistryOpen* **2021**, 4, 1–8.

### Appendix C

Porubský, M.; Gurská, S.; Stanková, J.; Hajdúch, M.; Džubák, P.; Hlaváč, J. *Mol. Pharm.* **2021**, 18, 2385–2396.

---



Cite this: *RSC Adv.*, 2019, 9, 25075

# Amino-BODIPY as the ratiometric fluorescent sensor for monitoring drug release or “power supply” selector for molecular electronics†

Martin Porubský,<sup>a</sup> Soňa Gurská,<sup>b</sup> Jarmila Stanková,<sup>b</sup> Marián Hajdúch,<sup>b</sup> Petr Džubák<sup>b</sup> and Jan Hlaváč \*<sup>a</sup>

The glutathione cleavable conjugates of amino-BODIPY dye with model drugs have been tested for monitoring the drug release *via* ratiometric fluorescence based on two excitation and one emission wavelength. As a self-immolative linker was used for the construction of conjugates, free amino-BODIPY was released with the drug. Different excitation profiles of the dye before and after conjugate cleavage and similar emission wavelengths that enabled monitoring the release of the drug *via* the OFF–ON effect were successfully tested inside the cancer cells. UV/Vis spectrometry could be used in the quantification of the conjugate/drug in an analyte irrespective of the cleavage grade. As the system functionality was based only on the altered acylamino-BODIPY present in the conjugate to amino-BODIPY released during the cleavage, the method could be applied as a ratiometric fluorescence theranostic system to other non-fluorescent drugs. Moreover, the present conjugates demonstrated their potential application in molecular electronics as a “power supply” selector enabling the application of two power sources for one “bulb” to maintain its light intensity.

Received 8th May 2019  
 Accepted 28th July 2019

DOI: 10.1039/c9ra03472b  
[rsc.li/rsc-advances](http://rsc.li/rsc-advances)

## Introduction

The ability to monitor a drug’s fate, including its conjugate penetration and the subsequent drug release is one of the key features in the development of new drug delivery systems (DDS) in cancer therapy.<sup>1</sup> The detection of relevant markers along with monitoring the drug release with time ranks these systems among the most intensively studied theranostics.<sup>2</sup>

The most frequently used visualization method for drug release is optical fluorescent spectroscopy, using various dyes such as cyanines, xanthene dyes, coumarines, *etc.* The frequently-used BODIPY dyes with total neutral charge, hydrophobic nature, and adjustable photochemical properties seem to be the first candidates of choice for penetration-visualization studies. In addition, BODIPYs are highly photostable and possess high quantum yields, high extinction coefficients, and sharp excitation/emission spectra.<sup>3</sup>

Optical imaging often utilizes activatable probes that effectuate amplified signal in the presence of selective or overexpressed biomarker or due to specific molecular events. This

phenomenon is fundamental for the OFF–ON or ON–OFF systems used in several diagnostic applications.<sup>4–10</sup> The greatest advantage of the fluorescent systems applied in chemical biology is the ratiometric measurement,<sup>11–13</sup> when two emission maxima are reached after excitation at one wavelength or when two excitation wavelengths cause one emission peak. Ratiometric systems easily overcome some drawbacks of simple intensimetric systems, especially false response caused by variation in the local concentration of the probe, light scattering by the sample matrix, excitation source fluctuation, or micro-environment effects around the probe.

Thiols, mainly glutathione (GSH), responsible for different redox state of the cancer cells,<sup>14</sup> are the key intracellular stimuli for the release of a drug from DDS or theranostics. Consequently, the level of glutathione in some tumors is up to 10-fold higher as compared to normal cells.<sup>15</sup> Elevated GSH level is typical of some cancer cells,<sup>16</sup> which makes them ideal triggers for the release of a drug from systems including disulfide linker.

Although a few disulfide theranostic prodrugs with an ability to monitor drug releasing *via* fluorescence have been introduced in recent years,<sup>17–22</sup> only a few were reported to have the ratiometric ability for monitoring the drug release.<sup>23,24</sup> These ratiometric OFF–ON systems are responsive to the presence of GSH and are based on one excitation/two emissions. However, the drawback of these systems is the application of the fluorescence resonance energy transfer (FRET) between camptothecin as the drug and the fluorescent dye. Thus, this system

<sup>a</sup>Department of Organic Chemistry, Faculty of Science, Palacký University, Tr. 17. Listopadu 12, 771 46 Olomouc, Czech Republic. E-mail: jan.hlavac@upol.cz

<sup>b</sup>Institute of Molecular and Translational Medicine, Faculty of Medicine and Dentistry, Palacký University, Hněvotínská 5, 779 00, Olomouc, Czech Republic

† Electronic supplementary information (ESI) available: Description of synthesis protocols, spectral properties of the probes and fluorescence spectroscopy recording of probes cleavage. See DOI: 10.1039/c9ra03472b



lacks the general application to drugs without regards to their fluorescent properties.

In the molecular electronics, the OFF-ON or ON-OFF concept could be used for the construction of molecular logic gates operated by various inputs, such as pH, the presence of metal ions, or other specific markers.<sup>25</sup> Although the molecular switches based on the (ir)reversible turn-on or turn-off effect giving the fluorescence response in the presence of appropriate marker has been described several times,<sup>26</sup> a selector as a molecular electronic device that can switch two different power supplies for one appliance while maintaining the level of power has not yet been described.

In this study, we report a new acylamino-BODIPY/amino-BODIPY system applicable in chemical biology or molecular electronics. As the specific spectral properties of the amino-BODIPY are exhibited together with the drug after conjugate cleavage, the drug release can be monitored *via* OFF-ON effect as well as ratiometric fluorescence irrespective of the fluorescent properties of the drug. The system could also serve as a molecular electronic selector activated by the presence of thiols and optimal pH.

## Experimental section

### Materials and methods

For the preparation and characterization of the compounds, LC/MS analyses were performed using UHPLC/MS with an UHPLC chromatograph (Acquity) with a PDA detector, a single quadrupole mass spectrometer (Waters), an X-Select C18 column at 30 °C and a flow rate of 600  $\mu\text{l min}^{-1}$ . The mobile phase consisted of (A) 0.01 M ammonium acetate in water and (B) acetonitrile, with a linear gradient over the course of 2.5 min; at the conclusion of the gradient, the final ratio was maintained for 1.5 min. The column was re-equilibrated with 10% B for 1 min. The APCI ionization operated at a discharge current of 5  $\mu\text{A}$ , a vaporizer temperature of 350 °C and a capillary temperature of 200 °C. Compound purity was determined using the ratio of the appropriate peak area to sum of areas of all peaks of the mixture. Areas were determined by integration of the peaks from the PDA detector response. Purity of final compounds was determined by this method and was >95%.

Purification was performed using semi-preparative HPLC with a Waters 1500 series HPLC equipped with a 2707 Autosampler, a 1525 binary HPLC pump, a 2998 Waters Photodiode Array Detector and a Waters Fraction Collector III with a YMC C18 reverse phase column (20  $\times$  100 mm, 5  $\mu\text{m}$  particle size). The mobile phase consisted of acetonitrile and a 10 mM aqueous ammonium acetate gradient over 6 min.

NMR spectra were measured in  $\text{CDCl}_3$  or  $\text{DMSO-d}_6$  using a Jeol ECX-500 (500 MHz) spectrometer. Chemical shifts ( $\delta$ ) are reported in parts per million (ppm), and coupling constants ( $J$ ) are reported in Hertz (Hz).

HR-MS analysis was performed using an Orbitrap Elite high-resolution mass spectrometer (Thermo Fischer Scientific, MA, USA) operating at positive full scan mode (120 000 FWHM) in the range of 2000–3000  $m/z$ . The settings for electrospray ionization were as follows: oven temperature of 300 °C, sheath gas

of 8 arb. units and source voltage of 1.5 kV. Samples were diluted to a final concentration of 20  $\mu\text{mol l}^{-1}$  with 0.1% formic acid in water and methanol (50 : 50, v/v).

Rink amide resin and Fmoc-amino acids were purchased from AAPPTec (Louisville, KY). Solvents and other chemicals were purchased from Sigma-Aldrich (Milwaukee, IL, <http://www.sigmaaldrich.com>).

Fluorescence spectra were recorded on a Varian Cary Eclipse fluorescence spectrophotometer equipped with a thermostat (FL1009M015). Excitation and emission slits were 5 nm. Absorption spectra were recorded on a Cary 300 UV/Vis spectrophotometer (UV111M031, Agilent). Excitation spectra of the model drugs 1–3 correspond to general observations published previously<sup>27,28</sup> and don't interfere with the spectra of the conjugates 4–6 or released dye 7.

### Quantum yield determination

Quantum yields ( $\Phi$ ) were calculated by standard procedure using Fluorescein as a reference ( $\Phi = 0.91$ ) according to eqn (1).

$$\Phi = \Phi_R \times I/I_R \times A_R/A \times \eta^2/(\eta_R^2) \quad (1)$$

where  $\Phi_R$  is the quantum yield of reference fluorophore,  $I$  is area under emission peak,  $A$  is absorbance at the excitation wavelength  $\eta$  is refractive index of the solvent.

### Cleavage of the conjugates 4–6 by glutathione and its LC/MS monitoring

0.25 ml of the conjugate 4, 5 and 6 solution (2 mM) in DMSO was mixed with 0.1 ml of GSH solution (50 mM) in HEPES (0.1 M, pH 7.4) and diluted with 0.65 ml DMSO/HEPES (2 : 1 v/v). The mixture was heated to 37 °C and analyzed by LC/MS within the time. Intracellular cleavage of conjugates 4–6 by glutathione and its fluorescence monitoring.

### Cleavage of the conjugates 4–6 by glutathione and its fluorescence monitoring

5  $\mu\text{l}$  of the probe 4, 5 or 6 solution (1 mM) in DMSO was mixed with 20  $\mu\text{l}$ , 60  $\mu\text{l}$  or 100  $\mu\text{l}$  of the GSH solution (50 mM) in HEPES buffer (0.1 M; pH 7.4) and diluted by HEPES buffer (0.1 M; pH 7.4) or DMSO/HEPES buffer (2 : 1) to 1 ml. The mixture was heated to 37 °C and the fluorescence was measured within the time.

### Intracellular cleavage of conjugates 4–6 by glutathione and its fluorescence monitoring

HeLa cells were added to black 96-well plates by MultiDrop Combi (Thermo Fisher Scientific, USA) at a cell density of  $1.25 \times 10^4$  per well and incubated overnight. Pre-treatment with GSH was performed by incubation of cells with GSH (20 mM in medium) for 2 h. The cells were washed with PBS, immediately treated with tested compounds for 2 min and washed with PBS again. Finally, 50  $\mu\text{l}$  of PBS was added to each well. Fluorescence intensity was measured by EnVision plate reader (PerkinElmer, USA), two reads for each time point (first with ex 510 nm/em 535 nm and second with ex 485 nm/em 535 nm).



## Fluorescent microscopy imaging

HeLa cells (3000 per well, 30  $\mu$ l per well) were seeded into 384 CellCarrier plates (PerkinElmer, USA) for live cell fluorescence imaging and preincubated for 24 h at 37  $^{\circ}$ C and 5% CO<sub>2</sub> to adhere. The cells were pretreated with 20 mM GSH for 2 h and stained by Hoechst dye in concentration 1.62  $\mu$ M within last 20 min. Further, the stained cells were rinsed with fresh media, treated with tested compounds (10  $\mu$ M) for 2 min and rinsed with fresh media again. The live-cell imaging was performed by Cell Voyager CV7000 (Yokogawa, Japan) spinning disc confocal microscopy system at 37  $^{\circ}$ C in 5% CO<sub>2</sub> atmosphere. Living cells were monitored by a 40 $\times$  water immersion objective. All images were post-processed, background subtracted and deconvolved using Image J software.

## Results and discussion

This novel system is suggested as the conjugate of amino-BODIPY dye acylated by (a) symmetrical self-immolative disulfide linker, connected to a drug predestinated to release. This system was designed based on the previous study by Jain *et al.*<sup>29</sup> The symmetrical linker can be used for binding of a drug with an amino or hydroxy group, whereas the asymmetrical linker can be used for binding of a drug *via* its thiol group (Scheme 1). The disulfide bridge provides a switch that triggers the release of the drug and free amino-BODIPY in the presence of thiols.

To study the possibility of monitoring a drug release, we used the compounds 1–3 from a group of 2-phenyl-3-hydroxy-4(1*H*)-quinolinone derivatives, known for their anticancer activity<sup>30</sup> as the model drugs. These drugs are substituted by the thiol, hydroxy, or amino group, suitable for conjugation with amino-BODIPY 7. The structure of these model drugs and their conjugates 4–6 are presented in Fig. 1.

The model drug 1 was synthesized from quinolinone 8 (ref. 30) by standard peptide synthesis with immobilized Fmoc-cysteine on Rink resin. Compound 2 was prepared by esterification of the starting derivative 9 with triethyleneglycol (Scheme 2). Compound 3 was synthesized according to the previously published procedure.<sup>30</sup>

Amino-BODIPY 7 was prepared by reaction of previously published chloroderivative 10 (ref. 31) with ammonia in

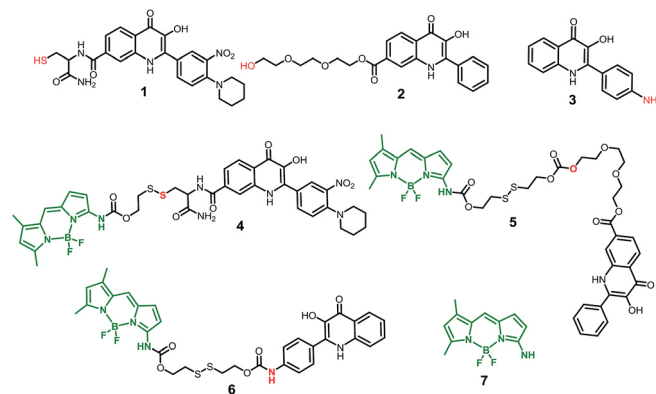


Fig. 1 Structure of model drugs 1, 2, and 3 (ref. 18) and their conjugates 4, 5, and 6 used for thiol-mediated cleavage studies.

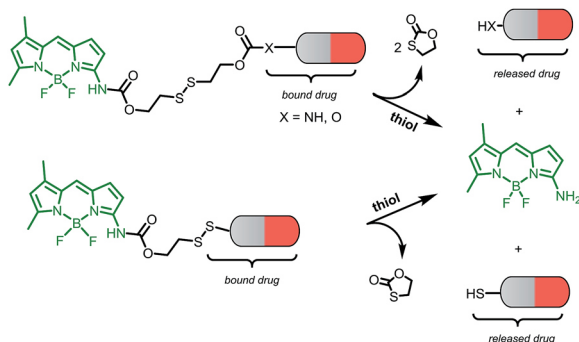
methanol/DCM as described previously. The reaction with disulfide precursor 11 (ref. 32) effectuated the intermediate 12. The disulfide exchange of this intermediate with mercapto derivative 1 afforded the final disulfide conjugate 4 (Scheme 3).

The coupling of amino-BODIPY 7 with linker precursor 13 and subsequent reaction with HOBT gave rise to compound 14 with activated carbonate group. Then, final conjugates 5 and 6 were prepared by coupling the derivative 14 with the corresponding quinolinones 2 or 3 respectively *via* carbamate or carbonate bond (Scheme 3).

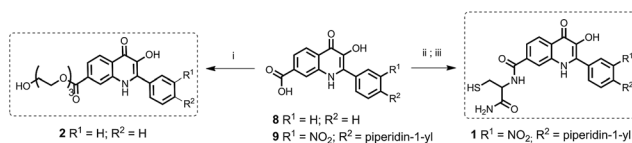
The fluorescence spectra of amino-BODIPY 7 and its conjugates 4–6 were first measured in HEPES buffer (0.1 M, pH 7.4) to meet the requirements for the planned biological experiments.

Amino-BODIPY 7 has one broad excitation maximum at 480 nm and emission at 523 nm (Table 1; Fig. 2). Acylamino-BODIPY in conjugates 4–6 possesses excitation maxima 515–517 nm, while emission of 525–527 nm is very close to the emission of amino-BODIPY 7 (Fig. 2; Table 1).

Besides the shift of excitation maxima, a significant difference was observed between amino-BODIPY 7 and its conjugates 4–6 with respect to the quantum yields and fluorescence intensity. When excitation wavelength at 480 nm, which is the characteristic maximum for amino-BODIPY 7, was used and emission at 525 nm was collected, a significant difference was observed between the fluorescence intensity of amino-BODIPY 7 and its conjugates 4–6 (Fig. 3), and thus, the system can work as OFF–ON during the cleavage. The intensity ratio of amino-BODIPY 7 to appropriate conjugate 4–6 differs probably due to different quenching effect of the bound derivatives 1–3.

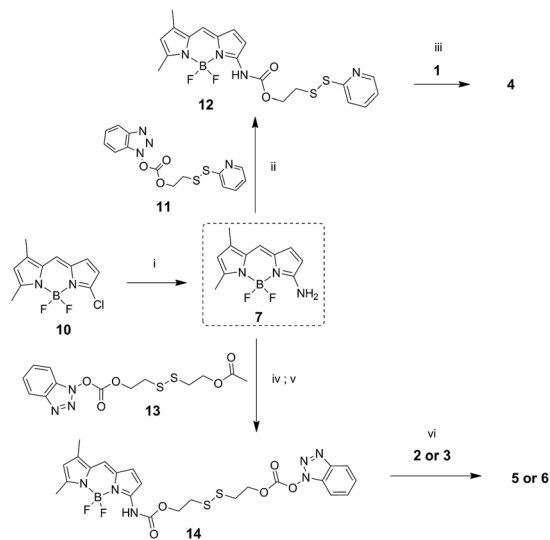


Scheme 1 Schematic illustration of the drug and amino-BODIPY release from their conjugates.



Scheme 2 Synthesis of model drugs 1 and 2. (i) 8, triethyleneglycol, H<sub>2</sub>SO<sub>4</sub> (cat.), THF, reflux, on; (ii) Rink amide resin preloaded with cysteine, 9, HOBT, DIC, DMF/Pyr, 3 h, rt. (iii) TFA/DCM/TES (2 : 1 : 0.05), 1 h, rt.





**Scheme 3** Synthesis of amino-BODIPY 7 and its conjugates 4–6. (i) 7.0 M  $\text{NH}_3/\text{MeOH}$ , DCM 70 °C, on; (ii) DMAP, TEA, DCM, rt, 3 h; (iii) DMF, 60 °C, on; (iv) TEA, DMAP, **13**, DCM, rt, 3 h. (v)  $\text{K}_2\text{CO}_3$ , THF/MeOH 3 : 1, rt, on; (vi) DMAP, TEA, DCM, rt, on.

Therefore a significant difference was observed between amino-BODIPY 7 and conjugate 4, in which the fluorescence is expectedly quenched by the nitro group.

When the excitation wavelength was selected at 510 nm, what is close to the excitation maxima of conjugates 4–6 and sufficiently distal from the emission maximum of BODIPY 7, the emission intensity was high for amino-BODIPY 7 due to its broad excitation spectrum and high quantum yield (Fig. 3; Table 1). The system could work as OFF-ON during the cleavage as well, but less efficiently.

To assess the effect of solvent polarity to OFF-ON effect, we mixed the HEPES buffer with DMSO (1 : 2 v/v). Based on the results from Table 1 and Fig. 4, the excitation as well as emission spectra of conjugates 4–6 exhibit bathochromic shift to approximately 520 nm and 530 nm, respectively and enhanced quantum yield.

**Table 1** Fluorescence profile of conjugates 4–6, **18**, **19** and BODIPY dyes **7**, **20**

Compound	Solvent	$\lambda_{\text{exc}}$ (nm)	$\lambda_{\text{em}}$ (nm)	$\Delta\lambda$ (nm)	QY (%)
4	HEPES	515	527	12	1.4
	DMSO/HEPES	517	531	14	7.7
5	HEPES	516	525	9	14
	DMSO/HEPES	520	530	10	58
6	HEPES	517	525	8	32
	DMSO/HEPES	521	532	11	53
7	HEPES	480	523	43	77
	DMSO/HEPES	496	523	40	95
<b>18</b>	DMSO/HEPES	521	549	28	23
<b>19</b>	DMSO/HEPES	520	531	11	95
<b>20</b>	DMSO/HEPES	521	550	29	48

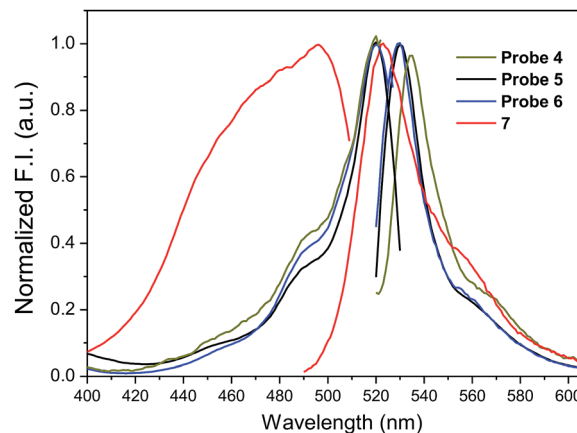


**Fig. 2** Normalized fluorescence excitation and emission spectra of amino-BODIPY 7 and its conjugates 4–6 (HEPES buffer, 0.1 M, pH 7.4).

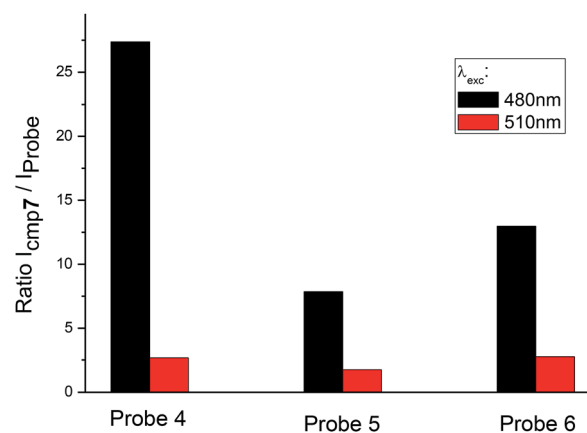


**Fig. 3** Ratio of fluorescence intensity of amino-BODIPY 7 to conjugates 4–6 at 525 nm after excitation at 480 nm or 510 nm (HEPES buffer, 0.1 M, pH 7.4).

When the excitation wavelength  $\lambda_{\text{exc}} = 480$  nm is applied, the emission intensity ratio for  $\lambda_{\text{em}} = 530$  nm between amino-BODIPY 7 and its conjugates 4–6 is approximately 2–3, and

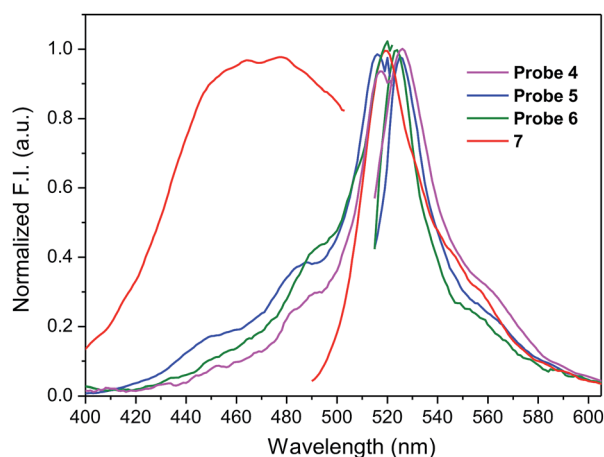


**Fig. 4** Fluorescence excitation and emission spectra of amino-BODIPY 7 and conjugates 4–6 (DMSO/HEPES buffer 2 : 1, 0.1 M, 7.4 pH).





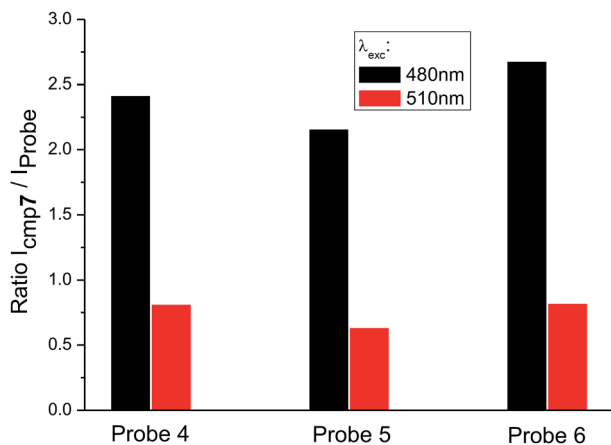


Fig. 5 Ratio of fluorescence intensity of amino-BODIPY 7 to conjugates 4–6 at 530 nm after excitation of the appropriate couple at 480 nm or 510 nm (DMSO/HEPES buffer 2 : 1, 0.1 M, pH 7.4).

hence, the OFF–ON effect is not as effective as in the HEPES buffer. When  $\lambda_{exc} = 510$  nm is used, the fluorescence intensity is lower for amino-BODIPY 7 as compared to conjugates 4–6 (Fig. 5).

To confirm the ability of disulfide linker to release the amino-BODIPY 7 and the model drugs 1–3 by thiols according to Scheme 1, conjugates 4–6 were treated with 0.5 mM glutathione at physiological conditions (37 °C, pH 7.4) and monitored by LC/MS. Because of the necessity to use a high concentration of the probes for such a detection, the present study was performed only in DMSO/HEPES buffer (2 : 1). As shown in Fig. 6, the treatment of prodrug 4 with GSH resulted in four products detected by HPLC. According to mass spectrometry, we detected the presence of the expected released drug 1 and amino-BODIPY 7 indicating complete cleavage of the conjugate, but also the formation of adducts 15 and 16 derived from the 3-HQ or BODIPY dye. Interestingly, the concentration of the adduct 15 increases in a time-dependent manner, which might be attributed to the equilibrium between 15 and 1. Conversely, the concentration of adduct 16 decreased with time because of the presence of self-immolative disulfide linker that prevents similar equilibrium.

The cleavage of the conjugates 5 and 6, wherein 3HQ is bound *via* carbonate and carbamate bonds, afforded the corresponding 3HQs 2 and 3, respectively. Although the GSH adducts 16 and 17 were also observed, these were subsequently converted to the final free 3HQ derivative 2 or 3 and amino-BODIPY 7 (Fig. 6B and C). The treatment using all prodrugs 4–6 was performed with 20  $\mu$ M in the extracellular matrix.<sup>33</sup> No cleavage was observed for any derivative in this case.

The difference in fluorescence profile of amino-BODIPY 7 and conjugates 4–6 should enable efficient monitoring of the cleavage of conjugates *via* OFF–ON mode in HEPES buffer (Fig. 3), which is optimal for potential biological applications. Next we performed the GSH-mediated cleavage of probes 4–6 monitored by fluorescence with excitation at 480 nm as well as 510 nm and emission at 525 nm. Within 180 min we observed

the expected enhancement of the fluorescence intensity for excitation at 480 nm and 510 nm (Fig. 7; Fig. S2 and S4†).

Furthermore, plotting the ratio of emission intensities at 525 nm after excitation at 480 nm and 510 nm ( $I_{480}/I_{510}$ ) *vs.* time allows ratiometric fluorescence monitoring the cleavage in a concentration independent manner (Fig. 8).

The rate of the GSH-mediated cleavage of disulfide bridge depends on the concentration of GSH. While 5 mM GSH normally present in some cancer cells,<sup>14</sup> was sufficient for full cleavage of conjugate 4 within 50 min and 120 min for conjugates 5 and 6, respectively; the low concentrations of GSH caused only partial cleavage during the same period (Fig. 8). The limit of detection (LOD) for GSH was determined for compounds 5 and 6 (HEPES buffer 7.4 pH, 37 °C, 2 h incubation). Obtained LOD values were 305 nM and 752 nM, respectively (ESI,† Fig. 12). In addition, the cleavage is pH dependent and proceeds rapidly in basic conditions. In acidic medium, none or only little conjugate is cleaved (Fig. 9).

As exemplified on probe 4 not only GSH but also cysteine, commonly present in a biological medium, can cause the amino-BODIPY 7 releasing. On the other hand, the system is resistant to all other amino acids (Fig. 10).

The release of amino-BODIPY 7 from conjugates 4–6 is accompanied by the release of drugs 1–3 (Fig. 6) and therefore enhancing the fluorescence of amino-BODIPY 7 reflects release of the drugs. Thus, the monitoring of the drug release is dependent only on the change of acylamino-BODIPY to amino-BODIPY derivative and is independent of the type of the drug. To prove this hypothesis, compounds 18, 19, and 20 with different substitutions on amino-BODIPY (Fig. 11) were synthesized as described in Scheme 3 (see ESI†). Conjugate 18 and released BODIPY dye 20 showed the same excitation/emission profile due to the same piperidyl substitution directly bound to the BODIPY scaffold. On the other hand, conjugate 19 effectuating amino-BODIPY 7 after cleavage follows the same excitation/emission profile changes as conjugates 4–6 (Fig. 11 and 4). Thus, we can conclude that the principle of OFF–ON effect is not influenced by the nature of a compound conjugated to BODIPY dye, but rather depends only on the transformation of acylamino-BODIPY to amino-BODIPY derivative.

Probe 4-based monitoring of the cleavage by UV/Vis spectroscopy resulted in the hyperchromic as well as hypochromic shift with an isosbestic point at approximately 490 nm (Fig. 12). As the absorption profile of quinolinones 1–3 bound in conjugates 4–6 did not interfere with this wavelength (see ESI†), the isosbestic point was connected with the change of acylamino-BODIPY to amino-BODIPY regardless of the bound drug. This phenomenon could be supported by the same results from UV/Vis-based monitoring of cleavage of conjugate 19 bearing cysteine having no absorption in the UV/Vis region (Fig. 12).

The developed system might be used for monitoring the release of a drug inside the cancer cells, well known for the increased level of redox potential due to high concentration of thiols, mainly GSH.<sup>14,15</sup> A maximal release of a drug within a time period corresponded to the maximal release of amino-BODIPY 7 from appropriate conjugate (Scheme 1; Fig. 6). To



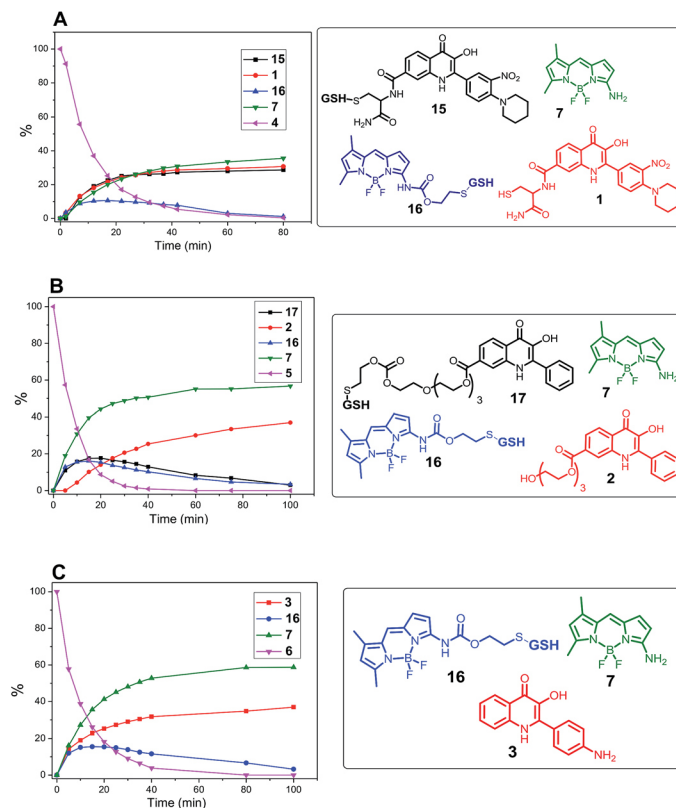


Fig. 6 Monitoring the drug release from conjugates 4, 5 and 6 (0.5 mM; DMSO/HEPES buffer 2 : 1, 0.1 M; pH 7.4; 37 °C) by GSH (5 mM) by HPLC/MS.

prove the real functioning of the system, we performed the cleavage experiment of conjugates 4–6 in HeLa cells that were pretreated with glutathione (20 mM). Due to the instrumental

limitation, excitation at 485 nm was used instead of  $\lambda_{exc} = 480$  nm. Although the inherent concentration of GSH in the cells was sufficient to cleave the disulfide conjugates 4–6, the

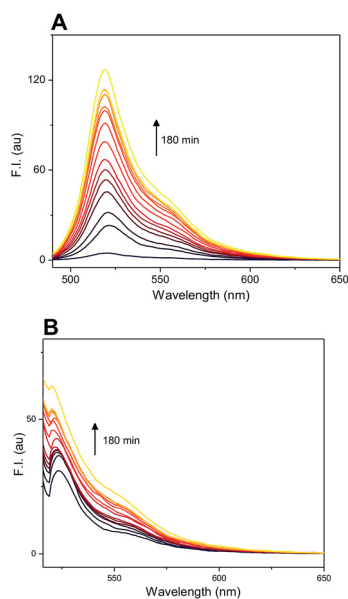


Fig. 7 GSH-mediated cleavage of probe 4 monitored within 180 min by fluorescence emission at 525 nm after excitation at 480 nm (A) and 510 nm (B) (5  $\mu$ M probe 4, 5 mM GSH; HEPES buffer, 0.1 M, pH 7.4, 37 °C).

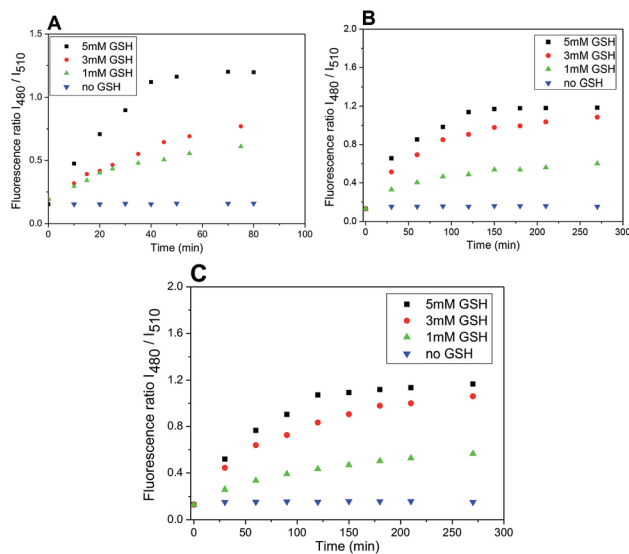


Fig. 8 Ratio of emission intensities at 525 nm upon excitation at 480 and 510 nm in time after treatment with different concentrations of GSH (5, 3, 1 mM). Probe 4 (A); probe 5 (B); probe 6 (C) (5  $\mu$ M probes 4–6; DMSO/HEPES buffer 2 : 1, 0.1 M, pH 7.4, 37 °C).



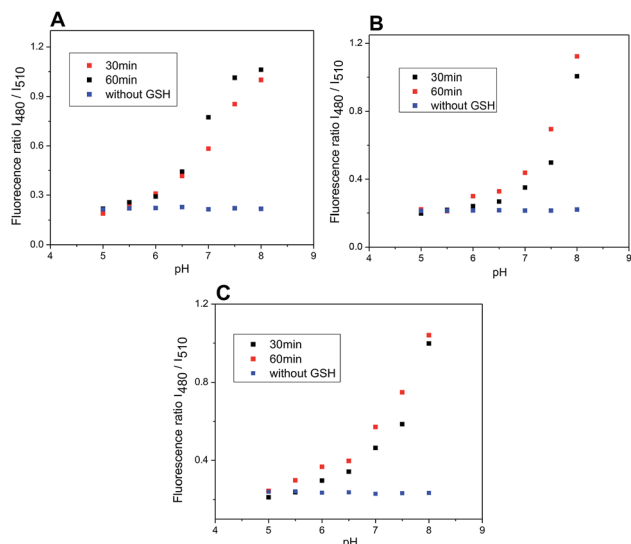


Fig. 9 Ratio of emission intensities at 525 nm upon excitation at 480 and 510 nm after 30 and 60 minutes of incubation of probes 4–6 with GSH at various pH (5.0–8.0) and without GSH after 60 minutes. Probe 4 (A); probe 5 (B); probe 6 (C) (5  $\mu$ M probe 4–6, 5 mM glutathione; DMSO/HEPES buffer 2 : 1, 0.1 M, 37  $^{\circ}$ C).

cleavage was efficient when conjugates were added to the cells preincubated with additional GSH (Fig. 13), which is similar to the previous results (Fig. 8). The exception is conjugate 5 with the most susceptible carbonate linker between dye and model drug. Supposedly, the GSH concentration in HeLa cells is sufficiently high for maximal cleavage of the linker, and the preincubation with GSH does not accelerate the disruption of the disulfide bond.

The release of a drug inside the cells can be monitored *via* the OFF–ON effect by fluorescence microscopy. For this purpose, the HeLa cells were localized by staining the nuclei by Hoechst dye (blue color) and then treated with the conjugate 4, generating green emission due to the release of amino-BODIPY

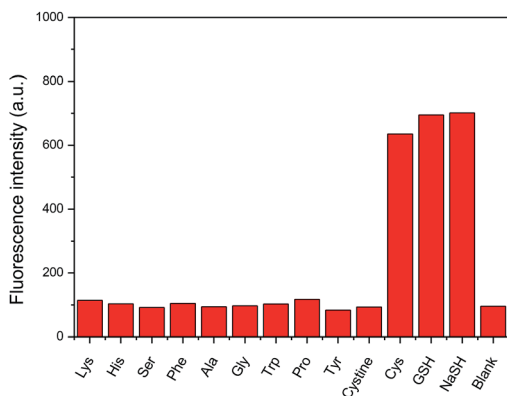


Fig. 10 Fluorescence intensity enhancement upon incubation of probe 4 (5  $\mu$ M) with various amino acids and NaSH (100 mM, DMSO/HEPES buffer 2 : 1, 0.1 M, pH 7.4) after 60 min. ( $\lambda_{\text{exc}} = 480$  nm,  $\lambda_{\text{em}} = 525$  nm).

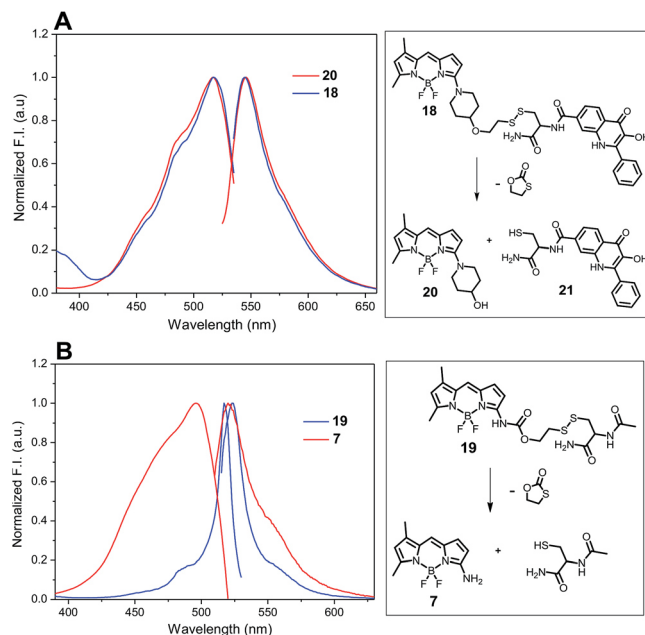


Fig. 11 Normalized excitation and emission profile of compounds 18, 19, and 20 (5  $\mu$ M in DMSO/HEPES buffer 2 : 1, 0.1 M, pH 7.4).

7 and the corresponding drug in a time-dependent manner (Fig. 14).

The other possible applicability of the introduced system can be demonstrated by the construction of a molecular electronic “selector” of two sources for one appliance. Therefore, the derivative 4 was studied in DMSO/HEPES (2 : 1 v/v) at a concentration of 5  $\mu$ M. If none or only one of the above-mentioned conditions (lack of thiols and pH < 6) were fulfilled, the conjugate was stable (Fig. 9). However, when both conditions were fulfilled, the conjugate was cleaved. In the case of intensity of emission at 527 nm or 543 nm, the excitation at  $\lambda_{\text{exc}} = 510$  nm before cleavage and at  $\lambda_{\text{exc}} = 480$  nm after cleavage was similar (Fig. 15).

The molecular selector represented schematically in Fig. 16, wherein two circuits with different power supplies are connected to one light. The selector able to change the source is operated by the tandem of molecular gates AND and NAND operated by thiol and pH inputs. Before the conjugate cleavage

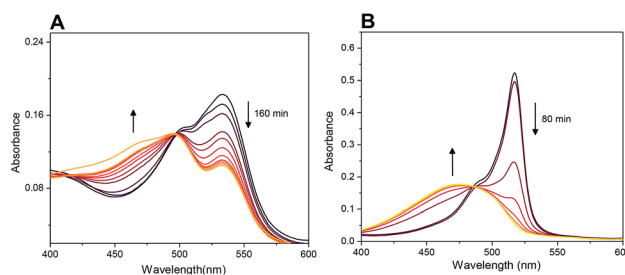


Fig. 12 Monitoring of cleavage of probes 4 (A) and 19 (B) by UV/Vis spectroscopy (5  $\mu$ M probes; 5 mM GSH, 0.1 M HEPES buffer, pH 7.4, 37  $^{\circ}$ C). For spectra highlighting change of fluorescence in time see Fig. 7 and S7.†



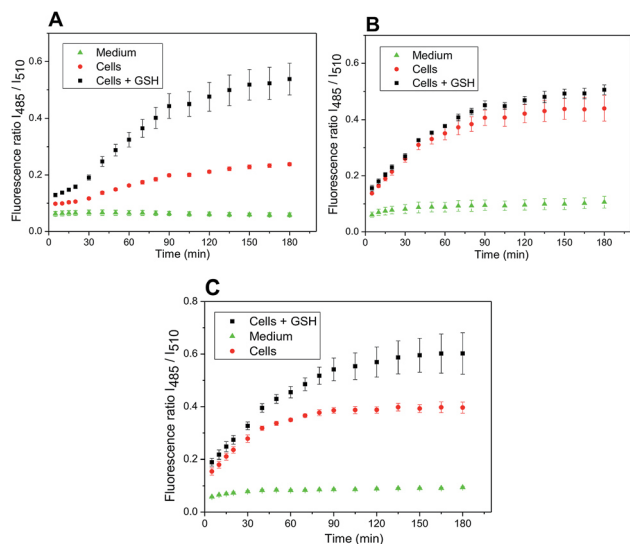


Fig. 13 Ratio of emission intensities at 525 nm upon excitation at 485 nm and 510 nm in HeLa cells corresponding to the cleavage of conjugate 4 (A), 5 (B), and 6 (C) within the prescribed period.

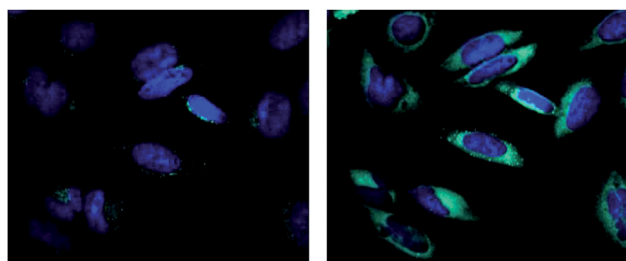


Fig. 14 Fluorescence intensity of released amino-BODIPY 7 (green color) after cleavage of conjugate 4 inside the HeLa cells pretreated with glutathione at time 0 min (left) and 120 min (right).  $\lambda_{exc} = 485$  nm.

the output of operator NAND is “one” and source 520 nm is active. When the conjugate is cleaved NAND operator has the output “zero” and immediately operator AND produces output

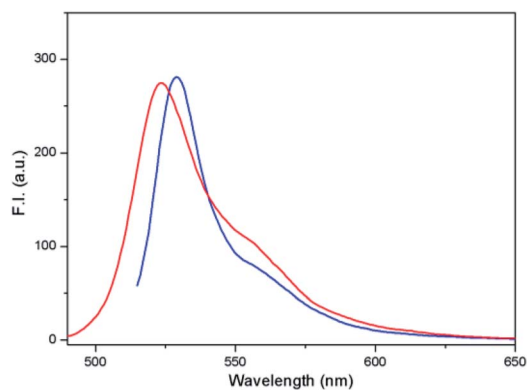
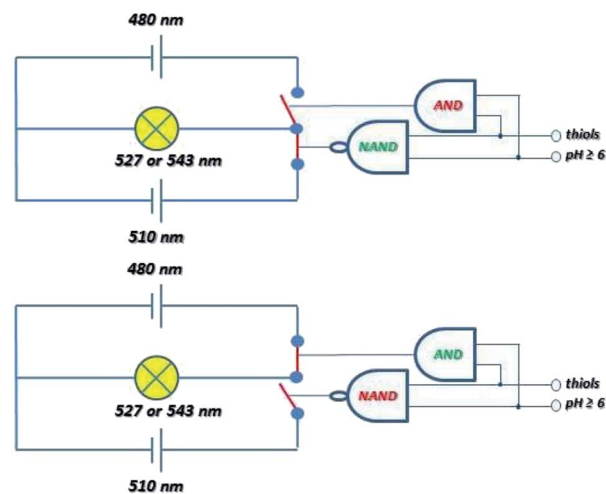


Fig. 15 Fluorescence emission spectra of compound 4 (5  $\mu$ M; DMSO/HEPES buffer 2 : 1, 0.1 M, pH 7.4) after excitation at 510 nm (blue) before cleavage and at 480 nm (red) after cleavage.



Thiols	pH $\geq$ 6.5	NAND	AND
0	0	1	0
0	1	1	0
1	0	1	0
1	1	0	1

Fig. 16 Schematic description of the selector based on cleavage of probe 4 able to switch the source of the light to maintain the same intensity and accuracy based on the truth table.

“one. The source 480 nm is then active. This circuitry imitates “emergency power unit” for the generation of energy for the “bulb” after the failure of the main source.

## Conclusion

In conclusion, the conjugates of amino-BODIPY and model drugs bound by self-immolative linker were synthesized and analyzed using glutathione for their cleavage with respect to the change in fluorescent properties. The spectral differences between acylamino-BODIPY in the conjugates and amino-BODIPY released after the glutathione attack enabled the monitoring of the release based on two excitations/one emission ratiometric fluorescence or *via* the OFF–ON effect. Thus, the drug release corresponded to the release of the amino-BODIPY used for monitoring, rendering the system valuable for monitoring the release of non-fluorescent drugs. Moreover, the drug interactions are effectuated *via* their amino, hydroxy, or thiol group that renders versatility to the compound structure. The rate of drug release is dependent on the concentration of glutathione as well as on the pH of the solution. The monitoring of the model drug release *via* ratiometric fluorescence as well as the OFF–ON effect was also verified in cancer cells with native and artificially increased concentration of glutathione. Furthermore, the UV/Vis spectroscopy allows the estimation of the concentration of conjugates independently on the extent of cleavage.



The altered excitation wavelengths post-cleavage also showed similar emission, and hence, was used for the construction of molecular electronic selector. This selector was operated by two logic gates for irreversible switching of the two sources to maintain the intensity of one light.

The concept of acylamino-BODIPY conjugates affording the amino-BODIPY dye after thiol-mediated cleavage based on the altered fluorescence offers development of various applications in chemical biology and molecular electronics in the future.

## Conflicts of interest

There are no conflicts to declare.

## Acknowledgements

This work was supported by the National Program of Sustainability (project LO1304) and by Technology Agency of the Czech Republic (project TE02000058).

## References

- Z.-R. Lu and P. Qiao, *Mol. Pharm.*, 2018, **15**, 3603–3616.
- S. S. Kelkar and T. M. Reineke, *Bioconjugate Chem.*, 2011, **22**, 1879–1903.
- T. Kowada, H. Maeda and K. Kikuchi, *Chem. Soc. Rev.*, 2015, **44**, 4953–4972.
- D. Zhang, J. R. Cochrane, A. Martinez and G. Gao, *RSC Adv.*, 2014, **4**, 29735–29749.
- S. Shanmugaraju and P. S. Mukherjee, *Chem. Commun.*, 2015, **51**, 16014–16032.
- T. Rasheed, C. Li, M. Bilal, C. Yu and H. M. N. Iqbal, *Sci. Total Environ.*, 2018, **640–641**, 174–193.
- W. Meng, Y. Chen, Y. Feng, H. Zhang, Q. Xu, M. Sun, W. Shi, J. Cen, J. Zhao and K. Xiao, *Org. Biomol. Chem.*, 2018, **16**, 6350–6357.
- Q. Huang, Q. Li, Y. Chen, L. Tong, X. Lin, J. Zhu and Q. Tong, *Sens. Actuators, B*, 2018, **276**, 82–88.
- R. Wang, R. Wang, D. Ju, W. Lu, C. Jiang, X. Shan, Q. Chen and G. Sun, *Analyst*, 2018, **143**, 5834–5840.
- A. Chabok, M. Shamsipur, A. Yeganeh-Faal, F. Molaabasi, K. Molaie and M. Sarparast, *Talanta*, 2019, **194**, 752–762.
- M. H. Lee, J. S. Kim and J. L. Sessler, *Chem. Soc. Rev.*, 2015, **44**, 4185–4191.
- P. Wu, X. Hou, J.-J. Xu and H.-Y. Chen, *Nanoscale*, 2016, **8**, 8427–8442.
- Q. Yang, J. Li, X. Wang, H. Peng, H. Xiong and L. Chen, *Biosens. Bioelectron.*, 2018, **112**, 54–71.
- F. Q. Schafer and G. R. Buettner, *Free Radicals Biol. Med.*, 2001, **30**, 1191–1212.
- R. A. Britten, J. A. Green and H. M. Warenius, *Int. J. Radiat. Oncol., Biol., Phys.*, 1992, **24**, 527–531.
- M. S. Kasibhatla, S. D. Teeter and O. M. Colvin, *Biomarkers*, 2012, **17**, 671–691.
- M. H. Lee, J. L. Sessler and J. S. Kim, *Acc. Chem. Res.*, 2015, **48**, 2935–2946.
- Y. Wang, L. Zhang, X. Zhang, X. Wei, Z. Tang and S. Zhou, *ACS Appl. Mater. Interfaces*, 2016, **8**, 5833–5846.
- J. Lai, B. P. Shah, E. Garfunkel and K. B. Lee, *ACS Nano*, 2013, **7**, 2741–2750.
- S. Santra, C. Kaittanis, O. J. Santiesteban and J. M. Perez, *J. Am. Chem. Soc.*, 2011, **133**, 16680–16688.
- M. H. Lee, J. Y. Kim, J. H. Han, S. Bhuniya, J. L. Sessler, C. Kang and J. S. Kim, *J. Am. Chem. Soc.*, 2012, **134**, 12668–12674.
- X. Wu, X. Sun, Z. Guo, J. Tang, Y. Shen, T. D. James, H. Tian and W. Zhu, *J. Am. Chem. Soc.*, 2014, **136**, 3579–3588.
- Y. Hu and F. Zeng, *Mater. Sci. Eng. C*, 2017, **72**, 77–85.
- Y. Liu, Q. Pei, L. Chen, Z. Li and Z. Xie, *J. Mater. Chem. B*, 2016, **4**, 2332–2337.
- S. Erbas-Cakmak, S. Kolemen, A. C. Sedgwick, T. Gunnlaugsson, T. D. James, J. Yoon and E. U. Akkaya, *Chem. Soc. Rev.*, 2018, **47**, 2228–2248.
- H. Li and J. C. Vaughan, *Chem. Rev.*, 2018, **118**, 9412–9454.
- K. Motyka, J. Hlaváč, M. Soral and P. Funk, *Tetrahedron Lett.*, 2010, **51**, 5060–5063.
- K. Motyka, J. Hlaváč, M. Soral, P. Hradil, P. Krejčí, L. Kvapil and M. Weiss, *Tetrahedron Lett.*, 2011, **52**, 715–717.
- A. K. Jain, M. G. Gund, D. C. Desai, N. Borhade, S. P. Senthilkumar, M. Dhiman, N. K. Mangu, S. V. Mali, N. P. Dubash, S. Halder and A. Satyam, *Bioorg. Chem.*, 2013, **49**, 40–48.
- M. Soral, J. Hlaváč, P. Hradil, I. Fryšová, M. Hajdúch, V. Bertolasi and M. Maloň, *Eur. J. Med. Chem.*, 2006, **41**, 467–474.
- V. Leen, T. Leemans, N. Boens and W. Dehaen, *Eur. J. Org. Chem.*, 2011, 4386–4396.
- J. Roy, T. X. Nguyen, A. K. Kanduluru, C. Venkatesh, W. Lv, P. V. N. Reddy, P. S. Low and M. Cushman, *J. Med. Chem.*, 2015, **58**, 3094–3103.
- D. Giustarini, F. Galvagni, A. Tesei, A. Farolfi, M. Zanoni, S. Pignatta, A. Milzani, I. M. Marone, I. Dalle-Donne, R. Nassini and R. Rossi, *Free Radicals Biol. Med.*, 2015, **89**, 972–981.



# Cytotoxicity of Amino-BODIPY Modulated via Conjugation with 2-Phenyl-3-Hydroxy-4(1*H*)-Quinolinones

Martin Porubský,<sup>[a]</sup> Kristýna Vychodilová,<sup>[b]</sup> David Miličević,<sup>[a]</sup> Miloš Buděšinský,<sup>[c]</sup> Jarmila Stanková,<sup>[b]</sup> Petr Džubák,<sup>[b]</sup> Marián Hajdúch,<sup>[b]</sup> and Jan Hlaváč<sup>\*[a]</sup>

The combination of cytotoxic amino-BODIPY dye and 2-phenyl-3-hydroxy-4(1*H*)-quinolinone (3-HQ) derivatives into one molecule gave rise to selective activity against lymphoblastic or myeloid leukemia and the simultaneous disappearance of the cytotoxicity against normal cells. Both species' conjugation can be realized via a disulfide linker cleavable in the presence of glutathione characteristic for cancer cells. The cleavage liberat-

ing the free amino-BODIPY dye and 3-HQ derivative can be monitored by ratiometric fluorescence or by the OFF-ON effect of the amino-BODIPY dye. A similar cytotoxic activity is observed when the amino-BODIPY dye and 3-HQ derivative are connected through a non-cleavable maleimide linker. The work reports the synthesis of several conjugates, the study of their cleavage inside cells, and cytotoxic screening.

## 1. Introduction

Fluorescent dyes conjugated with other molecules belong to essential bioimaging tools for several decades.<sup>[1–10]</sup> Their role in visualizing the appropriate process and detecting or determining the desired analyte is irreplaceable in contemporary chemical biology. As they have been extensively used in *in vitro* as well as *in vivo* assays, their toxicity should not affect the biological processes in the living system.

One of the most used dyes in fluorescent labeling and monitoring is the boron-dipyrromethene dye, frequently called BODIPY. Its derivatives have been used several times for detection of pH,<sup>[11–14]</sup> bio-labeling/bio-imaging<sup>[15,16]</sup> and in various other applications.<sup>[17–21]</sup> It is also frequently used in conjugates with various drugs,<sup>[22–25]</sup> nanoparticles,<sup>[26,27]</sup> or proteins.<sup>[18,28]</sup> The application of BODIPY dyes in medical research and chemical biology studies was nicely reviewed by Marfin et al. in 2017.<sup>[29]</sup>

Very recently, a model fluorescent system able to reflect the enhanced concentration of glutathione causing the drug release has been described by our group.<sup>[30]</sup> This new drug-

delivery system is based on 3-hydroxyquinolin-4(1*H*)-ones (3-HQ) as a model drug conjugation with fluorescent amino-BODIPY dye enabling the tracking of the whole system and detection of the drug release. Importantly, the drug and the dye are connected through a self-immolative disulfide linker allowing its selective cleavage inside a cancer cell.<sup>[31,32]</sup> This phenomenon is possible due to glutathione (GSH) as a linker cleavage agent. Its concentration in cancer cells, reaching up to 10 mM,<sup>[33,34]</sup> is by 2–3 orders of magnitude higher than in plasma and blood.<sup>[35,36]</sup>

According to numerous previously published studies, the BODIPY dyes are used as the fluorescent species with high intensity and low toxicity.<sup>[29]</sup> Although many of the recently developed BODIPY-drug conjugates<sup>[37–42]</sup> indicate the BODIPY as a promising candidate for biological applications, to the best of our knowledge, none of the studies describe its potential cytotoxicity or even direct application as an cytotoxic agent.

Here we report the amino-BODIPY dye as an anticancer agent. Its cytotoxicity is possible to modulate via conjugation with 3-HQs to achieve selective cytotoxicity against leukemia cell lines.


## 2. Results and Discussion


For the amino-BODIPY conjugation, we selected and synthesized five 3-HQ derivatives 1–5 (Figure 1) with different substitutions on the 2-phenyl ring as the counterparts. Compound 1 is derived from 2-phenyl-3-hydroxy-4(1*H*)-quinolinone reported to have no activity against cancer cells.<sup>[43]</sup> The derivative 2 is derived from the 2-(4-fluorophenyl)-3-hydroxy-4(1*H*)-quinolinone with low cytotoxicity against cancer cells.<sup>[44]</sup> The compound 3 comes from a modification of 2-(4-amino-3,5-dichlorophenyl)-3-hydroxy-4(1*H*)-quinolinone reported previously as the active derivative against various cancer cell lines. Product 4 was prepared by modification of the 2-(3-nitro-4-piperid-1-ylphenyl)-3-hydroxy-4(1*H*)-quinolinone having significant activity but low selectivity against cancer cell lines.<sup>[45]</sup>

[a] M. Porubský, Dr. D. Miličević, Prof. J. Hlaváč  
Department of Organic Chemistry  
Faculty of Science, Palacký University, Tr. 17. Listopadu 12  
771 46, Olomouc (Czech Republic)  
E-mail: jan.hlavac@upol.cz

[b] Dr. K. Vychodilová, J. Stanková, Dr. P. Džubák, Dr. M. Hajdúch  
Institute of Molecular and Translational Medicine  
Faculty of Medicine and Dentistry, Palacký University, Hněvotínská 5  
779 00, Olomouc (Czech Republic)

[c] Dr. M. Buděšinský  
Institute of Organic Chemistry and Biochemistry of the Czech Academy of Sciences  
Flemingovo nám. 542/2  
160 00, Prague (Czech Republic)

 Supporting information for this article is available on the WWW under <https://doi.org/10.1002/open.202100025>

 © 2021 The Authors. Published by Wiley-VCH GmbH. This is an open access article under the terms of the Creative Commons Attribution License, which permits use, distribution and reproduction in any medium, provided the original work is properly cited.

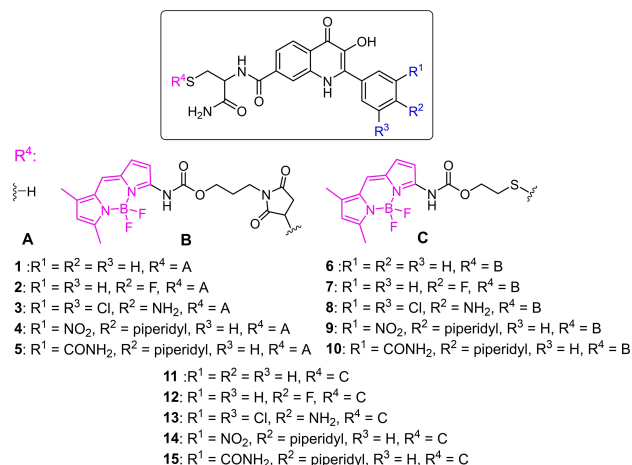


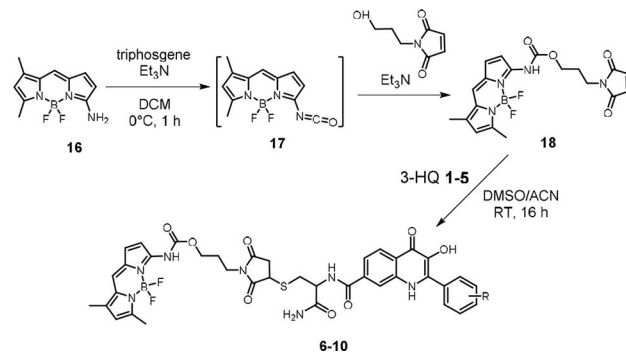
Figure 1. Prepared and studied 3-HQ derivatives 1–15

Compound 5 is then derived from active 2-(3-carboxamide-4-piperid-1-ylphenyl)-3-hydroxy-4(1*H*)-quinolinone with significant activity and increased selectivity toward cancer cells.<sup>[46]</sup> Carboxamide moiety with lipophilic *N*-substitution in position 7 was previously reported as the substituent co-responsible for cytotoxic activity when combined with suitable substituents on the 2-phenyl ring.<sup>[47]</sup> The substituted carboxamide effect is possibly connected with the ability of compounds to penetrate through the cell membrane. We have implemented cysteineamide to position 7 of the quinolinone framework for our studies to enable the conjugation with the amino-BODIPY dye 16. Thus, these compounds 1–5 were then incorporated into two sets of conjugates bearing amino-BODIPY. Conjugates 6–10 include maleimide linker, which is expected to be uncleavable under GSH treatment. Contrary, conjugates 11–15 contain the disulfide linker sensitive to GSH cleavage followed by drug/dye liberation as described previously.<sup>[30]</sup>

## 2.1 Synthesis

The synthetic approach to compounds 1–5 and 11–15 was inspired by the described procedure<sup>[30]</sup> (for details, see Experimental part). The conjugates 6–10 were prepared according to the following Scheme 1. Amino-BODIPY 16 was transformed to isocyanate 17 followed by reaction with 1-(3-hydroxypropyl)-1*H*-pyrrole-2,5-dione to obtain derivative 18. It was then reacted with 3-HQs 1–5 to get a targeted set of BODIPY-3HQs conjugates 6–10.

As reported previously, the GSH mediated cleavage of the disulfide linker results in the release of the 3-HQ derivative together with the Amino-BODIPY.<sup>[30]</sup> Different excitation and very similar emission profile of the free Amino-BODIPY 16 and the one bound in the conjugates enabling the OFF-ON effect is demonstrated for conjugate 11 in Figure 2, where excitation and emission spectra of compounds 16 and 11 are presented. As the mechanism of GSH-mediated cleavage and LC/MS analysis in Figure 2A and 2B depict nucleophilic thiol group on



Scheme 1. Synthesis of maleimide conjugates 6–10. For the structure of the compounds 1–5 and the substituents R see Figure 1.

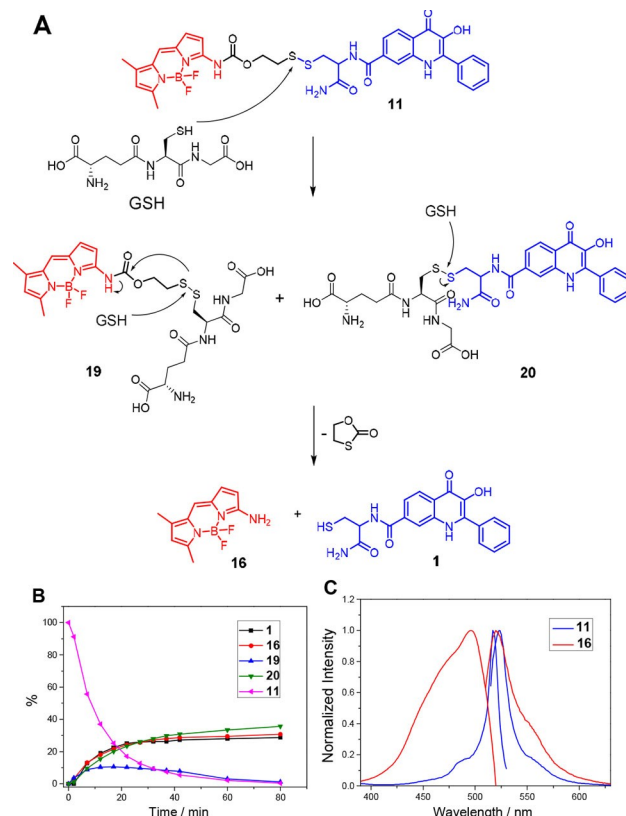


Figure 2. (A) Mechanism of GSH-mediated cleavage of conjugate 11 (5 mM GSH, 5  $\mu$ M conjugate 11 in HEPES buffer, 7.4 pH, 37 °C). (B) Time-dependent stability of compounds 1, 11, 16, 19 and 20 monitored by LC/MS. (C) Excitation/emission spectra of the conjugate 11 and the released Amino-BODIPY 16 enabling the OFF-ON fluorescence effect when excitation at 485 nm and emission at 530 nm is applied.

glutathione attacks the disulfide bond resulting in the formation of GSH adducts 19 and 20. Intermediate 19 further reacts with excess of GSH and self-immolative linker is cyclized while free Amino-BODIPY 16 is released. According to LC/MS analysis the intermediate 20 is relatively stable and further conversion to free 3-HQ 1 was not observed.

To evaluate the cleavability of conjugates 6–15, their fluorescence spectra were measured in HEPES buffer with and without the presence of GSH (5 mM). The cleavable conjugates

11–15 have an emission maximum at around 530 nm after excitation by 510 nm. Their cleavage affords the amino-BODIPY 16 with the similar emission maximum (530 nm) achieved after excitation at different wavelength (485 nm). Thus, when the ratio of emission intensities at 530 nm obtained after excitation at 485 nm and 510 nm was monitored within the time, the total conjugate cleavage was possible to detect by ratiometric fluorescence sensing (see Figure 3). As demonstrated in Figure 3A, conjugates 11–15 exhibit sufficient stability within the first three hours of the experiment when dissolved in HEPES buffer in the absence of GSH. When GSH as the cleavage agent is added, the Amino-BODIPY 16 releasing accompanied by the 3-HQs detachment<sup>[30]</sup> is indicated by a substantial increase of the 530 nm emission intensity ratio obtained after 485 nm and 510 nm excitation ( $I_{485}/I_{510}$ ) (Figure 3A).

## 2.2 Study of Conjugate Cleavage Inside Cells

Precise time monitoring of the drug release was performed in HeLa cells, where the conjugate was disrupted to a maximal level within the first several tens of minutes as demonstrated in Figure 3B and Figures S1–S3 in the Supporting Information. When the HeLa cells were pretreated by glutathione to increase the internal concentration of thiol, the cleavage was faster. The value of  $I_{485}/I_{510}$  responding to the amino-BODIPY, and drug release responded to a higher concentration of these liberated compounds.

Additionally, HeLa cells were treated with these conjugates, and microscopy images of their cellular internalization before

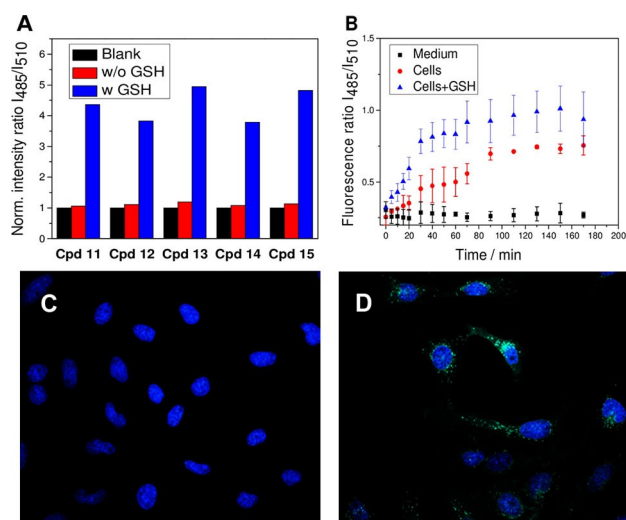


**Figure 3.** (A) Schematic representation of the ratiometric change of fluorescence intensities at 530 nm after excitation at 485 nm and 510 nm (Fluorescence ratio  $I_{485}/I_{510}$ ) for conjugates 11–15 incubated in HEPES buffer and measured at 0 h (black columns), HEPES buffer without GSH for 3 h (red columns) and in HEPES buffer with GSH (5 mM) for 3 h at 37 °C (blue columns). (B) Time monitored cleavage of conjugate 13 in medium without GSH (black), after treatment of the HeLa cells (red) or HeLa cells pretreated by 20 mM GSH (blue) with conjugate 13. (C) The microscopy images of the internalization of conjugate 13 inside the HeLa cells before treatment and (D) 2 h after treatment with GSH (20 mM).

and after treatment with GSH (20 mM) were recorded. It is apparent that after GSH treatment, the green fluorescence of released Amino-BODIPY 16 has appeared. Thus OFF-ON effect is observed as exemplified in Figures 3C and 3D.

Similarly, fluorescence ratio  $I_{485}/I_{510}$  of non-cleavable conjugates 6–10 was monitored in DMSO/HEPES buffer (2:1) (Figure 4, Figure S4). In these cases, no significant changes were observed, confirming the conjugates' inertness towards the GSH. The conjugates are also stable in HeLa cells, as demonstrated on representative derivative 9 (Figure 4).

## 2.3 Cytotoxic Activity

Finally, the amino-BODIPY 16 and all prepared conjugates 1–15 were tested for cytotoxic activity against selected cancer cell lines (Table 1). The tests were performed on cancer cell lines derived from solid tumors as well as hematological malignancies: CCRF-CEM (acute lymphoblastic leukemia), K562 (chronic myeloid leukemia), A549 (lung adenocarcinoma), colorectal carcinoma cell lines HCT116 with and without functional p53 protein HCT116p53, respectively. The panel also included chemoresistant subclone CCRF-CEM-DNR (resistant to daunorubicin) overexpressing P-glycoprotein and/or lung resistance-related protein (LRP), which are pumps or detoxifying systems responsible for the most common forms of clinical resistance. To evaluate non-tumor cells' toxicity, we used human skin fibroblast cell line BJ and lung fibroblast cell line MRC-5. From Table 1, we can see that non-conjugated 3-HQs (1–5) do not exhibit any cytotoxic activity, while amino-BODIPY 16 is active against lymphoblastic as well as myeloid leukemia cell lines and also against colorectal carcinoma. This dye is also slightly toxic to normal fibroblast BJ and MRC with  $IC_{50} > 40 \mu\text{M}$  and low-density seeding variants BJ-LD and MRC-LD with higher proliferation and no contact inhibition. Connection of amino-BODIPY 16 with 3-HQs via non-cleavable maleimide linker (conjugates 6–10) as well as via cleavable linker (compounds 11–15) causes higher selectivity toward CCRF-CEM lines. The exception is derivative 9 having the selectivity to K562 line and derivative 15, which is entirely inactive, probably due to low

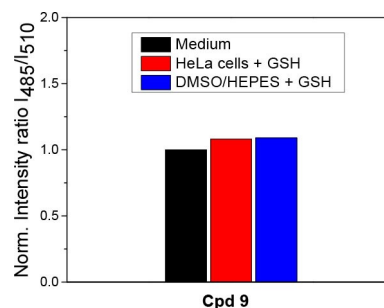


**Figure 4.** Ratio of fluorescence intensities at 530 nm after excitation at 485 nm and 510 nm ( $I_{485}/I_{510}$ ) after 180 min. incubation of non-cleavable conjugate 9 (5  $\mu\text{M}$ ) in free medium (black column), HeLa cells with additional GSH (20 mM) (red column) and in the presence of GSH (5 mM) in DMSO/HEPES buffer 2:1 (0.1 M, pH 7.4) (blue column). All experiments were carried out upon incubation at 37 °C.



**Table 1.** Cytotoxic activities of prepared compounds (IC<sub>50</sub> [μM]).

Cmp. N°	CCRF-CEM	CEM-DNR	K562	K562-TAX	A549	HCT116	HCT116p53	U2OS	BJ	BJ-LD	MRC	MRC-LD
1-5	> 50	> 50	> 50	> 50	> 50	> 50	> 50	> 50	> 50	ND	> 50	ND
6	14.60	> 50	> 50	> 50	> 50	> 50	> 50	> 50	> 50	> 50	> 50	> 50
7	6.37	> 50	> 50	> 50	> 50	> 50	> 50	> 50	> 50	> 50	> 50	> 50
8	12.70	> 50	> 50	> 50	> 50	> 50	> 50	> 50	> 50	> 50	> 50	> 50
9	> 50	> 50	4.05	> 50	> 50	> 50	> 50	> 50	> 50	ND	> 50	ND
10	5.10	> 50	> 50	49.55	> 50	> 50	> 50	> 50	> 50	> 50	> 50	> 50
11	19.73	34.42	49.82	39.77	49.89	> 50	> 50	> 50	> 50	> 50	> 50	> 50
12	8.14	26.51	44.65	33.59	46.43	> 50	49.79	42.30	> 50	> 50	> 50	> 50
13	2.59	40.09	41.43	41.83	> 50	> 50	> 50	> 50	> 50	> 50	> 50	> 50
14	1.52	37.91	29.91	40.61	46.27	39.71	42.60	44.15	> 50	> 50	> 50	> 50
15	> 50	46.25	> 50	46.16	> 50	> 50	> 50	> 50	> 50	> 50	> 50	> 50
16	4.25	5.08	3.29	6.41	47.2	11.56	12.74	19.80	49.66	28.10	40.11	26.94

[a] Average values of IC<sub>50</sub> from at least three independent experiments with SD ranging from 1 to 20% of the average values.

solubility. Contrary to the free Amino-BODIPY **16** none of the conjugates exhibit toxicity against the BJ, MRC, BJ-LD, or MRC-LD lines, suggesting the selectivity of conjugates to cancer cells. According to these results, we can conclude that the conjugation of cytotoxic Amino-BODIPY and inactive 3-HQs alters its cytotoxicity profile and gives the selectivity to leukemia cell lines. This effect is surprisingly independent of the cleavability of conjugates, what can be explained by the ability of pharmacophore to interact with a target regardless of release from the conjugate. The selectivity of conjugates toward leukemia cells could be caused by interaction with a specific target for the CCRF-CEM or K562 cells, respectively, or by particular transport to these cell lines. The later reason could explain the lower toxicity of amino-BODIPY released from the conjugate compared to free amino-BODIPY **16** directly applied to the cells.

### 3. Conclusion

A series of target conjugates were synthesized by combining 2-phenyl-3-hydroxy-4(1*H*)-quinolinone (3-HQ) derivatives with Amino-BODIPY dye. While some of them (**6-10**) were uncleavable in the presence of glutathione in increased concentration, disruption of cleavable conjugates (**11-15**) within the time was possible to monitor using ratiometric fluorescence. The released Amino-BODIPY is possible to detect also by the OFF-ON effect. While the prepared 3-HQs appeared to be quite inactive to selected cancer cell lines, the Amino-BODIPY was proved to possess cytotoxic activity against almost all of them as well as against proliferating non-tumor cells. When these cell lines were treated with Amino-BODIPY conjugated with 3HQs, the selectivity against lymphoblastic or myeloid leukemia has appeared. The cytotoxicity of the conjugates against normal cells has disappeared regardless of the linker cleavability. The specific toxicity of the system to leukemia cells and a possibility of a synergic effect of the Amino-BODIPY and maybe any other anticancer agent accompanied by a possibility of the cleavage monitoring could make this system attractive for future studies of new theranostics.

## Experimental Section

### Materials and Methods

All chemicals and solvents for the synthesis were obtained from Sigma-Aldrich. NMR spectra were measured in DMSO-*d*<sub>6</sub> and CDCl<sub>3</sub> using a Jeol ECX-500 (500 MHz) spectrometer. Chemical shifts ( $\delta$ ) are reported in parts per million (ppm) and coupling constants (*J*) are reported in Hertz (Hz). HRMS analysis was performed using an Exactive Plus Orbitrap high-resolution (Thermo Fischer Scientific, MA, USA). The machine was operated at the positive full scan mode (120 000 FWHM). The chromatographic separation was performed using column Phenomenex Gemini (C18, 50×2 mm, 3 μm particles) in isocratic mode with mobile phase using 95% MeOH and 5% H<sub>2</sub>O with 0.1% of formic acid.

### Cleavage of Conjugates 6-10 and 11-15 by Glutathione and its Fluorescence Monitoring

First, 5 μl of the solution of conjugates **6-10** and **11-15** (1 mM) in DMSO was mixed with 20 μl, 60 μl or 100 μl of the GSH solution (50 mM) in HEPES buffer (0.1 M; pH 7.4) and diluted with HEPES buffer (0.1 M; pH 7.4) or DMSO/HEPES buffer (2:1) to 1 ml. The mixture was heated to 37 °C, and the fluorescence was measured in time. after

### Intracellular Cleavage of Conjugates 6-10 and 11-15 by Glutathione and its Fluorescence Monitoring

HeLa cells were added to blank 96-well plates by MultiDrop Combi (Thermo Fisher Scientific, USA) at a cell density of 1.25×10<sup>4</sup> per well and incubated overnight. The pretreatment with GSH was performed by the incubation of cells with GSH (20 mM in medium) for 2 h. The cells were washed with PBS, immediately treated with the tested compounds for 2 min at 37 °C and washed with PBS again. Finally, 50 μL of PBS was added to each well. The fluorescence intensity was measured by an EnVision plate reader (Perkin Elmer, USA), with two reads for each time point (first, with ex 510 nm/em 535 nm, and second, with ex 485 nm/em 535 nm).

### Quantum Yield Determination

Quantum yields ( $\Phi$ ) were calculated by the standard procedure using fluorescein in 0.1M NaOH as a reference ( $\Phi = 0.91$ ) and according to equation (1).

$$\Phi = \Phi_R \times I/I_R \times A_R/A \times \eta^2/(\eta_R^2) \quad (1);$$

where  $\Phi_R$  is the quantum yield of the reference fluorophore,  $I$  is the area under the emission peak,  $A$  is absorbance at the excitation wavelength, and  $\eta$  is the refractive index of the solvent.

### Synthesis of BODIPY Conjugates

The compounds 1–5 were prepared by solid-phase chemistry approach according to the published procedure.<sup>[30]</sup>

#### Characterization of compound 1 was in accordance with the published data<sup>[30]</sup>

1: <sup>1</sup>H NMR (500 MHz, DMSO-*d*<sub>6</sub>)  $\delta$  11.82 (bs, 1H), 8.60 (d,  $J=7.9$  Hz, 1H), 8.26 (s, 1H), 8.22 (d,  $J=8.50$  Hz, 1H), 7.82 (d,  $J=7.2$  Hz, 2H), 7.76 (dd,  $J=1.2, 8.5$  Hz, 1H), 7.50–7.60 (m, 4H), 7.22 (s, 1H), 4.50–4.58 (m, 1H), 2.94–3.03 (m, 1H), 2.82–2.93 (m, 1H), 2.39 (t,  $J=8.4$  Hz, 1H). <sup>13</sup>C NMR  $\delta$  = 171.69, 169.48, 166.09, 138.55, 137.38, 135.93, 132.64, 132.09, 129.03, 129.28, 128.31, 124.59, 123.09, 120.26, 118.90, 55.97, 26.00. HRMS (ESI)  $m/z$  calcd for C<sub>19</sub>H<sub>17</sub>N<sub>3</sub>O<sub>4</sub>S<sup>+</sup> [M+H]<sup>+</sup>: 383.0940; found: 383.0944. Yield: 95%. Obtained as a light-yellow solid.

2: <sup>1</sup>H NMR (500 MHz, DMSO-*d*<sub>6</sub>)  $\delta$  11.80 (s, 1H), 8.60 (d,  $J=7.9$  Hz, 1H), 8.25 (s, 1H), 8.22 (d,  $J=8.5$  Hz, 1H), 7.89 (dd,  $J=8.4, 5.6$  Hz, 2H), 7.76 (d,  $J=8.6$  Hz, 1H), 7.55 (s, 1H), 7.42 (t,  $J=8.8$  Hz, 2H), 7.22 (s, 1H), 4.58–4.50 (m, 1H), 2.98 (dd,  $J=8.7, 4.7$  Hz, 1H), 2.89 (dd,  $J=15.1, 6.9$  Hz, 1H), 2.39 (t,  $J=8.4$  Hz, 1H). <sup>13</sup>C NMR (50 MHz, DMSO-*d*<sub>6</sub>)  $\delta$  171.66, 166.05, 163.49, 161.52, 138.52, 137.39, 135.94, 131.67, 131.60, 124.61, 123.13, 120.21, 115.37, 115.20, 55.94, 25.99. HRMS (ESI)  $m/z$  calcd. for C<sub>19</sub>H<sub>17</sub>FN<sub>3</sub>O<sub>4</sub>S<sup>+</sup> [M+H]<sup>+</sup>: 402.0918, found: 402.0920. Yield: 92%. Obtained as a light-yellow solid.

3: <sup>1</sup>H NMR (500 MHz, DMSO-*d*<sub>6</sub>)  $\delta$  11.62 (s, 1H), 8.58 (t,  $J=7.9$  Hz, 1H), 8.27 (d,  $J=1.1$  Hz, 1H), 8.20 (t,  $J=8.2$  Hz, 1H), 7.84 (d,  $J=12.7$  Hz, 2H), 7.75 (dd,  $J=8.6, 1.4$  Hz, 1H), 7.54 (s, 1H), 7.22 (s, 1H), 4.59–4.52 (m, 1H), 3.02–2.95 (m, 1H), 2.91–2.86 (m, 1H), 2.54 (s, 2H), 2.39 (t,  $J=8.4$  Hz, 1H). <sup>13</sup>C NMR (50 MHz, DMSO-*d*<sub>6</sub>)  $\delta$  171.66, 166.05, 142.14, 138.32, 137.34, 135.81, 128.66, 124.49, 122.92, 120.17, 119.92, 117.44, 55.94, 25.99. HRMS (ESI)  $m/z$  calcd. for C<sub>19</sub>H<sub>17</sub>Cl<sub>2</sub>N<sub>3</sub>O<sub>4</sub>S<sup>+</sup> [M+H]<sup>+</sup>: 467.0342, found: 467.0344. Yield: 89%. Obtained as a yellow-greenish solid.

Characterization of the compound 4 was in accordance with the published data.<sup>[30]</sup>

4: <sup>1</sup>H NMR (500 MHz, DMSO-*d*<sub>6</sub>)  $\delta$  11.74 (bs, 1H), 8.61 (d,  $J=7.9$  Hz, 1H), 8.30 (s, 1H), 8.25 (s, 1H), 8.21 (d,  $J=8.5$  Hz, 1H), 8.03 (d,  $J=8.5$  Hz, 1H), 7.75 (d,  $J=8.5$  Hz, 1H), 7.54 (s, 1H), 7.43 (d,  $J=8.8$  Hz, 1H), 7.22 (s, 1H), 4.54 (dd,  $J=8.3, 12.7$  Hz, 1H), 3.10 (s, 4H), 2.95–3.03 (m, 1H), 2.83–2.92 (m, 1H), 2.39 (t,  $J=8.4$  Hz, 1H), 1.60–1.64 (s, 6H). <sup>13</sup>C NMR  $\delta$  = 172.20, 170.13, 166.58, 145.75, 140.80, 139.22, 137.95, 136.50, 134.83, 130.69, 127.19, 125.15, 123.67, 123.56, 120.88, 120.75, 119.28, 56.51, 52.29, 26.52, 25.91, 23.93. HRMS (ESI)  $m/z$  calcd for C<sub>24</sub>H<sub>25</sub>N<sub>3</sub>O<sub>6</sub>S<sup>+</sup> [M+H]<sup>+</sup>: 512.1598; found: 512.1608. Yield: 94%. Obtained as an orange solid.

5: <sup>1</sup>H NMR (500 MHz, DMSO-*d*<sub>6</sub>)  $\delta$  11.82 (s, 1H), 8.60 (d,  $J=8.0$  Hz, 1H), 8.56 (s, 1H), 8.26 (dd,  $J=11.8, 1.7$  Hz, 2H), 8.22 (d,  $J=8.6$  Hz, 1H), 7.95 (dd,  $J=8.4, 2.2$  Hz, 1H), 7.79 (s, 1H), 7.75 (dd,  $J=8.6, 1.5$  Hz, 1H), 7.54 (s, 1H), 7.46 (d,  $J=8.3$  Hz, 1H), 7.21 (s, 1H), 4.54 (td,  $J=8.5, 4.7$  Hz, 1H), 3.12–3.05 (m, 4H), 3.02–2.96 (m, 1H), 2.92–2.85 (m, 1H), 2.39 (t,  $J=8.4$  Hz, 1H), 1.88 (s, 1H), 1.77–1.71 (m, 4H), 1.61–1.56 (m, 2H). <sup>13</sup>C NMR (50 MHz, DMSO-*d*<sub>6</sub>)  $\delta$  171.80, 171.66, 169.39, 168.21, 166.09, 158.22, 157.94, 138.56, 137.40, 135.91, 132.73, 131.66, 130.95, 127.35, 124.58, 123.09, 120.23, 119.69, 118.79, 55.97, 54.73, 53.83, 26.10, 25.99, 25.59, 22.97, 22.56. HRMS (ESI)  $m/z$  calcd.

for C<sub>25</sub>H<sub>28</sub>N<sub>3</sub>O<sub>5</sub>S<sup>+</sup> [M+H]<sup>+</sup>: 510.1806, found: 510.1803. Yield: 62%. Obtained as a light-yellow solid.

18: Solution of amino-BODIPY 16 (258 mg, 1.098 mmol) and triethylamine (160  $\mu$ L, 1.153 mmol) in DCM (3 mL) was added to the solution of triphosgene (108 mg, 0.362 mmol) while cooled to 0 °C. After stirring for 1 h at 0 °C the solution of *N*-(3-hydroxypropyl) maleimide (170 mg, 1.098 mmol) and triethylamine (160  $\mu$ L, 1.153 mmol) in DCM (3 mL) was added slowly. Reaction mixture was then warmed to RT and stirred for 16 h. Ethylacetate (100 mL) was added to the reaction mixture and it was washed with water and brine 3 times. Organic layer was dried over anhydrous sodium sulfate and concentrated under reduced pressure. Crude product was purified by column chromatography (hexane/ethylacetate 2:1) to obtain 240 mg (53%) of pure compound. <sup>1</sup>H NMR (500 MHz, CDCl<sub>3</sub>)  $\delta$  7.97 (s, 1H), 7.00 (s, 1H), 6.99 (d,  $J=4.5$  Hz, 1H), 6.88 (d,  $J=4.4$  Hz, 1H), 6.73 (s, 2H), 6.04 (s, 1H), 4.23 (t,  $J=6.2$  Hz, 2H), 3.68 (t,  $J=6.7$  Hz, 2H), 2.52 (s, 3H), 2.22 (s, 3H), 2.02 (p,  $J=6.5$  Hz, 2H). <sup>13</sup>C NMR (50 MHz, CDCl<sub>3</sub>)  $\delta$  170.82, 155.43, 151.61, 149.94, 141.05, 134.43, 133.58, 131.03, 129.86, 122.03, 118.89, 109.44, 64.23, 35.14, 27.72, 14.67, 11.38. MS (ESI)  $m/z$  calcd. for C<sub>19</sub>H<sub>20</sub>BF<sub>2</sub>N<sub>4</sub>O<sub>4</sub><sup>+</sup> [M+H]<sup>+</sup>: 417.15; found: 417.50. Obtained as a dark red solid.

Preparation of Compounds 6–10: Starting compound 18 (30 mg, 0.072 mmol) in DMSO/MeCN (1:1, v/v, 1 mL) was mixed with triethylamine (50  $\mu$ L, 0.360 mmol) and corresponding 3-HQ 2, 3 or 5 (0.072 mmol). The resulting mixture was stirred 16 h at RT. Product was then extracted with EtOAc (50 mL) and washed with water and brine 3 times. Organic layer was dried over anhydrous sodium sulphate and concentrated under reduced pressure to give 45 mg (78%) of crude product. Purification by column chromatography (DCM/MeOH gradient) or by HPLC (CH<sub>3</sub>COONH<sub>4</sub>/MeCN) was performed for all final compounds.

6: <sup>1</sup>H NMR (500 MHz, DMSO-*d*<sub>6</sub>)  $\delta$  11.80 (s, 1H), 8.75 (d,  $J=8.1$  Hz, 1H), 8.27 (s, 1H), 8.23 (d,  $J=8.5$  Hz, 1H), 7.83 (d,  $J=7.3$  Hz, 2H), 7.75 (d,  $J=8.6$  Hz, 1H), 7.61–7.49 (m, 5H), 7.30–7.21 (m, 2H), 6.80 (t,  $J=4.5$  Hz, 1H), 6.18 (s, 1H), 4.73–4.65 (m, 1H), 4.16 (t,  $J=5.7$  Hz, 2H), 4.13–4.07 (m, 1H), 3.54 (t,  $J=6.7$  Hz, 2H), 3.37 (dd,  $J=13.3, 4.5$  Hz, 1H), 3.27–3.19 (m, 2H), 3.06 (dd,  $J=13.3, 9.9$  Hz, 1H), 2.62–2.54 (m, 1H), 2.42 (s, 3H), 2.22 (s, 3H), 1.91–1.87 (m, 2H). <sup>13</sup>C NMR (50 MHz, DMSO-*d*<sub>6</sub>)  $\delta$  176.83, 176.70, 175.14, 172.01, 171.75, 171.70, 169.66, 166.09, 165.94, 151.72, 138.60, 137.43, 135.81, 135.77, 132.86, 132.39, 132.12, 131.73, 129.58, 129.37, 129.26, 128.27, 124.62, 123.12, 120.10, 118.94, 118.67, 109.39, 63.93, 63.87, 52.97, 52.80, 48.61, 36.05, 35.87, 35.28, 32.97, 26.37, 26.35, 21.03, 14.17, 10.91. HRMS (ESI)  $m/z$  calcd. for C<sub>38</sub>H<sub>37</sub>BF<sub>2</sub>N<sub>7</sub>O<sub>6</sub>S<sup>+</sup> [M+H]<sup>+</sup>: 800.2480, found: 800.2489. Yield: 34%.  $\Phi_F=0.24$ . Obtained as a dark red solid.

7: <sup>1</sup>H NMR (500 MHz, DMSO-*d*<sub>6</sub>)  $\delta$  11.80 (s, 1H), 8.75 (d,  $J=8.0$  Hz, 1H), 8.25 (s, 1H), 8.22 (d,  $J=8.5$  Hz, 1H), 7.88 (dd,  $J=8.3, 5.7$  Hz, 2H), 7.75 (d,  $J=8.6$  Hz, 1H), 7.57 (dd,  $J=10.4, 6.1$  Hz, 2H), 7.41 (t,  $J=8.5$  Hz, 2H), 7.25 (d,  $J=6.0$  Hz, 2H), 6.80 (t,  $J=4.7$  Hz, 1H), 6.19 (s, 1H), 4.73–4.65 (m, 1H), 4.16 (t,  $J=5.7$  Hz, 2H), 4.10 (ddd,  $J=9.0, 7.1, 3.9$  Hz, 1H), 3.54 (t,  $J=6.7$  Hz, 2H), 3.37 (dd,  $J=13.3, 4.4$  Hz, 1H), 3.23 (dd,  $J=18.3, 8.8$  Hz, 2H), 3.06 (dd,  $J=13.3, 10.0$  Hz, 1H), 2.62–2.55 (m, 1H), 2.42 (s, 3H), 2.22 (s, 3H), 1.93–1.87 (m, 3H). <sup>13</sup>C NMR (50 MHz, DMSO-*d*<sub>6</sub>)  $\delta$  176.82, 176.70, 175.14, 175.13, 172.00, 171.75, 171.70, 169.66, 166.06, 165.90, 163.49, 161.52, 154.45, 151.61, 149.43, 141.11, 138.56, 137.41, 135.83, 132.90, 131.85, 131.82, 131.80, 131.78, 131.73, 131.68, 131.61, 131.55, 131.39, 129.52, 128.47, 124.63, 123.36, 123.16, 120.13, 118.90, 118.74, 115.35, 115.18, 109.30, 63.95, 63.89, 54.89, 52.95, 52.80, 26.38, 26.35, 21.03, 14.17, 14.16, 10.91. HRMS (ESI)  $m/z$  calcd. for C<sub>38</sub>H<sub>36</sub>BF<sub>3</sub>N<sub>7</sub>O<sub>6</sub>S<sup>+</sup> [M+H]<sup>+</sup>: 818.2386, found: 818.2397. Yield: 35%.  $\Phi_F=0.25$ . Obtained as a dark red solid.

8: <sup>1</sup>H NMR (500 MHz, DMSO-*d*<sub>6</sub>) δ 8.74 (d, *J*=8.2 Hz, 1H), 8.26 (s, 1H), 8.18 (dd, *J*=8.5, 1.8 Hz, 1H), 7.82 (s, 2H), 7.73 (dd, *J*=8.6, 1.3 Hz, 1H), 7.60–7.51 (m, 1H), 7.27–7.21 (m, 2H), 6.79 (dd, *J*=6.0, 4.4 Hz, 1H), 6.17 (s, 1H), 6.01 (s, 2H), 4.73–4.64 (m, 1H), 4.18–4.13 (m, 2H), 4.12–4.07 (m, 1H), 3.54 (t, *J*=6.7 Hz, 2H), 3.36 (dd, *J*=13.3, 4.5 Hz, 1H), 3.27–3.19 (m, 2H), 3.06 (dd, *J*=13.3, 9.9 Hz, 1H), 2.62–2.53 (m, 1H), 2.41 (s, 3H), 2.21 (s, 3H), 1.95–1.86 (m, 4H). <sup>13</sup>C NMR (50 MHz, DMSO-*d*<sub>6</sub>) δ 176.83, 176.71, 175.15, 175.14, 172.01, 171.74, 171.69, 166.06, 165.91, 142.11, 138.37, 137.38, 135.69, 132.77, 131.73, 129.68, 128.65, 124.51, 122.95, 120.06, 118.87, 118.50, 117.45, 109.56, 63.88, 52.94, 52.79, 48.60, 26.35, 21.05, 14.16, 10.90. HRMS (ESI) *m/z* calcd. for C<sub>38</sub>H<sub>36</sub>BCl<sub>2</sub>F<sub>2</sub>N<sub>9</sub>O<sub>8</sub>S<sup>+</sup> [M+H]<sup>+</sup>: 883.1810, found: 883.1821. Yield: 29%. Φ<sub>F</sub>=0.19. Obtained as a dark red solid.

9: <sup>1</sup>H NMR (500 MHz, DMSO-*d*<sub>6</sub>) δ 8.76 (d, *J*=8.1 Hz, 1H), 8.30 (d, *J*=1.9 Hz, 1H), 8.25 (s, 1H), 8.20 (dd, *J*=8.5, 1.8 Hz, 1H), 8.02 (d, *J*=8.5 Hz, 1H), 7.74 (d, *J*=8.6 Hz, 1H), 7.56 (dd, *J*=17.8, 5.6 Hz, 2H), 7.41 (dd, *J*=8.9, 1.7 Hz, 1H), 7.24 (dd, *J*=9.3, 4.2 Hz, 2H), 6.79 (dd, *J*=6.3, 4.4 Hz, 1H), 6.18 (s, 1H), 4.73–4.64 (m, 1H), 4.15 (t, *J*=6.0 Hz, 2H), 4.12–4.07 (m, 1H), 3.54 (t, *J*=6.7 Hz, 2H), 3.36 (dd, *J*=13.3, 4.4 Hz, 1H), 3.24 (d, *J*=9.0 Hz, 1H), 3.21 (d, *J*=9.1 Hz, 1H), 3.11–3.07 (m, 4H), 2.61–2.53 (m, 1H), 2.41 (s, 3H), 2.21 (s, 3H), 1.93–1.86 (m, 3H), 1.67–1.61 (m, 4H), 1.61–1.56 (m, 2H). <sup>13</sup>C NMR (50 MHz, DMSO-*d*<sub>6</sub>) δ 176.82, 176.70, 175.13, 175.12, 171.99, 171.73, 171.69, 171.05, 166.04, 165.89, 146.20, 140.26, 138.69, 134.52, 134.27, 132.84, 131.73, 129.58, 126.64, 124.59, 123.13, 120.30, 120.15, 118.63, 109.42, 63.91, 63.86, 56.03, 54.89, 52.95, 52.80, 51.75, 48.59, 26.37, 26.34, 25.37, 23.38, 21.03, 18.53, 14.16, 10.91, 10.90. HRMS (ESI) *m/z* calcd. for C<sub>43</sub>H<sub>45</sub>BF<sub>2</sub>N<sub>9</sub>O<sub>10</sub>S<sup>+</sup> [M+H]<sup>+</sup>: 926.2920, found: 926.2941. Yield: 44%. Φ<sub>F</sub>=0.05. Obtained as a dark red solid.

10: <sup>1</sup>H NMR (500 MHz, DMSO-*d*<sub>6</sub>) δ 11.77 (s, 1H), 8.76 (d, *J*=8.0 Hz, 1H), 8.49 (s, 1H), 8.27 (s, 1H), 8.21 (dd, *J*=8.7, 1.4 Hz, 2H), 7.90 (d, *J*=8.2 Hz, 1H), 7.73 (d, *J*=8.6 Hz, 1H), 7.64 (s, 1H), 7.61–7.52 (m, 2H), 7.34–7.29 (m, 1H), 7.28–7.20 (m, 2H), 6.80 (t, *J*=4.5 Hz, 1H), 6.18 (s, 1H), 4.73–4.64 (m, 1H), 4.16 (t, *J*=5.8 Hz, 2H), 4.10 (ddd, *J*=9.1, 6.5, 3.9 Hz, 1H), 4.10 (ddd, *J*=9.1, 6.5, 3.9 Hz, 1H), 3.54 (t, *J*=6.7 Hz, 2H), 3.37 (dd, *J*=13.3, 4.4 Hz, 1H), 3.24 (d, *J*=8.8 Hz, 1H), 3.21 (d, *J*=8.8 Hz, 1H), 3.06 (dd, *J*=13.3, 10.0 Hz, 1H), 3.01–2.94 (m, 4H), 2.61–2.54 (m, 1H), 2.42 (s, 3H), 2.22 (s, 3H), 1.93–1.87 (m, 3H), 1.70 (s, 4H), 1.58–1.51 (m, 2H). <sup>13</sup>C NMR (50 MHz, DMSO-*d*<sub>6</sub>) δ 176.83, 176.71, 175.15, 175.13, 172.01, 171.77, 171.72, 168.02, 166.14, 165.99, 154.43, 152.66, 151.63, 149.46, 141.08, 138.56, 137.42, 135.77, 132.90, 132.35, 131.73, 131.13, 129.53, 128.12, 125.84, 124.58, 123.34, 123.11, 120.10, 120.08, 119.20, 118.87, 118.73, 109.31, 63.96, 63.90, 56.05, 53.58, 52.97, 52.81, 48.60, 26.38, 26.35, 25.77, 23.35, 21.04, 18.54, 14.18, 10.91. HRMS (ESI) *m/z* calcd. for C<sub>44</sub>H<sub>47</sub>BF<sub>2</sub>N<sub>9</sub>O<sub>9</sub>S<sup>+</sup> [M+H]<sup>+</sup>: 926.3273, found: 926.3285. Yield: 23%. Φ<sub>F</sub>=0.22. Obtained as a dark red solid.

**Preparation of Compounds 11–15:** The compounds 11–15 were prepared according to the published procedure.<sup>[30]</sup>

11: <sup>1</sup>H NMR (500 MHz, DMSO-*d*<sub>6</sub>) δ 11.78 (s, 1H), 8.82 (d, *J*=8.2 Hz, 1H), 8.33 (bs, 1H), 8.25 (d, *J*=1.5 Hz, 1H), 8.21 (d, *J*=8.6 Hz, 1H), 7.80 (m, 2H), 7.74 (dd, *J*=8.6, 1.5 Hz, 1H), 7.62 (bd, *J*=1.5 Hz, 1H), 7.58 (bs, 1H), 7.55 (m, 2H), 7.51 (m, 1H), 7.26 (bd, *J*=1.5 Hz, 1H), 7.21 (d, *J*=4.3 Hz, 1H), 6.71 (d, *J*=4.3 Hz, 1H), 6.21 (s, 1H), 4.73 (ddd, *J*=13.5, 10.2, 4.3 Hz, 1H), 4.41 (m, 2H), 3.29 (dd, *J*=13.5, 4.3 Hz, 1H), 3.13 (dd, *J*=13.5, 10.5, 1H), 3.08 (m, 2H), 2.42 (s, 3H), 2.22 (s, 3H). Hz. <sup>13</sup>C NMR δ 171.92, 169.84, 166.27, 155.07, 151.45, 149.02, 141.75, 138.77, 137.59, 135.99, 133.22, 132.28, 131.77, 131.51, 129.58, 129.53, 129.45, 128.44, 124.80, 123.89, 123.32, 120.25, 119.10, 119.08, 109.26, 64.02, 52.76, 40.52, 36.04, 14.39, 11.14. HRMS (ESI) *m/z* calcd. for C<sub>33</sub>H<sub>31</sub>BF<sub>2</sub>N<sub>6</sub>O<sub>6</sub>S<sub>2</sub><sup>+</sup> [M+H]<sup>+</sup>: 721.1880; found: 721.1886. Yield: 56%. Φ<sub>F</sub>=0.16. Obtained as a dark red solid.

12: <sup>1</sup>H NMR (500 MHz, DMSO-*d*<sub>6</sub>) δ 11.77 (s, 1H), 8.82 (d, *J*=8.2 Hz, 1H), 8.32 (bs, 1H), 8.24 (d, *J*=8.6 Hz, 1H), 8.20 (d, *J*=8.6 Hz, 1H), 7.86 (m, 2H), 7.74 (dd, *J*=8.6, 1.6 Hz, 1H), 7.62 (bd, *J*=1.5 Hz, 1H), 7.58 (s, 1H), 7.39 (m, 2H), 7.26 (bd, *J*=1.5 Hz, 1H), 7.21 (d, *J*=4.4 Hz, 1H), 6.70 (d, *J*=4.4 Hz, 1H), 6.21 (s, 1H), 4.73 (ddd, *J*=10.2, 8.2, 4.3 Hz, 1H), 4.40 (m, 2H), 3.29 (dd, *J*=13.5, 4.3 Hz, 1H), 3.12 (dd, *J*=13.5, 10.2 Hz, 1H), 3.08 (m, 2H), 2.41 (s, 3H), 2.22 (s, 3H). <sup>13</sup>C NMR (50 MHz, DMSO-*d*<sub>6</sub>) δ 171.94, 169.88, 166.24, 162.67 (*J*<sub>C-F</sub>=247 Hz), 155.07, 151.45, 149.02, 141.75, 138.75, 137.58, 136.01, 133.23, 131.82 (*J*<sub>C-F</sub>=8.6 Hz), 131.80, 131.57, 129.58, 128.63, 123.88, 123.36, 124.83, 120.28, 119.11, 119.08, 115.44 (*J*<sub>C-F</sub>=21.4 Hz), 109.25, 64.03, 52.76, 40.51, 36.01, 14.39, 11.13. MS (ESI) *m/z* calcd. for C<sub>33</sub>H<sub>31</sub>BF<sub>2</sub>N<sub>6</sub>O<sub>6</sub>S<sub>2</sub><sup>+</sup> [M+H]<sup>+</sup>: 739.179; found: 739.253. Yield: 29%. Φ<sub>F</sub>=0.22. Obtained as a dark red solid.

13: <sup>1</sup>H NMR DMSO-*d*<sub>6</sub> δ = 11.55 (s, 1H), 8.83 (d, *J*=8.2 Hz, 1H), 8.29 (bs, 1H), 8.26 (d, *J*=1.7 Hz, 1H), 8.17 (d, *J*=8.6 Hz, 1H), 7.80 (s, 2H), 7.74 (dd, *J*=8.6, 1.7 Hz, 1H), 7.63 (bd, *J*=1.5 Hz, 1H) 7.55 (bs, 1H), 7.26 (bd, *J*=1.5 Hz, 1H), 7.18 (d, *J*=4.3 Hz, 1H), 6.67 (d, *J*=4.3 Hz, 1H), 6.19 (s, 1H), 6.02 (bs, 2H), 4.74 (ddd, *J*=10.2, 8.2, 4.2 Hz, 1H), 4.40 (m, 2H), 3.29 (dd, *J*=13.6, 4.2 Hz, 1H), 3.13 (dd, *J*=13.6, 10.2 Hz, 1H), 3.07 (m, 2H), 2.41 (s, 3H), 2.21 (s, 3H). <sup>13</sup>C NMR (50 MHz, DMSO-*d*<sub>6</sub>) δ 171.96, 169.60, 166.23, 155.06, 151.40, 148.96, 142.29, 141.72, 138.59, 137.54, 135.84, 133.22, 131.74, 130.23, 129.55, 128.80, 124.71, 123.82, 123.14, 120.18, 120.09, 119.10, 119.08, 117.61, 109.19, 64.05, 52.74, 40.52, 35.95, 14.11, 11.14. MS (ESI) *m/z* calcd. for C<sub>33</sub>H<sub>31</sub>BCl<sub>2</sub>F<sub>2</sub>N<sub>6</sub>O<sub>6</sub>S<sub>2</sub><sup>+</sup> [M+H]<sup>+</sup>: 804.121; found: 804.419. Yield: 50%. Φ<sub>F</sub>=0.15. Obtained as a dark red solid.

Characterization of the compound 14 was in accordance with the published data.<sup>[30]</sup>

14: <sup>1</sup>H NMR (500 MHz, DMSO-*d*<sub>6</sub>) δ 11.23 (s, 1H), 8.09–7.99 (m, 3H), 7.96 (d, *J*=7.1 Hz, 1H), 7.79 (d, *J*=8.2 Hz, 1H), 7.65 (s, 1H), 7.39 (d, *J*=8.3 Hz, 1H), 7.00 (s, 1H), 6.85 (d, *J*=8.5 Hz, 1H), 6.74–6.70 (m, 1H), 6.67–6.63 (m, 1H), 6.42–6.37 (m, 1H), 6.21 (s, 1H), 5.71 (s, 1H), 4.68–4.58 (m, 1H), 4.18–4.06 (m, 2H), 3.12–2.99 (m, 4.4 Hz, 2H), 2.96–2.87 (m, 2H), 2.79 (s, 4H), 2.72–2.67 (m, 2H), 2.12 (s, 3H), 1.87 (s, 3H), 1.40 (s, 4H), 1.32 (s, 2H). <sup>13</sup>C NMR δ = 166.77, 166.59, 155.12, 151.11, 149.07, 146.73, 141.81, 141.18, 140.50, 137.70, 135.94, 135.69, 134.10, 133.27, 130.80, 129.38, 127.21, 126.65, 125.00, 122.72, 122.35, 122.11, 120.25, 119.83, 118.83, 118.74, 108.87, 63.99, 52.10, 40.87, 40.77, 36.46, 25.56, 23.69, 14.34, 11.09. HRMS (ESI) *m/z* calcd for C<sub>38</sub>H<sub>39</sub>BF<sub>2</sub>N<sub>9</sub>O<sub>8</sub>S<sub>2</sub><sup>-</sup> [M-H]<sup>-</sup>: 847.2310; found: 847.2307. Yield: 34%. Obtained as a dark red solid.

15: <sup>1</sup>H NMR DMSO-*d*<sub>6</sub> δ = 11.75 (s, 1H), 8.83 (d, *J*=8.2 Hz, 1H), 8.48 (bd, *J*=3.0 Hz, 1H), 8.26 (d, *J*=1.6 Hz, 3H), 8.19 (d, *J*=8.5 Hz, 1H), 8.18 (d, *J*=2.4 Hz, 1H), 7.87 (s, 1H), 7.73 (dd, *J*=8.5, 1.6 Hz, 1H), 7.66 (bd, *J*=3.0 Hz, 1H), 7.62 (bs, 1H), 7.59 (bs, 1H), 7.31 (d, *J*=8.5 Hz, 1H), 7.26 (bs, 1H), 7.21 (d, *J*=4.3 Hz, 1H), 6.71 (d, *J*=4.3 Hz, 1H), 6.21 (s, 1H), 4.73 (ddd, *J*=13.5, 10.5, 4.3 Hz, 1H), 4.41 (m, 2H), 3.29 (ddd, *J*=13.5, 4.3 Hz, 1H), 3.08 (m, 2H), 2.98 (m, 4H), 2.41 (s, 1H), 2.22 (s, 3H), 1.78 (m, 4H), 1.56 (m, 2H). <sup>13</sup>C NMR (50 MHz, DMSO-*d*<sub>6</sub>) δ 171.93, 169.67, 168.21, 166.32, 155.08, 152.79, 151.46, 149.03, 141.74, 138.73, 137.58, 135.94, 133.22, 132.51, 131.88, 131.78, 131.31, 129.5, 128.26, 125.99, 124.76, 123.89, 123.29, 120.25, 119.35, 119.11, 119.03, 109.28, 64.03, 53.79, 52.78, 40.52, 36.05, 25.90, 23.54, 14.40, 11.14. MS (ESI) *m/z* calcd. for C<sub>39</sub>H<sub>42</sub>BF<sub>2</sub>N<sub>8</sub>O<sub>7</sub>S<sub>2</sub><sup>+</sup> [M+H]<sup>+</sup>: 847.267; found: 847.435. Yield: 43%. Φ<sub>F</sub>=0.18. Obtained as a dark red solid.

## Acknowledgements

This work was supported by the Czech Science Foundation (reg. No. 18-26557Y), the Czech Ministry of Education, Youth and Sports

(CZ-OPENSREEN-LM2018130, and EATRIS-CZ- LM2018133) and internal grant of Palacky University (IGA\_LF\_2020\_019).

## Conflict of Interest

The authors declare no conflict of interest.

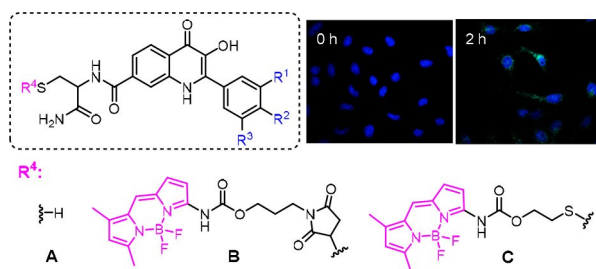
**Keywords:** amino-BODIPY dyes · cytotoxic activity · disulfide linkers · glutathione · hydroxyquinolinones

- [1] A. S. Klymchenko, F. Liu, M. Collot, N. Anton, *Adv. Healthcare Mater.* **2021**, *10*, 2001289.
- [2] Z. Shi, X. Han, W. Hu, H. Bai, B. Peng, L. Ji, Q. Fan, L. Li, W. Huang, *Chem. Soc. Rev.* **2020**, *49*, 7533–7567.
- [3] J. Wang, Q. Gong, L. Wang, E. Hao, L. Jiao, J. Wang, Q. Gong, L. Wang, E. Hao, L. Jiao, *J. Porphyrins Phthalocyanines* **2019**, *24*, 603–635.
- [4] J. Jiao, J. Zhang, F. Yang, W. Song, D. Han, W. Wen, *Eur. J. Pharm. Biopharm.* **2020**, *152*, 123–143.
- [5] L. Xu, J. Zhang, L. Yin, X. Long, W. Zhang, Q. Zhang, *J. Mater. Chem. C* **2020**, *8*, 6342–6349.
- [6] S. Schramm, D. Weiß, *Fluorescent Heterocycles: Recent Trends and New Developments*, Elsevier Inc., **2018**.
- [7] M. Shamsipur, A. Barati, Z. Nematifar, *J. Photochem. Photobiol. C* **2019**, *39*, 76–141.
- [8] W. J. Peveler, W. R. Algar, *ACS Chem. Biol.* **2018**, *13*, 1752–1766.
- [9] Y. Yue, F. Huo, F. Cheng, X. Zhu, T. Mafireyi, R. M. Strongin, C. Yin, *Chem. Soc. Rev.* **2019**, *48*, 4155–4177.
- [10] H. Zhang, L. Xu, W. Chen, J. Huang, C. Huang, J. Sheng, X. Song, *Anal. Chem.* **2019**, *91*, 1904–1911.
- [11] T. Rappitsch, I. Klimant, S. M. Borisov, *Dyes Pigment.* **2020**, *174*, 108037.
- [12] D. Pfeifer, A. Russegger, I. Klimant, S. M. Borisov, *Sens. Actuators B* **2020**, *304*, 127312.
- [13] Y. Ni, J. Wu, *Org. Biomol. Chem.* **2014**, *12*, 3774–3791.
- [14] V. Leen, W. Dehaen, *Chem. Soc. Rev.* **2012**, *41*, 1130–1172.
- [15] T. Kowada, H. Maeda, K. Kikuchi, *Chem. Soc. Rev.* **2015**, *44*, 4953–72.
- [16] E. Bodio, F. Denat, C. Goze, *J. Porphyrins Phthalocyanines* **2019**, *23*, 1159–1183.
- [17] B. M. Squeo, M. Pasini, B. M. Squeo, M. Pasini, *Supramol. Chem.* **2019**, *1*–15.
- [18] O. S. Vodyanova, B. A. Kochergin, S. D. Usoltsev, Y. S. Mar, E. V. Rumyantsev, E. L. Aleksakhina, I. K. Tomilova, *J. Photochem. Photobiol. A* **2018**, *350*, 44–51.
- [19] Y. Liu, X. Lv, M. Hou, Y. Shi, W. Guo, *Anal. Chem.* **2015**, 11475–11483.
- [20] M. Y. Jia, L. Y. Niu, Y. Zhang, Q. Z. Yang, C. H. Tung, Y. F. Guan, L. Feng, *ACS Appl. Mater. Interfaces* **2015**, *7*, 5907–5914.
- [21] F. Wang, L. Zhou, C. Zhao, R. Wang, Q. Fei, S. Luo, Z. Guo, H. Tian, W. H. Zhu, *Chem. Sci.* **2015**, *6*, 2584–2589.
- [22] S. Shukla, A. P. Skoumbourdis, M. J. Walsh, A. M. S. Hartz, K. L. Fung, C. Wu, M. M. Gottesman, C. J. Thomas, S. V. Ambudkar, *Mol. Pharm.* **2011**, *8*, 1292–1302.
- [23] T. Ruml, M. Jurásek, S. Rimpelová, V. Pavlík, P. B. Drašar, *Steroids* **2015**, *97*, 62–66.
- [24] N. Fishkin, *Mol. Pharm.* **2015**, *15*, 1745–751.
- [25] Z. X. Yang Liu, Q. Pei, L. Chen, Z. Li, *J. Mater. Chem. B* **2016**, 2332–2337.
- [26] T. Zhang, C. Ma, T. Sun, Z. Xie, *Coord. Chem. Rev.* **2019**, *390*, 76–85.
- [27] L. Huang, G. Han, *Small Methods* **2018**, 1700370.
- [28] N. Dorh, S. Zhu, K. B. Dhungana, R. Pati, F. Luo, H. Liu, *Sci. Rep.* **2015**, *5*, 1–10.
- [29] Y. S. Marfin, A. V. Solomonov, A. S. Timin, E. V. Rumyantsev, *Curr. Med. Chem.* **2017**, *24*, 2745–2772.
- [30] M. Porubský, S. Gurská, J. Stanková, M. Hajdúch, P. Džubák, J. Hlaváč, *RSC Adv.* **2019**, *9*, 25075–25083.
- [31] D. Yang, W. Chen, J. Hu, *J. Phys. Chem. B* **2014**, *118*, 12311–12317.
- [32] M. H. Lee, Z. Yang, C. W. Lim, Y. H. Lee, S. Dongbang, C. Kang, J. S. Kim, *Chem. Rev.* **2013**, *113*, 5071–5109.
- [33] R. A. Britten, J. A. Green, H. M. Wahrenius, *Int. J. Radiat. Oncol.* **1992**, *24*, 527–531.
- [34] M. Gamcsik, M. Kasibhatla, S. Teeter, O. Colvin, *Biomarkers* **2012**, *17*, 671–691.
- [35] A. G. Cheetham, P. Zhang, Y. Lin, L. L. Lock, H. Cui, *J. Am. Chem. Soc.* **2013**, *135*, 2907–2910.
- [36] S. Qin, A. Zhang, S. Cheng, L. Rong, X. Zhang, *Biomaterials* **2017**, *112*, 234–247.
- [37] S. Yin, A. Kamkaew, N. Fu, C. Siang, L. Yong, L. Voon, J. Wittayakun, K. Burgess, H. Boon, *Int. J. Pharm.* **2020**, *579*, 119189.
- [38] S. J. Scales, S. P. Tsai, N. Zacharias, J. Cruz-chuh, G. Bullen, E. Velasquez, J. Chang, E. Bruguera, K. R. Kozak, J. Sadowsky, *Bioconjugate Chem.* **2019**, *30*, 3046–3056.
- [39] S. Krajčovičová, J. Stanková, P. Džubák, M. Hajdúch, M. Soral, *Chem. A Eur. J.* **2018**, *24*, 4957–4966.
- [40] V. Ramu, S. Gautam, A. Garai, P. Kondaiah, A. R. Chakravarty, *Inorg. Chem.* **2018**, *57*, 1717–1726.
- [41] M. H. Y. Cheng, A. Maruani, H. Savoie, V. Chudasama, R. W. Boyle, *Org. Biomol. Chem.* **2018**, *16*, 1144–1149.
- [42] Q. Zhang, Y. Cai, Q. Li, L. Hao, Z. Ma, X. Wang, *Chem. A Eur. J.* **2017**, *23*, 14307–14315.
- [43] P. Hradil, J. Hlavac, M. Soral, M. Hajduch, M. Kolar, R. Vecerova, *Mini-Rev. Med. Chem.* **2009**, *9*, 696–702.
- [44] J. Řehulka, K. Vychodilová, P. Krejčí, S. Gurská, P. Hradil, M. Hajdúch, P. Džubák, J. Hlaváč, *Eur. J. Med. Chem.* **2020**, *192*, 112176.
- [45] P. Krejčí, P. Hradil, J. Hlaváč, M. Hajdúch, *Preparation of 2-Phenyl-3-Hydroxyquinolin-4(1H)-Ones for Treatment of Immune System and Proliferative Disorders*, **2008**, WO2008028427 A1.
- [46] K. Burglová, G. Rylová, A. Markos, H. Přichystalová, M. Soral, M. Petráček, M. Medvedíková, G. Tejral, B. Sopko, P. Hradil, P. Džubák, M. Hajdúch, J. Hlaváč, *J. Med. Chem.* **2018**, *61*, 3027–3036.
- [47] M. Soral, J. Hlaváč, P. Funk, P. Džubák, M. Hajdúch, *ACS Comb. Sci.* **2011**, *4*, 39–44.

Manuscript received: January 29, 2021

Revised manuscript received: July 11, 2021

## FULL PAPERS



**Amino-BODIPY conjugates** with various 2-phenyl-3-hydroxyquinolinones (3-HQs) connected via cleavable disulfide linker and non-cleavable maleimide linker were prepared and tested on cytotoxic activity and fluorescent ratiometric "OFF-ON" monitoring of cleavage inside the cells was demonstrated.

Disulfide conjugates exhibited improved cytotoxicity compared to the free 3-HQs whereas non-cleavable maleimide conjugates stayed inactive proving that disulfide linker is responsible for cleavage inside the cells and therefore resulting in cytotoxicity of disulfide Amino-BODIPY-3HQ conjugates.

M. Porubský, Dr. K. Vychodilová, Dr. D. Miličević, Dr. M. Buděšinský, J. Stanková, Dr. P. Džubák, Dr. M. Hajdúch, Prof. J. Hlaváč\*

1 – 8

**Cytotoxicity of Amino-BODIPY Modulated via Conjugation with 2-Phenyl-3-Hydroxy-4(1H)-Quinolinones**



## AminoBODIPY Conjugates for Targeted Drug Delivery Systems and Real-Time Monitoring of Drug Release

Martin Porubský, Soňa Gurská, Jarmila Stanková, Marián Hajdúch, Petr Džubák, and Jan Hlaváč\*



Cite This: *Mol. Pharmaceutics* 2021, 18, 2385–2396



Read Online

ACCESS |



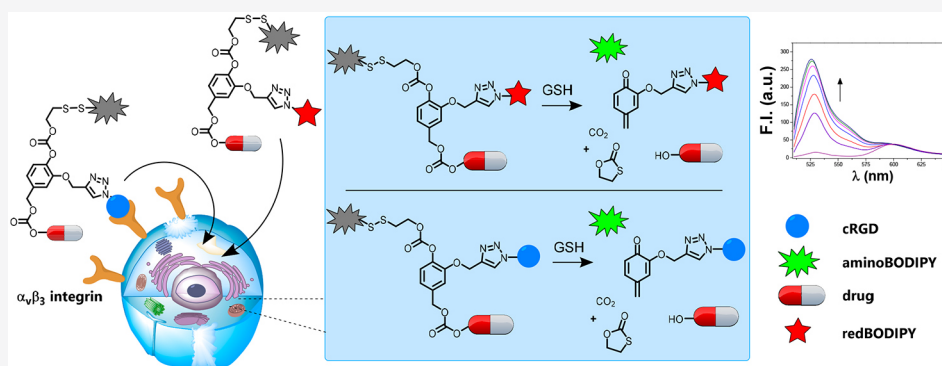
Metrics & More



Article Recommendations



Supporting Information



**ABSTRACT:** In this work, we report two concepts of drug delivery based on small-molecule drug conjugates with the ability of specific targeting and drug release monitoring via ratiometric fluorescence. The functionality of these concepts has been verified by two model systems consisting of three parts: (i) fluorescent aminoBODIPY for real-time detection of conjugate cleavage, (ii) a c(RGDfK) peptide specific for  $\alpha_v\beta_3$  integrin receptors targeting angiogenesis in most solid tumors or redBODIPY for conjugate cleavage monitoring via FRET, and (iii) pegylated-2-phenyl-3-hydroxy-4(1H)-quinolinone (3HQ) as a model drug. The model drug release is based on a self-immolative disulfide linker sensitive to environments containing thiols, especially glutathione, which is overexpressed in cancer cells. The results show effective thiol-mediated cleavage of the fluorescent reporter and the subsequent liberation of the drug in a tube. The conjugate with c(RGDfK) was confirmed to penetrate the cells via interaction with integrin receptors. Drug release from this conjugate is possible to monitor inside the cells. Further, the synthetic approach to the conjugates and the method of fluorescence monitoring of the drug release have also been described.

**KEYWORDS:** BODIPY, drug delivery, controlled release, targeting, conjugate

### INTRODUCTION

Glutathione in its reduced (GSH) or oxidized form (GSSG) is a ubiquitous component of all living organisms. It can prevent the oxidation of critical cellular components by reactive oxygen species, free radicals, and peroxides. It is also required in many aspects of the immune response.<sup>1</sup> Healthy cells maintain glutathione concentration at low submicromolar levels. However, in many cancers, the elevated glutathione levels protect against drugs and establish resistance only after developing resistance to chemotherapeutics.<sup>2</sup> The high concentration of GSH in cancer cells (up to 10 mM),<sup>3,4</sup> which is approximately 100–1000 times higher than that in human plasma and blood, is considered a suitable target for effective stimuli triggered cargo delivery.<sup>5,6</sup> Many small-molecule drug conjugates (SMDCs) have been synthesized/studied utilizing thiol-cleavable linkers involving various formulations such as dendrimers,<sup>7</sup> polymers,<sup>8</sup> nanoparticles,<sup>9</sup> and micelles.<sup>10</sup>

Although the activation of these prodrugs under particular conditions in tumors is advantageous for enhancing the specificity of anticancer drugs, the next major step toward improving the therapeutic index involves the active targeting of drugs to cancerous tissues.<sup>11</sup> One of the most effective approaches for the selective delivery of drugs to the appropriate cells is based on the interaction of a drug–ligand conjugate able to target the specific receptor.<sup>12–16</sup> A possible receptor that can be targeted is the heterodimeric transmembrane receptor integrin  $\alpha_v\beta_3$ ,<sup>17</sup> which is highly expressed on activated endothelial cells and newborn vessels, but it is absent in resting endothelial cells and most normal organ

**Received:** March 18, 2021

**Revised:** April 22, 2021

**Accepted:** April 23, 2021

**Published:** May 7, 2021



systems. This fact makes this receptor a suitable target for the antiangiogenic cancer therapy.<sup>18</sup> In addition, integrin  $\alpha_v\beta_3$  is also frequently overexpressed in tumor cells, as observed in colon,<sup>19</sup> pancreas,<sup>20</sup> and lung<sup>21</sup> cancers, melanomas,<sup>22</sup> brain tumors,<sup>23</sup> or breast<sup>24</sup> cancers.

The integrins overexpressed in cancer cells interact with the RGD peptide motif (Arg-Gly-Asp), especially in its cyclic form (cRGD).<sup>20</sup> Cyclic RGD peptides conjugated with anticancer drugs, such as doxorubicin,<sup>25</sup> camptothecin,<sup>26</sup> and paclitaxel,<sup>27</sup> were shown to have improved therapeutic activities in vitro as well as in vivo as compared to the corresponding free drugs. In addition, cRGD binds to the integrins on many cancer cells, resulting in active internalization. Recently, it was shown that cRGD peptides could selectively bind to  $\alpha_v\beta_3$  integrins over  $\alpha_v\beta_5$  integrins with a very high affinity, an  $IC_{50}$  in the nanomolar range, and a negligible difference between the effects of the conjugated drug and free ligand.<sup>28</sup> The  $\alpha_v\beta_3$  integrin-targeting moiety was implemented with the cilengitide-c(RGDfV) conjugate, which has been promoted to clinical trials for the treatment of glioblastoma.<sup>29</sup>

The specific responses of drug delivery systems in the presence of a selected marker, causing the consequent drug release, give rise to the development of targeted small-molecule drug conjugates (T-SMDCs) or theranostics—the combination of therapeutics and diagnostics in one material.<sup>30</sup> The significance of these SMDCs in therapy is well discussed in the recent reviews and perspective.<sup>31–33</sup> Although the visualization is commonly performed via fluorescence, this technique usually relies on the fluorescent intensimetric or ratiometric response of the drugs such as camptothecin or doxorubicin.<sup>34,35</sup> Only a few drug conjugates contain a universal and simple fluorescent dye, which allows drug uptake and release monitoring.<sup>35,36</sup> Therefore, in this study, we have used aminoBODIPY as reported in our previous work.<sup>37</sup> Generally, BODIPY dyes are known for their exceptional fluorescence properties such as high quantum yield, extinction coefficient, and low photobleaching.<sup>38</sup>

Herein, we report a model system that overcomes some of the abovementioned drawbacks. We also describe the synthesis, characterization, optical properties, and biological properties of two conjugates, namely, (i) the fluorescent dye-cRGD-drug conjugate designed for integrin-targeted delivery of (non)fluorescent drugs, providing a drug-independent fluorescent response to high concentrations of glutathione causing the drug release and (ii) the aminoBODIPY-redBODIPY-drug conjugate for the ratiometric fluorescence monitoring of glutathione-triggered drug release utilizing the FRET effect (see Figure 1). Both conjugates comprise a central unit based on the *p*-hydroxybenzyl moiety to which the fluorescent dye is bound by the cleavable disulfide

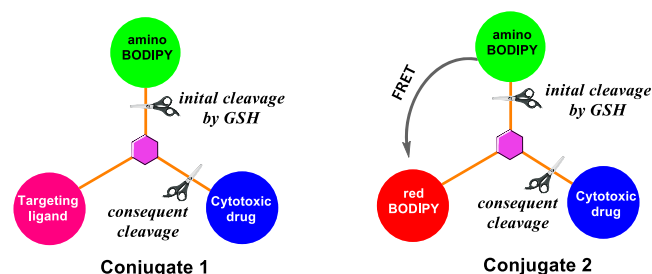


Figure 1. Suggested design of small-molecule drug conjugates.

self-immolative linker, as described originally by Satyam.<sup>39</sup> The cRGD targeting moiety (conjugate 1) or the second BODIPY dye (conjugate 2) is bound via a non-cleavable linker. After the glutathione attack, the disulfide linker releases the aminoBODIPY dye, and the central unit undergoes a 1,6-elimination reaction producing the quinone-methide moieties,<sup>40,41</sup> resulting in the release of the drug (Figure 1).

## EXPERIMENTAL SECTION

**Materials and Methods.** For the preparation and characterization of the compounds, LC/MS analyses were performed by UHPLC/MS via a UHPLC chromatograph (Acquity) with a PDA detector, a single quadrupole mass spectrometer (Waters), and an X-Select C18 column at 30 °C and a flow rate of 600  $\mu$ L/min. The mobile phase consisted of (A) 0.01 M ammonium acetate in water and (B) acetonitrile, with a linear gradient over the course of 2.5 min; at the conclusion of the gradient, the final ratio was maintained for 1.5 min. The column was re-equilibrated with 10% B for 1 min. The APCI ionization was operated at a discharge current of 5  $\mu$ A, a vaporizer temperature of 350 °C and a capillary temperature of 200 °C. Compound purity was determined using the ratio of the appropriate peak area to sum of the areas of all peaks of the mixture. Areas were determined by integration of the peaks from the PDA detector response. The purity of the final compounds was determined by this method and was estimated to be >95%.

The purification was performed using a semipreparative HPLC with a Waters 1500 series HPLC equipped with a 2707 autosampler, a 1525 binary HPLC pump, a 2998 Waters photodiode array detector, and a Waters Fraction Collector III with YMC C18 a reversed-phase column (20  $\times$  100 mm, 5  $\mu$ m particle size). The mobile phase consisted of acetonitrile and a 10 mM aqueous ammonium acetate gradient over 6 min.

NMR spectra were measured in  $CDCl_3$ ,  $DMSO-d_6$ , or  $CD_3OD$  using a JEOL ECX-500 (500 MHz) spectrometer. The chemical shifts ( $\delta$ ) are reported in parts per million (ppm) and the coupling constants ( $J$ ) are reported in Hertz (Hz).

The HR-MS analysis was performed using an Orbitrap Elite high-resolution mass spectrometer (Thermo Fischer Scientific, MA, USA) operating at positive full-scan mode (120,000 FWHM) in the range of 2000–3000  $m/z$ . The settings for electrospray ionization were as follows: an oven temperature of 300 °C, a sheath gas of 8 arb. units, and a source voltage of 1.5 kV. Samples were diluted to a final concentration of 20  $\mu$ mol/L with 0.1% formic acid in water and methanol (50:50 v/v).

Rink amide resin and Fmoc-amino acids were purchased from AAPPTec (Louisville, KY). Solvents and other chemicals were purchased from Sigma-Aldrich (Milwaukee, IL, [www.sigmaaldrich.com](http://www.sigmaaldrich.com)).

Fluorescence spectra were recorded on a Varian Cary Eclipse fluorescence spectrophotometer equipped with a thermostat (FL1009M015). The excitation and emission slits were 5 nm. Absorption spectra were recorded on a Cary 300 UV/VIS spectrophotometer (UV111M031, Agilent).

**Compound 4.** Compound 4 was prepared according to the previously published procedure.<sup>11</sup>

**Compound 5.** Compound 5 was prepared according to the previously published procedure.<sup>11</sup>

**Compound 6.** To a solution of the benzyl alcohol 5 (0.87 g, 4.89 mmol, 1.1 equiv) in dry DMF (20 mL) was added imidazole (366 mg, 1 equiv) and *tert*-butyldimethylsilyl chloride (811 mg, 1.1 equiv). The resulting solution was

stirred for 1 h at room temperature. The reaction mixture was then diluted with Et<sub>2</sub>O (150 mL) and washed with water five times to get rid of traces of DMF. The organic layer was then dried over Na<sub>2</sub>SO<sub>4</sub> and concentrated under reduced pressure. The crude product was purified using column chromatography (DCM/hexane 1:1) to give 1.27 g of pure compound (91% yield). <sup>1</sup>H NMR (500 MHz, CDCl<sub>3</sub>): δ 7.03–7.01 (m, 1H), 6.89 (d, *J* = 8.1 Hz, 1H), 6.85–6.82 (m, 1H), 5.53 (s, 1H), 4.75 (d, *J* = 2.4 Hz, 2H), 4.67–4.66 (m, 2H), 2.54 (t, *J* = 2.4 Hz, 1H), 0.94 (s, 9H), 0.09 (s, 6H). <sup>13</sup>C NMR (50 MHz, CDCl<sub>3</sub>): δ 145.11, 144.72, 133.71, 120.37, 114.82, 111.23, 78.32, 76.21, 64.91, 57.15, 26.12, 18.55, –5.04. MS (ESI): calculated for C<sub>16</sub>H<sub>23</sub>O<sub>3</sub>Si: 291.142. Found: 291.656.

**Compound 7.** Compound 7 was prepared according to our previously published procedure.<sup>37</sup>

**Compound 8.** To a solution of phenol 6 (147 mg, 0.503 mmol, 1 equiv) in dry DCM (6 mL) were added TEA (84 μL, 1.2 equiv), DMAP (74 mg, 1.2 equiv), and the solution of the amino-BODIPY disulfide linker 7 (280 mg, 1 equiv) in dry DCM (2 mL). The reaction mixture was then stirred for 30 min at room temperature. The mixture was then diluted with Et<sub>2</sub>O (50 mL) and washed with water three times and then with brine solution. The organic layer was dried over Na<sub>2</sub>SO<sub>4</sub> and concentrated under reduced pressure. The crude product was purified using column chromatography (DCM) to give 299 mg of pure compound 8 (81% yield). <sup>1</sup>H NMR (500 MHz, CDCl<sub>3</sub>): δ 8.05 (s, 1H), 7.15 (d, *J* = 1.7 Hz, 1H), 7.10 (d, *J* = 8.2 Hz, 1H), 7.00 (s, 1H), 6.98 (d, *J* = 4.4 Hz, 1H), 6.92–6.89 (m, 1H), 6.89–6.87 (m, 1H), 6.04 (s, 1H), 4.74–4.71 (m, 4H), 4.50 (dt, *J* = 10.6, 6.6 Hz, 4H), 3.06 (t, *J* = 6.6 Hz, 2H), 3.01 (t, *J* = 6.6 Hz, 2H), 2.52 (t, *J* = 2.4 Hz, 1H), 2.51 (s, 3H), 2.22 (s, 3H), 0.95 (s, 9H), 0.11 (s, 6H). <sup>13</sup>C NMR (50 MHz, CDCl<sub>3</sub>): δ 155.64, 153.17, 151.56, 149.71, 149.18, 145.09, 141.21, 140.90, 139.31, 133.66, 130.94, 129.77, 122.23, 122.09, 120.32, 119.02, 112.20, 111.23, 109.35, 78.31, 76.16, 66.55, 64.44, 64.27, 56.82, 37.14, 37.10, 26.09, 26.05, 26.04, 26.03, 26.02, 18.48, 14.65, 11.35, –5.17. MS (ESI): calculated for C<sub>33</sub>H<sub>43</sub>BF<sub>2</sub>N<sub>3</sub>O<sub>7</sub>S<sub>2</sub>Si<sup>+</sup>: 734.237. Found: 734.582.

**Compound 9.** To a solution of compound 8 (340 mg, 0.46 mmol, 1 equiv) in methanol (20 mL) was added pTSA (13 mg, 0.15 equiv), and the resulting solution was stirred for 2 h at room temperature. The reaction mixture was diluted with EtOAc (50 mL) and washed with water three times. The organic layer was dried over Na<sub>2</sub>SO<sub>4</sub> and concentrated under reduced pressure to yield 255 mg of crude product (89% yield), which was used without further purification. <sup>1</sup>H NMR (500 MHz, CDCl<sub>3</sub>): δ 8.05 (s, 1H), 7.16–7.12 (m, 2H), 7.05–6.95 (m, 4H), 6.94–6.84 (m, 2H), 6.05 (s, 1H), 4.75–4.73 (m, 2H), 4.67 (d, *J* = 4.8 Hz, 2H), 4.54–4.50 (m, 2H), 4.50–4.46 (m, 2H), 3.08–3.04 (m, 2H), 3.02–2.99 (m, 2H), 2.56–2.53 (m, 1H), 2.51 (s, 3H), 2.23 (s, 3H). <sup>13</sup>C NMR (50 MHz, CDCl<sub>3</sub>): δ 155.72, 153.07, 151.61, 149.36, 140.35, 139.95, 130.94, 122.61, 122.13, 120.12, 113.08, 109.36, 78.17, 76.32, 66.59, 64.91, 64.29, 56.92, 42.96, 37.23, 37.09, 14.68, 11.38. MS (ESI): calculated for C<sub>27</sub>H<sub>29</sub>BF<sub>2</sub>N<sub>3</sub>O<sub>7</sub>S<sub>2</sub><sup>+</sup>: 620.1503. Found: 620.406.

**Compound 10.** To a solution of alcohol 9 (95 mg, 0.153 mmol, 1 equiv) in dry THF (4 mL) were added pyridine (25 μL, 3 equiv) and the solution of 4-nitrophenylchloroformate (93 mg, 2 equiv) in dry THF (1 mL). The reaction mixture was stirred for 2.5 h at room temperature and then diluted with EtOAc (50 mL) and washed with water three times and brine. The organic layer was dried over Na<sub>2</sub>SO<sub>4</sub> and concentrated

under reduced pressure. The crude product was purified using column chromatography (DCM/hexane 1:1 to DCM) to afford 115 mg of pure product (91% yield). <sup>1</sup>H NMR (500 MHz, CDCl<sub>3</sub>): δ 8.26–8.22 (m, 1H), 8.11–8.08 (m, 2H), 8.04 (s, 1H), 7.18 (t, *J* = 5.2 Hz, 2H), 7.06 (dd, *J* = 8.1, 1.9 Hz, 1H), 6.99 (s, 1H), 6.96 (d, *J* = 4.4 Hz, 1H), 6.86–6.83 (m, 3H), 5.25 (s, 2H), 4.75 (d, *J* = 2.4 Hz, 2H), 4.53 (t, *J* = 6.5 Hz, 2H), 4.48 (t, *J* = 6.6 Hz, 2H), 3.05 (t, *J* = 6.5 Hz, 2H), 3.00 (t, *J* = 6.6 Hz, 2H), 2.56 (t, *J* = 2.4 Hz, 1H), 2.49 (s, 3H), 2.20 (s, 3H). <sup>13</sup>C NMR (50 MHz, CDCl<sub>3</sub>): δ 162.19, 155.91, 155.53, 153.02, 152.46, 151.65, 149.37, 145.50, 141.56, 141.29, 140.93, 133.69, 133.48, 130.84, 129.68, 126.21, 125.38, 122.95, 122.19, 121.85, 115.70, 114.78, 109.12, 77.78, 76.63, 70.33, 66.78, 64.28, 56.96, 37.07, 37.03, 14.19, 11.28. MS (ESI): calculated for C<sub>34</sub>H<sub>32</sub>BF<sub>2</sub>N<sub>4</sub>O<sub>11</sub>S<sub>2</sub><sup>+</sup>: 785.156. Found: 785.754.

**Compound 11.** The compound was synthesized according to our previously published procedure.<sup>37</sup>

**Compound 12.** To a solution of the activated carbonate 10 (93 mg, 0.119 mmol, 1 equiv) in dry DMF (1.5 mL) were added TEA (33 μL, 2 equiv) and the solution of 3HQ 11 (49 mg, 1 equiv) in dry DMF (0.5 mL). The resulting solution was stirred overnight at room temperature. After consumption of the starting material, the reaction mixture was diluted with EtOAc (50 mL) and successively washed with water three times and brine solution. The organic layer was dried over Na<sub>2</sub>SO<sub>4</sub> and concentrated under reduced pressure. The crude product was purified using column chromatography (DCM/EtOAc 1:1 to DCM/MeOH 50:1) to give 90 mg (72% yield) of the desired product. <sup>1</sup>H NMR (500 MHz, CDCl<sub>3</sub>): δ 10.94 (s, 1H), 8.36 (d, *J* = 8.5 Hz, 1H), 8.32 (s, 1H), 8.02 (s, 1H), 7.96 (s, 1H), 7.88 (d, *J* = 8.5 Hz, 1H), 7.60–7.50 (m, 2H), 7.47–7.36 (m, 3H), 7.07 (dd, *J* = 8.0, 4.9 Hz, 2H), 6.98 (s, 1H), 6.96 (d, *J* = 4.4 Hz, 1H), 6.88 (dd, *J* = 8.2, 1.7 Hz, 1H), 6.84 (d, *J* = 4.1 Hz, 1H), 6.02 (s, 1H), 5.11 (s, 2H), 4.68 (d, *J* = 2.3 Hz, 2H), 4.49 (dt, *J* = 14.6, 6.6 Hz, 4H), 4.45–4.42 (m, 2H), 3.80–3.74 (m, 2H), 3.66 (d, *J* = 2.9 Hz, 3H), 3.64–3.58 (m, 4H), 3.05 (t, *J* = 6.6 Hz, 2H), 3.00 (t, *J* = 6.6 Hz, 2H), 2.52 (t, *J* = 2.3 Hz, 1H), 2.49 (s, 3H), 2.19 (s, 3H). <sup>13</sup>C NMR (50 MHz, CDCl<sub>3</sub>): δ 165.58, 155.64, 153.10, 152.88, 151.54, 149.59, 149.27, 144.08, 141.27, 140.55, 138.74, 134.25, 133.63, 133.08, 132.88, 130.94, 130.81, 130.67, 129.77, 128.85, 128.62, 128.19, 126.53, 123.52, 122.59, 122.13, 121.47, 120.58, 118.96, 114.25, 109.28, 77.98, 76.47, 72.00, 70.72, 70.07, 69.81, 68.98, 66.63, 64.42, 64.25, 61.78, 57.00, 37.11, 37.09, 14.63, 11.33. MS (ESI): calculated for C<sub>50</sub>H<sub>50</sub>BF<sub>2</sub>N<sub>4</sub>O<sub>15</sub>S<sub>2</sub><sup>+</sup>: 1059.277. Found: 1059.468.

**Compound 1.** To the starting compound 12 (40 mg, 0.038 mmol, 1 equiv) in DMF/ACN (1 mL) were added CuSO<sub>4</sub>·5H<sub>2</sub>O (5 mg, 0.5 equiv), sodium ascorbate (4 mg, 0.5 equiv), and cRGD peptide 13 (85 mg, 2 equiv; for the synthesis, see Scheme S1), and the resulting solution was heated to 50 °C and stirred overnight. The reaction was monitored by LC/MS to the full conversion of the starting material. Then, the reaction mixture was diluted with DCM (50 mL) and washed with water three times. The organic layer was dried over Na<sub>2</sub>SO<sub>4</sub> and concentrated under reduced pressure. The crude product was purified using preparative HPLC with (ACN/CH<sub>3</sub>COONH<sub>4</sub> buffer 40 to 70% gradient) to afford 40 mg (56% yield) of pure compound 1. <sup>1</sup>H NMR (500 MHz, DMSO-*d*<sub>6</sub>): δ 8.44 (s, 1H), 8.34 (s, 1H), 8.28 (d, *J* = 8.5 Hz, 1H), 8.19–8.12 (m, 3H), 7.95 (s, 3H), 7.90–7.85 (m, 1H), 7.67–7.56 (m, 6H), 7.39 (s, 1H), 7.25–7.20 (m, 5H), 7.15 (dd, *J* = 10.7, 2.7 Hz, 3H), 6.93 (d, *J* = 8.2 Hz, 1H), 6.79



(d,  $J = 4.2$  Hz, 1H), 6.19 (s, 1H), 5.23 (s, 2H), 5.19 (s, 2H), 4.59–4.51 (m, 4H), 4.48–4.44 (m, 2H), 4.42 (dd,  $J = 11.3, 5.5$  Hz, 4H), 4.28–4.22 (m, 1H), 4.06 (dd,  $J = 15.3, 7.9$  Hz, 2H), 3.86–3.78 (m, 6H), 3.61 (dd,  $J = 5.8, 3.6$  Hz, 2H), 3.57–3.45 (m, 14H), 3.44–3.40 (m, 3H), 3.08 (t,  $J = 6.1$  Hz, 3H), 3.05–2.99 (m, 7H), 2.41 (s, 3H), 2.22 (s, 3H), 1.74–1.71 (m, 2H), 1.61–1.53 (m, 2H), 1.43–1.38 (m, 2H), 1.36–1.29 (m, 2H), 1.10–1.01 (m, 2H).  $^{13}\text{C}$  NMR (50 MHz, DMSO- $d_6$ )  $\delta$  172.08, 171.08, 170.52, 169.06, 165.01, 162.49, 156.67, 152.56, 152.27, 149.47, 141.97, 139.65, 138.84, 134.41, 132.48, 132.01, 131.64, 130.62, 129.05, 128.77, 128.69, 128.05, 127.53, 126.16, 125.67, 124.93, 122.75, 122.43, 120.29, 113.91, 72.34, 70.15, 69.95, 69.90, 69.74, 69.56, 69.51, 68.68, 68.28, 66.25, 64.68, 63.68, 62.01, 60.20, 53.97, 51.61, 49.43, 48.84, 45.86, 45.83, 43.16, 40.39, 37.86, 37.18, 36.24, 35.94, 28.57, 25.92, 25.86, 24.91, 22.86, 14.16, 10.91. MS (ESI): calculated for  $\text{C}_{88}\text{H}_{104}\text{BF}_2\text{N}_{16}\text{O}_{26}\text{S}_2^+$ : 1877.6805. Found: 1877.483.

**Compound 2.** To a solution of compound **12** (127 mg, 0.120 mmol, 1 equiv) in DMF/ACN (3 mL) were added  $\text{CuSO}_4 \cdot 5\text{H}_2\text{O}$  (30 mg, 1.0 equiv), sodium ascorbate (24 mg, 1.0 equiv), and red-BODIPY **14** (116 mg, 1 equiv; for the synthesis, see Scheme S2). The resulting solution was stirred overnight at room temperature. Then, it was diluted with DCM (50 mL) and washed with water three times and brine solution. The organic layer was dried over  $\text{Na}_2\text{SO}_4$  and concentrated under reduced pressure. The obtained crude product was purified using preparative HPLC with (ACN/ $\text{CH}_3\text{COONH}_4$  buffer 50 to 80% gradient) to afford 35 mg (15% yield) of pure compound **2**.  $^1\text{H}$  NMR (500 MHz, DMSO- $d_6$ )  $\delta$  12.32 (s, 1H), 11.85 (s, 1H), 9.85 (d,  $J = 3.2$  Hz, 1H), 8.45 (d,  $J = 17.8$  Hz, 1H), 8.38 (s, 1H), 8.27 (dd,  $J = 8.4, 5.6$  Hz, 1H), 8.15 (d,  $J = 8.4$  Hz, 1H), 7.88–7.80 (m, 4H), 7.63–7.52 (m, 6H), 7.49–7.43 (m, 1H), 7.40 (s, 1H), 7.34 (s, 1H), 7.31 (t,  $J = 7.6$  Hz, 3H), 7.25–7.23 (m, 1H), 7.21 (dd,  $J = 8.1, 1.9$  Hz, 1H), 7.17 (s, 2H), 7.07 (d,  $J = 8.4$  Hz, 1H), 6.96 (ddd,  $J = 33.2, 8.2, 1.7$  Hz, 1H), 6.86 (d,  $J = 10.1$  Hz, 1H), 6.78 (d,  $J = 4.4$  Hz, 1H), 6.20 (d,  $J = 3.8$  Hz, 1H), 6.16 (d,  $J = 8.9$  Hz, 1H), 5.23 (s, 1H), 5.19 (d,  $J = 1.9$  Hz, 2H), 5.12 (s, 1H), 4.57–4.52 (m, 3H), 4.46–4.40 (m, 6H), 4.16 (s, 4H), 4.11 (d,  $J = 4.2$  Hz, 2H), 3.83 (d,  $J = 3.1$  Hz, 2H), 3.78 (dd,  $J = 9.4, 5.2$  Hz, 6H), 3.73 (s, 1H), 3.66 (d,  $J = 4.3$  Hz, 2H), 3.63–3.60 (m, 6H), 3.57–3.51 (m, 18H), 3.47 (s, 2H), 3.44–3.41 (m, 6H), 3.23 (d,  $J = 5.4$  Hz, 6H), 3.10–3.06 (m, 2H), 3.05–3.01 (m, 2H), 2.42 (s, 3H), 2.22 (d,  $J = 3.4$  Hz, 3H), 1.44 (d,  $J = 5.7$  Hz, 3H), 1.39 (d,  $J = 6.0$  Hz, 3H), 1.23 (s, 3H).  $^{13}\text{C}$  NMR (50 MHz, DMSO- $d_6$ )  $\delta$  169.39, 168.64, 164.97, 154.95, 153.89, 152.69, 152.55, 152.26, 151.31, 149.90, 149.46, 148.83, 148.45, 143.74, 142.26, 141.96, 141.84, 141.58, 140.08, 139.65, 139.21, 138.69, 137.06, 134.39, 133.05, 132.50, 132.34, 131.98, 131.56, 131.17, 130.62, 130.25, 129.40, 129.30, 129.23, 128.93, 128.75, 128.67, 128.55, 128.29, 127.47, 125.66, 124.92, 123.66, 122.76, 122.39, 121.09, 120.79, 120.29, 119.77, 118.92, 117.97, 116.07, 114.15, 113.89, 113.11, 109.05, 72.33, 71.26, 70.38, 70.27, 70.00, 69.89, 69.85, 69.82, 69.73, 69.58, 69.54, 69.00, 68.87, 68.67, 68.54, 68.43, 68.27, 66.23, 64.66, 63.78, 62.00, 60.19, 58.02, 58.00, 54.78, 49.43, 36.12, 35.92, 28.99, 22.06, 14.39, 14.30, 14.15, 10.89. MS (ESI): calculated for  $\text{C}_{98}\text{H}_{115}\text{B}_2\text{F}_4\text{N}_{10}\text{O}_{27}\text{S}_2^+$ : 2025.749. Found: 2025.149.

**Quantum Yield Determination.** Quantum yields ( $\Phi$ ) were calculated by the standard procedure using fluorescein as a reference ( $\Phi = 0.91$ ) and according to eq 1.

$$\Phi = \Phi_{\text{R}} \times I/I_{\text{R}} \times A_{\text{R}}/A \times \eta^2/\eta_{\text{R}}^2 \quad (1)$$

where  $\Phi_{\text{R}}$  is the quantum yield of the reference fluorophore,  $I$  is the area under the emission peak,  $A$  is the absorbance at the excitation wavelength, and  $\eta$  is the refractive index of the solvent.

**FRET Efficiency.** FRET efficiency was calculated for conjugate **2** using standard eq 2.

$$\text{FRET} = F_{\text{a}}/(F_{\text{a}} + F_{\text{d}}) \quad (2)$$

where  $F_{\text{a}}$  is the emission intensity of the acceptor and  $F_{\text{d}}$  is the emission of the donor.

**Cleavage of Conjugates 1 and 2 by Glutathione and Its LC/MS Monitoring.** First, 0.25 mL of the conjugate **1** and **2** solution (2 mM) in DMSO was mixed with 0.1 mL of GSH solution (50 mM) in HEPES (0.1 M, pH 7.4) and diluted with 0.65 mL DMSO/HEPES (2:1 v/v). The mixture was heated to 37 °C and analyzed using LC/MS at the same time.

**Cleavage of Conjugates 1 and 2 by Glutathione and Its Fluorescence Monitoring.** First, 5  $\mu\text{L}$  of the solution of conjugate **1** or **2** (1 mM) in DMSO was mixed with 20, 60, or 100  $\mu\text{L}$  of GSH solution (50 mM) in HEPES buffer (0.1 M; pH 7.4) and diluted with 1 mL of HEPES buffer (0.1 M; pH 7.4) or DMSO/HEPES buffer (2:1). Then, the mixture was heated to 37 °C and the fluorescence was measured at the same time.

**Fluorescence Microscopy.** HeLa cells (10,000 well $^{-1}$ , 100  $\mu\text{L}$  per well) were seeded into 96 CellCarrier plates (PerkinElmer, USA) for live cell fluorescence imaging and pre-incubated for 24 h at 37 °C and 5%  $\text{CO}_2$  to adhere. The first group of cells was pretreated with 1 mM NEM for 30 min, then rinsed with fresh media, incubated with test compounds **1** and **2** (50  $\mu\text{M}$ ) for 1 h, and again rinsed with fresh media. The second group of cells was only incubated with test compounds **1** and **2** (50  $\mu\text{M}$ ) for 1 h and rinsed with fresh media. Finally, the third group of cells was incubated with test compounds **1** and **2** (50  $\mu\text{M}$ ) for 1 h and rinsed with fresh media with 20 mM GSHOEt. The live-cell imaging was performed using a Cell Voyager CV7000 (Yokogawa, Japan) spinning disc confocal microscopy system at 37 °C in a 5%  $\text{CO}_2$  atmosphere. Living cells were monitored with a 60 $\times$  water immersion objective at 0 and 2 h. Microscopy images were taken separately with excitation at 488 nm using a laser and emissions detected using band pass filters (BP 515/30 and BP 595/20). All the obtained images were post-processed, background-subtracted, and deconvolved using Image J software. Fluorescence intensity quantification of microscopy images was interpreted as a median of two technical replicates calculated in a total of 10 microscopy fields.

**Intracellular Cleavage of Conjugate 1 by Glutathione and Its Fluorescence Monitoring.** HeLa cells (10,000 well $^{-1}$ , 100  $\mu\text{L}$  per well) were seeded into 96 CellCarrier plates (Perkin Elmer, USA) and incubated overnight at 37 °C and 5%  $\text{CO}_2$  in order to adhere. The first group of cells was pretreated with 1 mM NEM for 30 min, then rinsed with fresh media, incubated with test compound **1** (50  $\mu\text{M}$ ) for 10 min, and again rinsed with fresh media. The second group of cells was only incubated with test compound **1** (50  $\mu\text{M}$ ) for 10 min and rinsed with fresh media. Finally, the third group of cells was incubated with test compound **1** (50  $\mu\text{M}$ ) for 10 min and rinsed with fresh media with 20 mM GSHOEt. The fluorescence intensity was measured using an EnSpire multimode plate reader (Perkin Elmer, USA), with two reads for each time point and each conjugate (conjugate **1** - first with

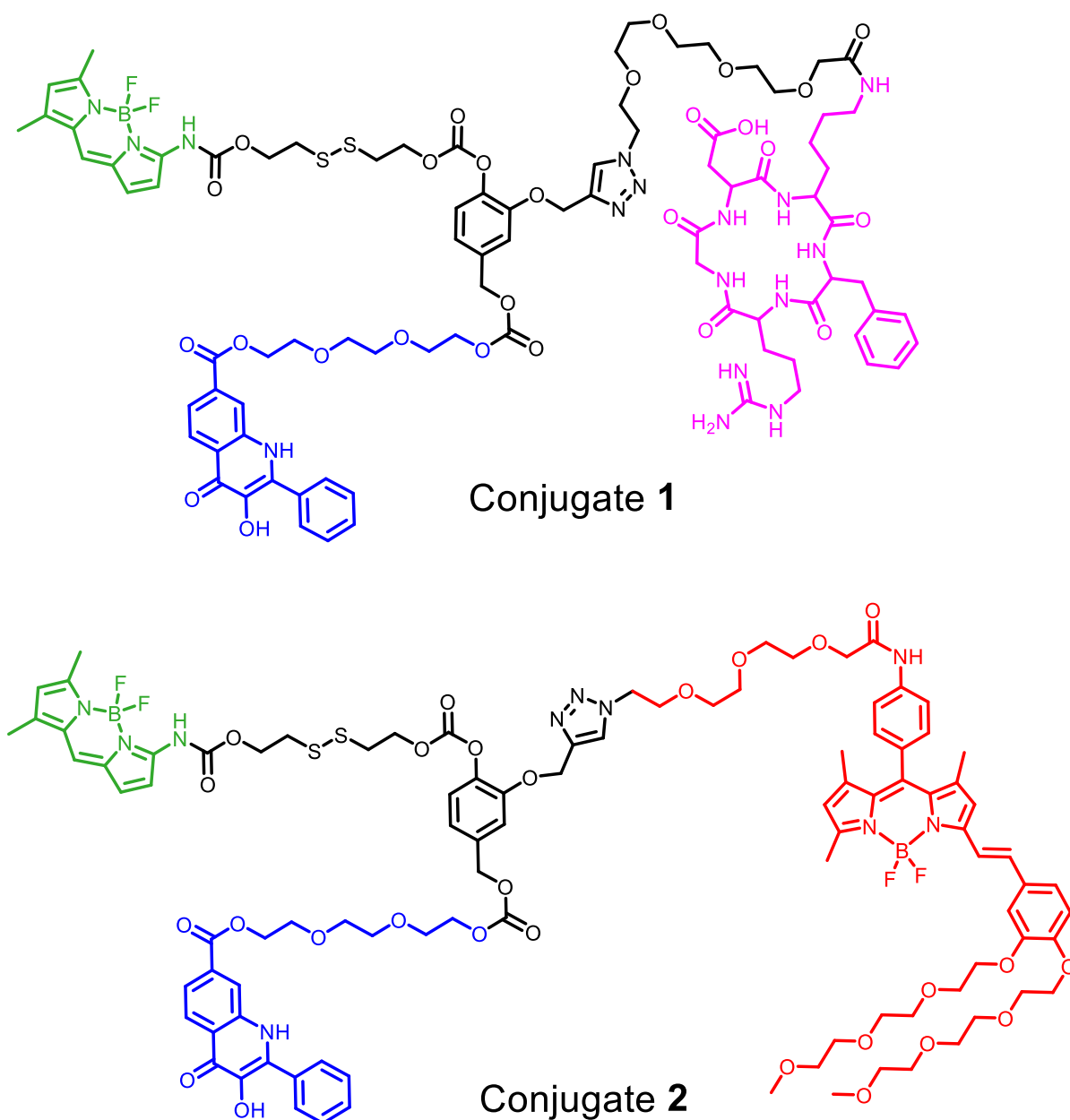


**Figure 2.** Structures of SMDCs aminoBDP-cRGD-3HQ **1** and T-SMDC aminoBDP-redBDP-3HQ **2**.

excitation at 485 nm/emission at 530 nm and second with excitation at 510 nm/emission at 530 nm).

**cRGD Binding Assay.** HeLa cells (10,000 well<sup>-1</sup>, 100  $\mu$ L per well) were seeded into 96 CellCarrier plates (Perkin Elmer, USA) and incubated overnight at 37 °C and 5% CO<sub>2</sub> in order to adhere. The cells were pretreated with a free RGD peptide in concentration from 0 to 100  $\mu$ M for 30 min, and after that, the content of the wells was discarded and the cells were treated with conjugate **1** at a concentration of 10  $\mu$ M for 10 min. Subsequently, the cells were rinsed with fresh media and the fluorescent emission intensity was measured using an EnSpire multimode plate reader (Perkin Elmer, USA), with excitation at 485 nm and emission at 530 nm.

## RESULTS AND DISCUSSION

The structures of conjugates **1** and **2** are presented in Figure 2. For both compounds, we chose 4-(hydroxymethyl) benzene-1,2-diol, a versatile building central unit suitable for

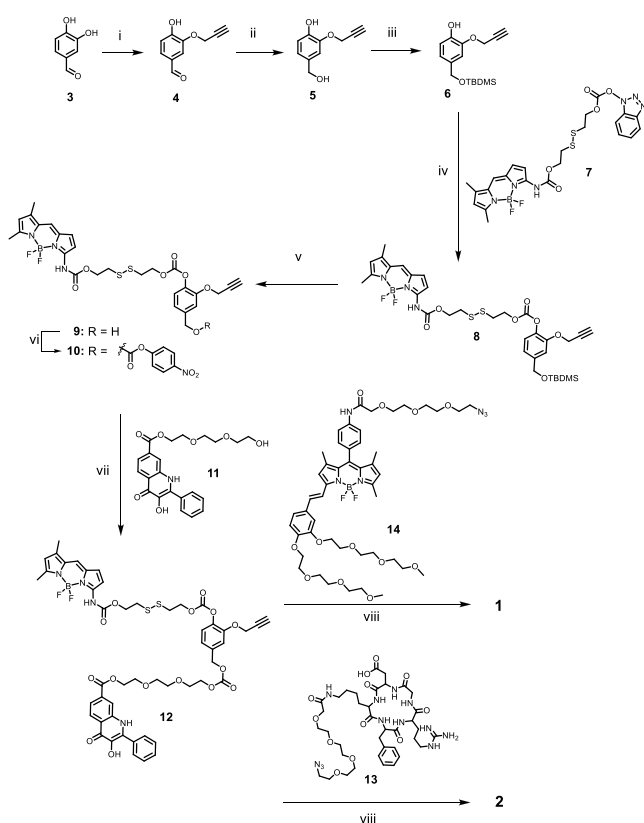
incorporating up to three different moieties as follows: For conjugate **1**, (i) the model drug 2-phenyl-3-hydroxyquinolin-4-(1*H*)-one(3HQ), (ii) integrin-specific cRGD-peptide-targeting ligand, and (iii) the previously characterized aminoBODIPY fluorescent dye for cleavage monitoring.<sup>42</sup> For conjugate **2**, it consisted of (i) aminoBODIPY dye, serving as a “green light” FRET donor; (ii) redBODIPY dye as the FRET acceptor; and (iii) 3HQ as the model drug bound to the central unit via a carbonate bond. The tethering of the fluorescent aminoBODIPY dye to the central frame is provided by the disulfide self-immolative linker for both probes. The linker allows the controlled release of the drug upon stimulation, such as the reductive microenvironment of cancer cells (e.g., elevated concentrations of GSH or thiols), so that it can subsequently liberate the drug via 1,6-elimination and lead to the formation of quinone methide (QM) species (Figure 1 and Scheme 2). Both conjugates are capable of making a ratiometric response based on the emission intensity measurements at one

wavelength after applying two different excitation wavelengths (conjugate 1) or intensities of two emission wavelengths after one excitation (conjugate 2).

In both prepared conjugates (Figure 2), we have used a derivative of 2-phenyl-3-hydroxyquinolin-4-(1H)-one as a model drug possessing the anticancer activity but suffering from poor aqueous solubility and often causing the toxicity to normal healthy cells.<sup>42–45</sup> Generally, binding such a compound to these developed conjugates could improve their physicochemical properties, the selectivity toward cancer cells, and pharmacological properties. The introduction of amino-BODIPY fluorophore, as the reporter responding to the presence of an elevated concentration of thiols together with a targeting unit, could lead to the formation of a targeted theranostic agent suitable for the studies in the field of personalized medicine.<sup>46</sup>

### Synthesis and Characterization of Conjugates 1 and 2. The synthesis of conjugates 1 and 2 is depicted in Scheme 1.

**Scheme 1. Synthesis of Conjugates 1 and 2<sup>a</sup>**



<sup>a</sup>Conditions: (i) propargyl bromide, NaH, DMSO, 0 °C, on; (ii) NaBH<sub>4</sub>, MeOH/H<sub>2</sub>O, 0 °C, 1 h; (iii) imidazole, TBDMS-Cl, DMF, rt, 1 h; (iv) DMAP, TEA, DCM, rt, 30 min; (v) pTSA, MeOH, rt, 2 h; (vi) 4-nitrophenylchloroformate, pyridine, THF, rt, 2.5 h; (vii) TEA, DMF, rt, on; (viii) CuSO<sub>4</sub>·5H<sub>2</sub>O, sodium ascorbate, ACN/DMF, 50 °C, on.

To form a central frame, 3,4-dihydroxy benzaldehyde 3 was alkylated with propargyl bromide and reduced with NaBH<sub>4</sub> to form 4-(hydroxymethyl)-2-(prop-2-yn-1-yloxy)phenol 5, with 31% yield according to the described procedure.<sup>11</sup> The benzylic hydroxyl group of intermediate 5 was then protected with *tert*-butyldimethylsilyl chloride (TBDMS-Cl) to afford a derivative 6 with 91% yield after purification. Compound 6 was

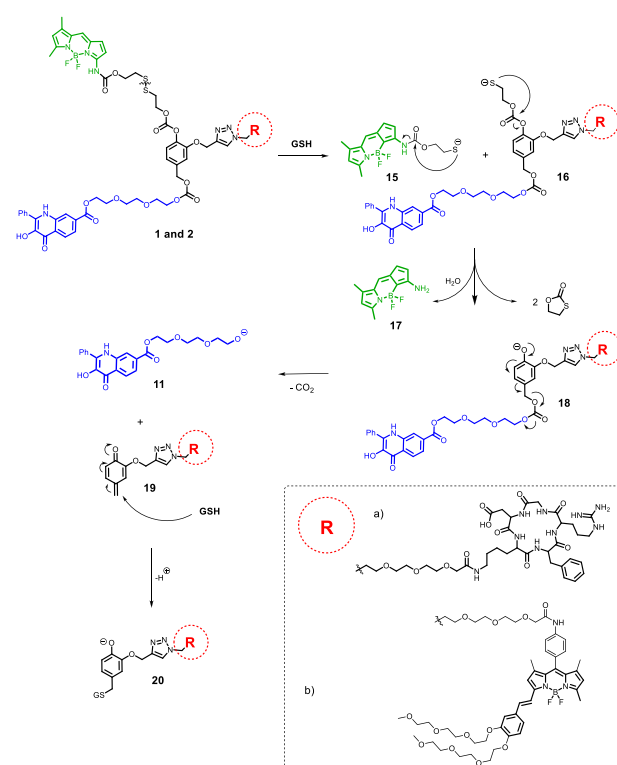
then reacted with amino-BODIPY disulfide linker 7 with the HOBT-activated carbonate group, which is synthesized according to our published procedure,<sup>37</sup> to form compound 8 with 81% yield after purification. The TBDMS protecting group was then removed under acidic conditions using pTSA and reacted with *p*-nitrophenyl chloroformate to obtain the acylated compound 10 with 96% yield.

In the next step, the 3HQ drug 11 was incorporated into the central QM frame under basic conditions through a carbonate bond using triethylamine to afford compound 12 with 45% yield after purification. Compound 12 was then used as a precursor to prepare the final conjugates 1 and 2 via a copper(I)-catalyzed cycloaddition reaction with azide 13 or 14, respectively.

The cRGD peptide derivative 13 was synthesized using the solid-phase peptide synthesis on the 2-chlorotrityl resin. RedBODIPY azido derivative 14 was synthesized by the standard Knoevenagel condensation of azido-BODIPY with 3,4-bis-[2-[2-(2-methoxy-ethoxy)-ethoxy]-ethoxy]-benzaldehyde, available similarly to that from the reported procedures<sup>47</sup> (see the Experimental Section). This BODIPY dye motif was considered for its optical properties as a suitable FRET acceptor for the green light-emitting amino-BODIPY 17.<sup>37</sup>

**LC/MS Monitoring of the GSH Cleavage.** To demonstrate the effective cleavage of the drug and the potential formation of any byproducts during the cleavage, we performed the UHPLC analysis with MS detection. The mechanism for the GSH-mediated cleavage of conjugates 1 and 2 is depicted in Scheme 2. In the first step, the disulfide bridge is attacked by the thiol group of GSH. After disrupting the SS bond, the linker's self-immolation occurs, where it forms

**Scheme 2. Mechanism for the GSH-Promoted Cleavage of Conjugates 1 and 2 to Quinone-Methide Species 19 with the Subsequent Liberation of the Drug 11 via 1,6-elimination**



two molecules of thiolactone and leaves the free aminoBODIPY 17 and intermediate 18. The push–pull effect of electrons in this intermediate causes the release of the drug 11 via 1,4-elimination and the subsequent formation of quinone methide 19. This QM 19, being a very good Michael acceptor, can be promptly captured by a nucleophile – GSH to form a fully aromatic system 20.

The obtained LCMS data showed that the total cleavage of conjugates 1 and 2 occurred within 80 and 60 min, respectively, along with the formation of the aminoBODIPY 17. In the case of conjugate 1, the formation of intermediate 16a is also observed. Similarly, the process of the elimination reaction of conjugate 2 to 19b and the liberation of the drug 11 occurred along with the formation of intermediate 16b (Figure 3).

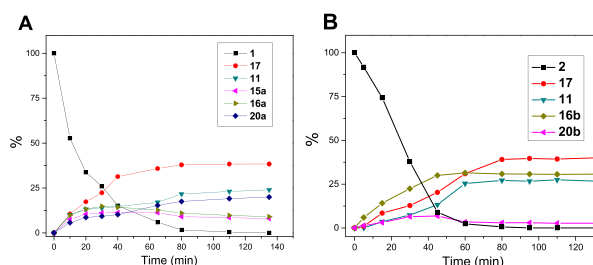


**Figure 3.** (A) GSH-mediated cleavage of the conjugate 1 (0.5 mM, 5 mM GSH, DMSO/HEPES buffer 0.1 M, 2:1, 37 °C) and (B) GSH-mediated cleavage of the conjugate 2 (0.5 mM, 2 mM GSH, DMSO/HEPES buffer 0.1 M, 2:1, 37 °C), with the detection of resulting products by LCMS.

**Optical Properties of SMDCs 1 and 2.** According to the results described previously,<sup>37</sup> the optical response of acylaminoBODIPY in conjugate 1 and the released aminoBODIPY 17 should differ significantly in excitation wavelengths, while the emission maxima should remain almost identical. To demonstrate the validity of this feature of conjugate 1, we have compared the excitation and emission spectra of the newly synthesized cRGD-aminoBODIPY-3HQ conjugate 1 to aminoBODIPY 17. As shown in Figure 4A, the comparison of optical properties fits well with the previously described system,<sup>37</sup> allowing the OFF–ON ratiometric drug release monitoring. The fluorescence quantum yield ( $\Phi_f$ ) of compound 1 in HEPES was calculated to be 0.15, taking fluorescein as a reference. The quantum yield of the aminoBODIPY dye released after conjugate disruption was previously calculated to be 0.77 (in HEPES buffer).<sup>37</sup>

In the case of conjugate 2 measured in DMSO/HEPES buffer, the emission of bound aminoBODIPY is expectedly transferred to redBODIPY and used for its excitation. The FRET between these two dyes is depicted in Figure 4B. The first excitation maximum belongs to the bound aminoBODIPY as observed from the comparison of excitation spectra of compounds 1 and 2. The similar emission maxima of conjugates 1 and 2 at around 530 nm can be attributed to aminoBODIPY itself. The second emission maximum of compound 2 at 592 nm belongs to redBODIPY. This emission can be achieved after excitation of aminoBODIPY (the first excitation maximum) or by redBODIPY itself (the second excitation maximum). The FRET effect is considerable in DMSO/HEPES buffer but decreases with a lower DMSO concentration (Figure 4C). The advantage of the FRET system

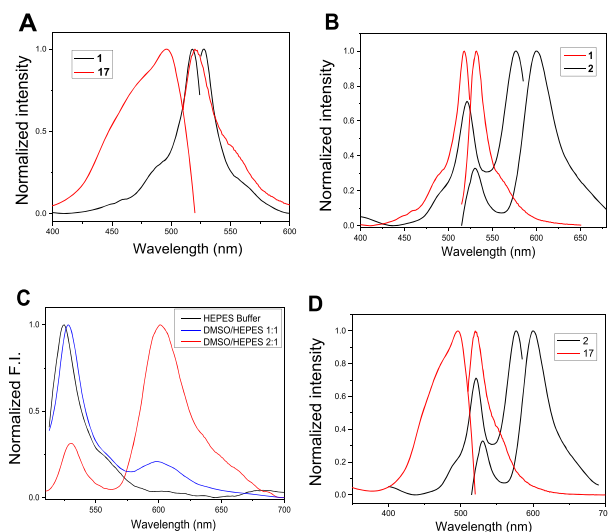


**Figure 4.** (A) Normalized excitation and emission spectra of conjugate 1 and aminoBODIPY 17 (HEPES buffer, 0.1 M, pH 7.4). (B) Normalized excitation and emission spectra of conjugates 1 and 2 (DMSO/HEPES buffer 0.1 M, 2:1, pH 7.4). (C) Normalized emission spectra of FRET conjugate 2 in different solvents. Excitation wavelength  $\lambda_{exc} = 510$  nm. (D) Normalized excitation and emission spectra of conjugate 2 and aminoBODIPY 17.

2 also includes the fact that in the case of excitation around 510 nm, not only the conjugated aminoBODIPY but the released aminoBODIPY 17 also emits light at around 530 nm (Figure 4D). Due to the significant difference in quantum yields of bound and released aminoBODIPY, the emission ratio in the given environment should increase much more significantly during the cleavage of the conjugate than during the suppression of FRET due to other effects.

To prove the ability to monitor the fluorescence of conjugates 1 and 2 in GSH-mediated cleavage and the subsequent liberation of the drug, we performed a series of fluorescence measurements using GSH in HEPES buffer and DMSO/HEPES buffer (2:1), in which conjugate 2 exhibited a significant FRET. GSH concentration used in our experiments was in the range generally found in many cancer cells (i.e., up to 5 mM).<sup>3,4</sup>

As shown in Figure 5, upon subjecting conjugate 1 to 5 mM concentration of GSH, the rapid liberation of aminoBODIPY occurred via disrupting the disulfide bond. Similarly, the self-immolative elimination of thiolactone (Scheme 2) caused the increase in the fluorescence intensity at 530 nm with excitation at 485 nm in HEPES as well as the 2:1 HEPES/DMSO mixture (Figure 5A,C). In contrast, the emission intensity at 530 nm excited at 510 nm, belonging to the conjugate, slightly increases with time in HEPES but decreases in the DMSO/HEPES mixture at a ratio of 2:1 (Figure 5B,D). When the emission intensity ratio of 530 nm (excited at 485 nm) and 510 nm (i.e.,  $I_{485}/I_{510}$ ) is followed with time, it is possible to monitor the conjugate cleavage. In HEPES buffer, conjugate 1 is fully cleaved within approximately 50 min, as indicated by reaching the plateau formation. However, the cleavage in DMSO/HEPES is found to be slightly slower. In addition, the cleavage is accompanied by a significant 6-fold change in the  $I_{485}/I_{510}$  ratio in HEPES buffer or a 2.5-fold change in the DMSO/HEPES (2:1) mixture (Figure 5E).

Apart from aminoBODIPY, conjugate 2 carries the additional dye, redBODIPY—designed for the efficient FRET from

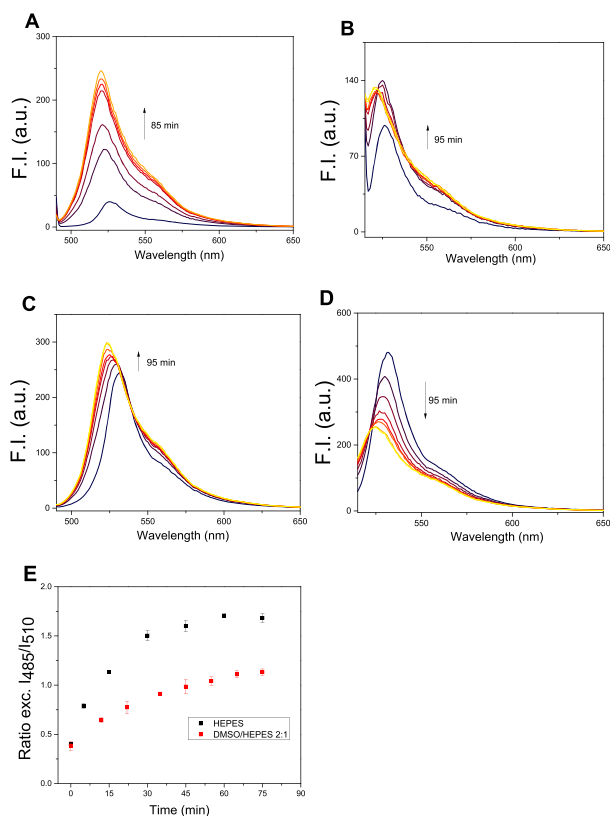


**Figure 5.** Fluorescence spectra of GSH-mediated cleavage (5 mM GSH) of conjugate 1 (5  $\mu$ M) upon excitation at (A) 485 nm or (B) 510 nm in HEPES buffer (0.1 M, pH 7.4). Fluorescence spectra of GSH-mediated cleavage (5 mM GSH) of conjugate 1 (5  $\mu$ M) upon excitation at (C) 485 nm and (D) 510 nm in DMSO/HEPES buffer (0.1 M, 2:1, 37  $^{\circ}$ C). (E) Schematic representation of the ratiometric change of fluorescence intensities at 530 nm after excitation at 485 nm and 510 nm ( $I_{485}/I_{510}$  ratio) with slit widths of 2.5 and 2.5 nm.

the aminoBODIPY dye. As demonstrated in Figure 6, before the GSH-mediated cleavage of conjugate 2 in DMSO/HEPES

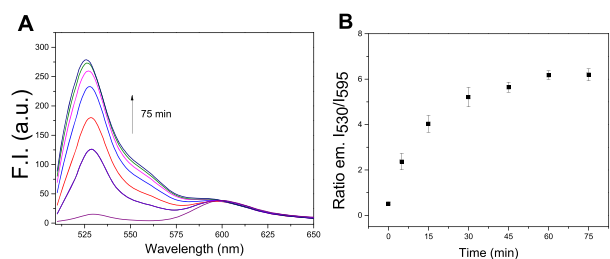


**Figure 6.** (A) Fluorescence spectra of conjugate 2 (1  $\mu$ M) during GSH-mediated cleavage (3 mM GSH) upon excitation at 510 nm and (B) schematic representation of the ratiometric change of  $I_{530}/I_{595}$  emissions ratio (3 mM GSH, DMSO/HEPES buffer 0.1 M, 2:1, 37  $^{\circ}$ C).

(2:1), the system affords the fluorescence of redBODIPY ( $\lambda_{em} = 595$  nm) upon excitation of aminoBODIPY ( $\lambda_{exc} = 510$  nm) due to the effective FRET transfer. During the cleavage, the green emission (530 nm) of the released aminoBODIPY appears and increases with time (Figure 6A). FRET efficiency of conjugate 2 was determined to be 72% in DMSO/HEPES (2:1) buffer.

When the ratio of both emission intensities at 530 and 595 nm upon excitation at 510 nm (i.e.,  $I_{530}/I_{595}$ ) is followed with time, the plateau is achieved in approximately 30 min. In this case, the fluorescence response enhancement is remarkably higher than that in conjugate 1, and it stands for a one-order increase in the emission ratio of  $I_{530}/I_{595}$  (Figure 6B).

Next, we examined the stability of the conjugates 1 and 2 at various pH values and the rate of cleavage by 5 mM GSH at 37  $^{\circ}$ C in the pH range of 5–8. It is known that the disulfide bond is stable in the presence of thiols at lower pH, while the linker readily cleaves at higher pH. The same pH stability is also observed for both conjugates 1 and 2, as shown in Figures 7 and 8, respectively. Both conjugates were found to be stable in the presence of GSH (5 mM) at acidic pH (5–5.5) and readily cleaved at higher pH (7–8).

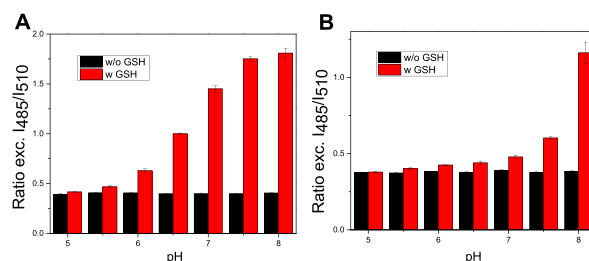


**Figure 7.** (A) Stability of conjugate 1 (1  $\mu$ M) at various pH 5–8 in HEPES buffer (0.1 M, 37  $^{\circ}$ C) and (B) DMSO/HEPES buffer (0.1 M, 2:1, 37  $^{\circ}$ C) without GSH and the cleavage of conjugate 1 (1  $\mu$ M) in the presence of GSH (3 mM) upon incubation for 1 h. All the data points were acquired upon excitation at 485 and 510 nm with emission at 530 nm and were performed in three repetitions.

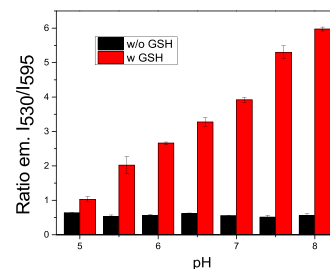


**Figure 8.** Stability of conjugate 2 (1  $\mu$ M) at various pH values (pH 5–8) (DMSO/HEPES buffer 0.1 M, 2:1, 37  $^{\circ}$ C) without GSH and cleavage of conjugate 2 in the presence of GSH (3 mM) upon incubation for 1 h. All the data points were acquired upon excitation at 510 nm with emissions at 530 and 595 nm and were performed in three repetitions.

As expected, the cleavage of both conjugates increases with increasing pH. However, for conjugate 1, the cleavage rate in the range of 5–6.5 pH is significantly slower than that of conjugate 2. When the emission ratio  $I_{530}/I_{595}$  of conjugate 2 in the absence of GSH ( $I_{530}/I_{595} = 0.50$ ) is compared to the value obtained after the incubation of conjugate 2 with GSH at pH 5 for 1 h ( $I_{530}/I_{595} = 1.32$ ) and considering a value of  $I_{530}/I_{595} = 6.7$  as the full cleavage (see Figure 6B), we can estimate that the conjugate is cleaved by 13% even at pH 5. Also, both conjugates proved to be stable in the selected pH range without the presence of reduced GSH. Figure 9 and Table 1 summarize the GSH concentration and rate of the cleavage relationship followed by the abovementioned fluorescence

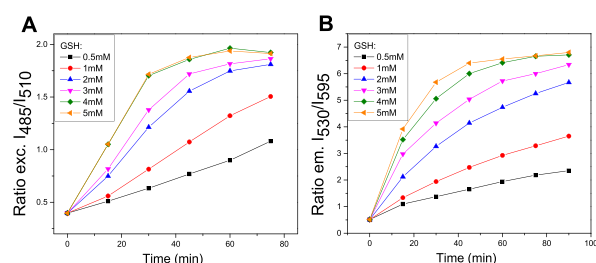


**Figure 9.** Influence of GSH concentration on the rate of cleavage of (A) conjugate 1 (1  $\mu$ M, HEPES buffer, 0.1 M, pH 7.4, 37  $^{\circ}$ C) demonstrated by the ratio of the emission intensities at 530 nm after excitation at 485 and 510 nm ( $I_{485}/I_{510}$ ) and (B) conjugate 2 (1  $\mu$ M, DMSO/HEPES buffer 0.1 M, 2:1, 37  $^{\circ}$ C) demonstrated by the ratio of the fluorescence intensities at 530 and 595 nm ( $I_{530}/I_{595}$ ) after excitation at 510 nm. All the data points were measured in three replicates, with SD ranging up to 5%.

**Table 1. Summary of Half-Lives of Conjugates 1 and 2 under Different Conditions<sup>d</sup>**

conjugate	GSH conc. (mM)	buffer	$t_{1/2}$ (min) <sup>c</sup>
1	5	HEPES <sup>a</sup>	22.3
1	4	HEPES <sup>a</sup>	23.1
1	3	HEPES <sup>a</sup>	38.2
1	2	HEPES <sup>a</sup>	54.6
2	5	DMSO/HEPES <sup>b</sup>	18.4
2	4	DMSO/HEPES <sup>b</sup>	23.6
2	3	DMSO/HEPES <sup>b</sup>	32.7
2	2	DMSO/HEPES <sup>b</sup>	51.5

<sup>a</sup>HEPES, 0.1 M, pH 7.4; <sup>b</sup>DMSO/HEPES 2:1, 0.1 M, pH 7.4. <sup>c</sup> $t_{1/2}$  was determined by the ExpDecay function in OriginLab software. <sup>d</sup>All the measurements were performed in three repetitions.

intensity ratios. The half-life of conjugate 1 was significantly longer than that of conjugate 2 under the same conditions.

**Monitoring of the Conjugate 1 Cleavage Inside the Cell.** Since compound 2 lacks the FRET effect in the buffer medium, we performed fluorescence monitoring of the drug release inside the cells only with compound 1.

Conjugate 1 was subjected to a series of experiments on HeLa cells, with and without pre-incubation by additional glutathione, to prove its cleavability. The pretreatment with the *N*-ethylmaleimide (NEM) was used for the total thiol activity inhibition in the assay.

The obtained fluorescence microscopy images of HeLa cells pretreated with NEM show that our model system 1 emits green light at the beginning of the experiment and after 2 h (Figure 10A) with the same intensity (Figure 10D). This fact corresponds to the assumption that NEM depletes the active thiols in the cells so that conjugate 1 is not cleaved, and no or negligible changes in fluorescence intensity are observed. Additionally, from the microscopy images, an altered distribution of compound 1 inside the NEM-treated cells and slightly higher green emission intensity at the beginning of the experiment was observed (Figure 10A) as compared to non-treated cells (Figure 10A,B). Arguably, this behavior may be explained by the fact that SH groups play crucial roles in regulating the permeability of transition pores. NEM is a membrane-permeant alkylating agent, and its binding to cysteine residues may affect the transition pores in membranes. This hypothesis results from the literature confirmed the fact

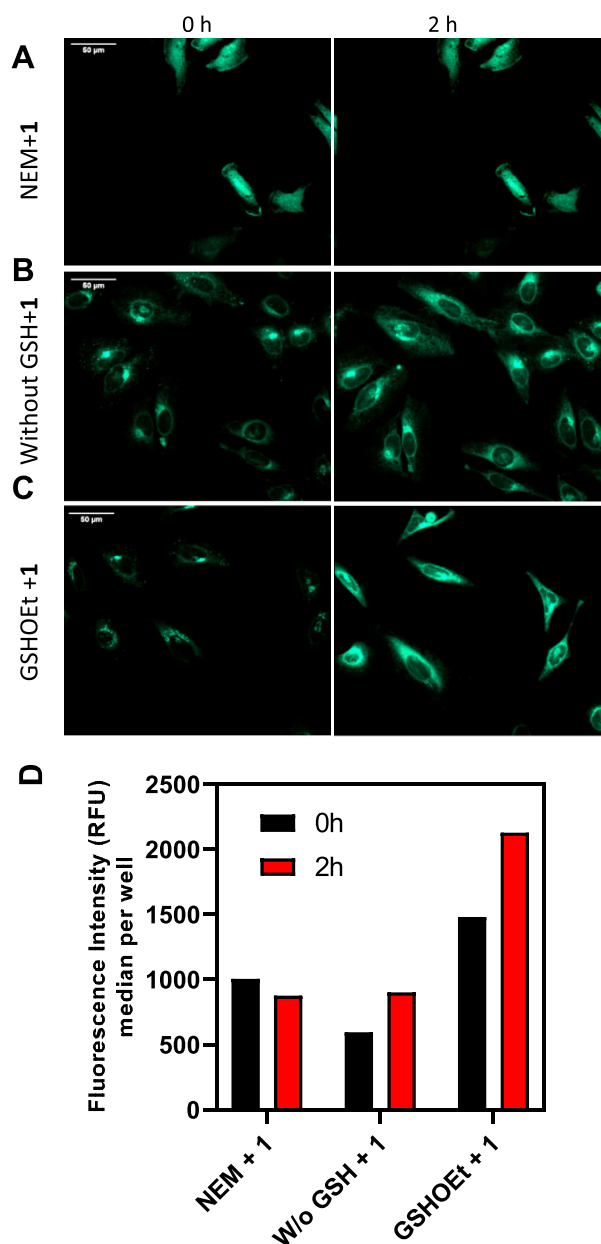


**Figure 10.** (A) Microscopy images of the conjugate 1 internalization inside the HeLa cells after the pretreatment with 1 mM NEM, (B) without any pretreatment, and (C) after pretreatment with 20 mM GSHOEt. (D) Quantification of fluorescence intensity in HeLa cells. Excitation/emission wavelengths of 488/515–530 nm.

that the high concentrations of NEM (0.5–1.0 mM) induce the pore opening in membranes.<sup>48,49</sup>

When the cells without NEM pretreatment are incubated with conjugate 1, the fluorescence is found to be increased in 2 h (Figure 10B,D) as the conjugate is cleaved by native GSH to release the aminoBODIPY together with the drug (see Scheme 2). On the other hand, the emission intensity is significantly enhanced in 2 h when the cells are pretreated with GSHOEt (Figure 10C,D), and a significant amount of aminoBODIPY as well as the drug is released. Thus, the drug release can be easily detected by the OFF–ON effect and confirmed by the experiments with real-time monitoring of cleavage using a cell EnVision plate reader (Figure 11).

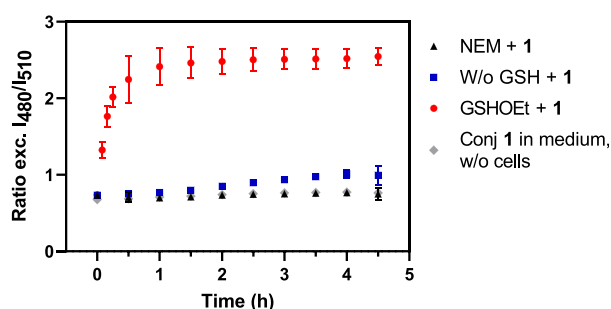


**Figure 11.** Time-dependent conjugate 1 cleavage monitoring inside HeLa cells pretreated with NEM (1 mM, 30 min) and HeLa cells with or without treatment with GSHOEt (20 mM). Excitation/emission wavelengths for conjugate 1 were selected as 485/530 and 510/530 nm.

To prove the enhanced uptake of conjugate 1 by HeLa cells, which possess overexpressed levels of  $\alpha_v\beta_3$  integrins,<sup>50,51</sup> the cRGD binding assay was performed by adopting the described protocol.<sup>52</sup> In the process, the cells were pre-incubated with various cRGD peptide concentrations (0–100  $\mu\text{M}$ ) and then treated with conjugate 1 (10  $\mu\text{M}$ ). As Figure 12 depicts, the

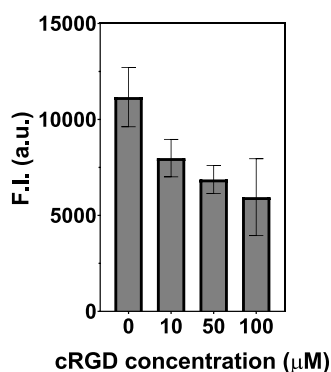


**Figure 12.** Uptake of conjugate 1 (10  $\mu\text{M}$ ) by HeLa cells pre-incubated with the cRGD peptide (0–100  $\mu\text{M}$ ). Fluorescence intensity was measured at  $\lambda_{\text{em}} = 530$  nm upon excitation at  $\lambda_{\text{exc}} = 485$  nm. All measurements were performed in at least five repetitions.

decreased fluorescence response with higher cRGD peptide concentrations suggested that the binding sites at  $\alpha_v\beta_3$  integrins were occupied by free cRGD peptides. This essentially results in reducing the penetration of conjugate 1 into the cells. The pre-incubation with 100  $\mu\text{M}$  cRGD led to an approximately 53% reduction in the cell uptake of conjugate 1 according to the fluorescence intensity at 530 nm.

In this study, the next-generation small-molecule drug conjugates (SMDCs) based on aminoBODIPY ratiometric fluorescence system were prepared utilizing a quinone methide (QM) central frame for the incorporation of three moieties, namely, (i) fluorescent aminoBODIPY for real-time detection of prodrug cleavage; (ii) the c(RGDfK) peptide, which is specific for targeting  $\alpha_v\beta_3$  integrin receptors or the redBODIPY dye with a bathochromic shift of absorption for real-time FRET monitoring of drug release; and (iii) pegylated-2-phenyl-3-hydroxy-4(1*H*)-quinolinone (3HQ) as a model drug. Both the targeting SMDC 1 and di-BODIPY FRET conjugate 2 were proven to be functional as cleavable conjugates in the presence of high concentrations of GSH (0.5–5 mM). The monitoring of the conjugates' cleavage was possible via the

fluorescence response with the advantage of ratiometric mode. System 2 showed an enhanced FRET effect in a mixture of HEPES buffer and DMSO, but this effect was significantly suppressed in an aqueous buffer alone.

Conjugate 1 was proven to be an effective drug delivery system with enhanced selectivity toward the cells having  $\alpha_v\beta_3$  integrins, serving as the cRGD binding sites. Drug release became possible to be monitored inside the cell via ratiometric fluorescence.

In summary, we have prepared and tested the first thiol-cleavable system based on QM elimination. The synthetic protocol enabled the modification of the system by different drugs and target moieties while keeping the fluorescence properties for drug release monitored. Increased selectivity toward cancer cells was assured by a thiol cleavable linker (both types of conjugates) or by combination with a cRGD targeting unit (conjugate 1). As system 1, which is based on the QM motif, can reflect the drug release inside the cells, it can potentially serve as a motif for the development of real-time theranostics system in anticancer therapy.

## ■ ASSOCIATED CONTENT

### SI Supporting Information

The Supporting Information is available free of charge at <https://pubs.acs.org/doi/10.1021/acs.molpharmaceut.1c00219>.

NMR spectra of newly synthesized compounds; synthesis of the compounds 13 and 14 (PDF)

## ■ AUTHOR INFORMATION

### Corresponding Author

Jan Hlaváč – Department of Organic Chemistry, Faculty of Science, Palacký University, 771 46 Olomouc, Czech Republic; [orcid.org/0000-0002-4652-7751](https://orcid.org/0000-0002-4652-7751); Email: [jan.hlavac@upol.cz](mailto:jan.hlavac@upol.cz)

### Authors

Martin Porubský – Department of Organic Chemistry, Faculty of Science, Palacký University, 771 46 Olomouc, Czech Republic

Soňa Gurská – Institute of Molecular and Translational Medicine, Faculty of Medicine and Dentistry, Palacký University, 779 00 Olomouc, Czech Republic

Jarmila Stanková – Institute of Molecular and Translational Medicine, Faculty of Medicine and Dentistry, Palacký University, 779 00 Olomouc, Czech Republic

Marián Hajdúch – Institute of Molecular and Translational Medicine, Faculty of Medicine and Dentistry, Palacký University, 779 00 Olomouc, Czech Republic

Petr Džubák – Institute of Molecular and Translational Medicine, Faculty of Medicine and Dentistry, Palacký University, 779 00 Olomouc, Czech Republic

Complete contact information is available at:

<https://pubs.acs.org/doi/10.1021/acs.molpharmaceut.1c00219>

### Author Contributions

The manuscript was written through the contributions of all authors.

### Notes

The authors declare no competing financial interest.

## ACKNOWLEDGMENTS

This work was supported by the Czech Science Foundation (GACR project 19-23972S), Czech Ministry of Education, Youth, and Sports (projects IGA\_PrF\_2020\_012, IGA\_LF\_2021-038) and by grants from the Czech Ministry of Education, Youth and Sports (LM2018133, LM2018130) and by the European Regional Development Fund - Project ENOCH (No. CZ.02.1.01/0.0/0.0/16\_019/0000868).

## REFERENCES

- (1) Pompella, A.; Visvikis, A.; Paolicchi, A.; De Tata, V.; Casini, A. F. The changing faces of glutathione, a cellular protagonist. *Biochem. Pharmacol.* **2003**, *66*, 1499–1503.
- (2) Balendiran, G. K.; Dabur, R.; Fraser, D. The role of glutathione in cancer. *Cell Biochem. Funct.* **2004**, *22*, 343–352.
- (3) Britten, R. A.; Green, J. A.; Warenius, H. M. Cellular glutathione (GSH) and glutathione S-transferase (GST) activity in human ovarian tumor biopsies following exposure to alkylating agents. *Int. J. Radiat. Oncol.* **1992**, *24*, 527–531.
- (4) Gamcsik, M. P.; Kasibhatla, M. S.; Teeter, S. D.; Colvin, O. M. Glutathione levels in human tumors. *Biomarkers* **2012**, *17*, 671–691.
- (5) Cheetham, A. G.; Zhang, P.; Lin, Y.; Lin Lock, L.; Cui, H. Supramolecular Nanostructures Formed by Anticancer Drug Assembly. *J. Am. Chem. Soc.* **2013**, *135*, 2907–2910.
- (6) Qin, S. Y.; Zhang, A. Q.; Cheng, S. X.; Rong, L.; Zhang, X. Z. Drug self-delivery systems for cancer therapy. *Biomaterials* **2017**, *112*, 234–247.
- (7) Kurtoglu, Y. E.; Navath, R. S.; Wang, B.; Kannan, S.; Romero, R.; Kannan, R. M. Biomaterials Poly (amidoamine) dendrimer – drug conjugates with disulfide linkages for intracellular drug delivery. *Biomaterials* **2009**, *30*, 2112–2121.
- (8) Dragojevic, S.; Ryu, J.; Raucher, D. Polymer-based prodrugs: Improving tumor targeting and the solubility of small molecule drugs in cancer therapy. *Molecules* **2015**, *20*, 21750–21769.
- (9) Zhang, J.; Yuan, Z. F.; Wang, Y.; Chen, W. H.; Luo, G. F.; Cheng, S. X.; Zhuo, R. X.; Zhang, X. Z. Multifunctional Envelope-Type Mesoporous Silica Nanoparticles for Tumor-Triggered Targeting Drug Delivery. *JACS* **2012**, *6*.
- (10) Mura, S.; Nicolas, J.; Couvreur, P. Stimuli-responsive nanocarriers for drug delivery. *Nat. Mater.* **2013**, *12*, 991–1003.
- (11) Shin, W. S.; Han, J.; Verwilst, P.; Kumar, R.; Kim, J. H.; Kim, J. S. Cancer Targeted Enzymatic Theranostic Prodrug: Precise Diagnosis and Chemotherapy. *Bioconjugate Chem.* **2016**, *27*, 1419–1426.
- (12) Chen, S.; Zhao, X.; Chen, J.; Chen, J.; Kuznetsova, L.; Wong, S. S.; Ojima, I. Mechanism-Based Tumor-Targeting Drug Delivery System. Validation of Efficient Vitamin Receptor-Mediated Endocytosis and Drug Release. *Bioconjugate Chem.* **2010**, *21*, 979–987.
- (13) Dcona, M. M.; Sheldon, J. E.; Mitra, D.; Hartman, M. C. T. Light induced drug release from a folic acid-drug conjugate. *Bioorg. Med. Chem. Lett.* **2016**, *27*, 466–469.
- (14) Cho, H. J.; Lee, S. J.; Park, S. J.; Paik, C. H.; Lee, S. M.; Kim, S.; Lee, Y. S. Activatable iRGD-based peptide monolith: Targeting, internalization, and fluorescence activation for precise tumor imaging. *J. Controlled Release* **2016**, *237*, 177–184.
- (15) Ranyuk, E.; Cauchon, N.; Klarskov, K.; Guérin, B.; Van Lier, J. E. Phthalocyanine-peptide conjugates: Receptor-targeting bifunctional agents for imaging and photodynamic therapy. *J. Med. Chem.* **2013**, *56*, 1520–1534.
- (16) Pillow, T. H.; Sadowsky, J. D.; Zhang, D.; Yu, S.-F.; Del Rosario, G.; Xu, K.; He, J.; Bhakta, S.; Ohri, R.; Kozak, K. R.; et al. Decoupling stability and release in disulfide bonds with antibody-small molecule conjugates. *Chem. Sci.* **2017**, *8*, 366–370.
- (17) Liu, Z.; Wang, F.; Chen, X. Integrin alphaV-beta3-targeted cancer therapy. *Drug Dev. Res.* **2008**, *69*, 329–339.
- (18) Sancey, L.; Garanger, E.; Foillard, S.; Schoehn, G.; Hurbin, A.; Albiges-Rizo, C.; Boturyn, D.; Souchier, C.; Grichine, A.; Dumy, P.; Coll, J.-L. Clustering and Internalization of Integrin  $\alpha v \beta 3$  With a Tetrameric RGD-synthetic Peptide. *Mol. Ther.* **2009**, *17*, 837–843.
- (19) Danhier, F.; Le Breton, A.; Preat, V. RGD-Based Strategies To Target Alpha (  $\alpha$  ) Beta (  $\beta$  ) Integrin in Cancer Therapy and Diagnosis. *Mol. Pharmaceutics* **2012**, *9*, 2961–2973.
- (20) Nieberler, M.; Reuning, U.; Reichart, F.; Notni, J.; Wester, H. J.; Schwaiger, M.; Weinmüller, M.; Räder, A.; Steiger, K.; Kessler, H. Exploring the role of RGD-recognizing integrins in cancer. *Cancers (Basel)*. **2017**, *9*, 116.
- (21) Chen, X.; Sievers, E.; Hou, Y.; Park, R.; Tohme, M.; Bart, R.; Bremner, R.; Bading, J. R.; Conti, P. S. Integrin  $\alpha\beta 3$  – Targeted Imaging of Lung Cancer. *Neoplasia* **2005**, *7*, 271–279.
- (22) SefTOR, R. E.; SefTort, E. A.; Gehlsen, K. R.; Stetler-Stevenson, W. G.; Brown, P. D.; Ruoslahti, E.; Hendrix, M. J. Role of the  $\alpha v \beta 3$  integrin in human melanoma cell invasion. *Proc. Natl. Acad. Sci.* **1992**, *89*, 1557–1561.
- (23) Gladson, C. L.; Cheresch, D. A. Glioblastoma expression of vitronectin and the  $\alpha v \beta 3$  integrin: Adhesion mechanism for transformed glial cells. *J. Clin. Invest.* **1991**, *88*, 1924–1932.
- (24) Rolli, M.; Fransvea, E.; Pilch, J.; Saven, A.; Felding-habermann, B. Activated integrin  $\alpha v \beta 3$  cooperates with metalloproteinase MMP-9 in regulating migration of metastatic breast cancer cells. *PNAS* **2003**, *100*, 9482–9487.
- (25) Arap, W.; Pasqualini, R.; Ruoslahti, E. Cancer Treatment by Targeted Drug Delivery to Tumor Vasculature in a Mouse Model. *Science (80- )* **1997**, *279*, 377–380.
- (26) Dal Pozzo, A.; Ni, M. H.; Esposito, E.; Dallavalle, S.; Musso, L.; Bargiotti, A.; Pisano, C.; Vesci, L.; Bucci, F.; Castorina, M.; Fodera, R.; Giannini, G.; Aulicino, C.; Penco, S. Novel tumor-targeted RGD peptide-camptothecin conjugates: Synthesis and biological evaluation. *Bioorganic Med. Chem.* **2010**, *18*, 64–72.
- (27) Chen, X.; Plasencia, C.; Hou, Y.; Neamati, N. Synthesis and Biological Evaluation of Dimeric RGD Peptide - Paclitaxel Conjugate as a Model for Integrin-Targeted Drug Delivery. *J. Med. Chem.* **2005**, *48*, 1098–1106.
- (28) Rivas, P. L.; Randelović, I.; Moreira, R.; Pina, A.; Arosio, D.; Tóvári, J.; Mező, G.; Corso, D.; Pignataro, L.; Gennari, C. Synthesis and Biological Evaluation of Paclitaxel Conjugates Involving Linkers Cleavable by Lysosomal Enzymes and  $\alpha V 3$  - Integrin Ligands for Tumor Targeting. *Eur. J. Org. Chem.* **2018**, 2902–2909.
- (29) Goodman, S. L.; Hölzemann, G.; Sulyok, G. A. G.; Kessler, H. Nanomolar Small Molecule Inhibitors for  $\alpha v \beta 6$ ,  $\alpha v \beta 5$ , and  $\alpha v \beta 3$  Integrins. *J. Med. Chem.* **2002**, *45*, 1045–1051.
- (30) Ma, Y.; Huang, J.; Song, S.; Chen, H.; Zhang, Z. Cancer-Targeted Nano-theranostics: Recent Advances and Perspectives. *Small* **2016**, *1*–4954.
- (31) Fernandez, A.; Vendrell, M. Fluorophore–Drug Conjugates To Unravel the Mechanisms of Action of Therapeutic Assets. *Biochemistry* **2017**, *57*, 175–176.
- (32) Zhuang, C.; Guan, X.; Ma, H.; Cong, H.; Zhang, W.; Miao, Z. Small molecule-drug conjugates: A novel strategy for cancer-targeted treatment. *Eur. J. Med. Chem.* **2019**, *163*, 883–895.
- (33) Casi, G.; Neri, D. Antibody–Drug Conjugates and Small Molecule–Drug Conjugates: Opportunities and Challenges for the Development of Selective Anticancer Cytotoxic Agents. *J. Med. Chem.* **2015**, *58*, 8751–8761.
- (34) Santra, S.; Kaittani, C.; Santiesteban, O. J.; Perez, J. M. Cell-specific, activatable, and theranostic prodrug for dual-targeted cancer imaging and therapy. *J. Am. Chem. Soc.* **2011**, *133*, 16680–16688.
- (35) Hu, Y.; Zeng, F. A theranostic prodrug based on FRET for real-time drug release monitoring in response to biothiols. *Mater. Sci. Eng. C* **2017**, *72*, 77–85.
- (36) Liu, Y.; Pei, Q.; Chen, L.; Li, Z.; Xie, Z. Reduction-responsive fluorescence off – on BODIPY – camptothecin conjugates for. *J. Mater. Chem. B* **2016**, *4*, 2332–2337.
- (37) Porubský, M.; Gurská, S.; Stanková, J.; Hajdúch, M.; Džubák, P.; Hlaváč, J. Amino-BODIPY as the ratiometric fluorescent sensor for monitoring drug release or “power supply” selector for molecular electronics. *RSC Adv.* **2019**, *9*, 25075–25083.



(38) Loudet, A.; Burgess, K. BODIPY dyes and their derivatives: Syntheses and spectroscopic properties. *Chem. Rev.* **2007**, *107*, 4891–4932.

(39) Satyam, A. Design and synthesis of releasable folate-drug conjugates using a novel heterobifunctional disulfide-containing linker. *Bioorganic Med. Chem. Lett.* **2008**, *18*, 3196–3199.

(40) Gnaim, S.; Shabat, D. Quinone-Methide Species, A Gateway to Functional Molecular Systems: From Self-Immolative Dendrimers to Long-Wavelength Fluorescent Dyes. *Acc. Chem. Res.* **2014**, *47*, 2970–2984.

(41) Polaske, N. W.; Kelly, B. D.; Ashworth-Sharpe, J.; Bieniarz, C. Quinone Methide Signal Amplification: Covalent Reporter Labeling of Cancer Epitopes using Alkaline Phosphatase Substrates. *Bioconjugate Chem.* **2016**, *27*, 660–666.

(42) Funk, P.; Motyka, K.; Džubák, P.; Znojek, P.; Gurská, S.; Kusz, J.; McMaster, C.; Hajdúch, M.; Soral, M. Preparation of 2-phenyl-3-hydroxyquinoline-4(1H)-one-5-carboxamides as potential anticancer and fluorescence agents. *RSC Adv.* **2015**, *5*, 48861–48867.

(43) Motyka, K.; Hlaváč, J.; Soral, M.; Funk, P. Fluorescence properties of 2-aryl-3-hydroxyquinolin-4(1H)-one-carboxamides. *Tetrahedron Lett.* **2010**, *51*, 5060–5063.

(44) di Cagno, M.; Stýskala, J.; Hlaváč, J.; Brandl, M.; Bauer-Brandl, A.; Skalko-Basnet, N. Liposomal solubilization of new 3-hydroxyquinolinone derivatives with promising anticancer activity: a screening method to identify maximum incorporation capacity. *J. Liposome Res.* **2011**, *21*, 272–278.

(45) di Cagno, M.; Stein, P. C.; Stýskala, J.; Hlaváč, J.; Skalko-Basnet, N.; Bauer-Brandl, A. Overcoming instability and low solubility of new cytostatic compounds: A comparison of two approaches. *Eur. J. Pharm. Biopharm.* **2012**, *80*, 657–662.

(46) Jo, S. D.; Ku, S. H.; Won, Y. Y.; Kim, S. H.; Kwon, I. C. Targeted Nanotheranostics for Future Personalized Medicine: Recent Progress in Cancer Therapy. *Theranostics* **2016**, *6*, 1362–1377.

(47) Poolman, J. M.; Maity, C.; Boekhoven, J.; Van Der Mee, L.; Le Sage, V. A. A.; Groenewold, G. J. M.; Van Kasteren, S. I.; Versluis, F.; Van Esch, J. H.; Eelkema, R. A toolbox for controlling the properties and functionalisation of hydrazone-based supramolecular hydrogels. *J. Mater. Chem. B* **2016**, *4*, 852–858.

(48) Costantini, P.; Colonna, R.; Bernardi, P. Induction of the mitochondrial permeability transition by N-ethylmaleimide depends on secondary oxidation of critical thiol groups. Potentiation by copper-ortho-phenanthroline without dimerization of the adenine nucleotide translocase. *Biochim. Biophys. Acta, Bioenerg.* **1998**, *1365*, 385–392.

(49) Garcia, N.; Pavón, N.; Chávez, E. The effect of N-ethylmaleimide on permeability transition as induced by carboxyatractyloside, agaric acid, and oleate. *Cell Biochem. Biophys.* **2008**, *51*, 81–87.

(50) Liu, Y.; Zhao, F.; Gu, W.; Yang, H.; Meng, Q.; Zhang, Y.; Yang, H.; Duan, Q. The roles of platelet GPIIb/IIIa and  $\alpha v\beta 3$  integrins during HeLa cells adhesion, migration, and invasion to monolayer endothelium under static and dynamic shear flow. *J. Biomed. Biotechnol.* **2009**, *2009*, 1.

(51) Orgovan, N.; Peter, B.; Bosze, S.; Ramsden, J. J.; Szabó, B.; Horvath, R. Dependence of cancer cell adhesion kinetics on integrin ligand surface density measured by a high-throughput label-free resonant waveguide grating biosensor. *Sci. Rep.* **2014**, *4*, 1–8.

(52) Jang, J. H.; Kim, W. R.; Sharma, A.; Cho, S. H.; James, T. D.; Kang, C.; Kim, J. S. Targeted tumor detection: guidelines for developing biotinylated diagnostics. *Chem. Commun.* **2017**, *53*, 2154–2157.



---

Palacký University  
Olomouc



---

Faculty  
of Science



---

Department of Organic  
Chemistry

PALACKÝ UNIVERSITY

Olomouc

Faculty of Science

Department of Organic Chemistry

**Development of new fluorescent conjugates  
for intracellular imaging, drug delivery and  
diagnostics**

Summary of the Ph.D. Thesis

Mgr. Martin Porubský

Supervisor: prof. RNDr. Jan Hlaváč, Ph.D.

Academic Year: 2021/2022

This Ph.D. thesis was elaborated within the framework of the Ph.D. study program P1417 Chemistry, field of study Organic Chemistry, guaranteed by the Department of Organic Chemistry, Faculty of Science, Palacký University, Olomouc in the years 2015 – 2021.

**Author:** Mgr. Martin Porubský  
Faculty of Science, Palacký University  
Department of Organic Chemistry  
Olomouc

**Supervisor:** prof. RNDr. Jan Hlaváč, Ph.D.  
Faculty of Science, Palacký University  
Department of Organic Chemistry  
Olomouc

**Referees:**

The oral defense will take place on ..... in front of the committee for defense of the doctoral thesis at the Department of Organic Chemistry, Faculty of Science, Palacký University, Olomouc. At the same place is the thesis available since 13.12.2021.

I declare hereby with my signature, that this abovementioned thesis is my own original work. Furthermore, I confirm that I have clearly referenced in accordance with departmental requirements.

13.12.2021, Olomouc

.....  
Mgr. Martin Porubský

## Abstract

Ratiometric fluorescent intracellular imaging and drug delivery represent interesting strategy in current medicinal chemistry and study of various therapeutics for its personalized approach and deeper study of drug penetration and localization in cells taking advantage mainly of being non-destructive technique. Controlled and targeted delivery and real-time monitoring of drug release is of great importance due to reducing or lessening of adverse side effects in process of medication.

In the first part of this thesis, the design, synthesis and spectral properties of fluorescent conjugates of BODIPY and 3-hydroxyquinolinones (3HQs) are discussed. First generation involves BODIPY-3HQ conjugates connected with disulfide linker allowing a cleavage by increased level of glutathione. Second generation of conjugates were equipped either with two fluorescent dyes to allowing the FRET ratiometric detection or with one fluorescent tag and targeting unit to provide selective localization in the cancer cells. Both generations of conjugates were studied with respect to biological activity and fluorescent properties.

The second part is dedicated to description of design, synthesis and optimization of novel fluorescent three-fluorophore dual-FRET peptide probe for detection and quantification of proteolytic enzymes – caspase-8 and caspase-9. The probe was designed as a ratiometric single-excitation triple-emission system which function is driven by a change of fluorescence intensities during the enzymatic cleavage of specific linkers. Several probes were prepared by solid-phase chemistry approach and mathematical model for unambiguous caspases detection and determination of their relative activities was developed. The functionality of proposed system was tested in biological media, specifically on cell lysates with selectively activated caspase-8 and caspase-9.

## Abstrakt

Poměrové fluorescenční zobrazování uvnitř buněk a systémy pro doručování léků představují v současné medicíně zajímavou strategii zejména pro její osobní přístup a detailnější studium penetrace a lokalizace léků v buňkách s využitím nedestruktivních technik. Řízené a cílené doručování léků a monitorování jejich uvolňování v reálném čase má velký význam kvůli snížení nebo zmírnění nežádoucích vedlejších účinků v procesu léčby.

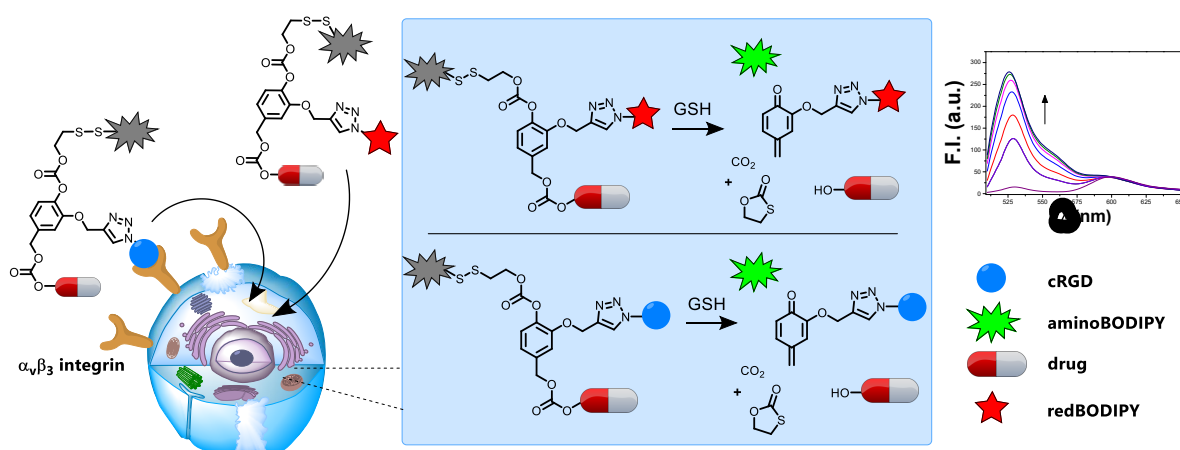
V první části této disertační práce je diskutován design, syntéza a spektrální vlastnosti fluorescenčních konjugátů BODIPY a 3-hydroxychinolonů. První generace těchto látek zahrnuje konjugáty BODIPY-3HQ spojené disulfidovým linkerem, aby se umožnilo štěpení díky zvýšené koncentraci glutathionu. Druhá generace konjugátů byla vybavena buď dvěma fluorescenčními barvivy umožňujícími FRET poměrovou detekci nebo jednou fluorescenční značkou a cílicí jednotkou tak, aby byla umožněna selektivní lokalizace v rakovinných buňkách. Aktivita obou generací konjugátů byla studována na buněčných liniích za použití fluorescenční mikroskopie.

Druhá část disertační práce je věnována popisu designu, syntézy a optimalizace nové tří-fluoroforové duální-FRET sondy pro detekci a kvantifikaci proteolytických enzymů – kaspázy-8 a kaspázy-9. Sonda byla navržena jako poměrová s jednou excitací a trojitou emisí, které se mění během enzymatického štěpení specifických linkerů. Testované sondy byly připraveny syntézou na pevné fázi a byl vyvinut matematický model pro jednoznačnou detekci obou kaspáz samostatně nebo ve směsi a pro stanovení jejich relativní aktivity. Funkčnost navrhovaného systému byla testována v biologickém médiu, konkrétně na buněčných lyzátech se selektivně aktivovanými kaspázami -8 a -9.

## Thesis objectives

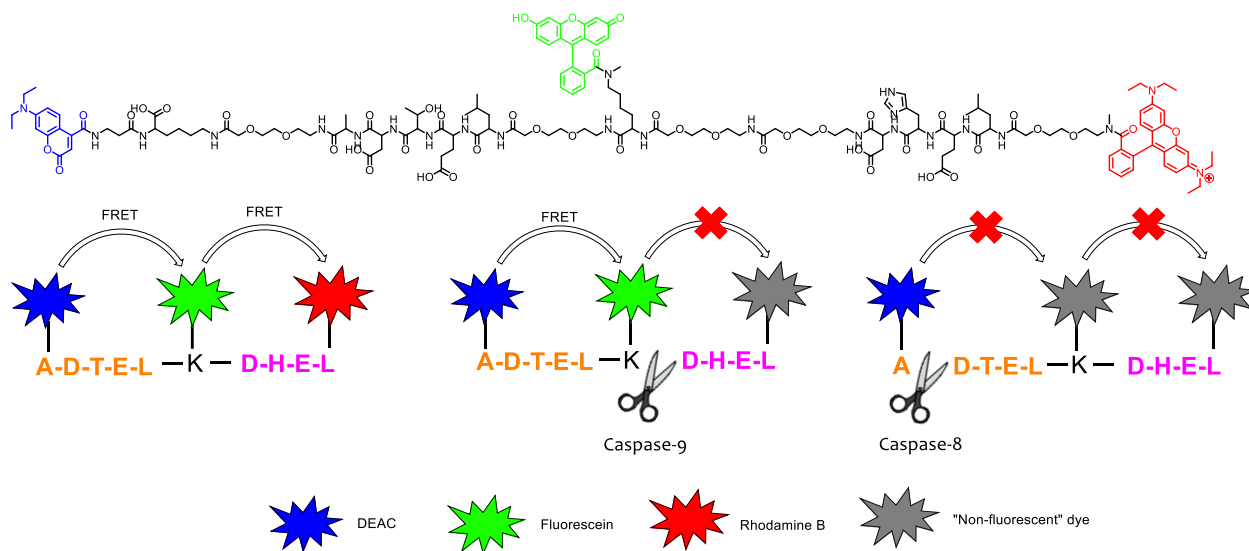
This work is divided into three separate parts which discuss design, synthesis, optimization and biological activity of conjugates that may be generally assigned as theranostics or diagnostic tools. The common denominator of all projects is the use of fluorescent labels for intracellular imaging or diagnostic purposes. The chemistry of fluorescent labels was not thoroughly established previously in the group of Jan Hlaváč and this work may provide new insight in development of intracellular ratiometric imaging agents and theranostics. Currently, a lot of effort in medicinal chemistry is put into development of more selective and personalized chemotherapeutic agents together with reduction of undesired effects. Moreover, ratiometric or “OFF-ON” fluorescent probes are attractive for their ability to selectively visualize tumor sites what may be utilized in imaging-guided surgery.

The first project was devoted to various ways of conjugation of model drug 3-hydroxyquinolinone with fluorescent tag and to monitor the fate of these conjugates in biological medium. 3HQs were synthesized and derivatized previously in our group as novel anticancer agents. Some derivatives were therefore used as model drugs for conjugates development. The aim was to prepare various conjugates bearing fluorescent dye - BODIPY that would easily penetrate and would be cleaved readily in the presence of microenvironment stimuli inside the cancer cells releasing the free drug. Our goal was also to study the optical properties and compare biological activity of cleavable and non-cleavable conjugates. Further, our intention was also to incorporate targeting unit specific for cancer cells such as biotin or cRGD peptide to the previously prepared conjugates and monitor its cleavability as well as biological activity.



The second project deals with design and synthesis of dual-FRET probes for detection of caspases -8 and -9, proteolytic enzymes that take a part in programmed cell death – apoptosis. Chosen caspases represent two main initiator caspases which are activated in the cells by different pathways and facile distinguishing between them would provide valuable information about mechanism of action of drugs. Synthesis of dual-FRET probes by solid phase chemistry approach would lead to optimization of structure for optimal caspase cleavage selectivity and FRET efficiency. Further, the functionality of probes was aimed to be tested with active recombinant enzymes and cell lysates with selectively activated caspases. The big challenge

remained to develop mathematical model that would be able to provide detection and relative quantification of enzymes as well.





# 1 Fluorescent conjugates for delivery of 2-phenyl-3-hydroxy-4(1H)-quinolinones to the cancer cells and their release monitoring

## 1.1 Introduction

In the last decades a lot of effort is oriented towards development of drugs and drug delivery systems with higher selectivity to the desired target such as certain cancer cell type, tissue or enzyme. Growing understanding of cancer biology encourages the drug developers to identify new targeting tools based on predictive biomarkers with the aim of achieving selective personalized cancer treatment.<sup>1</sup> Selective targeting by cell targeting moieties, e.g. vitamins, antibodies, peptides or aptamers may in turn provide lower toxicity against normal healthy tissues and thus reducing the side effects associated with conventional therapies.

It is suggesting that the use of targeting techniques represents logical, smart and more effective way to deliver the therapeutic agents selectively to the place of action (Figure 1). In addition, targeted delivery of therapeutic agents may overcome some difficulties generally connected with conventional anticancer drugs including rapid clearance from body, low bioavailability and most of all lack of selectivity.<sup>2</sup> The most prominent and recently thoroughly studied strategies for cancer targeting involve (i) passive targeting by enhanced permeability and retention (EPR) effect mainly applicable for nanoparticles (NPs)<sup>3</sup>, (ii) active targeting by incorporation of targeting moiety to cargoes such as peptides, antibodies, vitamins or small-molecule ligands<sup>4</sup>, (iii) introduction of the cell penetrating peptides (CPPs)<sup>5</sup> or (iv) conjugation of drugs with delivery vehicles via cleavable linkers responsive to tumor microenvironment (glutathione, pH, hypoxia, enzymes, ROS or temperature).<sup>6</sup>

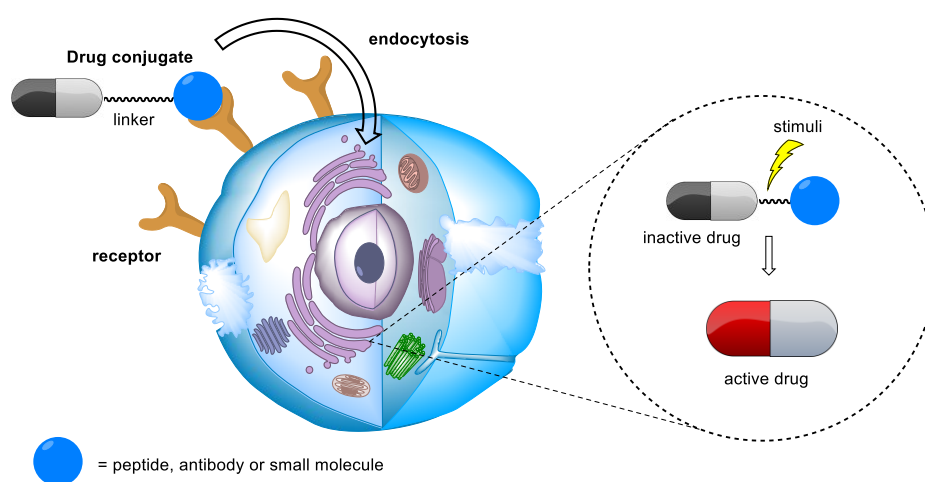
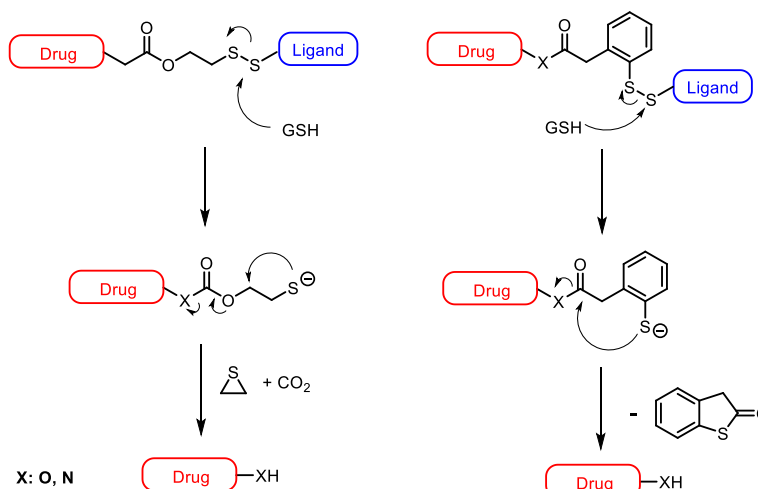


**Figure 1** Active targeting.

Reductively cleavable linkers such as disulfide or diselenide linkers offer an attractive concept for targeting cancer cells via glutathione mediated cleavage.<sup>7</sup> Glutathione (GSH) is responsible for damage prevention of cells due to the presence of reactive oxygen species such as free radicals, peroxides etc. and is found in 100-1000 times higher concentration in intracellular compartments than in plasma and blood. Moreover, in some tumor cells GSH is overexpressed and found in concentrations 2-10 mM allowing a cancer targeted delivery with good stability of the conjugates in bloodstream.<sup>8</sup> Disulfide linkers were broadly explored in

conjugation to numerous drugs, nanoparticles or mAbs.<sup>9,10</sup> Drugs containing disulfide linkers such as Vintafolide or Epopolate reached clinical studies. Several antibody containing conjugates were approved by FDA.<sup>9</sup> The cleavage of disulfide linker by GSH is depicted in the Scheme 1.



**Scheme 1** Cleavage of disulfide linker by GSH.

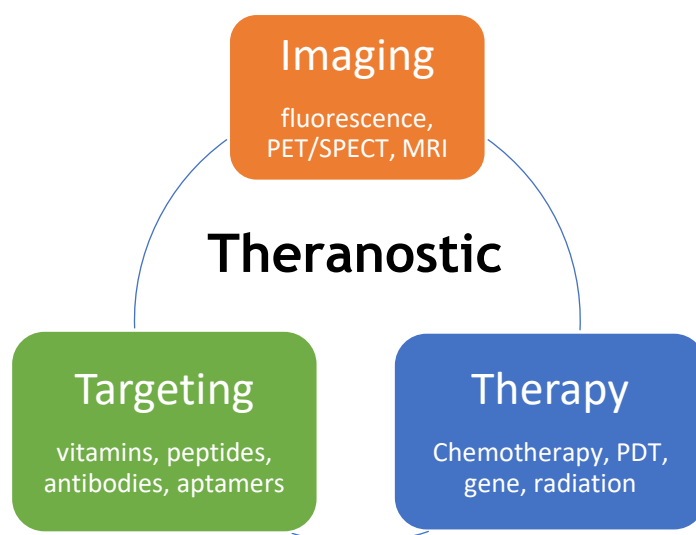


**Figure 2** Theranostic – combination of imaging, therapy and targeting.

An attractive strategy for achieving the desired cell specificity is to link an established therapeutic agent to a targeting ligand, which can deliver the attached cargo selectively to the cancer cell, and imaging agent (fluorophores, PET or MRI agents) for visualization of disease status. This theranostic strategy is a “smart” combination of diagnosis (imaging) and therapy (drug), which provides feedback information after cancer therapy and therefore it can lead directly to enhancement in treatment efficacy and fluorescence-guided surgery (Figure 2).<sup>11,12</sup>

One of the frequently used targeting motifs are RGD (Arg-Gly-Asp) peptides which selectively interact with integrin receptors on the cell surface (Figure 3). Integrins are a family of cell adhesion receptors that are involved in tumor-induced angiogenesis, vascularization and metastasis.<sup>13</sup> Integrin  $\alpha_v\beta_3$  is highly expressed on activated endothelial cells and new-born vessels, but it is absent in resting endothelial cells and most normal organ tissues.<sup>14</sup> Since

integrin  $\alpha_v\beta_3$  is also frequently overexpressed in tumor cells, as observed in colon,<sup>15</sup> pancreas,<sup>16</sup> lung<sup>17</sup> cancers, melanomas,<sup>18</sup> brain<sup>19</sup> or breast<sup>20</sup> tumors makes this receptor suitable target for the anti-angiogenic cancer therapy.<sup>21</sup> Attachment of cyclic RGD peptide to conventional drugs such as doxorubicin,<sup>22</sup> camptothecin,<sup>23</sup> and paclitaxel<sup>24</sup> was shown to have improved therapeutic activities *in vitro* as well as *in vivo* as compared to the corresponding free drugs.

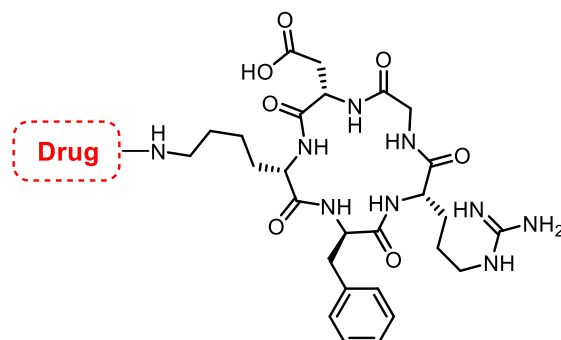


**Figure 3** cRGD peptide – drug conjugate.

Real-time imaging of the fate of the drug inside the tissue is essential for personalized medicine and assessment of efficacy of treatment. Fluorescence imaging is one of the most exploited techniques for visualization of proteins, molecular processes or structures *in vitro* and *in vivo* with the use of plentiful of suitable fluorophores (Figure 4). Among the most frequently used fluorophores belong boron difluoride complexes of dipyrromethenes, 4,4-difluoro-4-bora-3a,4a-diaza-s-indacene or abbreviated BODIPYs are among the most popular dyes recently and thanks to their outstanding properties they have become extremely valuable fluorophores. BODIPYs are hydrophobic dyes with neutral overall charge despite bearing formal charges on boron and nitrogen. They usually tend to strongly absorb in the visible range having high absorption coefficient ( $\epsilon$ ) and emit sharp fluorescence bands with high quantum yield ( $\Phi$ ). Common feature of BODIPY dyes is also relatively small Stoke's shift, insensitivity to polarity and pH of the solvent and stability in under physiological conditions. Arguably, the major advantage of BODIPY dyes is their extremely high spectral tunability and diversification. BODIPYs are used for imaging of the target proteins, membranes, organelles,<sup>25</sup> antibodies, enzymes,<sup>26</sup> as chemosensors for detection of metals, gases,<sup>27</sup> ROSs,<sup>28</sup> thiols,<sup>29</sup> as pH<sup>30</sup> and hypoxia indicators<sup>31</sup> or as agents in fluorescence guided drug delivery and precision therapy.<sup>32</sup>

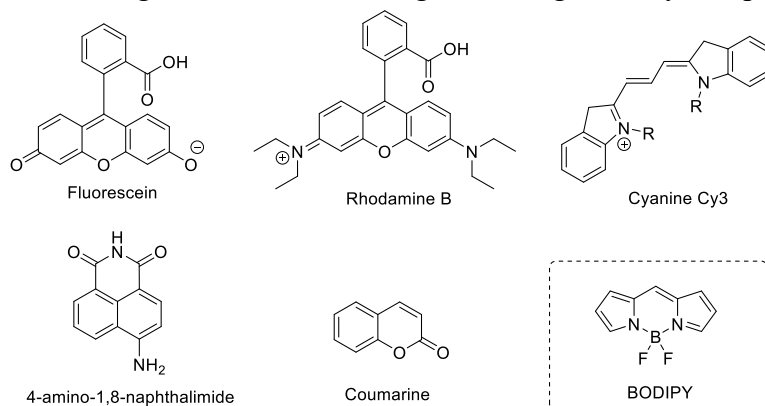


**Figure 4** Commonly used fluorescent dyes.

The motivation of the main project of this work was to prepare fluorescent conjugates with 3-hydroxy-2-phenyl-(4*H*)quinolinones (3HQs) with a possibility to monitor their penetration into the cells as well as to study the liberation to the free 3HQ drug. The choice of 3HQ derivatives as conjugated drugs was based on thorough experience with their synthesis and properties in our group together with their potential to become a hit molecule in the cancer or antimicrobial research in the future. However, 3HQs possess some undesirable properties - their insolubility in aqueous media and high polarity causes significant disadvantages for advanced biological testing. Moreover, 3HQs are generally highly toxic not only to cancer cells but also show unfavorable toxicity to normal healthy cells.<sup>33,34</sup> Despite their native fluorescence around 540 nm, they can't be used alone as molecular fluorescent probes for cell imaging because excitation wavelength around 350 nm is usually in the window where ever-present cofactors such as NAD/NADH are excited as well. Therefore, we chose fluorescent BODIPY dye for further conjugation and improvement of the spectral properties. As described above, BODIPYs are great fluorophores - mainly high quantum yield, stability against photobleaching and ease of chemical modification. Additionally, the hydrophobic character of BODIPY dyes could increase penetrating ability of 3HQs into the cells. Moreover 3HQ-BODIPY conjugation via disulfide cleavable linker could preferentially release the 3HQs in the cancer cells due to higher concentration of glutathione.

## 1.2 Results and discussion

In the early phase of my work on this project, I focused on synthesis of simple 3HQ-SS-BODIPY conjugates and study of their fluorescent properties in order to effectively follow their cleavage in the living cells. This led to development of the first generation of 3HQ conjugates (1<sup>st</sup> generation, Figure 5). The conjugates were potent against cancer cells but lacked the possibility of active targeting to cancer cells resulting in lower selectivity and lower fluorescent resolution towards real-time monitoring for bioimaging. Thus, next steps in the synthesis led to the attempts to synthesize conjugates decorated with CPPs and finally second generation with cell targeting peptide (CTP) - cRGD peptide as an effective cell targeting moiety together with “smart” quinone methide central core and redBODIPY with higher absorption for FRET monitoring (2<sup>nd</sup> generation, Figure 5). This approach represented current trends for development of novel theranostics as combined diagnostic and therapeutic tools.

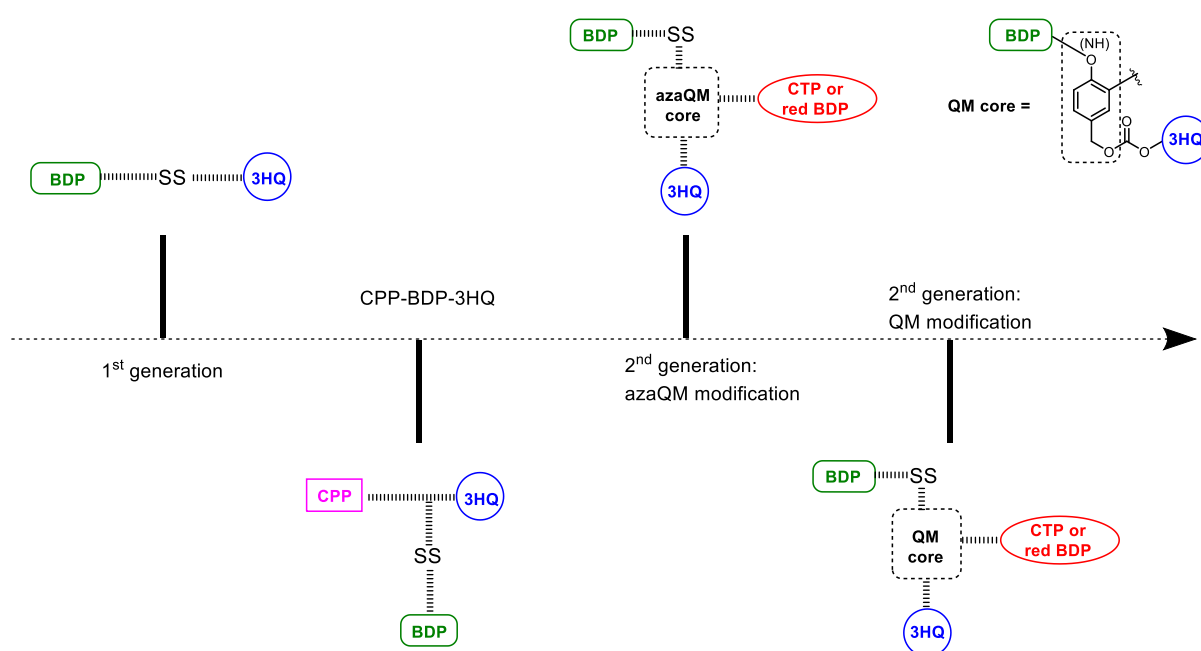
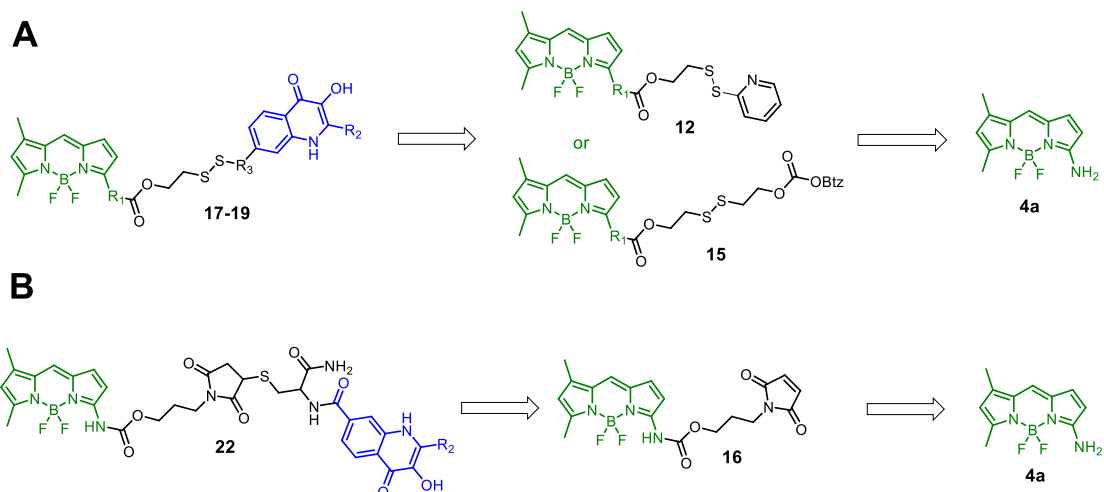


**Figure 5** Timeline of development of 3HQ-BODIPY conjugates.

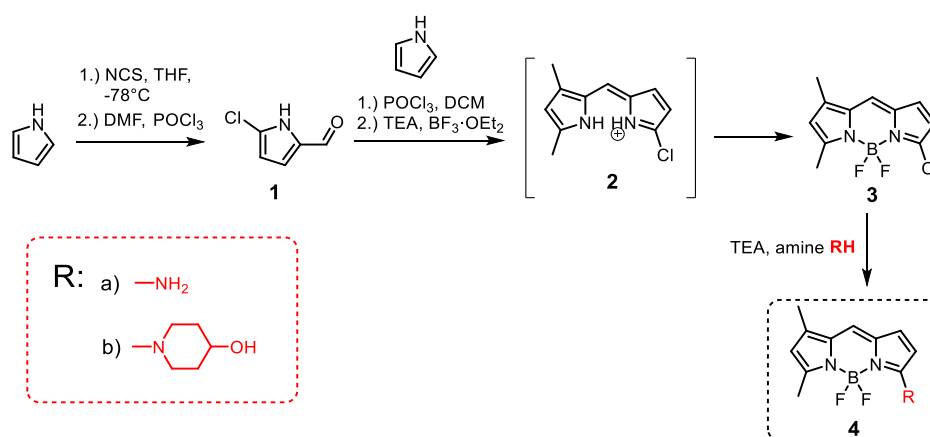
### 1.1.1 Synthesis of the 1<sup>st</sup> generation conjugates

The first generation of 3HQ-BODIPY conjugates represents the connection of 3HQ drug with BODIPY dye through disulfide cleavable linker or maleimide non-cleavable linker (Scheme 2). Non-cleavable conjugates (Scheme 2 B) were synthesized in order to monitor the role of disulfide bond in cleavable conjugates and their cytotoxicity. Synthesis of 3HQ-BODIPY conjugates begins with appropriate modification of BODIPY dye followed by introduction of cleavable disulfide or non-cleavable maleimide linker. Attachment of 3HQ drugs was carried out through amino, hydroxy and thiol group (Scheme 2 A, R<sub>3</sub> substitution) to investigate the cleavage efficiency of final conjugates.



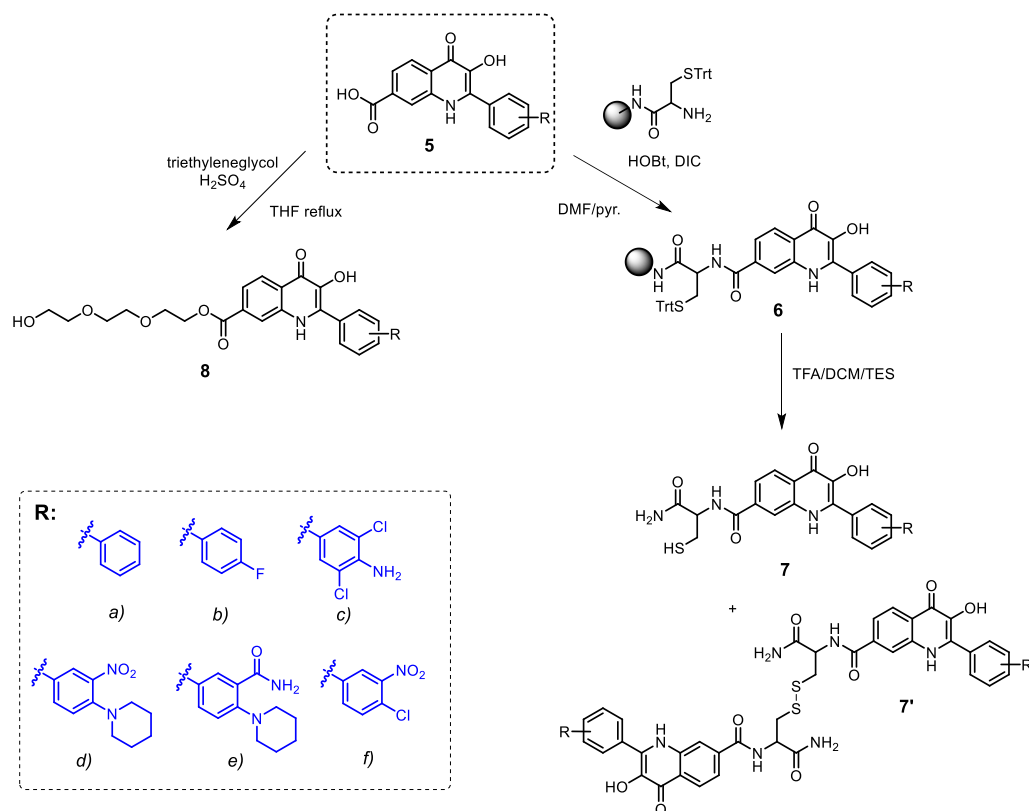
**Scheme 2** Retrosynthetic approach towards (A) cleavable conjugates and (B) non-cleavable maleimide conjugates of 1<sup>st</sup> generation.

As the fluorescent dye for the conjugate of the 1<sup>st</sup> generation we used aminoBODIPY dyes **4a,b** which were synthesized according to the Scheme 3 from pyrrole. Modification of BODIPY dye with amino and 4-hydroxypiperidyl group was necessary for further incorporation of disulfide or maleimide linker and 3HQ model drug later in the synthesis. Both BODIPY dyes **4a** and **4b** showed slightly different spectroscopic properties as will be discussed later.



**Scheme 3** Synthesis of aminoBODIPY **4a** and **4b**.

3HQs became the drugs of our choice on which we demonstrated functionality of the proposed system. 3HQ carboxylic acids **5a-f** were synthesized according to the described procedure bearing six different substitution patterns on 2-phenyl ring and were further modified in order to attach to the disulfide or maleimide linker with cysteine or triethyleneglycol chain as shown in the Scheme 4. Modification with cysteine was performed on the solid phase support using Rink amide resin and provided Cys-3HQs **7a-e**. Triethyleneglycol was attached to the carboxylic acid **5a-e** by acid catalyzed esterification yielding PEG-3HQs **8a-e**.



**Scheme 4** Modification of 3HQs with cysteine and triethyleneglycol.

Connection of 3HQs **7** or **8** with aminoBODIPY dyes **4a,b** was realized by two cleavable disulfide linkers non-symmetrical linker **9** and symmetrical linker **10** or non-cleavable maleimide linker **11** as shown in the Figure 6. We used two types of disulfide linkers in order to investigate the stability together with the cleavage rate and cytotoxicity of resulting conjugates.

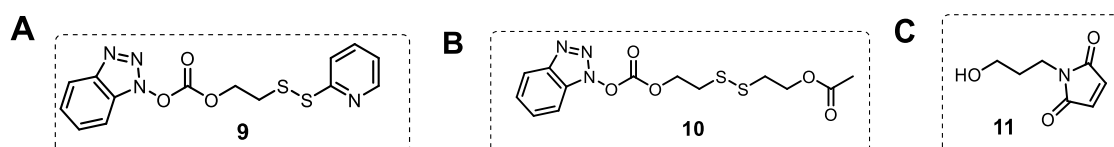
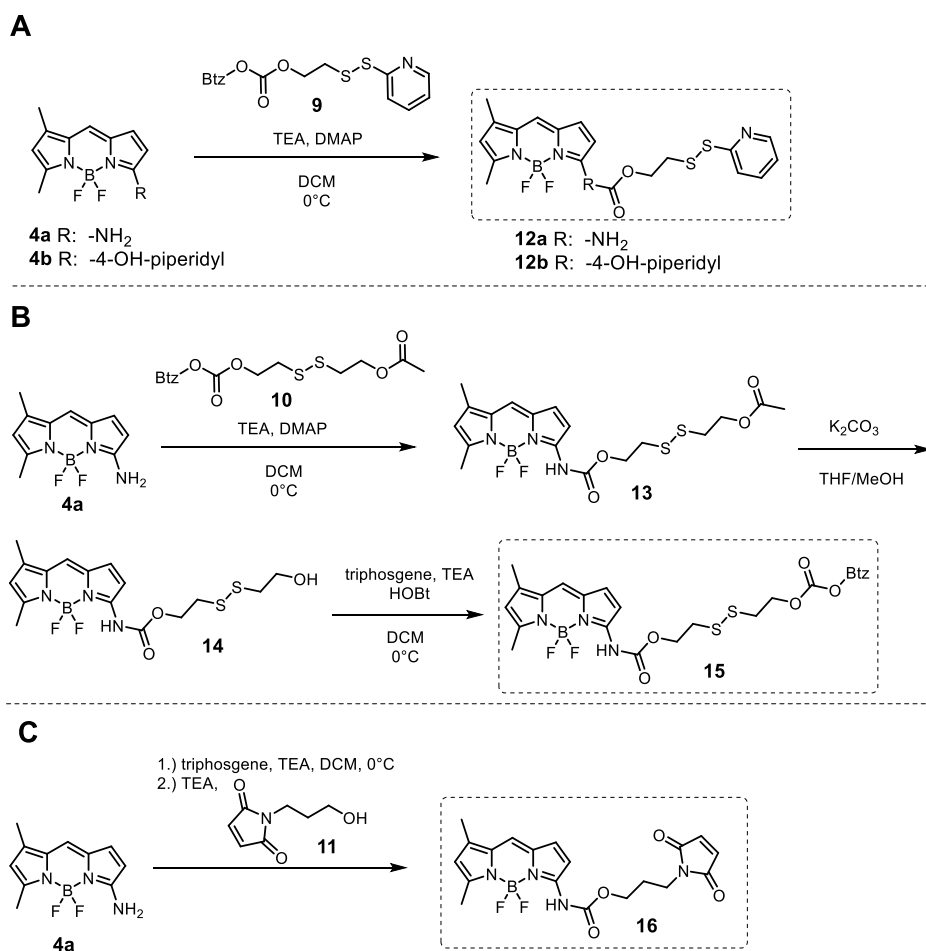


**Figure 6** (A) Non-symmetrical disulfide linker **9**, (B) symmetrical disulfide linker **10** and (C) non-cleavable maleimide **11** linker.

After synthesis of all the three parts – BODIPY dyes, linkers and 3HQs the next step was the conjugation – connecting the parts together. The first step involved attachment of linkers to BODIPY dyes (Scheme 5). This was accomplished by reacting amino-BODIPY **4a,b** with disulfide linkers **9** or **10** to afford intermediates **12**, resp. **15**. BODIPY-maleimide linker **16** was prepared in similar fashion by first activation of BODIPY **4a** with triphosgene followed by treatment with maleimide **11**.

The final conjugates were prepared by reaction of BODIPY-linkers with corresponding 3HQs as depicted in the Scheme 6.

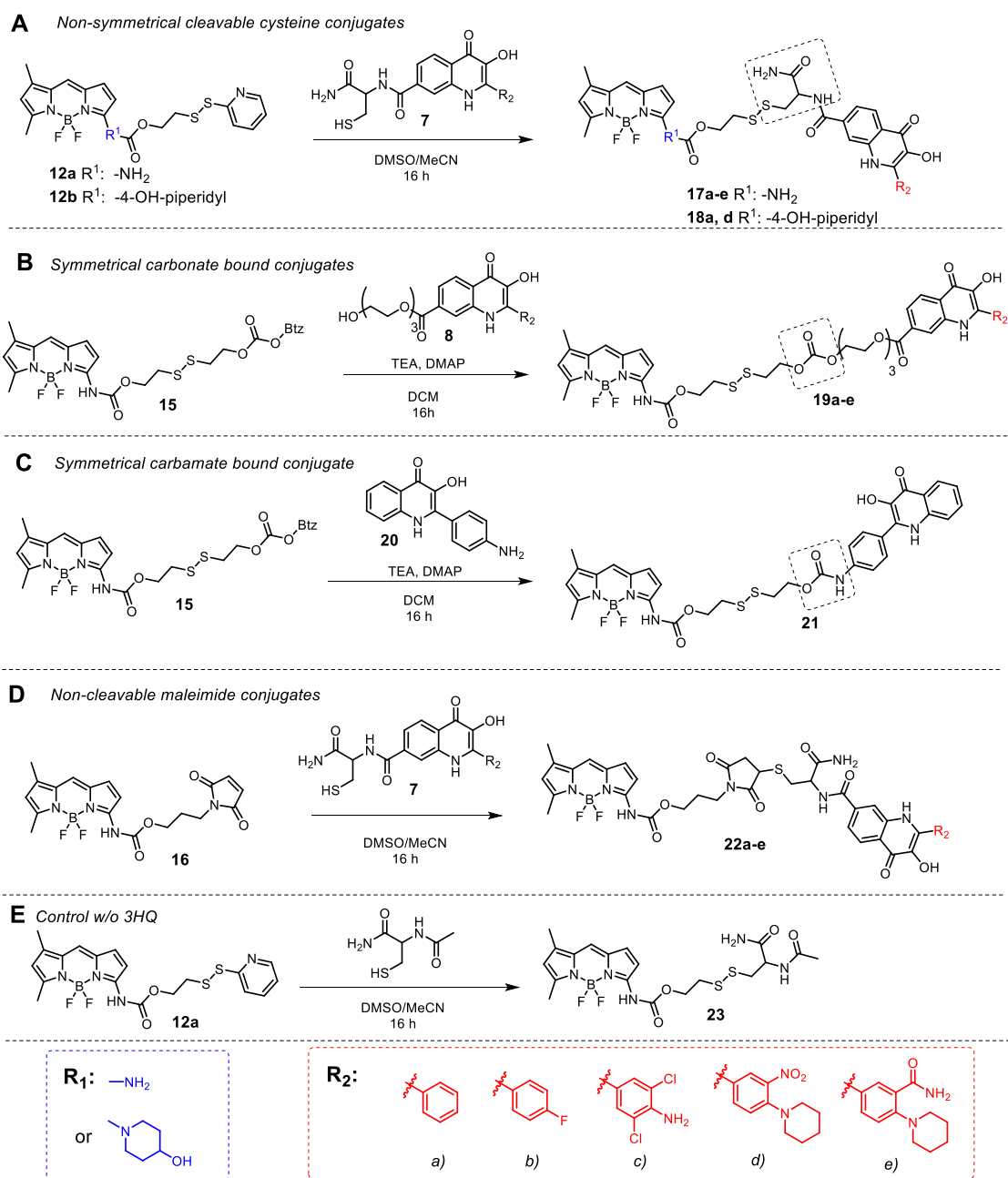


**Scheme 5** Modification of BODIPY dyes **4a,b** with (A) non-symmetrical disulfide linker **9**, (B) symmetrical disulfide linker **10** and (C) non-cleavable maleimide linker **11**.

### 1.1.2 Synthesis of the 2<sup>nd</sup> generation conjugates

Next aim of the project was to develop such compounds that would bear multiple moieties including drug, fluorescent dyes and/or targeting moieties (CPPs, CTPs) connected with aminoBODIPY by disulfide bond for GSH responsive system and “OFF-ON” fluorescence monitoring. Various approaches to prepare such conjugates were attempted as depicted in the Figure 7. By the **Approach A** several compounds with PKKKRKV cell penetrating peptide and different spacers were synthesized and tested on cytotoxicity. However, these compounds lacked the central unit capable of simultaneous releasing of the free drug. As a consequence, the CPP-SS-BDP-3HQ conjugates exhibited only poor toxicity against cancer cell lines.





**Scheme 6** Synthesis of (A) cysteine cleavable conjugates **17** and **18**, (B) carbonate bound conjugates **19**, (C) carbamate bound conjugate **21** and (D) non-cleavable maleimide conjugates **22**. (E) Synthesis of cysteamide-BODIPY **23**.

Therefore, this approach was abandoned and more emphasis was focused on finding suitable “smart” central unit. **Approach B** where the 1,3,5-triazine was used as a central unit provided only preliminary unsuccessful modifications with disulfide linkers and the fact that two equal disulfide linkers had to be used discouraged us from further continuation of this route. Therefore, results from synthesis of conjugates by Approach A and B are not discussed in this summary.

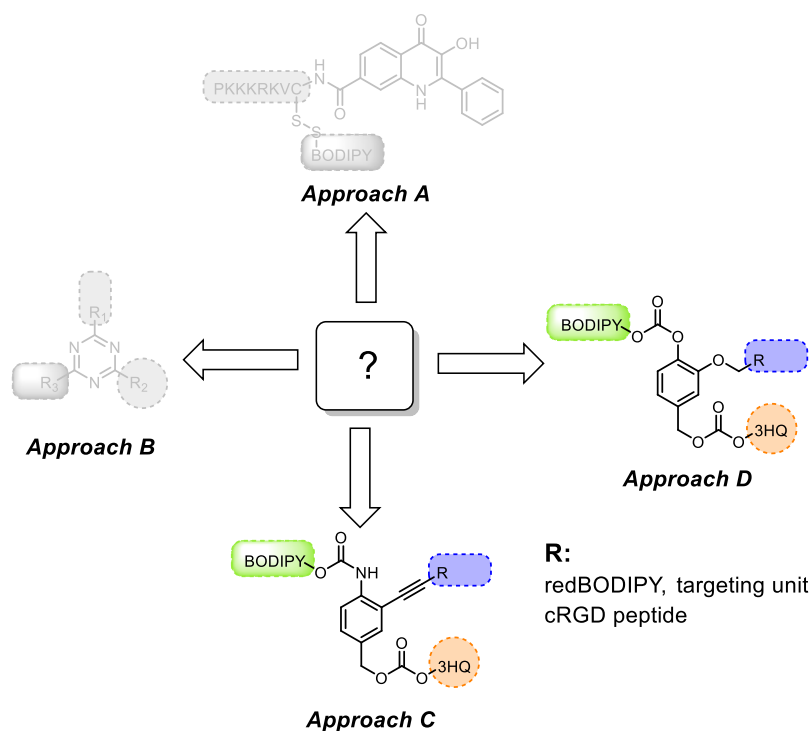


**Figure 7** Approaches towards conjugates with three-component central unit.

**Approach C and D** involved modification of central unit – aza-quinone methide (QM, Approach C) or quinone methide (Approach D) with three parts: (i) aminoBODIPY with cleavable disulfide linker bound via carbamate or carbonate bond (green box), (ii) 3HQ bound to central unit via carbonate bond (orange box) and (iii) redBODIPY dye or cRGD peptide (blue box) attached by two different linkages– alkynyl (Approach C) and ether bond (Approach D). Aza-quinone methide and quinone methide linkers function as stable spacers between an enzyme- or reagent- responsive group and a reporter moiety, drug molecule and can undergo 1,4-, 1,6-, or 1,8-type elimination reactions after cleavage of the triggering group (Figure 8). Such reactivity results in the release of the reporter group through formation of a quinone-methide species.<sup>35–37</sup> We designed system utilizing this scaffold in order to prepare targeted, self-immolative and fluorescent theranostic.

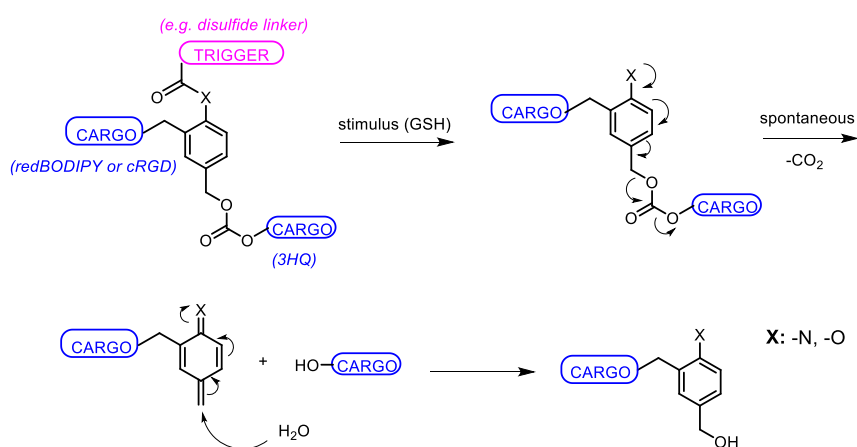
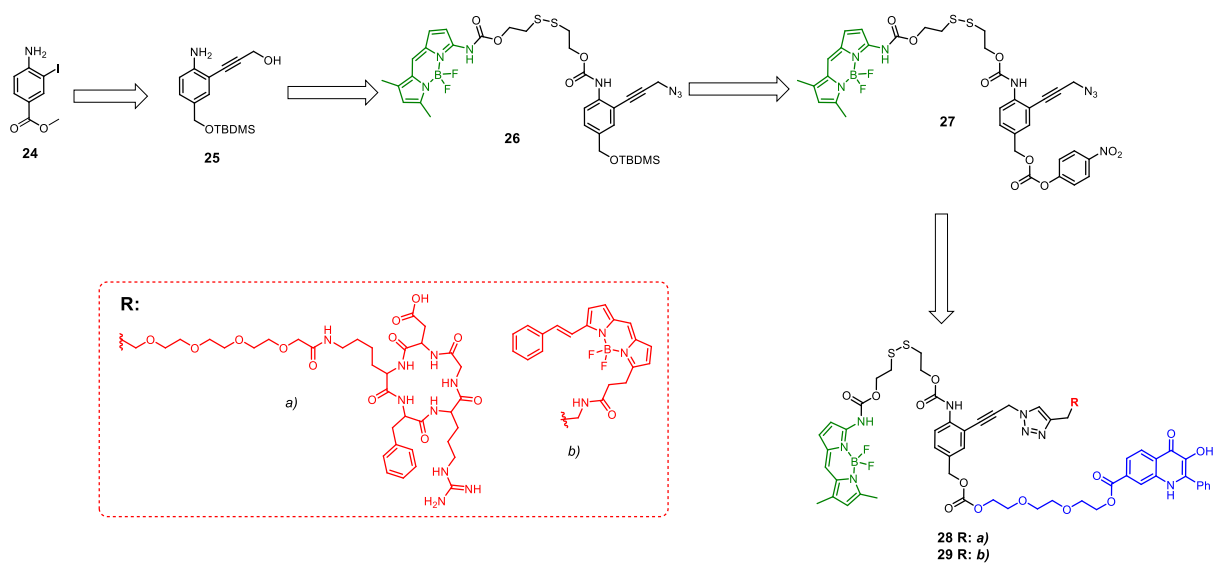


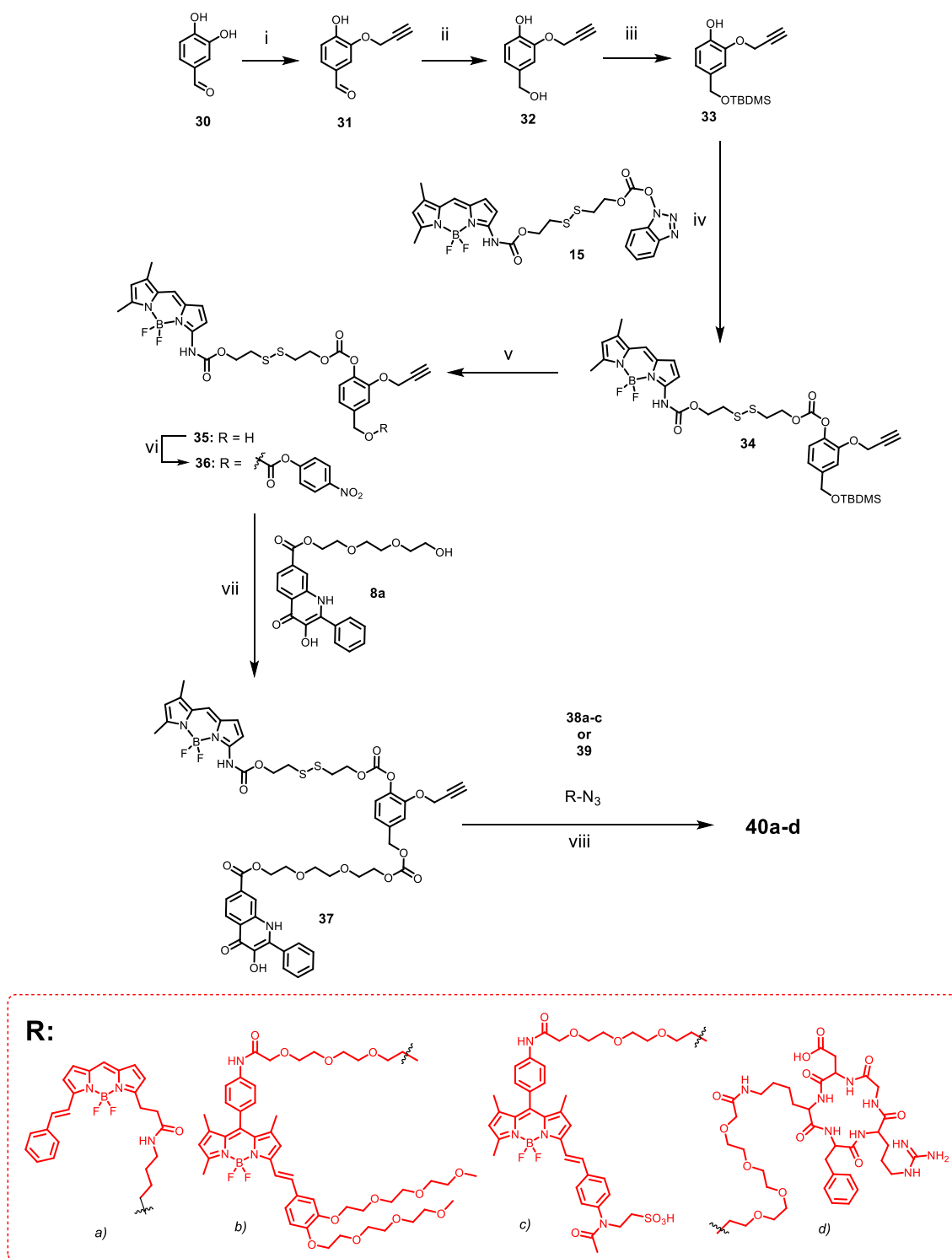
**Figure 8** Quinone-methide elimination.

Synthesis of the aza-quinone analogs was performed as depicted according to the retrosynthetic Scheme 7. Methyl 4-amino-3-iodobenzoate **24** was firstly reduced to benzyl alcohol which was after protection by TBDMS modified by Sonogashira coupling reaction with propargyl alcohol to the intermediate **25**. Afterwards aminoBODIPY **4a** was attached via disulfide linker to amino group of central unit to intermediate **26** and TBDMS was deprotected under acidic conditions. Resulting benzyl alcohol was activated with 4-nitrophenyl chloroformate to intermediate **27**. Activated carbonate was reacted with PEG-3HQ **8a** and azido group was clicked with corresponding propargylated redBODIPY or cRGD peptide to obtain the final conjugates **28** and **29**.



**Scheme 7** Retrosynthetic route to aza-quinone 2<sup>nd</sup> generation conjugates **28** and **29**.

In similar fashion the synthesis of conjugates with quinone-methide central unit were synthesized as depicted in the Scheme 8. During the synthesis which started from 1,2-dihydroxy benzaldehyde **30**, aminoBODIPY was introduced in the position C1 and 3HQ was bound through carbonate group in the position C4 of the central unit. The position C2 was derivatized with three different redBODIPY dyes or cRGD peptide (Scheme 8). redBODIPY dyes modified with groups of different polarity (phenyl, PEG chains and sulfonic group) were introduced in order to investigate its influence on FRET efficiency due to better solvation of resulting conjugate in aqueous medium (see fluorescence studies).



**Scheme 8** The synthesis of conjugates **40a-d**. Conditions: (i) propargyl bromide, NaH, DMSO, 0 °C, on; (ii) NaBH<sub>4</sub>, MeOH/H<sub>2</sub>O, 0 °C, 1 h; (iii) imidazole, TBDMSCl, DMF, rt, 1 h; (iv) DMAP, TEA, DCM, rt, 30 min; (v) pTSA, MeOH, rt, 2 h; (vi) 4-nitrophenylchloroformate, pyridine, THF, rt, 2.5 h; (vii) TEA, DMF, rt, on; (viii) CuSO<sub>4</sub>·5H<sub>2</sub>O, sodium ascorbate, ACN/DMF, 50 °C, on.

### 1.1.3 Fluorescence studies

At first, the optical properties of free BODIPY dyes and conjugates were measured in different solvents (Table 1). AminoBODIPY **4a** showed interesting feature – in the bound/acylated form (conjugates **17-19**, **21-23**) the BODIPY core has an excitation maximum

at  $\lambda_{exc.} = 515$  nm in the free form (**4a**, BODIPY-NH<sub>2</sub>) the excitation wavelength is significantly shifted to the lower wavelengths with maximum at  $\lambda_{exc} = 480$  nm. In the acylated form the BODIPY core is excited at higher wavelengths ( $\lambda_{exc.} = 515$  nm). Interestingly, the emission maximum remained approximately the same 523 nm and 527 nm, respectively (Figure 9 A). The shift of the excitation maxima is caused probably due to alteration of electronical properties at the amino group that is bound directly to the BODIPY core. Free amino group is good electron donor, but turning it to carbamate group results in formation of electron more deficient structure.

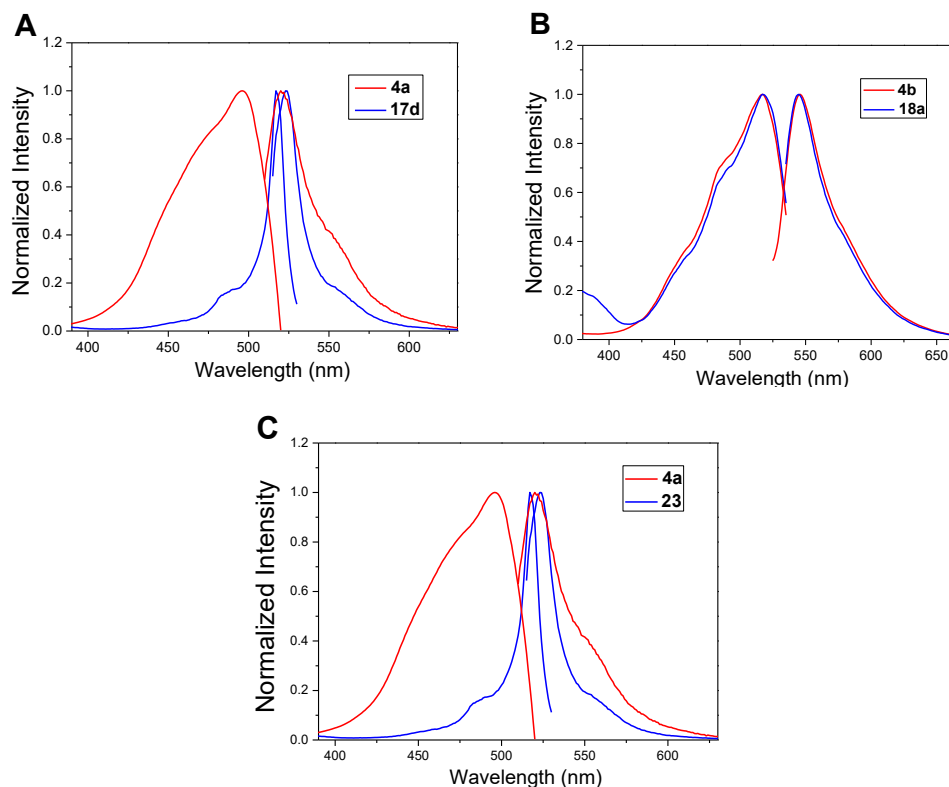
Compound	Solvent	$\lambda_{exc}$ (nm)	$\lambda_{em}$ (nm)	$\Delta\lambda$ (nm)	QY (%)	
<b>17d</b>	Conjugate – Cysteine linker	HEPES DMSO/HEPES	515 517	527 531	12 14	1.4 7.7
	<b>19a</b>	Conjugate – symmetrical linker	HEPES DMSO/HEPES	516 520	525 530	9 10
<b>19d</b>		Conjugate – symmetrical linker	DMSO/HEPES	521	549	28
<b>21</b>	Conjugate – symmetrical linker	HEPES DMSO/HEPES	517 521	525 532	8 11	32 53
	<b>23</b>	Cysteamide-BODIPY	DMSO/HEPES	520	531	11
<b>4a</b>	aminoBODIPY	HEPES	480	523	43	77
		DMSO/HEPES	496	523	40	95
<b>4b</b>	piperidylBODIPY	DMSO/HEPES	521	550	29	48

**Table 1** Spectral properties of some prepared conjugates.

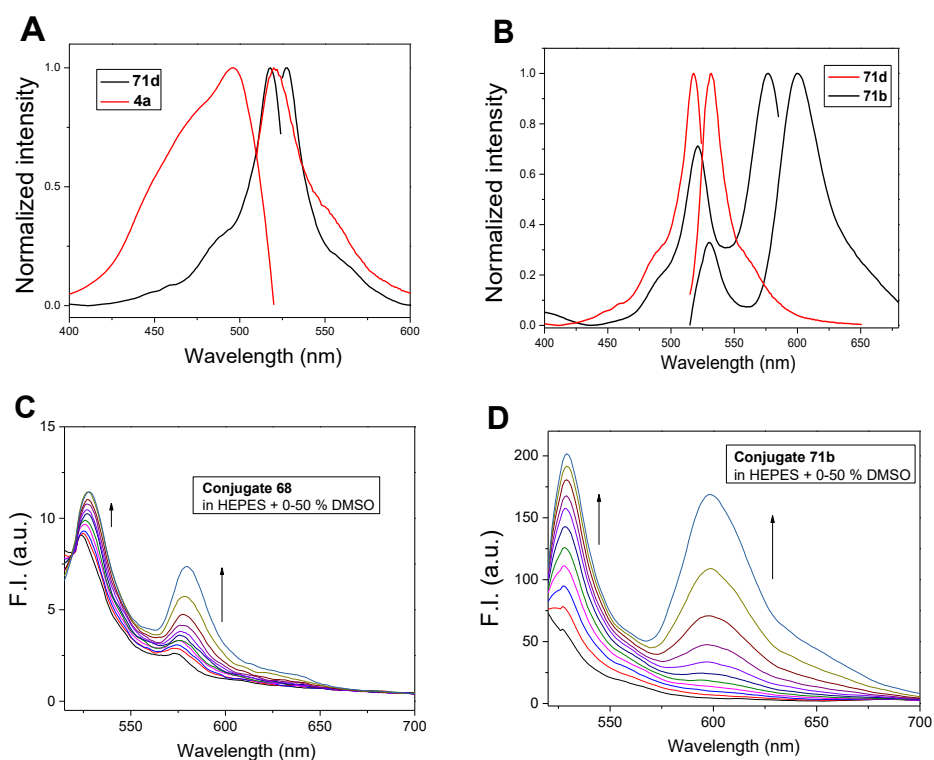
This fact can be supported by optical properties of piperidineBODIPY **4b** in which the linker is attached not directly to the core of BODIPY. No such shift of excitation maxima was observed and thus conjugates **18** have the same excitation and emission as the free piperidineBODIPY **4b** (Figure 9B). Moreover, the excitation wavelength shift in the case of aminoBODIPY **4a** is universal - it does not depend on the conjugated counterpart and is not typical only for 3HQs as was confirmed by the preparation and measurement of optical properties of cysteamide-BODIPY conjugate **23** (Figure 9C).

In the case of 2<sup>nd</sup> generation conjugates bearing aminoBODIPY dye the spectral properties are expectedly similar to the previously described 1<sup>st</sup> generation system, allowing the “OFF-ON” ratiometric drug release monitoring (Figure 10A). Emission of aminoBODIPY in FRET conjugates **29** and **40a-c** (aza-QM and QM conjugates) is expectedly transferred to the redBODIPY and the emission at approximately 595 nm is observed (Figure 10 B) in DMSO/HEPES buffer. However, arguably due to the hydrophobic character and low water solubility, despite the attached ethyleneglycol chains on redBODIPY **40b** or -SO<sub>3</sub>H group on **40c**, the FRET efficiency drastically dropped in HEPES buffer. The effect of hydrophobicity of redBODIPY dyes is demonstrated in the Figure 10 C-E. Addition of DMSO into the HEPES buffer (pH 7.4) solution of conjugates **29** and **40-b,c** with different redBODIPY dyes resulted probably in better solvation and increased efficiency of FRET fluorescence. Conjugate **40c** with redBODIPY modified with more hydrophilic SO<sub>3</sub>H group showed at least two times higher efficiency compared to the conjugate **40b** with PEGylated redBODIPY in the same media (e.g.

50% DMSO). However, we did not continue to further cleavage and biological experiments with conjugate **40c** due to low amount of compound available and difficulties in its synthesis. FRET efficiency of conjugate **40b** was determined as 72 % in DMSO/HEPES (2:1) buffer.



**Figure 9** Normalized excitation and emission spectra of (A) aminoBODIPY **4a** and 3HQ conjugate **17d**, (B) BODIPY **4b** and 3HQ conjugate **18a** and (C) aminoBODIPY **4a** compared with cysteamideBODIPY **23**. Measured in DMSO/HEPES 2:1.



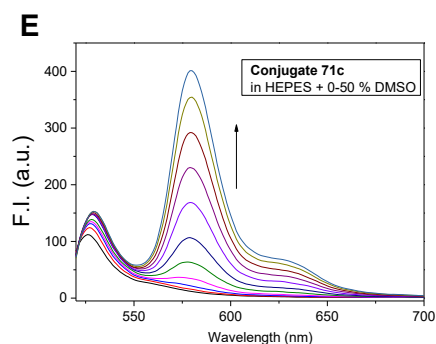
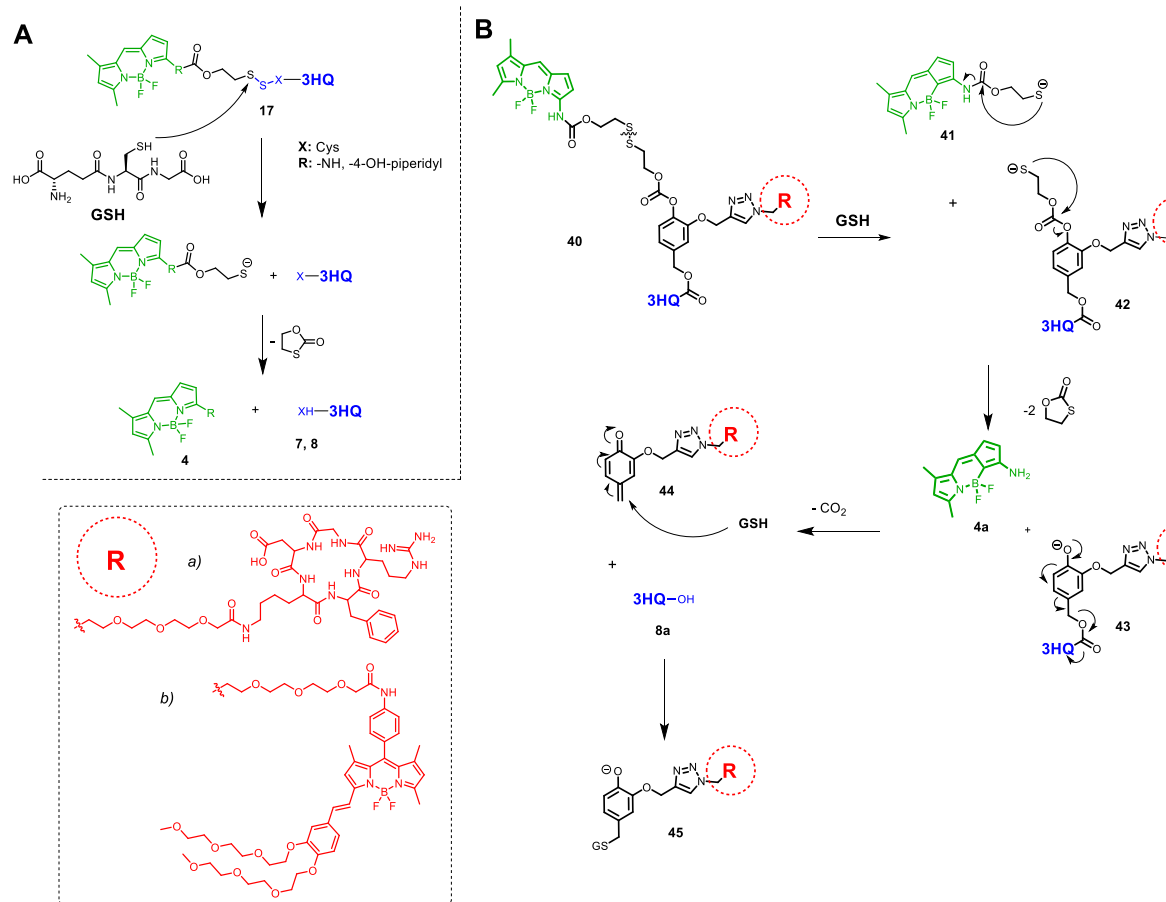


**Figure 10** (A) Normalized excitation and emission spectra of the conjugate **40d** and aminoBODIPY **4a** (HEPES buffer, 0.1 M, pH 7.4), (B) conjugate **40b** and conjugate **40d** (DMSO/HEPES buffer 0.1 M, 2:1, pH 7.4). Change of FRET efficiency by incremental addition of DMSO to HEPES solution of (C) conjugate **29**, (D) conjugate **40b** and (E) conjugate **40c**. Excitation wavelength  $\lambda_{\text{exc}} = 510$  nm.

#### 1.1.4 GSH cleavage study

Bathochromic shift in excitation maximum of aminoBODIPY conjugates enabled us to apply so called “OFF-ON” monitoring and further ratiometric monitoring of GSH-mediated cleavage (Scheme 9). Since conjugates themselves have only little absorption at 480 nm at the beginning of cleavage there is only weak fluorescence (OFF state). As the cleavage proceeds aminoBODIPY **4a** is liberated and strong green fluorescence appears (ON state) (Scheme 9, Figure 11 A). Furthermore, when the emission intensity upon excitation at 510 nm is followed, we observe strong emission at the beginning of the cleavage (compound is in conjugated form) and as the cleavage continues the increase of fluorescence is lower or even in some cases the fluorescence decreases as the conjugate disappears (conjugates **19d** and **40d**, Figure 11 B, Figure 12 D). Supported by the significant difference in quantum yields (Table 1) between the free BODIPY dyes (**4a,b**) and conjugates containing fluorescence quenching  $-\text{NO}_2$  group (e.g. conjugate **19d**) the change of fluorescence emission intensity during the GSH-mediated cleavage was observed to be 4-5 fold what was acceptable for further cleavage experiments.



**Scheme 9** GSH-mediated cleavage of disulfide 3HQ-BODIPY conjugates (A) **17** and (B) **40b,d**.

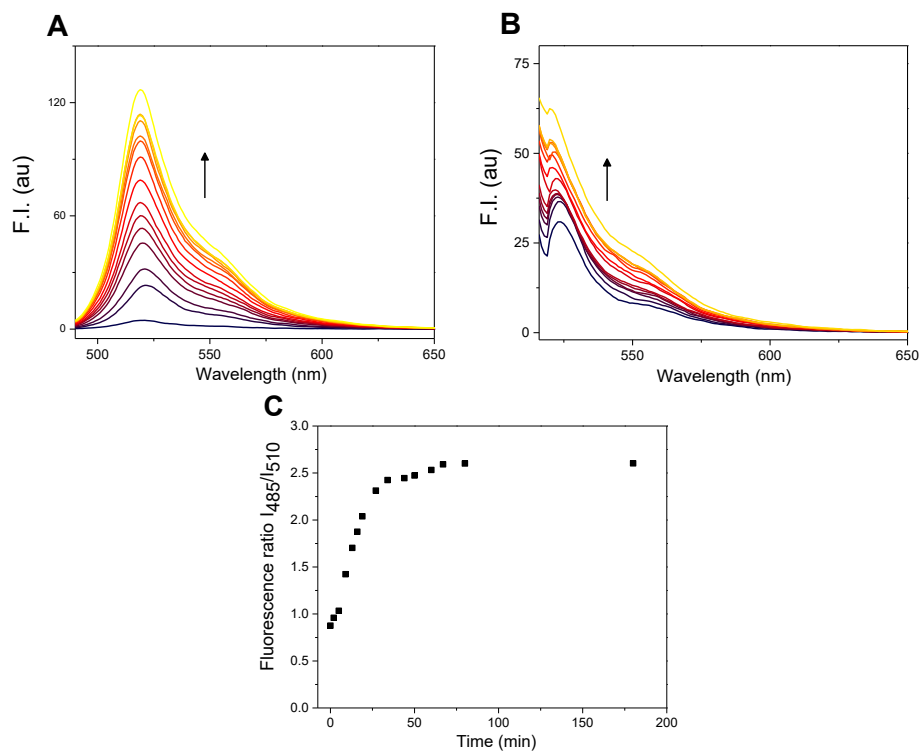


**Figure 11** GSH-mediated cleavage of probe the **17d** monitored within 180 min by fluorescence emission at 525 nm upon excitation at (A) 480 nm and (B) 510 nm (5  $\mu$ M probe **17d**, 5 mM GSH; HEPES buffer, 0.1M, pH 7.4, 37  $^{\circ}$ C). (C) Time dependent change of fluorescence ratio at 530nm upon dual excitation at 480 nm and 510 nm.



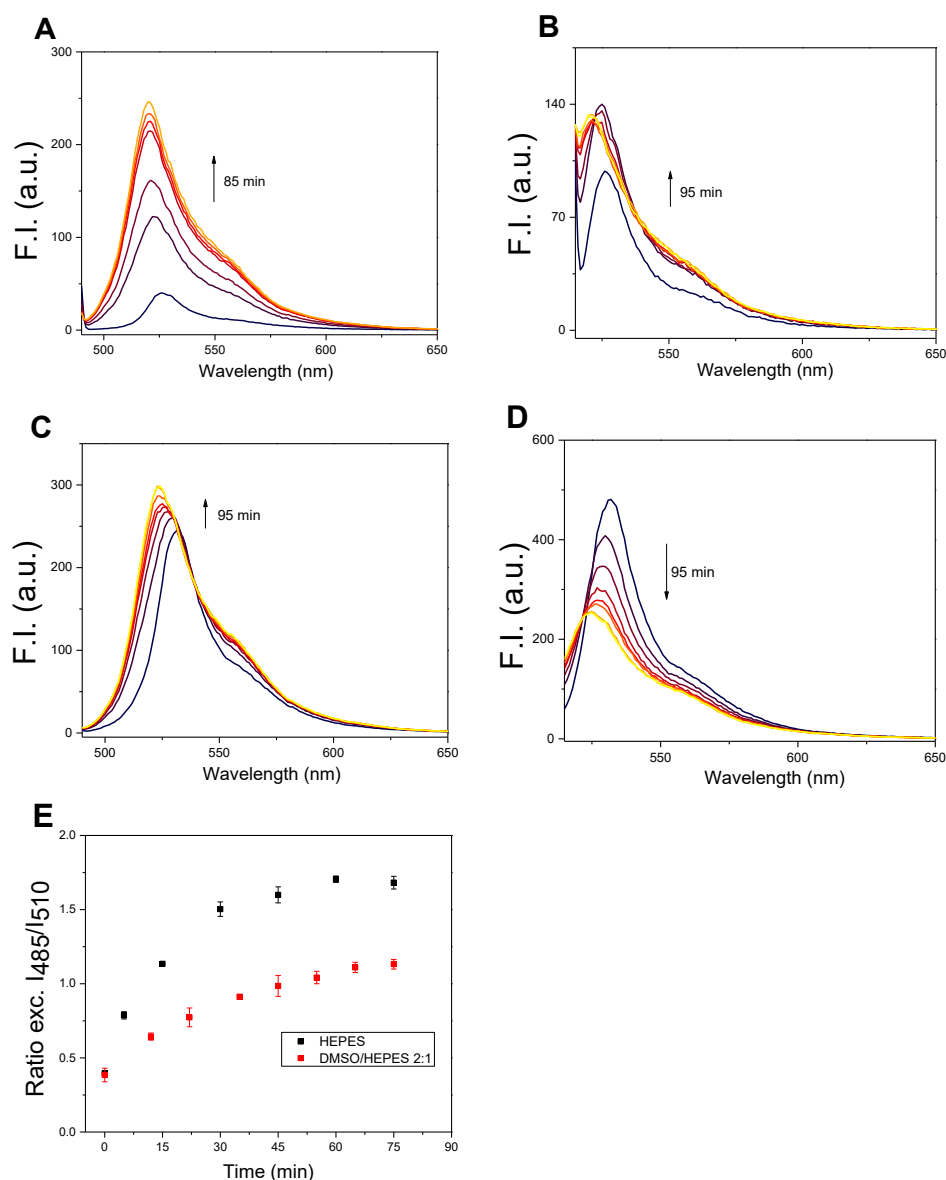


**Figure 12** (A) Fluorescence spectra of GSH-mediated cleavage (5 mM GSH) of the conjugate **40d** (5  $\mu$ M) upon excitation at 485 nm or (B) 510 nm in HEPES buffer (0.1 M, pH 7.4). (C) Fluorescence spectra of GSH-mediated cleavage (5 mM GSH) of the conjugate **40d** (5  $\mu$ M) upon excitation at 485 nm and (D) 510 nm in DMSO/HEPES buffer (0.1 M, 2:1, 37  $^{\circ}$ C). (E) Schematic representation of the ratiometric change of fluorescence intensities at 530 nm after excitation at 485 nm and 510 nm ( $I_{485}/I_{510}$  ratio).

Apart from the aminoBODIPY conjugates **17-19**, **21-23** and **40d**, conjugates **40a-c** carry the additional dye – redBODIPY – designed for efficient FRET. As demonstrated on conjugate **40b** (Figure 13), before the GSH-mediated cleavage of conjugate the system affords the fluorescence of the redBODIPY ( $\lambda_{em} = 595$  nm) upon the excitation of aminoBODIPY ( $\lambda_{exc} = 510$  nm). During the cleavage, the green emission (530 nm) of the released aminoBODIPY **4a** appears and increases with time (Figure 13 A). When the ratio of both emissions at 530 nm and 595 nm (herein  $I_{530}/I_{595}$ ) upon excitation at 510 nm is followed within the time, the plateau is achieved in approximately 30 minutes. The fluorescence response (emission ratio  $I_{530}/I_{595}$ ) enhancement in this case is particularly higher than in the case of aminoBODIPY conjugates and stands approximately for 12-fold increase (Figure 13 B).

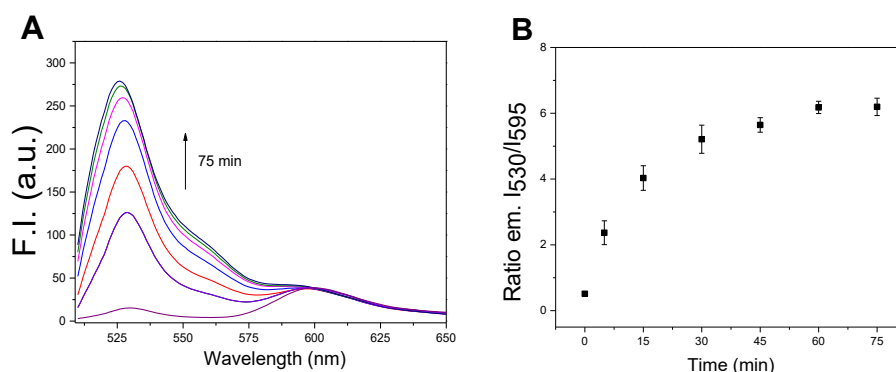


**Figure 13** (A) Fluorescence spectra of the conjugate **40b** (1  $\mu$ M) during GSH-mediated cleavage (3 mM GSH) upon excitation at 510 nm and (B) schematic representation of the ratiometric change of  $I_{530}/I_{595}$  emissions ratio (3 mM GSH, DMSO/HEPES buffer 0.1 M, 2:1, 37  $^{\circ}$ C).

Next, we examined the stability of conjugates **40b** and **40d** at various pH and the rate of cleavage by 5 mM GSH at 37  $^{\circ}$ C in the pH range of 5-8. It is known that the disulfide bond is stable in presence of thiols at lower pH and at higher pH the linker is readily cleaved. The same pH stability is observed for both conjugates as shown in the Figure 14 A and B. Both conjugates **40b** and **40d** were quite stable in the presence of GSH (3 mM) at acidic pH (5-5.5) and were readily cleaved at higher pH (7-8). In addition, both conjugates proved to be stable in the selected pH range without the presence of reduced GSH.

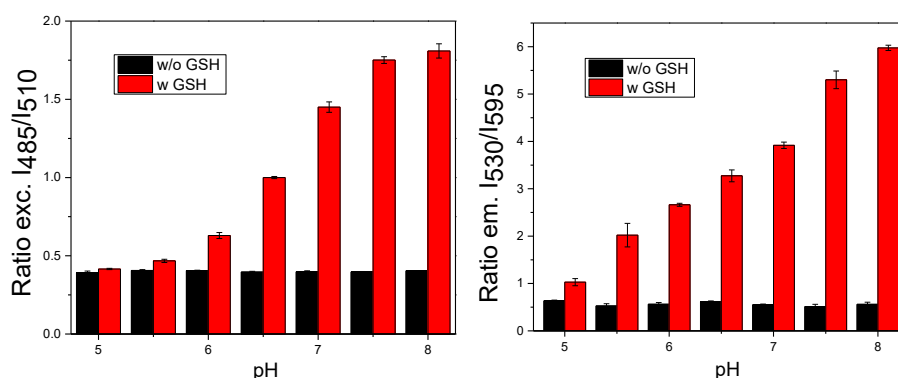


**Figure 14** (A) Stability of the conjugate **40d** (1  $\mu$ M) at various pH 5-8 in HEPES buffer (0.1 M, 37  $^{\circ}$ C) in the absence of GSH (black bars) and with 3mM GSH (red bars) upon incubation for 1 hour. (B) Stability of the conjugate **40b** (1  $\mu$ M) at various pH 5-8 in DMSO/HEPES buffer (0.1 M, 37  $^{\circ}$ C) in the absence of GSH (black bars) and with 3mM GSH (red bars) upon incubation for 1 hour. All datapoints were acquired upon irradiation at 485 nm and 510 nm with the following emission at 530 nm and were performed in 3 repetitions.

### 1.1.5 Biology

To prove the real functioning of the system, the cleavage of conjugates **17-22** in HeLa cells that were pretreated with glutathione (20 mM) was performed. Although the inherent concentration of GSH in the cells was sufficient to cleave the disulfide conjugates, the cleavage was more efficient when conjugates were added to the cells preincubated with additional GSH (Figure 15, Figure 16). However, conjugate **19a** with the more susceptible carbonate linker was cleaved efficiently inside native cells without preincubation with GSH. Arguably, the GSH concentration in the HeLa cells is sufficiently high for full cleavage of the linker, and the preincubation with GSH does not further accelerate the disruption of the disulfide bond.

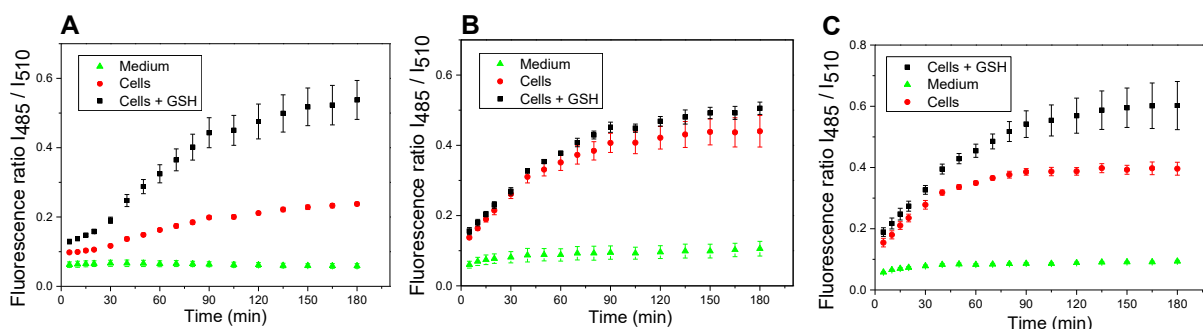


**Figure 15** Ratio of emission intensities at 525 nm upon excitation at 485 nm and 510 nm inside HeLa cells corresponding to the cleavage of the conjugate (A) **17d**, (B) **19a**, and (C) **21** within 3 h period.

Similarly, fluorescence ratio  $I_{485}/I_{510}$  of non-cleavable conjugates **22a-e** was monitored in DMSO/HEPES buffer (2:1) as well as in HeLa cells after treatment with GSH (Figure 16 B). In this case, no significant changes were observed, confirming the stability of conjugates towards thiols and GSH.

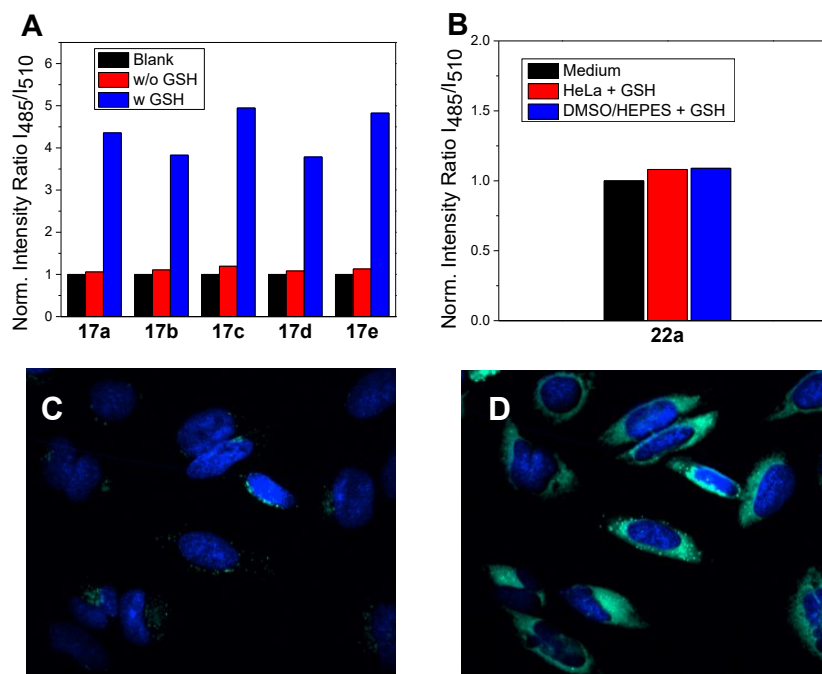
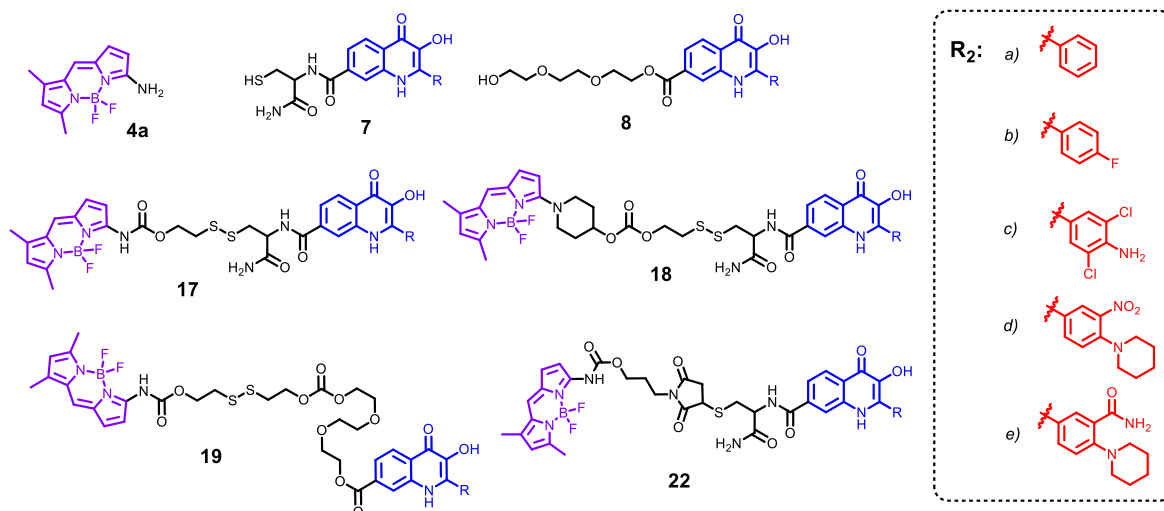


**Figure 16** (A) Schematic representation of the ratiometric change of fluorescence intensities at 530 nm after excitation at 485 nm and 510 nm (fluorescence ratio  $I_{485}/I_{510}$ ) for conjugates **17a-e** incubated in HEPES Buffer and measured at 0 h (black columns), HEPES buffer without GSH for 3 h (red columns) and in HEPES buffer with GSH (5 mM) for 3 h at 37 °C (blue columns). (B) Fluorescence ratio  $I_{485}/I_{510}$  change after incubation of the non-cleavable conjugate **22a** (5  $\mu$ M) in free medium (black column), HeLa cells with additional GSH (20 mM) (red column) and in the presence of GSH (5 mM) in DMSO/HEPES buffer 2:1 (0.1 M, pH 7.4, 37 °C) (blue column) for 180 min. (C) The microscopy images of the internalization of the conjugate **17d** inside the HeLa cells before treatment and (D) 2 h after treatment with GSH (20 mM).

All the prepared compounds were tested on cytotoxicity in collaboration Institute of molecular and translational medicine (IMTM) and biological screening department, and  $IC_{50}$  values were determined (Table 2). In general, free cysteine-3HQs **7a-e** exhibited no toxicity whatsoever probably due to their high polarity and impaired cell uptake. However, conjugation to

aminoBODIPY **4a** or **4b** led to the increased toxicity mainly in case of cleavable conjugates Cys-3HQ **17** and **18** and PEG-3HQ conjugates **19**. Cys-3HQ conjugates **17a-e** and **18a,d** showed moderate activity against CEM cells but only subtly increased toxicity to other cell lines compared with non-cleavable conjugates **22**. Non-cleavable conjugates exhibit only certain inherent toxicity to CCRF-CEM cells, arguably as a result of insufficient rendering of 3HQ toxicity, but exhibit completely no toxicity to other cell lines. The highest toxicity exhibited PEG-3HQs **8a-e** and their conjugates **19a-e**. Although, PEG-3HQ derivatives showed micromolar and in case of derivative **8d** sub-micromolar activity against CEM cell line and good-to-moderate toxicity against other cell types (HCT116, K562 and U2OS) they showed also substantial toxicity to healthy cell line MRC-5. The only exception was the compound **8e** which showed no toxicity probably due to its very low solubility. On the contrary, aminoBDP-PEG-3HQ conjugates **19** retained the toxicity of PEG-3HQs against cancer cells (CEM, K562, U2OS) and even demonstrated improved cytotoxicity to resistant cell lines (CEM-DNR, K562-TAX or HCT116-p53). Moreover, the toxicity to normal cell line MRC-5 was significantly lower. However, it is important to mention that unexpectedly also aminoBODIPY **4a** exhibited significant, non-specific toxicity to cancer cells (Table 2) and subtle toxicity to healthy MRC-5 cell line.



Code	Cell line/IC <sub>50</sub> (μM)									
	A549	BJ	CCRF-CEM	CEM-DNR	HCT116	HCT116 p53	K562	K562-TAX	MRC-5	U2OS
<b>7a</b>	50	50	50	50	50	50	50	50	50	50
<b>7b</b>	50	50	50	50	50	50	50	50	50	50
<b>7c</b>	50	50	50	50	50	50	50	50	50	50
<b>7d</b>	50	50	50	50	50	50	50	50	50	50
<b>7e</b>	50	50	50	50	50	50	50	50	50	50
<b>8a</b>	9.27	46.84	6.21	23.55	8.17	13.37	5.55	22.13	24.07	12.81
<b>8b</b>	50	50	9.1	45.19	32.31	33.71	50	43.49	41.79	50
<b>8c</b>	8.64	50	1.00	30.91	5.95	6.56	5.95	27.7	17.09	6.15
<b>8d</b>	13.13	50	0.39	7.6	3.35	3.55	4.55	7.04	7.62	13.06
<b>8e</b>	50	50	24.02	50	50	50	50	50	50	50
<b>19a</b>	11.55	50	1.99	15.3	10.39	9.66	6.83	19.23	43.31	8.69
<b>19b</b>	7.56	50	1.70	5.22	6.56	6.21	6.1	6.36	41.1	6.7

19d	3.2	50	0.45	7.97	2.85	2.07	1.94	9.79	50	2.41
19e	10.17	50	1.43	8.54	7.54	8.09	5.52	8.5	50	3.64
17a	50	50	19.73	34.42	50	50	49.82	39.77	50	50
17b	46.43	50	8.14	26.51	50	49.79	44.65	33.59	50	42.3
17c	50	50	2.59	40.09	50	50	41.43	41.83	50	50
17d	46.27	50	1.52	37.91	39.71	42.6	29.91	40.61	50	44.15
17e	50	50	50	46.25	50	50	50	46.16	50	50
22a	50	50	14.6	50	50	50	50	50	50	50
22b	50	50	6.37	50	50	50	50	50	50	50
22c	50	50	12.7	50	50	50	50	50	50	50
22d	50	50	50	50	50	50	50	50	50	50
22e	50	50	5.1	50	50	50	50	49.55	50	50
18a	50	50	3.01	50	12.9	9.76	7.09	50	50	48.98
18c	50	50	5.88	50	50	43.02	41.67	50	50	50
4a	47.2	50	4.25	5.08	11.56	12.74	3.29	6.41	40.11	19.8

**Table 2** IC<sub>50</sub> values of the prepared conjugates **30-32**, **34** and free 3HQs **12** and **13**.

Incubation of the 2<sup>nd</sup> generation conjugate **40d**, bearing cRGD targeting peptide, with cells pre-incubated with N-ethylmaleimide (agent that depletes intracellular thiols) led only to the slight increase of the fluorescence in 2 hours (Figure 17, Figure 18 A). The emission intensity was significantly enhanced when the cells were treated with GSHEt (Figure 17, Figure 18 C), and greater amount of the aminoBODIPY and drug is released. Cleavage of the conjugate **40b** (Figure 17 B) inside the HeLa cells was not well reproducible with high error and did not correspond with images from fluorescence microscopy arguably because of its low solubility.

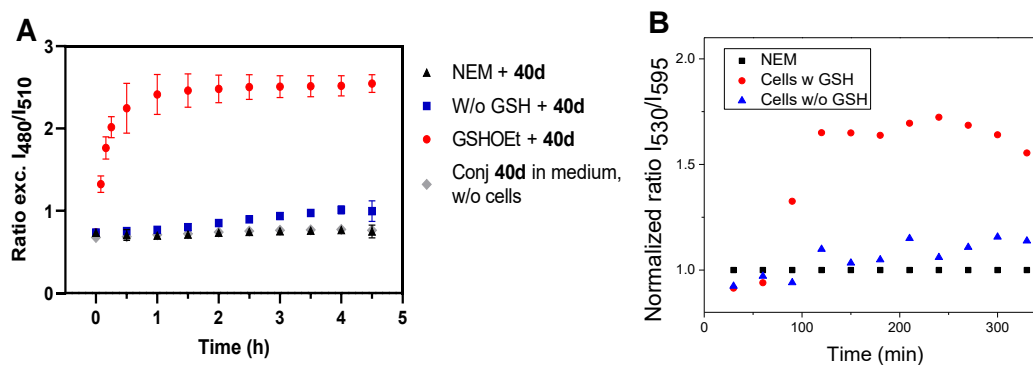


**Figure 17** Time-dependent cleavage monitoring of conjugates (A) **40d** and (B) **40b** inside HeLa cells pretreated with NEM (1 mM, 30min) and HeLa cells with or without treatment with GSHEt (20mM).

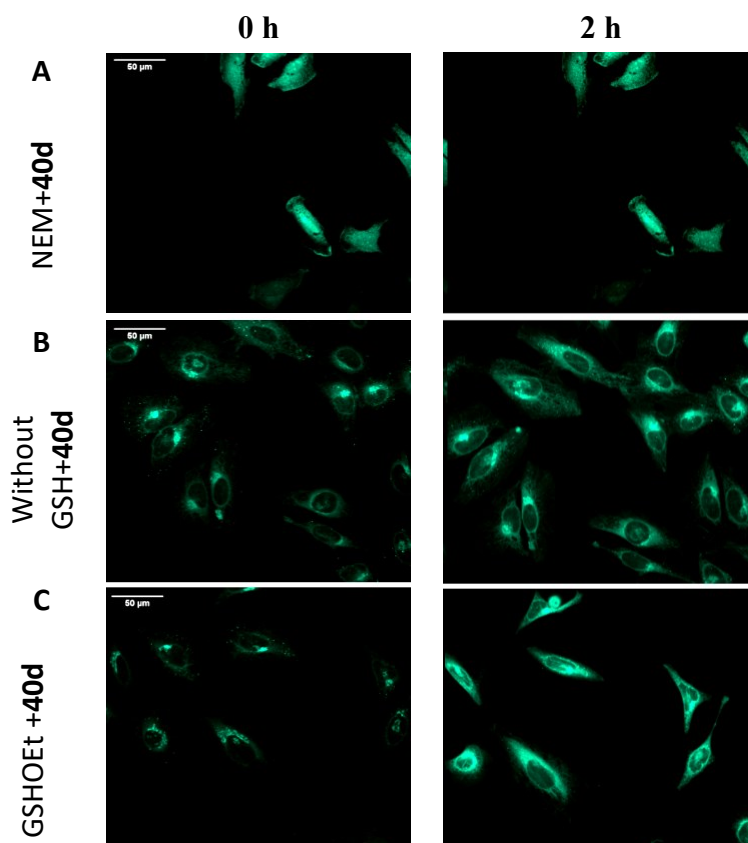


**Figure 18** (A) Microscopy images of the conjugate **40d** internalization inside the HeLa cells after pretreatment with 1mM NEM, (B) without any pretreatment and (C) after pretreatment with 20 mM GSHOEt. (D) Quantification of fluorescence intensity in HeLa cells. Excitation/emission wavelength 488/515-530 nm.

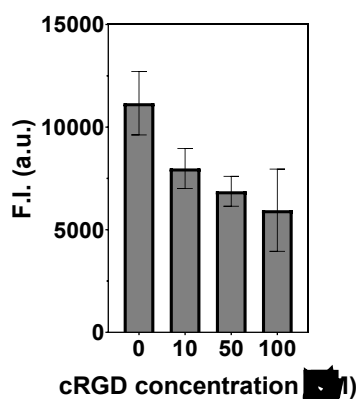


**Figure 19** Uptake of the conjugate **40d** (10  $\mu\text{M}$ ) by HeLa cells pre-incubated with cRGD peptide (0-100  $\mu\text{M}$ ). Fluorescence was measured at  $\lambda_{\text{em}} = 530\text{nm}$  upon excitation by  $\lambda_{\text{exc}} = 485\text{nm}$ . All measurements were performed in at least 5 repetitions.

Enhanced uptake of the cRGD conjugate **40d** by HeLa cells which possess overexpressed levels of  $\alpha_v\beta_3$  integrins<sup>38,39</sup> was proven by cRGD binding assay. Cells were pre-incubated with various cRGD peptide concentrations (0-100  $\mu\text{M}$ ) and then treated with conjugate **40d** (10  $\mu\text{M}$ ). As Figure 19 depicts, fluorescence response decreased with higher concentrations of cRGD peptide suggesting that binding sites at  $\alpha_v\beta_3$  integrins were occupied by free cRGD peptide and thus less conjugate penetrated into the cells. Pre-incubation with

100  $\mu$ M cRGD led approximately to 53 % reduction in the cell uptake of conjugate **40d** according to fluorescence intensity at 530 nm.

Cytotoxicity of aza-quinone methide conjugates **28** and **29** and quinone methide conjugates **40a-d** are summarized in the Table 3. Drug releasable conjugates **29** and **40a-c** with redBODIPY dye showed no activity regardless of the aza-quinone or quinone methide central unit probably as a result of poor solubility in aqueous medium. On the other hand, both conjugates **28** and **40d** with cRGD targeting peptide exhibited cytotoxic activity comparable with the free 3HQ-PEG model drug **8a**. This activity was probably the result of either effective targeting and penetration to cells or enhanced water solubility of the compounds. In addition, the toxicity of compounds **28** and **40d** against normal cells (MRC-5) was reduced.

Compound	Cell line/IC <sub>50</sub> ( $\mu$ M)									
	A549	BJ	CCRF-CEM	CEM-DNR	HCT116	HCT116 p53	K562	K562-TAX	MRC-5	U2OS
<b>29</b>	50	50	50	50	50	50	48.68	50	50	50
<b>28</b>	8.62	50	6.23	30.75	7.43	8.22	7.08	36.06	50	8.01
<b>40a</b>	50	50	46.35	50	50	50	49.84	50	50	50
<b>40d</b>	8.50	42.02	6.06	17.89	7.22	7.48	7.98	22.42	45.82	8.80
<b>40b</b>	50	50	50	50	50	50	50	50	50	50
<b>40c</b>	50	50	50	50	50	50	50	32.74	50	50
<b>8a</b>	9.27	46.84	6.21	23.55	8.17	13.37	5.55	22.13	24.07	12.81

**Table 3** IC<sub>50</sub> values of 2<sup>nd</sup> generation conjugates.

### 1.3 Conclusion

To summarize, in this project we successfully prepared and optimized synthetic route leading to two generations of BODIPY-3HQ conjugates. These potential theranostics were then evaluated through GSH-mediated cleavage and fluorescence monitoring of the drug release in glass cuvettes as well as inside the HeLa cells. In collaboration with cell biology department at IMTM we tested cytotoxicity of all final compounds on cancer cell lines and normal cell lines. Firstly, simple conjugation of aminoBODIPY **4a** and **4b** with various 3HQs as model drugs *via* disulfide cleavable or maleimide non-cleavable linkers resulted in the first generation of conjugates **17-19**, **21** and **22**. During the studies on fluorescent monitoring of drug release we discovered an interesting feature of aminoBODIPY dye **4a** – significantly different excitation maximum in the acylated form of aminoBODIPY (515 nm) compared to the free aminoBODIPY dye (480 nm) while emission spectra remained very similar (525 nm). Moreover, quantum yields of fluorescence of conjugates bearing nitro group were significantly lower. Followingly, we utilized this behavior to develop ratiometric and “OFF-ON” system based on dual excitation and single emission wavelength. We proved the universality of this system by attaching the drug part by three different disulfide cleavable linkages – cysteine (thiol), carbonate (-OH group) and carbamate (-NH group) linkers. In all cases, the drug and free aminoBODIPY dyes were efficiently released and monitored by fluorescence spectroscopy. In general, conjugates with more labile carbonate linker **19a-e** were more susceptible for nucleophilic attack and were strongly cytotoxic against cancer cell lines with IC<sub>50</sub> in sub-micromolar concentration in some cases, but not toxic to normal healthy cells. Conjugates with cysteine disulfide linker **17-e** and **18a,c** possessed improved cytotoxicity and

penetration ability in comparison to free Cys-3HQ **12a-e**. On the other hand, non-cleavable maleimide conjugates **22a-e** exhibited no toxicity with  $IC_{50} > 50$   $\mu$ M. Therefore, this demonstrates that cytotoxic effect is mainly based on the cleavage of disulfide linker and liberation of free 3HQs and BODIPY dye.

The main intention of second generation of conjugates was to develop GSH responsive system with possibility to introduce three parts: (i) cancer cell targeting moiety or second redBODIPY to provide FRET monitoring of drug release, (ii) 3HQ model drug and (iii) aminoBODIPY connected to central unit via disulfide linker. From various attempted synthetical approaches quinone methide and aza-quinone methide approach matched the requirements for central unit – one event (disulfide bond cleavage by GSH) triggers the cleavage of both aminoBODIPY dye and the free drug. Conjugates with quinone methide **40a-d** and aza-quinone methide central unit **28** and **29** decorated with either cRGD peptide, for targeting integrins overexpressed in cancer cells, or redBODIPY for more effective drug release monitoring via FRET were synthesized and tested. Aza-quinone methide conjugates showed slower rate of GSH cleavage compared to quinone methide conjugates **40**. However, FRET conjugates equipped with redBODIPY dyes showed no cytotoxicity probably as a result of low solubility or insufficient penetration into the cells. Conjugates **28** and **40d** equipped with integrin targeting cRGD peptide exhibited moderate cytotoxicity against cancer cells with improved toxicity to normal healthy cells.

#### Published articles:

- Porubský, M.; Gurská, S.; Stanková, J.; Hajdúch, M.; Džubák, P.; Hlaváč, J. *RSC Adv.* **2019**, *9*, 43, 25075–25083.
- Porubský, M.; Gurská, S.; Stanková, J.; Hajdúch, M.; Džubák, P.; Hlaváč, J. *Molecular Pharmaceutics*. **2021**, *18*, 6, 2385–2396.
- Porubský, M.; Vychodilová, K.; Miličević, D.; Buděšinský, M.; Stanková, J.; Džubák, P.; Hajdúch, M.; Hlaváč, J. *ChemistryOpen*. **2021**, *10*, 1-8.



## 2 Development of dual FRET probes for detection and quantification of caspases -8 and -9

### 1.2 Introduction

Fluorescent probes are powerful tools that have brought revolution to our ability to monitor biochemical processes and detect bioactive molecules.<sup>40</sup> Recently, many fluorescent probes based on simple or functionalized small organic dyes, fluorescent proteins, and nanoparticles have been developed.<sup>41–45</sup> Many of them enable a determination of biological and environmental molecules and ions with high sensitivity and selectivity and some of them even in the real-time manner. Moreover, fluorescence is widely used for single-analyte or multi-analyte probes being often superior to other techniques such as mass spectrometry, electrophoresis or other biochemical methods due to its high sensitivity, simplicity, tunability and cost of instrumental equipment.<sup>46</sup>

Recently, multiple-analyte probes have attracted attention thanks to addressing the challenges of selectivity among structurally similar targets and the visualization of the interactions in the complex mixture of the analytes.<sup>47,48</sup> Probes for differentiation among multiple small-molecule analytes have been synthesized but are usually limited only to thiols, ROS/RNS ( $H_2O_2$ ,  $HClO$  etc.), ATP sensing and few enzymes such as phosphodiesterase/ $\beta$ -D-glucosidase<sup>49</sup>, MMP-2/caspase-3<sup>50</sup> (Figure 20), cathepsin B<sup>51</sup> or trypsin/chymotrypsin<sup>52</sup>.

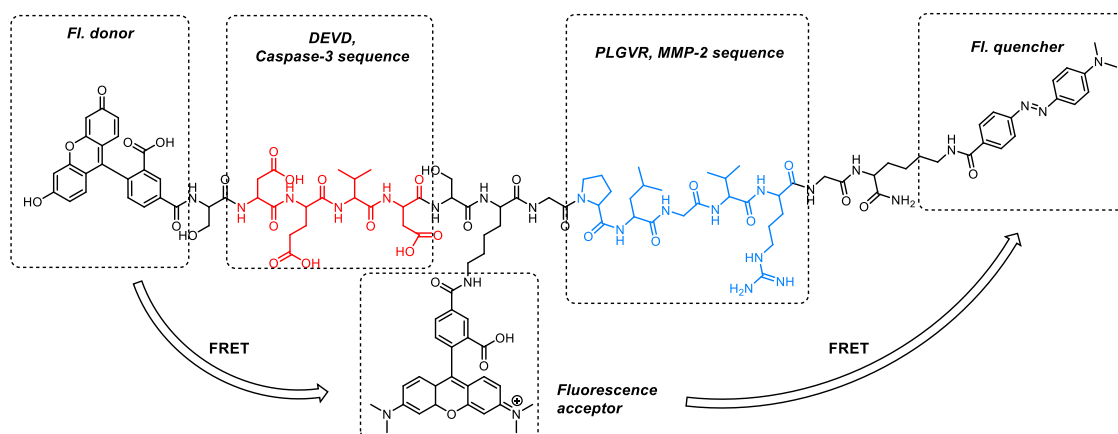


**Figure 20** Probe for simultaneous detection of MMP-2 and caspase-3.<sup>50</sup>

Caspases (**cysteine-aspartic proteases**) are a family of endo-proteases playing key role in maintaining homeostasis through programmed cell death, apoptosis, and involves the controlled dismantling of intracellular components while avoiding inflammation and damage to surrounding cells.

Simultaneous detection of more caspases can serve for elucidation of various metabolic pathways.<sup>53</sup> Usually the initiator caspases, caspases-8, -9, and -10 are overexpressed due to action of xenobiotics or other stimuli and they activate the executioner caspases in a proteolytic cascade to start the apoptotic process (Figure 21).<sup>54</sup> In mammals, it is well known that drug mediated apoptosis proceeds by two major signaling pathways. The extrinsic apoptotic pathway, is initiated by binding to the cell surface “death receptors” such as Fas.<sup>55</sup> In this pathway, apoptotic signals are mediated through the activation of the initiator caspase-8 and

executioner caspases such as caspase-3 and caspase-7. Intrinsic pathway is also known as mitochondrial apoptosis because it depends on factors released from the mitochondria. This pathway is activated by a cellular stresses, including growth factor deprivation, cytoskeletal disruption, DNA damage, accumulation of unfolded proteins or hypoxia and results in the activation of initiator caspase-9.<sup>54,56</sup>

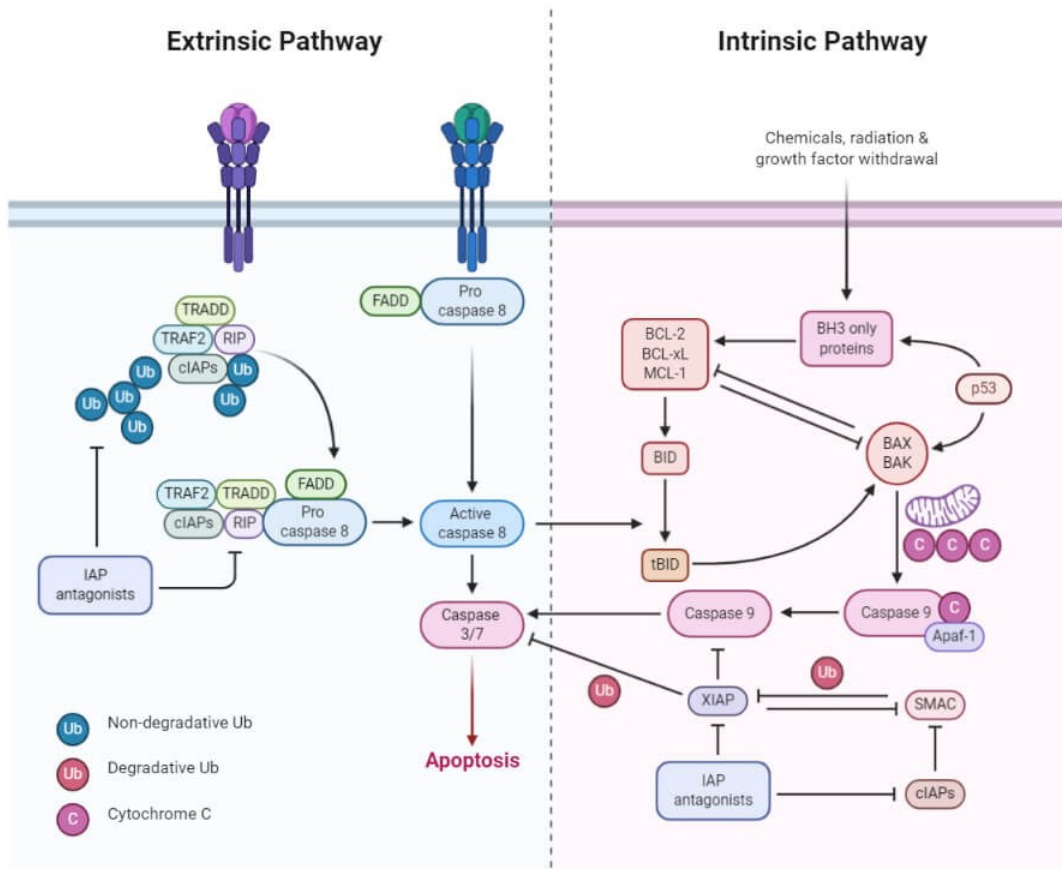
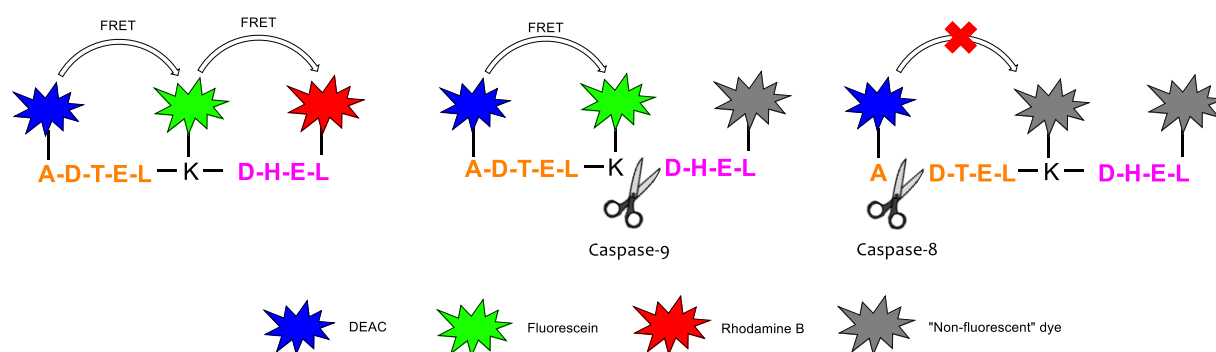


Figure 21 Extrinsic and intrinsic caspase pathway.<sup>57</sup>

### 1.3 Results and discussion

We describe three-fluorophore system containing coumarin, fluorescein and rhodamine B dyes connected with two peptide-like sequences that are recognized and cleaved by caspase-8 and caspase-9 (Figure 22). Cleavage of the caspase-9 peptide linker should lead to disappearance of the FRET between fluorescein and rhodamine (Figure 22, middle structure) and cleavage of the caspase-8 peptide linker should similarly result in total vanishing of the FRET (Figure 22, structure on the right). This system should provide simple FRET-based detection of caspase-8 and -9 and resolution of extrinsic and intrinsic mechanism of action of drugs together with relative quantification of caspase-8 and -9 activity in simple mixtures.

We chose DEAC, fluorescein and Rhodamine B based on our previous experience with the model chymotrypsin-trypsin system as fluorophores capable to serve as donor, acceptor/donor and acceptor of energy, respectively. Fluorophores are located at the beginning, in the middle and at the end of linear peptide backbone. The backbone itself consists of two specific sequences (I)LETDA and LEHD which are cleaved according to literature and previous studies with sufficient selectivity by caspase-8 and -9, respectively.



**Figure 22** Dual-FRET probe and basic principle of cleavage mechanism by caspase-8 and caspase-9.

Several probes were synthesized by standard solid phase chemistry on Wang resin using Fmoc-based protocol and six of them are shown in the Figure 23.

#### 1.3.1 Caspase cleavage studies

Firstly, the cleavage by caspase-9 was tested to see the expected increasing of fluorescein emission after cleavage of LEHD linker causing the termination of energy transfer between fluorescein and rhodamine. In other words, the Figure 24 demonstrates the sensitivity of the probes **46a-f** to the presence of caspase-9 in the model analyte. Probes **46a-d** (Figure 24 A-D) possessed only very low FRET efficiency that led to weak response during caspase cleavage as the most energy is emitted by fluorescein and only little is passed to rhodamine B. Probe **46e** showed satisfying response (almost 2-fold increase) during caspase-9 cleavage and superior FRET efficiency as well. The probe **46f** with the reversed order of peptide linkers showed suitable FRET efficiency but exhibited very poor selectivity towards the caspase-9 as demonstrated by significant increase of Fluorescein emission (528 nm, Figure 24 F). Therefore, we chose the Probe **46e** for further experiments.

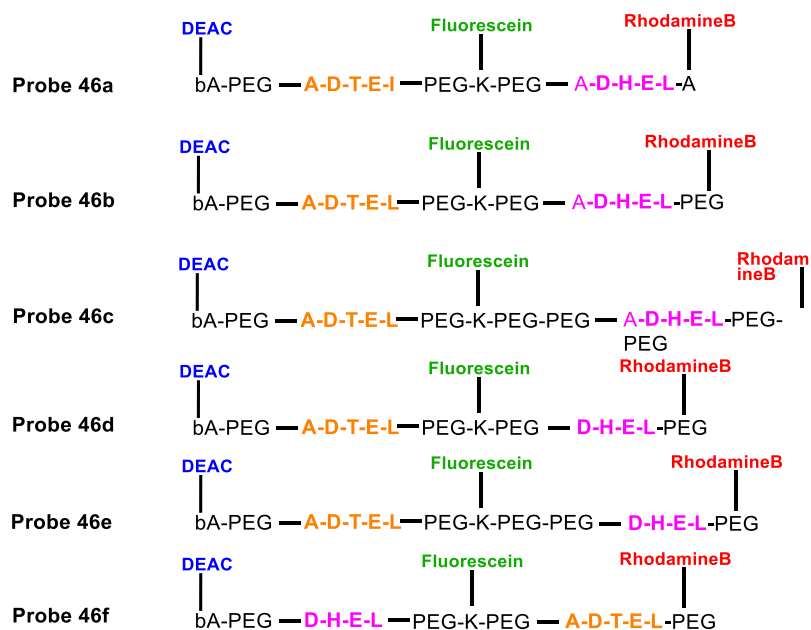


**Figure 23** Structures of Probes 46a-f (one letter code refers to individual amino acid).

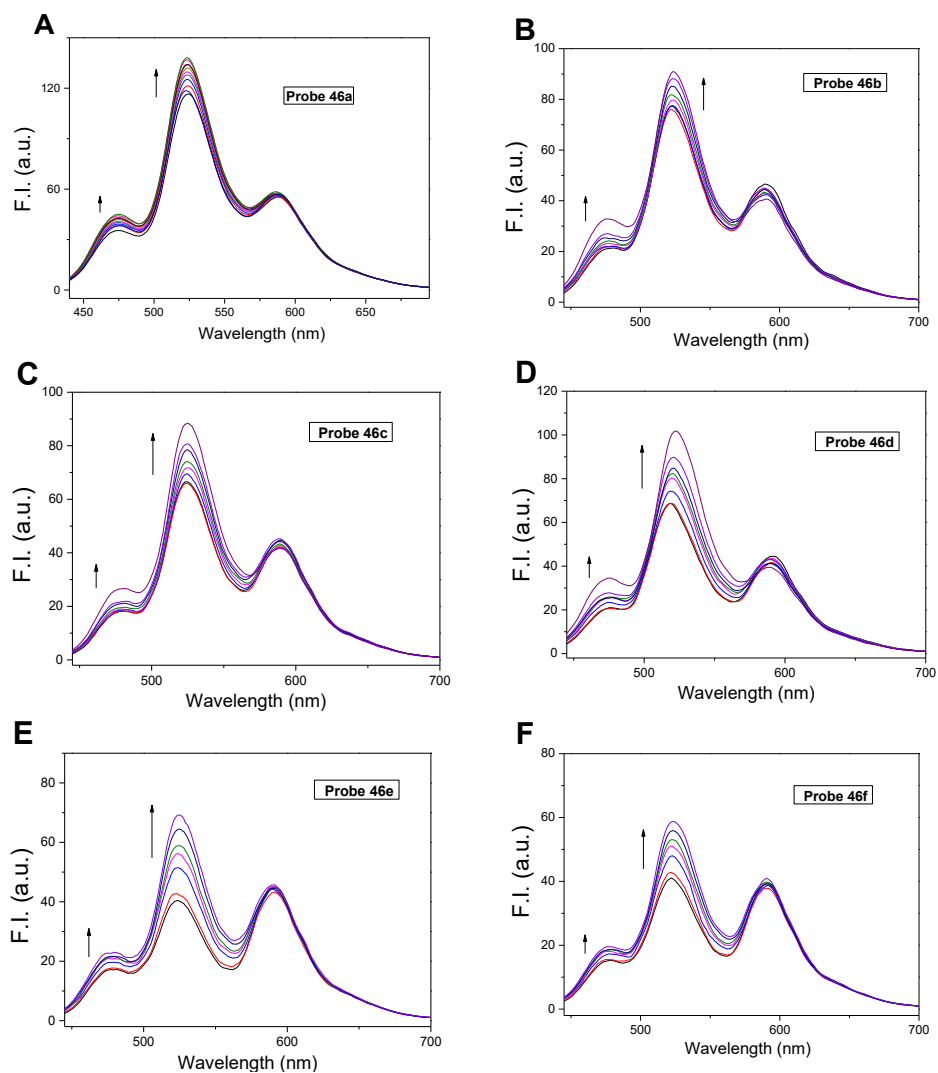


**Figure 24** Emission spectra of probes 46a-f (2  $\mu$ M, A-F) after treatment with active caspase-9 for 2 h (6 U/mL, HEPES Buffer, NaCl, EDTA, DTT, 5% glycerol).

As expected, cleavage by caspase-8 is considerably faster and emission of coumarin is rising significantly (almost 6-fold). According to LC/MS analysis the probe **46e** (2  $\mu$ M) is fully cleaved after 180 min in the presence of 20 Units/mL of caspase-8 yielding to cleavage products depicted in Figure 26. In the presence of 40 Units/mL of caspase-9 the increase in fluorescein emission is up to 5-fold.

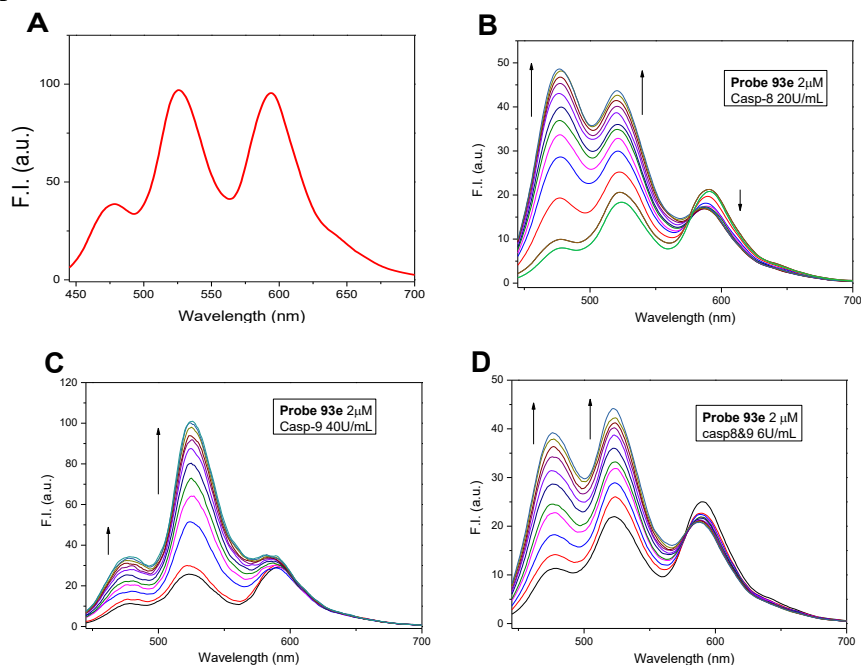


**Figure 25** (A) Emission profile of the intact Probe **46e** (50mM HEPES, pH 7.2, 50mM sodium chloride, 10mM EDTA, 5% glycerol, 10mM DTT; 37 °C), (B) after treatment with caspase-8 (2  $\mu$ M probe, 20 U/mL), (C) caspase-9 (2  $\mu$ M probe, 40 U/mL) and (D) mixture of both caspases-8 and -9 (2  $\mu$ M probe, 6 U/mL each caspase). Excitation wavelength 425nm.

However, according to LC/MS analysis cleavage by caspase-8 or -9 is usually incomplete after 3 h in concentration range that was used (up to 20 U/mL and 40 U/mL for caspase-8 and -9, respectively) and products of cross linker cleavage are formed due to non-selectivity of caspases to its substrate linker and different cleavage rates. Non-selectivity of the cleavage is more significant in the case of caspase-9 as the Figure 26 shows. Treatment by caspase-9 leads to formation of expected cleavage products **49** and **51** and cross linker cleavage by-products **47** and **48**. Treatment by caspase-8 was accompanied only with slight non-selective cleavage of caspase-9 linker to obtain main cleavage products **47** and **48** as demonstrated by Figure 27.

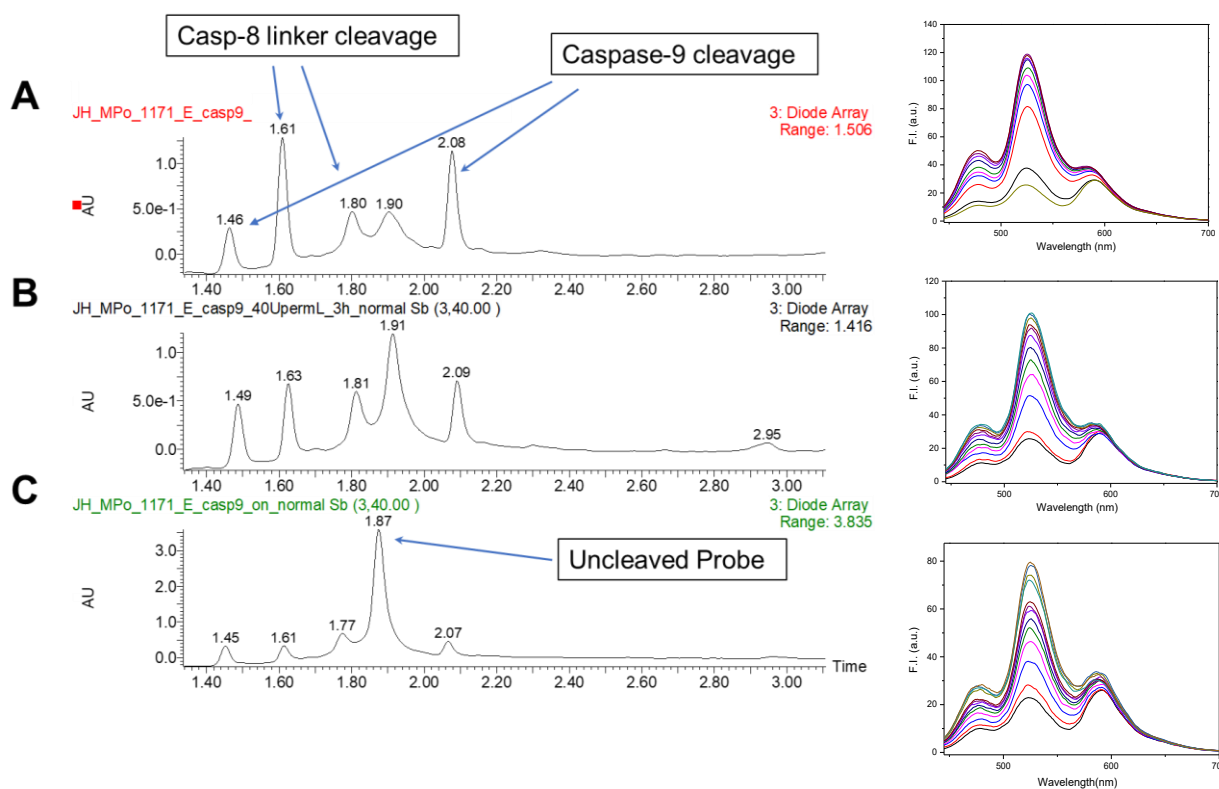
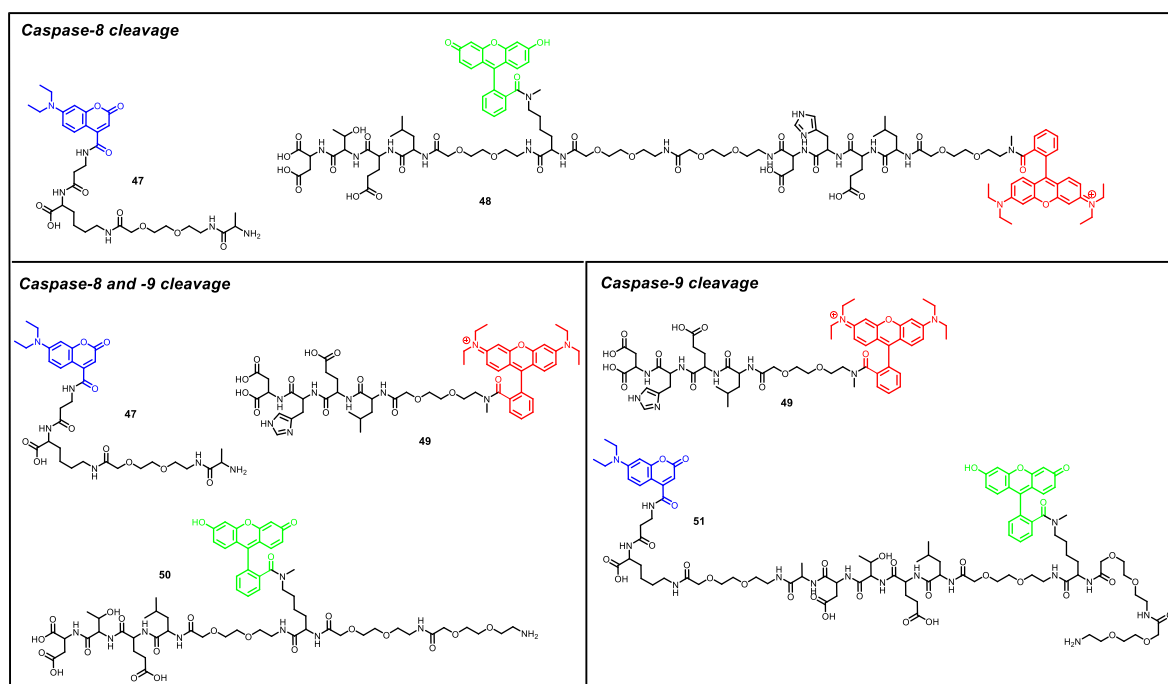


**Figure 26** LC/MS analysis of cleavage products after cleavage of the Probe 46e by caspase-9 and fluorescence response upon excitation at 425 nm. Caspase-9 concentration: (A) 80 U/mL, (B) 40 U/mL and (C) 20 U/mL.

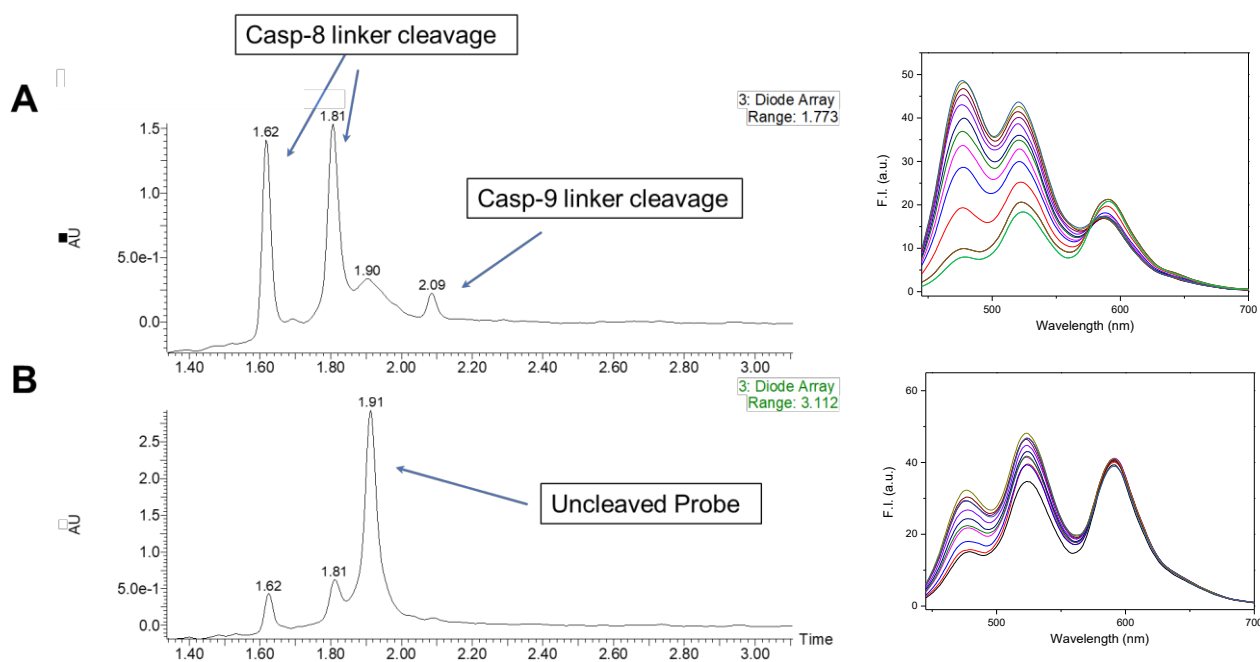


**Figure 27** LC/MS analysis of cleavage products after cleavage of the Probe **46e** (2  $\mu$ M) by caspase-8 and fluorescence response upon excitation at 425 nm. Caspase-8 concentration: (A) 2 U/mL and (B) 0.5 U/mL.

### 1.3.2 Mathematical model

To unambiguously distinguish between presence of any caspase solely or in their mixture we had to develop reliable mathematical model. The model used for previous model trypsin/chymotrypsin probe<sup>52</sup> we found insufficient mainly because of non-selectivity of caspase-9.<sup>58</sup> Therefore, in this case we applied new model where we used  $X = \text{Em}_{\text{DEAC}} / \text{Em}_{\text{FI}}$  against  $Y = \text{Em}_{\text{RHb}} / \text{Em}_{\text{FI}}$ . When we plot ratio  $X_0 / X_t$  ( $X_0$  is value in time = 0 min;  $X_t$  is value in appropriate time interval) against  $Y_0 / Y_t$  in Cartesian coordinate system, we obtained curve that starts from point [1,1] (as the  $X_t = X_0$  and  $Y_t = Y_0$ ) and is linear in adequately broad interval. These lines obtained from cleavage of probe **46e** by individual caspases-8 and-9 intersect at an angle approximately  $110^\circ$  (Figure 28, black and left red line) and lines corresponding to any mixture of both enzymes lie inside this sector.

We specified the operational region as depicted by the red box in Figure 29 A and B where valid datapoints should be located within limit of detection and quantification and are defined as 0.125-2 U/mL and 5-20 U/mL for individual caspase-8 and -9, respectively. Higher than upper limit concentrations of enzymes caused loss of linearity and bending of curves towards the central axis probably due to lower selectivity of enzymatic cleavage and rapid non-distinguishing consumption of substrate (Figure 29 C, D).

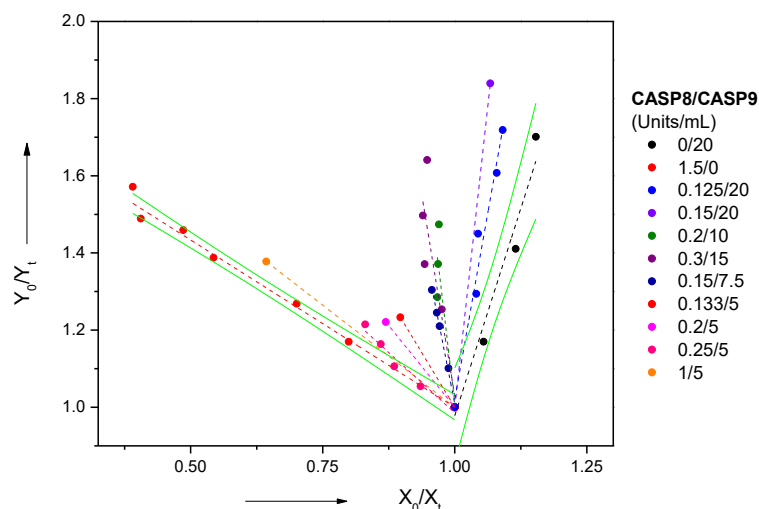


**Figure 28** “Sun watch” model for detection and quantification of caspases-8 and -9.

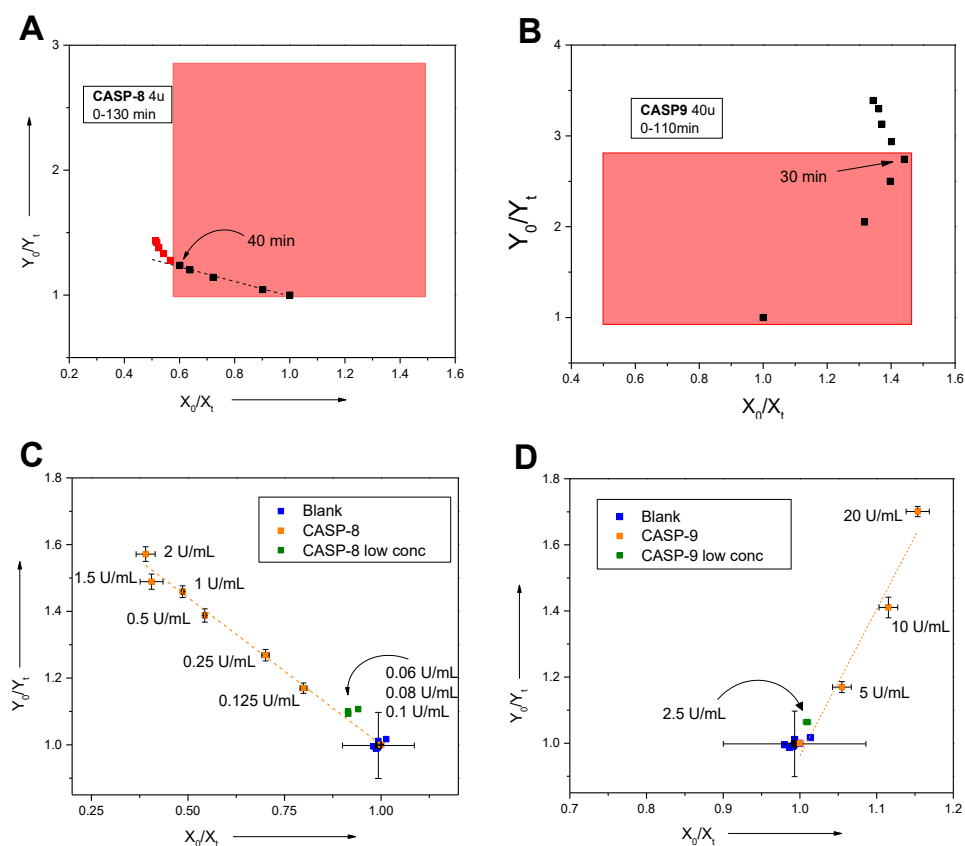


**Figure 29** Determination of linear region (red box) and overconcentrated non-linear region in samples containing (A) 4 U/mL of caspase-8 and (B) 40 U/mL of caspase-9 together with the Probe **46e** (2  $\mu$ M). Determination of LOD and LOQ for (C) caspase-8 and (D) caspase-9. Data points were measured in at least 3 repetitions after 120 min of incubation at 37  $^{\circ}$ C with corresponding enzyme concentration.

Since the process of apoptosis is accompanied by activation of other caspases than caspase-8 or -9, mainly executioner caspase-3 and caspase-7 we investigated also the selectivity of recombinant caspases -3 and -7 towards the probe **46e**. Probe **46e** was treated with 1, 3, 6 U/mL of caspase-3 and -7 in similar fashion as for the previous experiments with caspase-8 and -9 summarized in Figure 30. In the case of caspase-3, significant cleavage of caspase-8



linker (LETD) was observed resulting in the green data points following the trend of caspase-8 curve (red). Caspase-7 did not significantly cleave any of the peptide linkers in probe **46e** what is demonstrated by blue points close to or within standard deviation (error bars) of blank measurements (Figure 30).

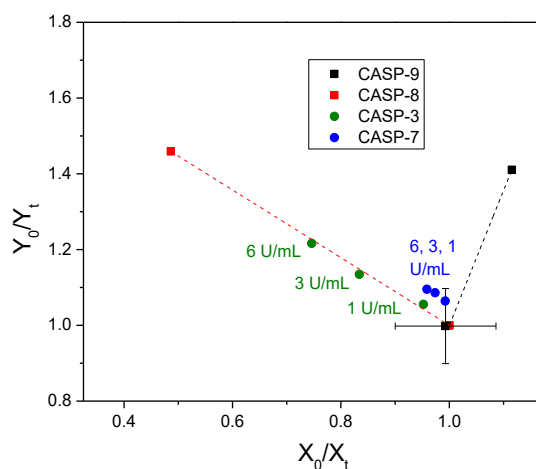


**Figure 30** Cleavage selectivity of caspase-3 and -7. Caspase-3 and -7 cleavage of the probe **46e** measured in concentration 1, 3, 6 Units/mL after 120 min of incubation.

### 1.3.3 Biology

In collaboration with the group of Vladimír Kryštof from Laboratory of Growth Regulators (LGR, Palacký University Olomouc) cell lysates of various cancer cell lines JURKAT wild-type (WT) and special caspase-8 deficient and caspase-9 deficient types<sup>59,60</sup> were prepared by treatment with several known agents inducing apoptosis including caspase-9 selective inducers doxorubicin (DOXO) and taxol (TAX) and caspase-8 selective inducer - tumor necrosis factor/cycloheximide (TNF/CHX). Treatment of selected cell lines these inducers initiated the programmed cell death – apoptosis as indicated by cleaved PARP-1 (Figure 31). PARP-1 is one of few known cellular substrates of caspases and acts as a mediator of apoptotic cell death and cleavage of PARP-1 is therefore considered as a hallmark of apoptosis.<sup>61,62</sup>

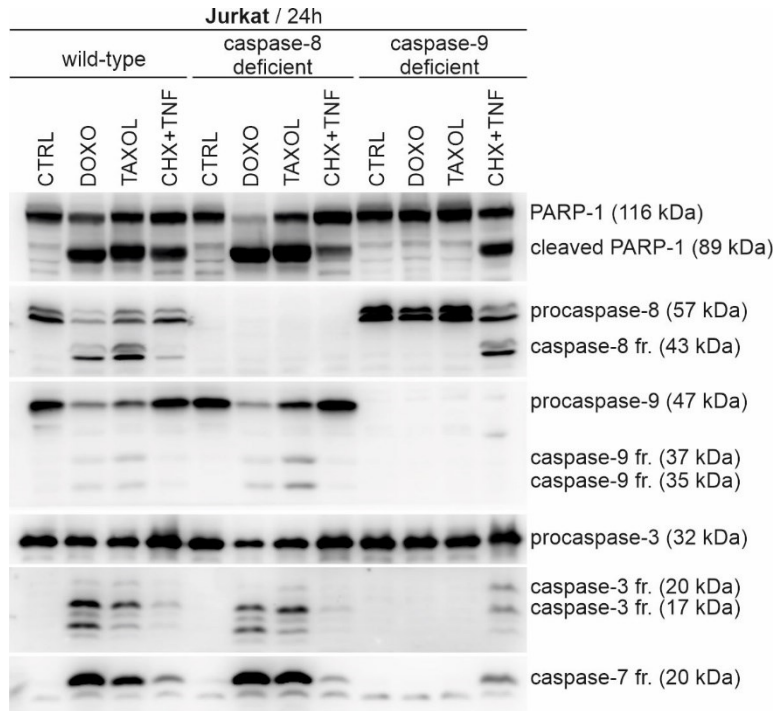
#### a) Testing of the probe on wild type cell line

In wild type cell line (WT) both caspase-8 and caspase-9 can be activated. Treatment by doxorubicin and taxol led to diminishing of the procaspase-8 and activation of caspase-8 in higher extent in comparison to the control experiment. Similarly, the active caspase-9 is generated from its procaspase, although less significantly. In case of CHX/TNF treatment caspase-8 is activated only slightly, while caspase-9 almost not at all. When we compare the observations of western blot results with our model, we can observe a very good agreement. The lines for DOXO and TAX treatment responded to a mixture of caspase-8 and caspase-9, while no significant response was observed for CHX/TNF treatment (Figure 32A).

#### b) Testing of the probe on caspase-8 deficient cell line

Significant cleavage of PARP-1 was observed in JURKAT caspase-8 deficient cells after treatment with doxorubicin and taxol as indicated by western blot Figure 31. However, treatment with CHX-TNF led only to insignificant PARP-1 cleavage and thus small amounts of activated caspases. However, doxorubicin and taxol treatment led to generation of high

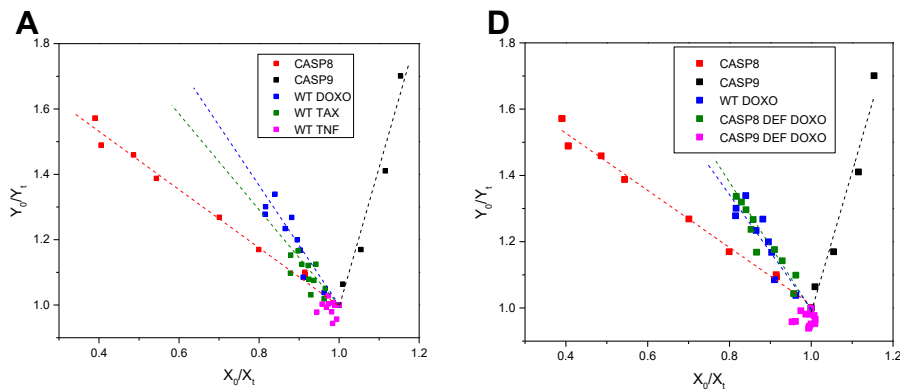
amount of caspase-7 and caspase-3 besides desired caspase-9 initiator caspase. Arguably, the presence of mixture of caspases caused the lower angle of the curves in model representation (Figure 32 B) mainly due to the presence of caspase-3 which causes false positive results for caspase-8.



**Figure 31** Western blot analysis of JURKAT cell lysates of WT, casp-8 and casp-9 deficient cell lines with activation by DOXO, TAX and CHX/TNF.

c) Testing of the probe on caspase-9 deficient cell line.

Based on the western blot analysis, only treatment with TNF-CHX resulted in apoptosis and cleavage of PARP-1 while activation of caspase-8, no caspase-9 and little amount of casp-3/7 occurred. This observation is in accordance with our model where the curve (CASP-9 DEF TNF/CHX, Figure 32 C) converge with the pure recombinant caspase-8 line (marked as red points).



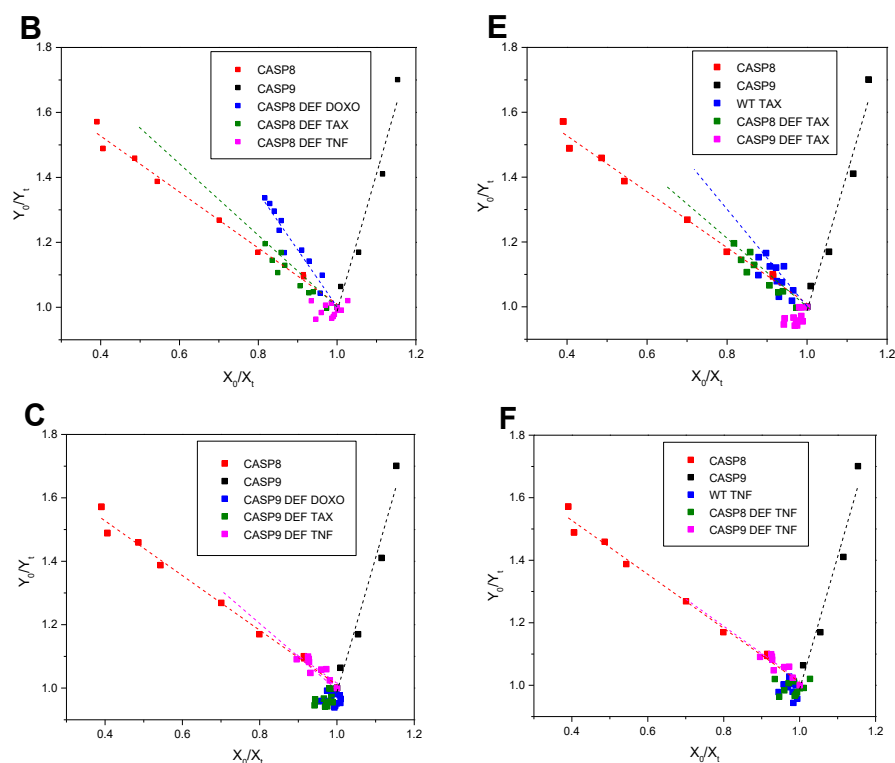


**Figure 32** Treatment of the Probe **46e** with cell lysates from WT, CASP-8 DEF and CASP-9 DEF cell lines with activated caspase by DOXO, TAX or TNF/CHX.

Since the generation of executioner caspases-3 and -7 in cell lysates was not negligible and contributed to a false response we considered also the use of caspase-3/7 inhibitor – the peptide sequence Ac-DEVD-CHO as their preferred substrate.<sup>55</sup> However, we discovered that not only desired inhibition of caspase-3/7 occurs but also the activity of caspase-8 in the various concentrations (10, 50, 100  $\mu$ M) is blocked as demonstrated in Figure 33.

To rule out the cleavage of Probe **46e** by caspase-3 in the cell lysates, mainly caspase-8 DEF cells which gave positively false results because of high abundance of caspase-3 we carried out series of inhibition experiments with caspase-3 inhibitor Ac-DEVD-CHO. As demonstrated by Figure 33, caspase-9 was not inhibited in chosen concentration range (0-100 nM), caspase-8 exhibited only partial inhibition and caspase-3 was effectively inhibited at 50nM of caspase-3 inhibitor. Treatment of Jurkat WT cell lysates with various concentrations of caspase-3 inhibitor - Ac-DEVD-CHO before incubation with the probe **46e** led to disappearance of the line in sundial model (Figure 14 A, B) without significant change of the angle. This can be explained by low amounts of induced caspases in lysates which were in turn fully inhibited even in presence of low concentration of the inhibitor.

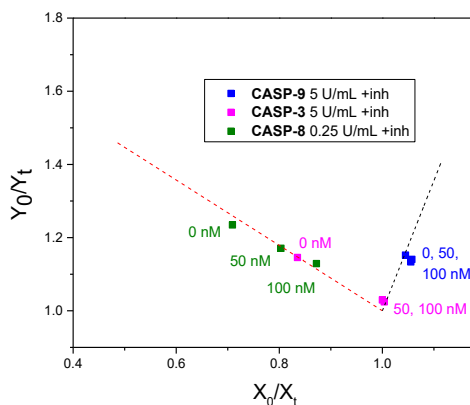


**Figure 33** Inhibition of caspase-3, -8, -9 by caspase-3 selective inhibitor Ac-DEVD-CHO in concentrations 0, 50, 100 nM (50mM HEPES buffer, 50mM NaCl, 10mM EDTA, 10mM DTT, 5% glycerol, pH 7.2, 37 °C) in presence of the Probe **46e** (2  $\mu$ M). Concentration of caspases: caspase-8 0.25 U/mL, caspase-9 5 U/mL, caspase-3 5 U/mL.

Treatment of JURKAT CASP-8 DEF cell lysates with caspase-3 inhibitor led to gradual shift of the curves (Figure 34 C, D) towards caspase-9 line (to the right) in the sun-watch model as expected. However, we were not able to credibly quantify activity of caspase-8 vs caspase-9 due to partial inhibition of caspase-8 by Ac-DEVD-CHO inhibitor. Therefore, the proposed model would be valid for relative quantification in samples containing only simple mixtures of caspase-8/9 or in cell lysates in combination with selective inhibitor of caspase-3. One of such inhibitors proposed by Wolan et al. could be of a good choice.<sup>63</sup>

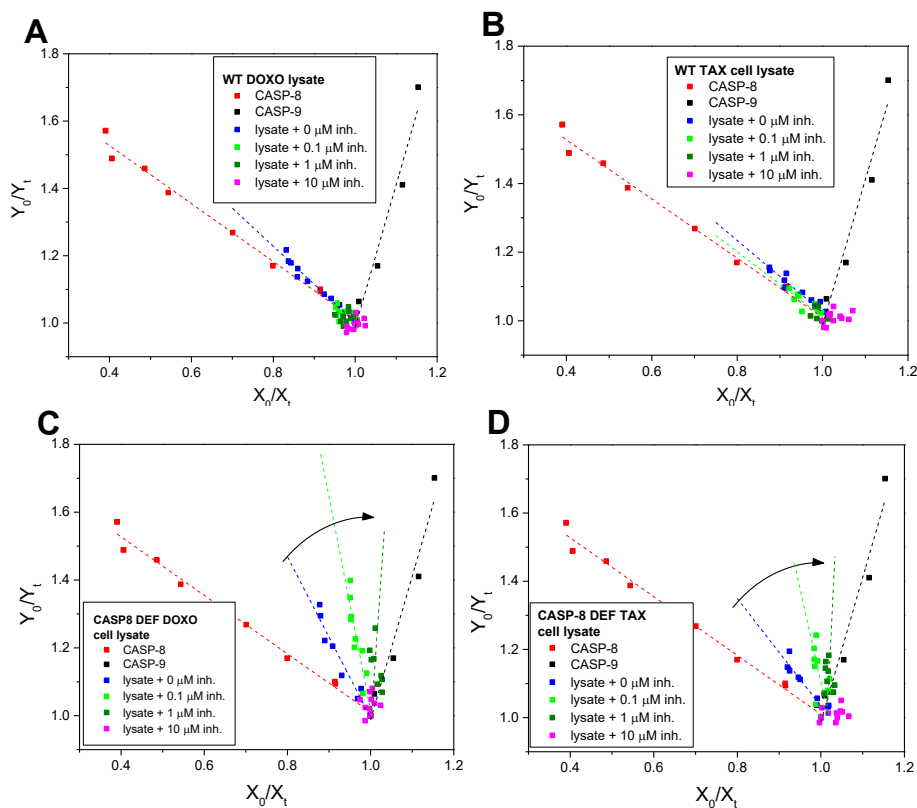


**Figure 34** Treatment of WT and CASP8-DEF cell lysates with caspase-3 inhibitor Ac-DEVD-CHO in concentrations 0, 0.1, 1 and 10  $\mu$ M in the presence of the Probe **46e**.

## 1.4 Conclusion

In summary, we prepared a series of three fluorophore multi-FRET probes for caspase-8 and -9 detection and relative quantification by solid phase chemistry approach. Peptide substrates - LETD and LEHD served as linkers and preferred cleavage sites for caspase-8, resp. caspase-9. Prepared compounds exhibited different FRET efficiencies and selectivity towards caspase cleavage and for further studies we chose Probe **46e** with moderate FRET efficiency and the best selectivity towards caspase-9 among tested probes. Mathematical "sun-watch" model was developed in order to evaluate the activity of caspase-8 and - 9 in cell lysates simultaneously. However, we found that executioner caspase-3 also cleaves the probe **46e** selectively at LETD (caspase-8) linker and the use of Ac-DEVD-CHO inhibitor was necessary in the cell lysates where whole cascade of caspases was activated. Inhibition of caspase-3 led to significant shift of the curve in mathematical model representation towards caspase-9 content in caspase-8 DEF cell lysate and no shift was observed in WT cell lysates. This means that caspase-8 was activated in much higher extent in wild type cells than caspase-9 or caspase-9 was activated in amount lower than detection limit (2.5 U/mL). On the other hand, since caspase-8 could not be activated in caspase-8 deficient cells apoptosis was triggered by activation of caspase-9 according to western blot and confirmed also by our model.

### Submitted articles:

- Porubský, M.; Řezníčková, E.; Kryštof, V.; Hlaváč, J. Development of fluorescent dual-FRET probe for simultaneous detection and relative quantification of caspase-8 and caspase-9. (*submitted*).

---

### 3 Literature:

- (1) Amit Sharma, Jonathan F. Arambula, Seyoung Koo, Rajesh Kumar, Hardev Singh, Jonathan L. Sessler, J. S. K. (2019) Hypoxia-targeted drug delivery. *Chem. Soc. Rev.*, 48, 771–813.
- (2) Yao, V. J.; D'Angelo, S.; Butler, K. S.; Theron, C.; Smith, T. L.; Marchiò, S.; Gelovani, J. G.; Sidman, R. L.; Dobroff, A. S.; Brinker, C. J.; et al. (2016) Ligand-targeted theranostic nanomedicines against cancer. *J. Control. Release*, 240, 267–286.
- (3) Matsumura, Y.; Maeda, H. (1986) A New Concept for Macromolecular Therapeutics in Cancer Chemotherapy: Mechanism of Tumor-tropic Accumulation of Proteins and the Antitumor Agent Smancs. *Cancer Res.*, 46, 6387–6392.
- (4) Mohanty, C.; Das, M.; R. Kanwar, J.; K. Sahoo, S. (2010) Receptor Mediated Tumor Targeting: An Emerging Approach for Cancer Therapy. *Curr. Drug Deliv.*, 8, 45–58.
- (5) Xie, J.; Bi, Y.; Zhang, H.; Dong, S.; Teng, L.; Lee, R. J.; Yang, Z. (2020) Cell-Penetrating Peptides in Diagnosis and Treatment of Human Diseases: From Preclinical Research to Clinical Application. *Front. Pharmacol.*, 11, 1–23.
- (6) Srinivasarao, M.; Low, P. S. (2017) Ligand-Targeted Drug Delivery. *Chem. Rev.*, 117, 12133–12164.
- (7) Santra, S.; Kaittanis, C.; Santiesteban, O. J.; Perez, J. M. (2011) Cell-specific, activatable, and theranostic prodrug for dual-targeted cancer imaging and therapy. *J. Am. Chem. Soc.*, 133, 16680–16688.
- (8) Balendiran, G. K.; Dabur, R.; Fraser, D. (2004) The role of glutathione in cancer. *Cell Biochem. Funct.*, 22, 343–352.
- (9) Wang, Q.; Guan, J.; Wan, J.; Li, Z. (2020) Disulfide based prodrugs for cancer therapy. *RSC Adv.*, 10, 24397–24409.
- (10) Lee, M. H.; Sessler, J. L.; Kim, J. S. (2015) Disulfide-Based Multifunctional Conjugates for Targeted Theranostic Drug Delivery. *Acc. Chem. Res.*, 48, 2935–2946.
- (11) Paulmurugan, R.; Oronsky, B.; Brouse, C. F.; Reid, T.; Knox, S.; Scicinski, J. (2013) Real time dynamic imaging and current targeted therapies in the war on cancer: A new paradigm. *Theranostics*, 3, 437–447.
- (12) Jiao, J.; Zhang, J.; Yang, F.; Song, W.; Han, D.; Wen, W. (2020) Quicker, deeper and stronger imaging : A review of tumor-targeted , near- infrared fluorescent dyes for fluorescence guided surgery in the preclinical and clinical stages. *Eur. J. Pharm. Biopharm.*, 152, 123–143.
- (13) Eble, J.; Haier, J. (2006) Integrins in Cancer Treatment. *Curr. Cancer Drug Targets*, 6, 89–105.
- (14) Liu, Z.; Wang, F.; Chen, X. (2008) Integrin alphaV-beta3-targeted cancer therapy. *Drug Dev. Res.*, 69, 329–339.
- (15) Danhier, F.; Breton, A. Le (2012) RGD-Based Strategies To Target Alpha (v)Beta(3) Integrin in Cancer Therapy and Diagnosis. *Mol. Pharm.*, 9, 2961–2973.
- (16) Nieberler, M.; Reuning, U.; Reichart, F.; Notni, J.; Wester, H. J.; Schwaiger, M.; Weinmüller, M.; Räder, A.; Steiger, K.; Kessler, H. (2017) Exploring the role of RGD-recognizing integrins in cancer. *Cancers (Basel)*, 9, 116.
- (17) Chen, X.; Sievers, E.; Hou, Y.; Park, R.; Tohme, M.; Bart, R.; Bremner, R.; Bading, J. R.; Conti, P. S. (2005) Integrin avB3 – Targeted Imaging of Lung Cancer. *Neoplasia*, 7, 271–279.
- (18) Seftor, R. E. B.; Seftor, E. A.; Gehlsent, K. R.; Stetler-stevenson, W. G.; Brown, P. D.; Ruoslahti, E.; Hendrix, M. J. C. (1992) Role of the avB3 integrin in human melanoma cell invasion. *Proc. Natl. Acad. Sci.*, 89, 1557–1561.
- (19) Gladson, C. L.; Cheresch, D. A. (1991) Glioblastoma expression of vitronectin and the avβ3 integrin: Adhesion mechanism for transformed glial cells. *J. Clin. Invest.*, 88, 1924–1932.
- (20) Rolli, M.; Fransvea, E.; Pilch, J.; Saven, A.; Felding-habermann, B. (2003) Activated integrin avB3 cooperates with metalloproteinase MMP-9 in regulating migration of metastatic breast cancer cells. *PNAS*, 100, 9482–9487.
- (21) Sancey, L.; Garanger, E.; Foillard, S.; Schoehn, G.; Hurbin, A.; Albiges-rizo, C.; Boturyn, D.; Souchier, C.; Grichine, A.; Dumy, P.; et al. (2009) Clustering and Internalization of Integrin avβ3 With a Tetrameric RGD-synthetic Peptide. *Mol. Ther.*, 17, 837–843.
- (22) Wadih Arap, R. P. and E. R. (1998) Cancer Treatment by Targeted Drug Delivery to Tumor Vasculature in a Mouse Model. *Am. Assoc. Adv. Sci.*, 279, 377–380.
- (23) Dal Pozzo, A.; Ni, M. H.; Esposito, E.; Dallavalle, S.; Musso, L.; Bargiotti, A.; Pisano, C.; Vesci, L.; Bucci, F.; Castorina, M.; et al. (2010) Novel tumor-targeted RGD peptide-camptothecin conjugates: Synthesis and biological evaluation. *Bioorganic Med. Chem.*, 18, 64–72.
- (24) Chen, X.; Plasencia, C.; Hou, Y.; Neamati, N. (2005) Synthesis and Biological Evaluation of Dimeric RGD Peptide - Paclitaxel Conjugate as a Model for Integrin-Targeted Drug Delivery. *J. Med. Chem.*, 48, 1098–1106.
- (25) Kaur, P.; Singh, K. (2019) Recent advances in the application of BODIPY in bioimaging and chemosensing. *J. Mater. Chem. C*, 7, 11361–11405.
- (26) Watzke, A.; Kosec, G.; Kindermann, M.; Jeske, V.; Nestler, H.; Turk, V.; Turk, B.; Wendt, K. U. (2008) Selective

- Activity-Based Probes for Cysteine Cathepsins. *Angew. Chemie Int. Ed.*, 47, 406–409.
- (27) Zhang, Q.; Zhu, Z.; Zheng, Y.; Cheng, J.; Zhang, N.; Long, Y. T.; Zheng, J.; Qian, X.; Yang, Y. (2012) A three-channel fluorescent probe that distinguishes peroxyntrite from hypochlorite. *J. Am. Chem. Soc.*, 134, 18479–18482.
- (28) Krumova, K.; Greene, L. E.; Cosa, G. (2013) Fluorogenic  $\alpha$ -tocopherol analogue for monitoring the antioxidant status within the inner mitochondrial membrane of live cells. *J. Am. Chem. Soc.*, 135, 17135–17143.
- (29) Guo, H.; Jing, Y.; Yuan, X.; Ji, S.; Zhao, J.; Li, X.; Kan, Y. (2011) Highly selective fluorescent OFF-ON thiol probes based on dyads of BODIPY and potent intramolecular electron sink 2,4-dinitrobenzenesulfonyl subunits. *Org. Biomol. Chem.*, 9, 3844–3853.
- (30) Hoogendoorn, S.; Blom, A. E. M.; Willems, L. I.; Van Der Marel, G. A.; Overkleeft, H. S. (2011) Synthesis of pH-activatable red fluorescent BODIPY dyes with distinct functionalities. *Org. Lett.*, 13, 5656–5659.
- (31) Wang, S.; Liu, H.; Mack, J.; Tian, J.; Zou, B.; Lu, H.; Li, Z.; Jiang, J.; Shen, Z. (2015) A BODIPY-based “turn-on” fluorescent probe for hypoxic cell imaging. *Chem. Commun.*, 51, 13389–13392.
- (32) Chen, C.; Tian, R.; Zeng, Y.; Chu, C.; Liu, G. (2020) Activatable Fluorescence Probes for “turn-On” and Ratiometric Biosensing and Bioimaging: From NIR-I to NIR-II. *Bioconjug. Chem.*, 31, 276–292.
- (33) Funk, P.; Motyka, K.; Džubák, P.; Znojek, P.; Gurská, S.; Kusz, J.; McMaster, C.; Hajdúch, M.; Soural, M. (2015) Preparation of 2-phenyl-3-hydroxyquinoline-4(1H)-one-5-carboxamides as potential anticancer and fluorescence agents. *RSC Adv.*, 5, 48861–48867.
- (34) Soural, M.; Hlaváč, J.; Funk, P.; Džubák, P.; Hajdúch, M. (2011) 2-Phenylsubstituted-3-Hydroxyquinolin-4(1H)-one-Carboxamides: Structure-Cytotoxic Activity Relationship Study. *ACS Comb. Sci.*, 4, 39–44.
- (35) Polaske, N. W.; Kelly, B. D.; Ashworth-Sharpe, J.; Bieniarz, C. (2016) Quinone Methide Signal Amplification: Covalent Reporter Labeling of Cancer Epitopes using Alkaline Phosphatase Substrates. *Bioconjug. Chem.*, 27, 660–666.
- (36) Luo, C. Q.; Zhou, Y. X.; Zhou, T. J.; Xing, L.; Cui, P. F.; Sun, M.; Jin, L.; Lu, N.; Jiang, H. L. (2018) Reactive oxygen species-responsive nanoprodug with quinone methides-mediated GSH depletion for improved chlorambucil breast cancers therapy. *J. Control. Release*, 274, 56–68.
- (37) Gnaïm, S.; Shabat, D. (2014) Quinone-Methide Species, A Gateway to Functional Molecular Systems: From Self-Immolative Dendrimers to Long-Wavelength Fluorescent Dyes. *Acc. Chem. Res.*, 47, 2970–2984.
- (38) Liu, Y.; Zhao, F.; Gu, W.; Yang, H.; Meng, Q.; Zhang, Y.; Yang, H.; Duan, Q. (2009) The roles of platelet GPIIb/IIIa and v3 integrins during HeLa cells adhesion, migration, and invasion to monolayer endothelium under static and dynamic shear flow. *J. Biomed. Biotechnol.*, 2009.
- (39) Orgovan, N.; Peter, B.; Bosze, S.; Ramsden, J. J.; Szabó, B.; Horvath, R. (2014) Dependence of cancer cell adhesion kinetics on integrin ligand surface density measured by a high-throughput label-free resonant waveguide grating biosensor. *Sci. Rep.*, 4, 1–8.
- (40) Ueno, T.; Nagano, T. (2011) Fluorescent probes for sensing and imaging. *Nat. Methods*, 8, 642–645.
- (41) Elmes, R. B. P. (2016) Bioreductive fluorescent imaging agents: Applications to tumour hypoxia. *Chem. Commun.*, 52, 8935–8956.
- (42) Yu, M. K.; Park, J.; Jon, S. (2012) Targeting strategies for multifunctional nanoparticles in cancer imaging and therapy. *Theranostics*, 2, 3–44.
- (43) Jo, S. D.; Ku, S. H.; Won, Y.; Kim, S. H.; Kwon, I. C. (2016) Targeted Nanotheranostics for Future Personalized Medicine: Recent Progress in Cancer Therapy. *Theranostics*, 6, 1362–1377.
- (44) Wang, R.; Wang, R.; Ju, D.; Lu, W.; Jiang, C.; Shan, X.; Chen, Q.; Sun, G. (2018) “ON-OFF-ON” fluorescent probes based on nitrogen-doped carbon dots for hypochlorite and bisulfite detection in living cells. *Analyst*, 143, 5834–5840.
- (45) Chabok, A.; Shamsipur, M.; Yeganeh-Faal, A.; Molaabasi, F.; Molaei, K.; Sarparast, M. (2019) A highly selective semiconducting polymer dots-based “off-on” fluorescent nanoprobe for iron, copper and histidine detection and imaging in living cells. *Talanta*, 194, 752–762.
- (46) Vendrell, M.; Zhai, D.; Er, J. C.; Chang, Y. T. (2012) Combinatorial strategies in fluorescent probe development. *Chem. Rev.*, 112, 4391–4420.
- (47) Yue, Y.; Huo, F.; Cheng, F.; Zhu, X.; Mafireyi, T.; Strongin, R. M.; Yin, C. (2019) Functional synthetic probes for selective targeting and multi-analyte detection and imaging. *Chem. Soc. Rev.*, 48, 4155–4177.
- (48) Kolanowski, J. L.; Liu, F.; New, E. J. (2018) Fluorescent probes for the simultaneous detection of multiple analytes in biology. *Chem. Soc. Rev.*, 47, 195–208.
- (49) Li, Y.; Wang, H.; Li, J.; Zheng, J.; Xu, X.; Yang, R. (2011) Simultaneous Intracellular  $\beta$ -D-Glucosidase and Phosphodiesterase I Activities Measurements Based on A Triple-Signaling Fluorescent Probe. *Anal. Chem.*, 83,

- 
- 1268–1274.
- (50) Li, S. Y.; Liu, L. H.; Cheng, H.; Li, B.; Qiu, W. X.; Zhang, X. Z. (2015) A dual-FRET-based fluorescence probe for the sequential detection of MMP-2 and caspase-3. *Chem. Commun.*, 51, 14520–14523.
- (51) Xu, J.; Fang, L.; Shi, M.; Huang, Y.; Yao, L.; Zhao, S.; Zhang, L.; Liang, H. (2019) A peptide-based four-color fluorescent polydopamine nanoprobe for multiplexed sensing and imaging of proteases in living cells. *Chem. Commun.*, 55, 1651–1654.
- (52) Okoročhenkova, Y.; Porubský, M.; Benická, S.; Hlaváč, J. (2018) A novel three-fluorophore system as a ratiometric sensor for multiple protease detection. *Chem. Commun.*, 54, 7589–7592.
- (53) Shalini, S.; Dorstyn, L.; Dawar, S.; Kumar, S. (2015) Old, new and emerging functions of caspases. *Cell Death Differ.*, 22, 526–539.
- (54) Kominami, K.; Nagai, T.; Sawasaki, T.; Tsujimura, Y.; Yashima, K.; Sunaga, Y.; Tsuchimochi, M.; Nishimura, J.; Chiba, K.; Nakabayashi, J.; et al. (2012) In Vivo Imaging of Hierarchical Spatiotemporal Activation of Caspase-8 during Apoptosis. *PLoS One*, 7.
- (55) Thornberry, N. A.; Rano, T. A.; Peterson, E. P.; Rasper, D. M.; Timkey, T.; Garcia-Calvo, M.; Houtzager, V. M.; Nordstrom, P. A.; Roy, S.; Vaillancourt, J. P.; et al. (1997) A combinatorial approach defines specificities of members of the caspase family and granzyme B: Functional relationships established for key mediators of apoptosis. *J. Biol. Chem.*, 272, 17907–17911.
- (56) Shi, Y. (2004) Caspase activation, inhibition, and reactivation: A mechanistic view. *Protein Sci.*, 13, 1979–1987.
- (57) <https://microbenotes.com/apoptosis/>. <https://microbenotes.com/apoptosis/>.
- (58) Okoročhenkova, Y.; Porubský, M.; Benická, S.; Hlaváč, J. (2018) A novel three-fluorophore system as a ratiometric sensor for multiple protease detection. *Chem. Commun.*, 54.
- (59) Juo, P.; Kuo, C. J.; Yuan, J.; Blenis, J. (1998) Essential requirement for caspase-8/FLICE in the initiation of the Fas-induced apoptotic cascade. *Curr. Biol.*, 8, 1001–1008.
- (60) Samraj, A. K.; Keil, E.; Ueffing, N.; Schulze-Osthoff, K.; Schmitz, I. (2006) Loss of caspase-9 provides genetic evidence for the type I/II concept of CD95-mediated apoptosis. *J. Biol. Chem.*, 281, 29652–29659.
- (61) Kaufmann, S. H.; Desnoyers, S.; Ottaviano, Y.; Davidson, N. E.; Poirier, G. G. (1993) Specific Proteolytic Cleavage of Poly(ADP-ribose) Polymerase: An Early Marker of Chemotherapy-induced Apoptosis. *Cancer Res.*, 53, 3976–3985.
- (62) Chaitanya, G. V.; Alexander, J. S.; Babu, P. P. (2010) PARP-1 cleavage fragments: Signatures of cell-death proteases in neurodegeneration. *Cell Commun. Signal.*, 8, 1–11.
- (63) Solania, A.; E. González-Páez, G.; W. Wolan, D. (2019) Selective and Rapid Cell-Permeable Inhibitor of Human Caspase-3. *ACS Chem. Biol.*, 14, 2463–2470.